




Pascal Hesse



**Radical Polymerization Kinetics in
Aqueous Solution and in Systems with
Secondary and Tertiary Radicals Studied
by Novel Pulsed-Laser Techniques**



Cuvillier Verlag Göttingen



Radical Polymerization Kinetics in Aqueous
Solution and in Systems with Secondary and
Tertiary Radicals Studied by Novel
Pulsed-Laser Techniques

Dissertation

zur Erlangung des Doktorgrades
der Mathematisch-Naturwissenschaftlichen Fakultäten
der Georg-August-Universität zu Göttingen

vorgelegt von
Pascal Hesse
aus Nordhausen

Göttingen 2008

Bibliografische Information der Deutschen Nationalbibliothek

Die Deutsche Nationalbibliothek verzeichnet diese Publikation in der Deutschen Nationalbibliografie; detaillierte bibliografische Daten sind im Internet über <http://dnb.ddb.de> abrufbar.

1. Aufl. - Göttingen : Cuvillier, 2008
Zugl.: Göttingen, Univ., Diss., 2008
978-3-86727-682-5

D 7

Referent: Prof. Dr. M. Buback

Korreferent: Prof. Dr. K. Hoyer mann

Tag der mündlichen Prüfung: 27.06.2008

© CUVILLIER VERLAG, Göttingen 2008
Nonnenstieg 8, 37075 Göttingen
Telefon: 0551-54724-0
Telefax: 0551-54724-21
www.cuvillier.de

Alle Rechte vorbehalten. Ohne ausdrückliche Genehmigung des Verlages ist es nicht gestattet, das Buch oder Teile daraus auf fotomechanischem Weg (Fotokopie, Mikrokopie) zu vervielfältigen.

1. Auflage, 2008

Gedruckt auf säurefreiem Papier

978-3-86727-682-5

Table of contents

1 Abstract	1
2 Introduction	3
3 Theoretical Background	9
3.1 Ideal Polymerization Kinetics.....	9
3.1.1 Initiation.....	10
3.1.2 Propagation.....	11
3.1.3 Termination	11
3.1.4 Integrated rate laws.....	12
3.2 Transfer reactions.....	13
3.2.1 Transfer to chain-transfer agents	13
3.2.2 Transfer-to-monomer / -solvent.....	14
3.2.3 Transfer-to-polymer.....	14
3.3 Conversion dependence of rate coefficients in FRP	17
3.3.1 Conversion dependence of propagation	17
3.3.2 Conversion dependence of initiator efficiency	19
3.3.3 Conversion dependence of termination	19
3.4 Chain-length dependence of rate coefficients in FRP.....	23
3.4.1 Chain-length dependence of propagation	23
3.4.2 Chain-length dependence of termination.....	23
3.4.3 Rate laws for chain-length-dependent k_t	27
3.5 RAFT-polymerization.....	30
3.6 Size-exclusion chromatography	33

4	Materials and Instrumentation	35
4.1	Chemicals	35
4.1.1	Monomers	35
4.1.2	Polymers.....	36
4.1.3	Saturated monomer analoga.....	36
4.1.4	Initiators	37
4.1.5	Solvents.....	38
4.1.6	Miscellaneous.....	38
4.2	High-pressure equipment	40
4.2.1	Optical high-pressure cell	40
4.2.2	Optical internal cell.....	41
4.2.3	Heating and temperature control.....	42
4.2.4	Pressure generation and control	42
4.3	FT-IR/NIR spectrometer	43
4.4	The PLP-SEC setup.....	44
4.4.1	Pulsed-laser polymerizations	44
4.4.2	Size-exclusion chromatography.....	44
4.5	The SP-PLP-NIR setup	46
4.6	The PLP-ESR setup.....	48
4.7	Simulations.....	49
5	Experimental Procedures and Data Evaluation	51
5.1	The PLP-SEC Technique	51
5.1.1	Experimental procedures.....	52

5.1.2	Data evaluation	54
5.2	Chemically initiated polymerizations	55
5.2.1	Experimental procedure.....	55
5.2.2	Determination of monomer-to-polymer conversion.....	55
5.3	The SP-PLP-NIR technique	58
5.3.1	Experimental procedure.....	59
5.3.2	Calculation of monomer concentration traces	60
5.4	The SP-PLP-ESR technique	60
5.4.1	Experimental procedure.....	61
5.4.2	Determination of radical concentrations.....	63
5.4.3	Interpretation of primary experimental data.....	71
5.5	Selection of experimental conditions.....	77
5.5.1	Photoinitiation	77
5.5.2	Reaction conditions	80
5.6	Data fitting procedures.....	81
5.7	Error estimates	82
6	Propagation Kinetics in Methacrylic Acid Polymerization	85
6.1	Propagation kinetics of non-ionized MAA at low conversions	86
6.2	Conversion dependence of k_p of non-ionized MAA	99
6.3	Dependence of k_p of MAA on monomer concentration and degree of ionization.....	108
6.3.1	Specific features of the polymerization system.....	109
6.3.2	Propagation kinetics of ionized MAA	112
7	Propagation Kinetics in <i>N</i>-Vinyl Pyrrolidone Polymerization	125

7.1	Dependence of k_p of NVP on monomer concentration and temperature.....	126
7.2	Conversion dependence of k_p for polymerization of NVP in water	134
7.3	Dependence of k_p on pH for polymerization of NVP in aqueous solution.....	136
8	Termination Kinetics in Methacrylic Acid Polymerization	139
8.1	Generalized k_p correlation	140
8.2	Determination of $\langle k_t \rangle$ by SP-PLP-NIR.....	142
8.3	Determination of $\langle k_t \rangle$ by chemically initiated polymerizations	150
9	Termination Kinetics in <i>N</i>-Vinyl Pyrrolidone Polymerization	157
9.1	Generalized k_p correlation	157
9.2	Dependence of $\langle k_t \rangle$ on initial monomer concentration, monomer-to-polymer conversion and pressure for polymerizations of NVP in D_2O	159
10	Midchain Radicals in Acrylate Polymerization	169
10.1	Acrylate polymerization scheme and basic kinetic equations	169
10.2	Impact of midchain radical formation on the kinetics of stationary polymerization.....	171
10.3	Impact of midchain radical formation on the kinetics of pseudo-stationary polymerization.....	173
10.4	Impact of midchain radical formation on the kinetics of instationary polymerization.....	189
11	Determination of Rate Coefficients for Acrylate Systems by PLP-SEC	205
11.1	Experimental and simulated MWDs for PLP of BA.....	206
11.2	Evaluation of k_{bb} , k_p^{eff} and k_p^t	212

11.3 Evaluation of c_R^0 and $b\sigma$	214
11.4 Analysis of experimental MWDs	216
11.5 Comparison of k_{bb} and k_p^t estimates with literature data.....	221
12 Determination of Rate Coefficients for Acrylate Systems by SP-PLP-ESR	225
12.1 The ESR spectrum of alkyl acrylates	226
12.2 PLP labeling of SPRs and MCRs in ESR analysis.....	229
12.3 Evaluation of midchain radical fractions determined during stationary and pseudo-stationary polymerization	232
12.4 SP-PLP-ESR of BA.....	238
12.4.1 SPR and MCR concentration traces after single pulse initiation.....	239
12.4.2 Strategy for kinetic analysis of $c_{SPR}(t)$ and $c_{MCR}(t)$ curves	241
12.4.3 Termination kinetics of BA at low temperatures	243
12.4.4 Termination and transfer kinetics of BA between 0 and 60 °C.....	247
13 Kinetics of Acrylic Acid Polymerization	255
13.1 Determination of x_{MCR} and k_{bb}/k_p^t by PLP-SEC experiments.....	256
13.2 Re-consideration of $\langle k_t^{app} \rangle$ data for AA polymerization in water	258
13.3 Chain-length-dependent termination in AA polymerization.....	262
14 General Aspects of Termination Kinetics in Free-Radical Polymerization	271
15 Closing Remarks	281
16 Glossary of Abbreviations	285
17 References	291

1 Abstract

Rate coefficients of propagation, k_p , of termination, k_t , and of intramolecular transfer-to-polymer, k_{bb} , have been studied via pulsed-laser polymerization (PLP) methods for systems with strong intermolecular interactions, such as hydrogen bonds, and for polymerizations with two types of distinctly different radicals being present.

The propagation kinetics of methacrylic acid (MAA) and *N*-vinyl pyrrolidone (NVP) in aqueous solution has been investigated by the PLP-SEC technique which combines PLP-initiation with subsequent analysis of the produced polymer by size-exclusion chromatography. The experimental conditions of monomer concentration, temperature, pressure and degree of monomer ionization have been varied in wide ranges. The dependence of k_p on monomer-to-polymer conversion has been determined from PLP-SEC experiments with pre-mixed polymer. The variation of k_p may be adequately explained by the interaction of solvent and monomer molecules with the transition state structure for propagation. The termination rate coefficients of MAA and NVP have been studied by the SP-PLP-NIR method in which the change in monomer concentration after single pulse (SP) initiation is monitored via μ s time-resolved near infrared spectroscopy (NIR). The variations of k_t with conversion for different initial monomer concentrations reflect the diffusion-controlled character of the termination step with k_t being governed by segmental, translational, and reaction diffusion.

In acrylate polymerization backbiting reactions may occur by which chain-end secondary propagating radicals (SPR) are transformed into tertiary midchain radicals (MCR) via 1,5-hydrogen shift. MCRs can react back to SPRs by monomer addition. The basic kinetic scheme has to be extended for additional reactions steps, as SPR and MCR species show widely different k_p and k_t , respectively. The impact of MCR formation on the applicability of the experimental techniques for k_p and k_t determination, i.e. PLP-SEC and SP-PLP-NIR, was investigated by PREDICI simulations. A novel experimental method has been developed by which k_{bb} and the rate coefficient for monomer addition to the MCR, k_p^t , for butyl acrylate (BA) have been determined from PLP-SEC experiments carried out under extended variation of laser pulse repetition rates. Insights into the kinetics, especially of the termination reactivity of secondary and tertiary acrylate radicals, have been obtained by measurements of full electron spin resonance (ESR) spectra under stationary UV and pseudo-stationary PLP

initiation, respectively, or by time-resolved monitoring of SPR and MCR concentrations after application of a laser single pulse (SP-PLP-ESR). By the latter technique also chain-length-dependent individual k_t values are accessible.

For acrylic acid (AA) polymerization in aqueous solution, the complexities associated with strong solvent effects on the rate coefficients and with the pronounced MCR build-up add to each other. Attempts were made to consider the resulting consequences for the kinetic data of AA polymerization in aqueous solution published so far.

2 Introduction

Synthetic polymers are extensively used in almost all technical fields today with applications ranging from simple packaging material over furniture, clothes and automotive parts to high-tech devices, e.g. for aerospace engineering and life sciences. This widespread distribution makes modern life hardly imaginable without polymeric materials. Synthetic polymers stand out due to their versatile and tunable physical properties and their inexpensive and raw material saving production.

The age of commercial synthetic polymers started about 100 years ago by the work of Baekeland,^[1] however it were the pioneering investigations of Staudinger^[2,3] that form the basis of the scientific fields of polymer chemistry and polymer physics; he discovered the macromolecular chain structure consisting of chemically bonded monomeric units. Since those early studies, polymer production grew rapidly and is nowadays one of the major fields in chemical industry with a turnover in 2006 of about 26 bn € in Germany alone.^[4]

Polymers may be synthesized via polycondensation, catalytic, ionic or free-radical polymerization (FRP). FRP is a robust and versatile technique which is employed to produce e.g. poly(ethylene), poly(styrene), poly(acrylates), poly(methacrylates), and corresponding copolymers as high-volume commodities. In conventional FRP the average lifetime of a growing chain is typically below 1 s which makes it impossible to actively intervene during chain growth. In controlled radical polymerization the lifetime of macroradicals is increased to hours, days or even longer by suppression of irreversible radical termination reactions. Since the breakthrough of such techniques in the 1990s, designing macromolecular architecture by radical polymerization has become possible providing easy access to e.g. blockcopolymers, star polymers and comb polymers.^[5]

The physical properties of polymeric materials are in principle governed by the composition and microstructure of each single macromolecule within the ensemble of chains which form the bulk material. Parameters describing such ensembles of macromolecules, beside others, are the molecular weight distribution (MWD) and mean values, e.g., of the degree of short- or long-chain branching. The microstructure of a macromolecule is established during the polymerization process and is hence a result of the kinetics of the individual reaction steps which occur during chain growth. To allow for strategic and rational design of new materials, which is of great academic and industrial interest, two types of information are required: (i)

the relation of microstructure and physical properties and (ii) the polymerization mechanism together with the associated reaction rates.

Estimation of polymer structure has become feasible in the last decade via sophisticated simulation programs by which not only the time-dependent change in concentration of the reacting species but also full MWDs, branching levels and (copolymer) composition of the formed polymer may be calculated. This development strengthens the need for accurate mechanistic models and rate coefficients. However, due to the mostly rather complex polymerization scheme these rate coefficients are not easily determined and are often not known with sufficient accuracy to allow for satisfactory simulation results. To resolve these problems, an IUPAC working party on “Modeling of Polymerization Kinetics and Processes” has been founded which addresses existing dilemmas and collates benchmark values, mostly for the propagation rate coefficient so far.^[6–15]

The reaction rate in FRP is essentially governed by the rates of initiation, propagation, and termination. The propagation reaction is chemically controlled up to high monomer-to-polymer conversions.^[16] The magnitude of the propagation rate coefficient, k_p , is determined by the properties of the transition state structure (TS) for propagation and its interactions with the solvent environment.^[17–21] Thus, pronounced solvent effects on k_p are expected for systems in which strong, but different, monomer–monomer and monomer–solvent interactions occur. The termination reaction is assumed to be diffusion controlled from low conversions on which introduces an enormous complexity toward the description of this reaction step, as the corresponding rate coefficient, k_t , may change dramatically with monomer-to-polymer conversion, X , which is associated with an increase in solution viscosity. Moreover, k_t may depend on radical chain length, i , on macroradical mobility, on the location of the radical within the chain, on the MWD of the background polymer matrix and on solvent content and quality. Theoretical models have been proposed which are based on the physical understanding of the diffusion-controlled nature of the termination step and adequately describe the variation of k_t with X ^[22,23] and with i ^[24–27]. These models, however, cannot be used to predict k_t for unknown polymerization systems without some additional experimental data.

Classical methods for investigations into the individual rate coefficients of propagation and termination require the combination of results from experiments with stationary and instationary radical concentration yielding the coupled parameters k_t/k_p^2 and k_t/k_p , respectively. Application of such techniques may however pose problems in cases where the

radical chain length distributions significantly differ in both experiments^[7] or side reactions such as transfer-to-polymer^[28] occur. The situation has been largely improved by the development of pulsed-laser polymerization (PLP) techniques about 20 years ago in which chain growth is induced by application of short laser pulses to reaction mixtures containing a photoinitiator. The propagation rate coefficient can be determined precisely by the PLP-SEC method, put forward by Olaj and co-workers,^[29,30] in which PLP is combined with subsequent analysis of the formed polymer by size-exclusion chromatography (SEC). The variation of the termination rate coefficient with conversion is accessible by the SP-PLP-NIR technique, introduced by Buback et al.,^[31] in which the change in monomer concentration after single pulse (SP) initiation is monitored via μs time-resolved near infrared (NIR) spectroscopy. Recently a novel technique was designed in which k_t is determined by direct tracing of radical concentrations after SP initiation using time-resolved electron spin resonance spectroscopy (ESR).^[32] This SP-PLP-ESR technique provides direct access to chain-length dependent k_t values in conventional FRP.^[32-34] However, the decrease of k_t toward increasing chain length may also be detected by SP-PLP-NIR applied to systems in which macroradical chain length is controlled by the addition of a reversible addition fragmentation transfer (RAFT)^[35,36] agent.^[37-39] Application of SP-PLP-NIR represents a significant improvement compared to the so-called RAFT-CLD-T technique^[40] in which k_t is determined from classical chemically induced polymerizations.

Beside the problems introduced by conversion and chain-length dependent rate coefficients, there are additional challenges with systems where two types of radicals with distinctly different reactivities occur, as is known since long from ethylene polymerization. It is now generally accepted^[13] that this difficulty also intervenes in acrylate polymerization where secondary propagating radicals (SPRs) are transformed into tertiary midchain radicals (MCRs) which propagate and terminate less rapidly than SPRs. This conclusion is based on experimental^[28,41-54] and theoretical^[55-58] evidence. The situation is further complicated by the back transformation of MCRs into SPRs through monomer addition which results in a dynamic interconversion between secondary and tertiary radicals by backbiting and MCR propagation steps. To comprehensively describe acrylate polymerization, MCR formation and the subsequent reaction pathways of tertiary radicals have to be implemented into the kinetic scheme. Besides initiation, propagation and termination of SPRs, backbiting, propagation from MCR position, and two additional termination steps need to be considered. For the associated rate coefficients only rough estimates were available before 2007.^[47,51]

Water-soluble homopolymers and copolymers are of high technical importance because of their wide-spread application in hydrogels, thickeners, viscosifiers, flocculants, membranes, coatings, etc.^[59] Mostly, these polymers are obtained from FRP in aqueous solution. Water-soluble monomers of particular technical relevance are acrylic acid (AA), methacrylic acid (MAA), and *N*-vinyl pyrrolidone (NVP). Investigations into the free-radical rate coefficients for polymerizations of these monomers in aqueous as well as organic solutions are scarce.^[16] Significant changes of the rate coefficients are expected as a consequence of the action of hydrogen bonds between monomer, polymer, growing radicals, and water. The complexity may be further enhanced in case that ionic interactions come into play. This requires the additional consideration of the degree of ionization for monomer, polymer, and free-radical species.

First studies into the kinetics of FRP in aqueous phase date back to the work of Katchalsky and Blauer in the early 1950s.^[60] In the 1970s and 1980s, polymerizations in aqueous solution were investigated mostly by Russian scientists, as reviewed by Gromov et al.^[61,62] Only a few individual rate coefficients have been determined by combining stationary methods with the instationary rotating sector technique. The quality of the so-obtained data may however be rather insufficient and reported data exhibit an enormous scatter.^[63–65] During recent years, the PLP-SEC technique has been used extensively for k_p measurements in aqueous phase and reliable k_p values^[8] became available for AA,^[66–69] MAA,^[66] *N*-*iso*-propyl acrylamide (NIPAm)^[70] and acrylamide (AAM).^[71] The implementation of aqueous-phase SEC into PLP-SEC studies on water-soluble monomers^[67] brought a significant improvement of k_p determination, as molecular weight distributions of polymer samples from PLP could be measured directly without the need for carrying out polymer modification reactions to produce samples which may be subjected to SEC analysis in organic phase.^[66] Such polymer modification may give rise to changes of the MWD and thus may result in unreliable k_p values.^[67]

The thesis in hand is mainly devoted to the propagation and termination kinetics in aqueous solution polymerization of MAA (Chapters 6 and 8),^[15,72–75] NVP (Chapters 7 and 9), and AA^[52] studied via PLP-SEC and SP-PLP-NIR, respectively. MAA and NVP are perfectly suited for systematic kinetic studies, as the produced polymers are well soluble in water and in both cases no backbiting reactions occur which would necessitate the use of an extended kinetic scheme. However, MCR formation has to be considered in AA polymerization as is indicated by the problems^[55–57] faced in PLP-SEC experiments at elevated

temperatures^[52,66–69]. Moreover MCR build up was directly demonstrated by ESR spectroscopy.^[41] As already mentioned, the kinetic description of acrylate polymerization is not even satisfactory addressed for polymerization in organic phase. Thus, new experimental methods were developed which are based on both, PLP-SEC experiments under extended variation of laser pulse repetition rate (Chapter 11)^[52,53] and ESR spectroscopic measurements under stationary, pseudo-stationary^[54] and instationary polymerization conditions (Chapter 12). These techniques were first applied to polymerizations of acrylic acid esters, mainly butyl acrylate (BA), in organic phase to prevent superposition with added complexity met in aqueous-phase polymerization. The understanding of the general kinetic trends observed in aqueous-solution polymerization of MAA and NVP is combined with the results for BA polymerization and with theoretical arguments (Chapter 10) toward describing the k_p and k_t data measured for AA (Chapter 13).

3 Theoretical Background

There is a close interlink between the physical properties of a polymer and its molecular weight distribution (MWD) and microstructure, respectively. As the microstructure of a polymer results from the kinetics of the individual reaction steps during polymerization, knowledge of the rate coefficients is an inevitable prerequisite for modeling MWDs and production processes as well as for tailoring product characteristics by suitable selection of reaction conditions and additives.

The basic kinetic description of a polymerization is the ideal polymerization scheme. This scheme, however, needs to be extended by additional reaction steps which occur during polymerization or by rate coefficients being dependent on conversion and radical chain length to adequately describe real polymerizations.

In this chapter, the ideal polymerization scheme is outlined first. Subsequently, this scheme is extended by introducing transfer reactions. The influence of conversion and chain length on rate coefficients in free-radical polymerization is then described in detail. The mechanism of reversible addition fragmentation chain transfer (RAFT) polymerization is briefly outlined. In the last section, the basic concepts of size-exclusion chromatography are presented.

3.1 Ideal Polymerization Kinetics

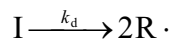
Ideal polymerization kinetics is based on four assumptions:

- all reactions are irreversible
- monomeric species are only consumed in propagation steps
- all macroradicals show the same reactivity, irrespective of their chain length
- termination takes place only by disproportionation or bimolecular radical combination

With these assumptions, the kinetic scheme of a free-radical polymerization can be characterized by three fundamental steps: the formation of radicals, chain growth of these radicals by propagation and termination of the radical chains.

3.1.1 Initiation

Formation of radicals proceeds by thermal, chemical or photochemical activation of an initiator or by direct excitation of the monomer.



The rate of initiation in chemically initiated polymerization, v_i , is given by:

$$v_i = \frac{dc_R}{dt} = 2 \cdot k_d \cdot f \cdot c_i \quad (3-1)$$

where c_R is the radical concentration, k_d is the initiator decomposition rate coefficient, c_i is the initiator concentration, and f is the initiator efficiency which is the fraction of initiator-derived radicals which actually start chain growth.

In case of photochemical initiated polymerization induced by short UV laser pulses (with a typical pulse width of about 20 ns of the lasers used in this work) fired on the reaction mixture containing initiator, monomer and perhaps solvent (pulsed laser polymerization, PLP), the laser pulse instantaneously creates a significant amount of primary radicals. The formation of radicals is fast in comparison to a subsequent termination or propagation step. The radical concentration, which is generated by a single laser pulse, c_R^0 , is given by:

$$c_R^0 = 2 \cdot \Phi \cdot \frac{n_{\text{abs}}}{V} \quad (3-2)$$

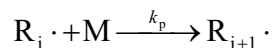
where Φ is the primary quantum yield, n_{abs} is the number of absorbed photons and V is the irradiated volume. The primary quantum yield is the product of the laser efficiency, φ , and the initiator efficiency, f . According to Beer-Lambert's law, the number of absorbed photons may be calculated by Eq. (3-3)

$$n_{\text{abs}} = \frac{E_p}{E_\lambda} \cdot (1 - 10^{-\varepsilon \cdot c_i \cdot l}) \quad (3-3)$$

in which E_p is the energy of one laser pulse, E_λ the energy of one mole of photons at the laser wavelength λ , ε the molar absorption coefficient of the initiator molecule at the laser wavelength, c_i the photoinitiator concentration, and l the optical path length.

3.1.2 Propagation

During the propagation step a monomer molecule adds to a radical.



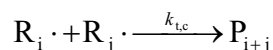
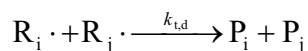
The change in monomer concentration can be expressed by the following rate law:

$$\frac{dc_M}{dt} = -k_p \cdot c_M \cdot c_R \quad (3-4)$$

with k_p being the propagation rate coefficient and c_M the monomer concentration.

3.1.3 Termination

The termination reaction proceeds either by disproportionation, which involves the transfer of a β -hydrogen from one radical to another, or by combination, which is usually a simple head-to-head coupling of the radicals.



The termination rate coefficient, k_t , is the sum of the rate coefficients for disproportionation, $k_{t,d}$, and for combination, $k_{t,c}$. In the termination step, the actual “dead” polymer is formed. The rate of termination is of second order in the radical concentration, c_R .

$$\frac{dc_R}{dt} = -2 \cdot k_t \cdot c_R^2 \quad (3-5)$$

It should be noted, that throughout this thesis, k_t refers to this IUPAC-recommended notation with the factor of two being included (see Eq. (3-5)).

3.1.4 Integrated rate laws

Integration of Eq. (3-5) yields the expression for radical concentration at time t after application of the laser pulse:

$$c_R(t) = \left(2 \cdot k_t \cdot t + \frac{1}{c_R^0} \right)^{-1} \quad (3-6)$$

Combination of Eqs. (3-4) and (3-6) followed by integration results in Eq. (3-7) which formula gives the time-dependent change in monomer concentration after single pulse initiation at $t = 0$:

$$\frac{c_M(t)}{c_M(t=0)} = \left(2 \cdot k_t \cdot c_R^0 \cdot t + 1 \right)^{-k_p/2k_t} \quad (3-7)$$

Unless chain transfer comes into play (see Chapter 3.2), the growth of the radicals in the dark time period after laser pulse initiation is close to monodisperse (of Poisson type). The kinetic chain length i may be calculated by Eq. (3-8) for any time after firing the laser pulse.

$$i = k_p \cdot c_M \cdot t \quad (3-8)$$

In case of stationary polymerization, the rate of radical formation by initiator decomposition (Eq. (3-1)) equals the one for radical loss by termination (Eq. (3-5)):

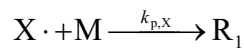
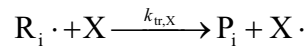
$$k_d \cdot c_1 \cdot f = k_t \cdot c_R^2 \quad (3-9)$$

Combination of Eqs. (3-4) and (3-9) yields the expression for the overall rate of polymerization, R_p , in an ideal stationary polymerization:

$$R_p = -\frac{dc_M}{dt} = c_M \cdot \frac{k_p}{\sqrt{k_t}} \cdot \sqrt{f \cdot k_d \cdot c_1} \quad (3-10)$$

3.2 Transfer reactions

Ideal polymerization kinetics does not include side reactions in which the radical functionality is transferred to another species. However, such reactions readily take place within many polymerization systems and the corresponding kinetic schemes need to be enhanced by radical transfer steps to allow for satisfactory modeling predictions.



X is the species to which the radical functionality is transferred. X may be monomer, initiator, polymer, solvent or an added chain-transfer agent (CTA). Transfer reactions reduce the average molecular weight of the formed polymer (provided that X is a small molecule) by introducing additional termination and initiation events. The rate of chain transfer is given by:

$$\frac{dc_X}{dt} = -k_{tr,X} \cdot c_R \cdot c_X \quad (3-11)$$

where $k_{tr,X}$ is the rate coefficient of chain transfer to a species X of concentration c_X . The radical may subsequently initiate chain growth by adding a monomer molecule with the rate coefficient $k_{p,X}$. Usually a lumped parameter, the transfer constant $C_{tr,X}$, is used to describe transfer reactions:

$$C_{tr,X} = \frac{k_{tr,X}}{k_p} \quad (3-12)$$

Transfer reactions of particular relevance for the present study are outlined below.

3.2.1 Transfer to chain-transfer agents

CTAs are used in conventional FRP for controlling polymer molecular. Whereas catalytic CTAs are not consumed during polymerization, non-catalytic CTAs are found as end-groups of the polymer. Typical non-catalytic CTAs are mercaptanes such as dodecyl mercaptan which easily forms sulfur-centered radicals by cleavage of the S-H bond.

3.2.2 Transfer-to-monomer / -solvent

Transfer reactions may also occur in systems without special additives by transfer of the radical functionality to a monomer or solvent molecule. Transfer-to-monomer has to be considered to take place to some extent with all polymerization systems. Relatively high transfer constants are found for allylic monomers and vinyl acetate and for some common solvents, such as toluene and heptane.^[65]

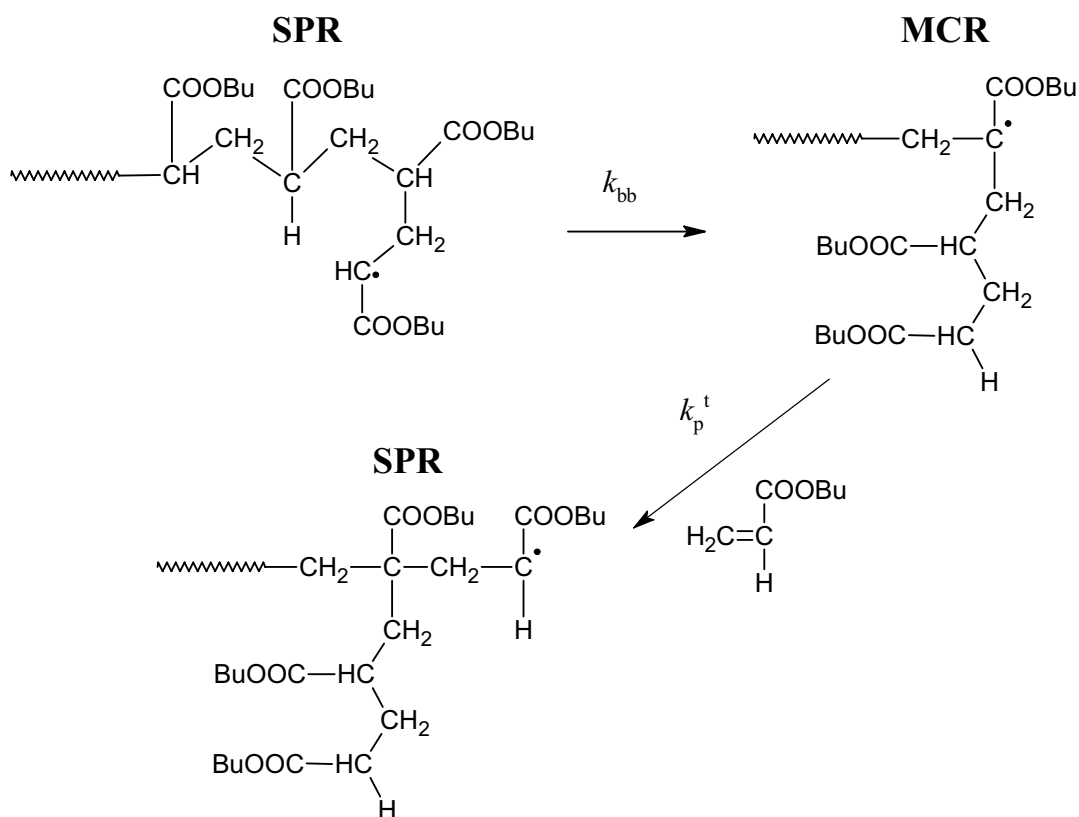
3.2.3 Transfer-to-polymer

Transfer-to-polymer proceeds by intra- or intermolecular abstraction of hydrogen atoms from the macroradical or polymer backbone. This process differs from the above-mentioned reactions in that with this transfer step the number of growing chains is not increased. Hence, the average molecular weight of the obtained polymer is not intrinsically lowered by transfer to polymer. However, short- and long-chain branches are introduced in the chains.

Transfer-to-polymer occurs at high rates when the chain-end propagating radical is less stabilized as compared to the situation where the radical site is located at the polymer backbone. This is known since long for ethylene polymerization but in recent years it became evident that also for acrylate polymerization transfer-to-polymer has to be considered^[13,28,41-58] by which a secondary propagating radical (SPR) is transformed into a tertiary "midchain" radical (MCR). Whereas the intermolecular step occurs at significant rate only for high polymer contents, i.e. monomer-to-polymer conversions,^[76] intramolecular transfer-to-polymer via hydrogen abstraction, most likely via the transition state being a six-membered ring, may readily occur from low conversions on. The latter reaction, often referred to as backbiting, is depicted in Scheme 3-1 with k_{bb} , the backbiting rate coefficient. Subsequent addition of monomer to the MCR creates a short-chain branch (SCB) in the polymer and leads to reformation of a chain-end radical. The propagation rate coefficient for monomer addition to the MCR, k_p^t , is significantly lower than for addition to the chain-end SPR (denoted by k_p^s).^[45,48,51-54]

Furthermore, the reactivity toward termination for MCRs is lower compared to the secondary radical species. Thus, formation of tertiary radicals in acrylate polymerization not only creates

branching points, but also considerably influences polymerization rates and necessitates the use of extended reaction schemes.



Scheme 3-1: Formation of a midchain tertiary radical (MCR) by intramolecular chain transfer of a chain-end secondary radical (SPR). Monomer addition to the new midchain radical structure creates a short-chain branch in the polymer and leads to reformation of a chain-end radical.

The relative concentrations of the two types of radicals, c_{SPR} and c_{MCR} , may be estimated by assuming that a dynamic equilibrium has been reached and making a quasi-steady state assumption on dc_{MCR}/dt :^[28]

$$\frac{c_{\text{MCR}}}{c_{\text{SPR}}} = \frac{k_{bb}}{k_p^t \cdot c_M + 2 \cdot k_t^{tt} \cdot c_{\text{MCR}} + 2 \cdot k_t^{st} \cdot c_{\text{SPR}}} \quad (3-13)$$

In Eq. (3-13), k_t^{tt} is the rate coefficient for termination of two midchain radicals, k_t^{st} is the rate coefficient for cross-termination of the two radical types. Other side reactions (i.e., β -scission of tertiary radicals^[77] and transfer-to-monomer) are assumed to be negligible. The fraction of midchain radicals, x_{MCR} , is hence given by:

$$x_{\text{MCR}} = \frac{c_{\text{MCR}}}{c_{\text{SPR}} + c_{\text{MCR}}} = \frac{k_{\text{bb}}}{k_{\text{p}}^{\text{t}} \cdot c_{\text{M}} + 2 \cdot k_{\text{t}}^{\text{tt}} \cdot c_{\text{MCR}} + 2 \cdot k_{\text{t}}^{\text{st}} \cdot c_{\text{SPR}} + k_{\text{bb}}} \quad (3-14)$$

The rate of polymerization for a system with SPRs and MCRs being present is:

$$\begin{aligned} R_{\text{p}} &= (k_{\text{p}}^{\text{t}} \cdot c_{\text{MCR}} + k_{\text{p}}^{\text{s}} \cdot c_{\text{SPR}}) \cdot c_{\text{M}} = (k_{\text{p}}^{\text{t}} \cdot x_{\text{MCR}} + k_{\text{p}}^{\text{s}} \cdot (1 - x_{\text{MCR}})) \cdot c_{\text{M}} \cdot (c_{\text{MCR}} + c_{\text{SPR}}) \\ &= k_{\text{p}}^{\text{eff}} \cdot c_{\text{M}} \cdot (c_{\text{MCR}} + c_{\text{SPR}}) = k_{\text{p}}^{\text{eff}} \cdot c_{\text{M}} \cdot c_{\text{R}} \end{aligned} \quad (3-15)$$

where Eqs. (3-4) and (3-15) lead to the definition of an effective propagation rate coefficient for the two-radical system. Assuming that for MCRs the probability of propagation is much higher than of termination ($k_{\text{p}}^{\text{t}} \cdot c_{\text{M}} \gg 2 \cdot k_{\text{t}}^{\text{tt}} \cdot c_{\text{MCR}} + 2 \cdot k_{\text{t}}^{\text{st}} \cdot c_{\text{SPR}}$ in Eq. (3-13), the so-called long-chain hypothesis).^[28,45,55]

$$k_{\text{p}}^{\text{eff}} = k_{\text{p}}^{\text{s}} - \frac{k_{\text{p}}^{\text{s}} - k_{\text{p}}^{\text{t}}}{1 + \frac{k_{\text{p}}^{\text{t}} \cdot c_{\text{M}}}{k_{\text{bb}}}} \quad (3-16)$$

which, as $k_{\text{p}}^{\text{t}} \ll k_{\text{p}}^{\text{s}}$, is transformed to:

$$\frac{k_{\text{bb}}}{k_{\text{p}}^{\text{t}}} = c_{\text{M}} \cdot \left(\frac{k_{\text{p}}^{\text{s}}}{k_{\text{p}}^{\text{eff}}} - 1 \right) \quad (3-17)$$

A particularly useful relation between $k_{\text{p}}^{\text{eff}}$ and the fraction of midchain radicals is derived for the case of $k_{\text{p}}^{\text{t}} \ll k_{\text{p}}^{\text{s}} \cdot c_{\text{SPR}} / c_{\text{MCR}}$:

$$k_{\text{p}}^{\text{eff}} = k_{\text{p}}^{\text{s}} \cdot (1 - x_{\text{MCR}}) \quad (3-18)$$

A comprehensive discussion of the impact of MCR formation on the kinetics of stationary, pseudo-stationary and instationary polymerization is given in Chapter 10. Novel experimental techniques directed toward the evaluation of k_{p}^{s} , $k_{\text{p}}^{\text{eff}}$, x_{MCR} , k_{p}^{t} , and the individual termination rate coefficients k_{t}^{ss} (termination of two SPRs), k_{t}^{st} , and k_{t}^{tt} are detailed in Chapters 11 and 12.

3.3 Conversion dependence of rate coefficients in FRP

During the course of a polymerization reaction small unsaturated monomer molecules are continuously transformed into saturated long-chain polymer molecules. This transformation induces significant changes in the properties of the reaction mixture. The most obvious is the orders of magnitude increase in viscosity, η , for bulk polymerizations which decelerates diffusive processes. Diffusion of reactants is the first stage of all bimolecular reactions, i.e. propagation, termination and initiator re-combination, being followed by the actual chemical reaction. An excellent review on the influence of diffusion limitations on polymerization reactions recently appeared in ref.^[78]

3.3.1 Conversion dependence of propagation

The propagation reaction consists of two stages, the diffusion of macroradical and monomer to reach sufficiently close proximity for the subsequent step, the actual chemical reaction. A diffusion controlled rate coefficient, k_D , may be expressed by the Smoluchowski equation^[79]

$$k_D = 4 \cdot \pi \cdot N_A \cdot (D_s^A + D_s^B) \cdot R_C \quad (3-19)$$

where N_A is Avogadro's number, D_s^A and D_s^B are the diffusion coefficients of species A and B, and R_C is the capture radius. The corresponding rate coefficient of the diffusive stage of propagation ($k_{p,D}$) is thus proportional to the sum of the diffusion coefficients of monomer and macroradical.

The individual diffusion coefficients may be approximated by the Stokes-Einstein-Equation for the case of negligible ionic interactions

$$D_s = \frac{k_B \cdot T}{6 \cdot \pi \cdot r_{s,i} \cdot \eta} \quad (3-20)$$

with the Boltzmann constant k_B , the absolute temperature T , and the hydrodynamic radius of the monomer or the macroradical of chain length i , $r_{s,i}$, respectively. Thus, $k_{p,D} \sim \eta_r(X)^{-1}$ and the absolute value of $k_{p,D}$ is mainly governed by the diffusion coefficient of the smaller

species, i.e. of the monomer. The relative viscosity of the reaction solution at monomer-to-polymer conversion X , $\eta_r(X)$, is defined as

$$\eta_r(X) = \frac{\eta(X)}{\eta_0} \quad (3-21)$$

with the absolute viscosity at monomer-to-polymer conversion X , $\eta(X)$, and the viscosity at zero conversion, η_0 . According to the relations given above, $k_{p,D}$ may be formulated as:

$$k_{p,D} = \frac{k_{p,D}^0}{\eta_r(X)} \quad (3-22)$$

where $k_{p,D}^0$ denotes the diffusion controlled part of the propagation rate coefficient at $X=0$. When $k_{p,0}$ denotes the propagation rate coefficient without the contribution of diffusion, overall k_p may be represented by the kinetic expression for a consecutive-type reaction:

$$\frac{1}{k_p} = \frac{1}{k_{p,0}} + \frac{1}{k_{p,D}} \quad (3-23)$$

A significant lowering of k_p due to the contribution of $k_{p,D}$ in Eq. (3-23) is only expected for very high viscosities as the actual chemical reaction is rather slow ($k_{p,0}$). Thus, k_p can be assumed constant up to conversions of about 80 to 90 % from which on a pronounced drop of the propagation rate may set in.^[80] Via ESR spectroscopy, this assumption has already been proven for styrene^[81] and methyl methacrylate (MMA)^[82-84] polymerization in non-polar solutions.

It needs to be stressed that during solution polymerization not only the viscosity of the reaction medium changes but also the solvent composition, as monomer, which actually is a co-solvent, is continuously transformed into polymer. Hence, in systems for which pronounced solvent effects on low-conversion k_p are observed, k_p may also change during polymerization from initial conversions on.

A thorough presentation and discussion of mechanistic models for solvent effects on the propagation rate is given in Chapters 6 and 7 together with the experimental results for k_p of MAA and NVP in water.

3.3.2 Conversion dependence of initiator efficiency

Initiator decomposition as a unimolecular reaction is unlikely to be affected by the viscosity of the reaction medium and should hence not change with conversion. After bond cleavage of the initiator, the two primary radicals have to add to a monomer molecule for inducing macroradical chain growth. In the time span between initiator decomposition and monomer addition the primary radicals may undergo irreversible side reactions which lower the initiator efficiency. This time span is significantly increased in case of diffusion controlled initiation which may, analogous to k_p , set in at high conversions at which also c_M is low.

Experimental evidence for a pronounced decrease of f at high conversions has been obtained from comparison of bulk and emulsion polymerization of MMA^[85] and by ESR studies^[84,86-88].

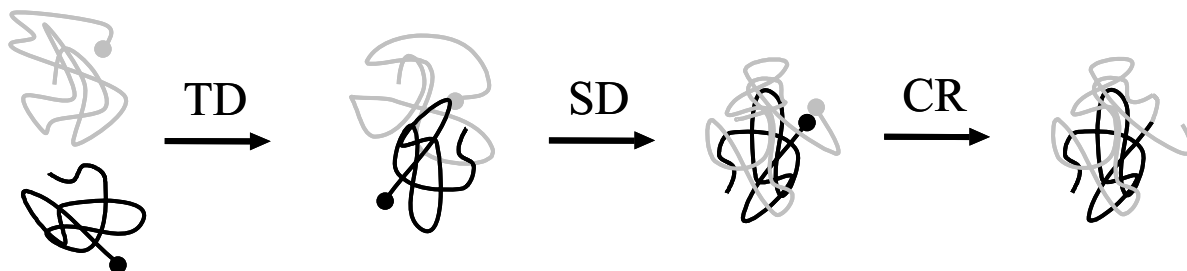
3.3.3 Conversion dependence of termination

Bimolecular termination involves the fast chemical reaction of two radicals and is therefore considered being diffusion controlled from zero per cent conversion on.^[11] Consequently, k_t scales with the diffusive mobility of the macroradicals which may strongly depend not only on temperature and pressure, as do all rate coefficients, but also on factors like solvent viscosity, monomer-to-polymer conversion, chain flexibility, dynamics of entanglements, macroradical chain length, and molecular weight distribution of the surrounding polymer matrix through which the radical has to diffuse. The diffusion coefficients and thus k_t of macroradicals are highly system specific and may vary over several orders of magnitude with conversion or in between two monomer systems. The enormous complexity which is introduced by the diffusion controlled nature of termination necessitates careful presentation of all reaction conditions when reporting k_t data to allow for comparability.^[6,7,11,14]

The termination reaction of two macroradicals proceeds in a three stage mechanism which is depicted in Scheme 3-2 and was introduced by Benson and North.^[89,90]

As is indicated in Scheme 3-2, both macroradicals first have to come into contact by translational (centre-of-mass) diffusion (TD). Subsequently, the radical functionalities have to come into close proximity for forming a radical-radical encounter pair by segmental diffusion (SD). The third and final step is the chemical reaction (CR) proceeding either by combination

or disproportionation. The individual rates of the two modes of termination do not manifest in experiments from which k_t is derived as far as they are not based on the analysis of the produced polymer. However, for modeling molecular weight distributions this information is of concern.



Scheme 3-2: Schematic view of the diffusion and reaction steps during termination of two macroradicals. For details see text.

Analogous to the description of the propagation reaction in Chapter 3.3.1, the diffusion controlled termination rate coefficient, $k_{t,D}$, may be expressed by:

$$\frac{1}{k_{t,D}} = \frac{1}{k_{SD}} + \frac{1}{k_{TD}} + \frac{1}{k_{CR}} \quad (3-24)$$

with the corresponding rate coefficients for SD, TD and CR. In accordance to Eq. (3-22), which accounts for the TD control of k_p , k_{TD} can be expressed as:

$$k_{TD} = \frac{k_{TD}^0}{\eta_r(X)} \quad (3-25)$$

where k_{TD}^0 is the translational diffusion rate coefficient at zero conversion.

The description above neglects the contribution of radical chain end motion by monomer addition, a mechanism denoted as reaction diffusion (RD).^[22,91] This process may become dominant in highly concentrated polymer solutions in which TD is very slow and most macroradicals are trapped in an environment of dead polymer.^[22,23] However, for highly cross-linked systems RD-control may already set in at low conversions.^[92] Radical mobility via RD is proportional to the rate of propagation, i.e. to $k_p \cdot c_M$ or $k_p \cdot (1-X)$. Thus, the reaction-diffusion controlled termination rate coefficient, $k_{t,RD}$, may be expressed by:

$$k_{t,RD} = C_{RD} \cdot k_p \cdot (1 - X) \quad (3-26)$$

where C_{RD} is the reaction-diffusion constant which is a measure for the efficiency of termination via reaction diffusion. The magnitude of C_{RD} is mainly determined by the dynamics of the macroradical chain end and its location relative to the ultimate entanglement mode.^[22,23,93] The termination rate coefficient, k_t , is given by:

$$k_t = k_{t,D} + k_{t,RD} \quad (3-27)$$

Implementation of Eqs. (3-23) to (3-26) in Eq. (3-27) yields for the case of $k_{CR} \gg k_{TD}$ and k_{CR} :

$$k_t = \frac{1}{k_{SD}^{-1} + \eta_r(X)/k_{TD}^0} + \frac{C_{RD} \cdot (1 - X)}{k_{p,0}^{-1} + \eta_r(X)/k_{p,D}^0} \quad (3-28)$$

Eq. (3-28) allows for an adequate representation of the conversion dependence of k_t for most polymerization systems.

The three modes of diffusion, i.e. SD, TD and RD, are not equally important over the entire range of conversions. Thus, the k_t variation may be subdivided into different conversion regimes as is indicated in Figure 3-1, which shows the variation of k_t with monomer-to-polymer conversion as is typically for some bulk methacrylate polymerizations. At low conversions, k_t remains almost constant. Such initial plateau regimes are indicative of SD being the rate determining diffusion step. Increasing monomer conversion is associated with an increase in bulk viscosity. As a consequence, TD may become rate determining which manifests itself in an, in some cases, orders of magnitude decrease in k_t . The strong decrease of termination rate in this regime, often referred to as gel-effect or Norrish-Trommsdorf effect,^[94,95] reflects the reduced translational mobility of the macroradicals at significantly increasing bulk viscosity (see Eq. (3-25)). At even higher degrees of monomer conversion (40 to 70 % in Figure 3-1), the lowering of k_t with X is less pronounced, an observation that indicates that k_t runs under reaction diffusion control. The stronger decrease of k_t at conversions above 70 % is caused by the pronounced deceleration of propagation rate (see Eq. (3-26)) at low monomer concentrations and perhaps even with diffusion controlled k_p .

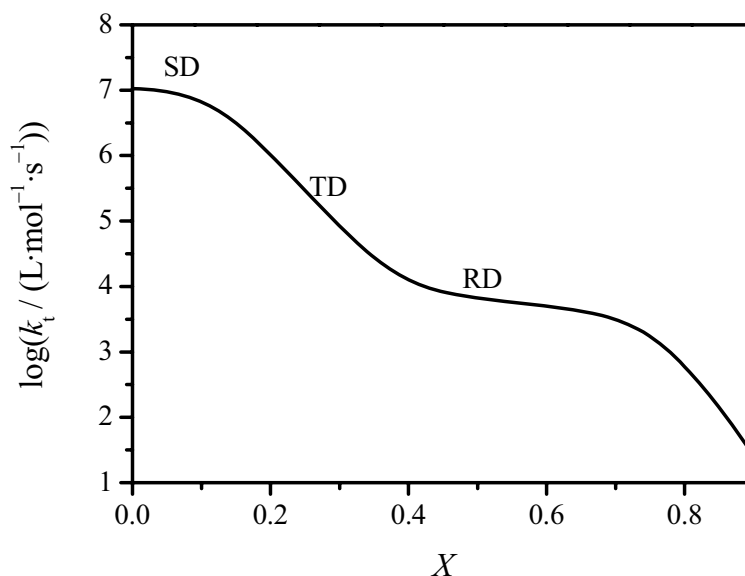


Figure 3-1: Variation of k_t with monomer-to-polymer conversion according to Eq. (3-28). Parameters are taken from ref.^[23]

It should be noted that the onset of the gel-effect and the magnitude of the decrease in k_t is strongly dependent on solvent concentration^[75,96] and the MWD of the formed background polymer.

Acrylate monomers are typically not featured by strong variations of k_t with conversion.^[16,97,98] For methyl acrylate (MA) and dodecyl acrylate (DA), SD control of the low conversion k_t was assumed. However, it was proposed that RD is dominant in the entire conversion range for polymerization of butyl acrylate (BA).^[23] This assumption was based on experimental data showing a decrease of k_t from low conversions on. In contrast, recent SP-PLP-NIR data for BA showed a constant termination rate coefficient at low conversions followed by a decrease in k_t setting in at $X \approx 30\%$.^[97] Consequently, this data implies SD control in the initial plateau range (followed by TD control) also of BA polymerization. Additional evidence for termination control by SD is provided by results from studies into the chain-length dependence of termination. This topic will be discussed in Chapters 13 and 14. The reason why different types of k_t vs. X dependencies were measured for BA polymerization is not yet clear. However, the more recent data, implying SD control, may be considered more reliable as care was taken to reduce effects arising from chain-length dependent termination (see Chapter 3.4.2) and MCR formation (see Chapter 10.4).^[97]

3.4 Chain-length dependence of rate coefficients in FRP

Macroradicals of widely different chain lengths are subject to propagation and termination reactions during conventional polymerization. Thus, the rate coefficients discussed so far are chain-length-averaged parameters and should correctly be denoted as $\langle k_p \rangle$ and $\langle k_t \rangle$, respectively. The magnitude of potential chain-length dependencies of k_p and k_t is supposed to be different, as the rates of the two reactions are controlled by different mechanisms, i.e. chemical and diffusion control.

3.4.1 Chain-length dependence of propagation

The propagation reaction can be assumed to be chemically controlled up to high conversions (see Chapter 3.3.1). Thus, the absolute value of k_p is determined by the geometries, vibrational frequencies, and energies of reactants and transition state (TS). Propagation rate coefficients may be accessed by applying transition state theory, e.g., in conjunction with *ab initio* quantum-chemical calculations.^[17–21] Such predictions indicate significantly higher k_p values for short radicals compared to long-chain ones^[17] as is supported by experimental evidence^[99–101]. Besides genuine kinetic effects, displacement of monomer by polymer in vicinity of the radical chain end reducing the local monomer concentration and hence the apparent k_p was discussed.^[102] It is not yet clear to which extent k_p may vary with chain length, whether strong effects are only seen for short chains ($i < 10$),^[103,104] and which functional form is most appropriate for describing the dependence of k_p on chain length^[102,105–107]. Recent simulations, however, indicate that even in case that the chain-length dependence of k_p does not exceed $i \sim 10$, strong macroscopic kinetic effects may be seen for systems with degrees of polymerization up to 100.^[106–110]

3.4.2 Chain-length dependence of termination

It is generally accepted that the diffusion-controlled termination rate coefficient k_t depends on chain lengths i and j of the terminating radicals resulting in individual $k_t(i,j)$ values for each combination of i and j . According to Eq. (3-20) the centre-of-mass diffusion coefficient is

inversely proportional to the hydrodynamic radius of the macroradical. Thus, the velocity of Fickian diffusion decreases toward increasing degree of polymerization of the terminating radicals. Also the propability that the reactive sites collide during coil overlap decreases toward higher i due to shielding effects.^[26]

For termination events between two radicals of different size, there are three commonly used models: the harmonic mean (hm), the diffusion mean (dm) and the geometric mean (gm) model, each representing a different weighting of the impact of the larger or the smaller radical on the rate coefficient.^[111–113]

$$k_t(i, j) = k_t(1, 1) \cdot \left(\frac{2 \cdot i \cdot j}{i + j} \right)^{-\alpha} \quad (\text{hm}) \quad (3-29)$$

$$k_t(i, j) = \frac{1}{2} \cdot k_t(1, 1) \cdot (i^{-\alpha} + j^{-\alpha}) \quad (\text{dm}) \quad (3-30)$$

$$k_t(i, j) = k_t(1, 1) \cdot (\sqrt{i \cdot j})^{-\alpha} \quad (\text{gm}) \quad (3-31)$$

$k_t(1, 1)$ denotes the rate coefficient for termination of two radicals with chain length unity and α is the power law exponent describing the chain-length dependence of k_t .

In single pulse initiated polymerization, unless chain transfer comes into play, the growth of radicals in the dark time after the laser pulse is close to monodisperse. Thus, termination occurs between radicals of the same degree of polymerization which linearly increases with time after the laser pulse according to Eq. (3-8). In such simplified case, Eqs. (3-29) to (3-31) reduce to:^[25]

$$k_t(i, i) = k_t(1, 1) \cdot i^{-\alpha} \quad (3-32)$$

The drawback of the above equations is that the power law does not account for changes in termination mechanism during chain growth which thus may induce a variation in the exponent α . Reviews on the wide range of existing models can be found in refs.^[27,114]

The so-called composite model introduced by Smith et al.^[27] suggests that $k_t(i, i)$ decreases strongly at short chain lengths and in a less pronounced fashion at longer chain lengths, that is, k_t may be described by two different exponents α_s and α_l for the short and long chain-

length regime, respectively. The transition between these regimes occurs at the so-called crossover chain length, i_c . The dependence of $k_t(i,i)$ on chain length may be expressed by:

$$k_t(i,i) = k_t(1,1) \cdot i^{-\alpha_s} \quad i \leq i_c \quad (3-33)$$

$$k_t(i,i) = k_t(1,1) \cdot i_c^{-\alpha_s + \alpha_1} \cdot i^{-\alpha_1} = k_t^0 \cdot i^{-\alpha_1} \quad i > i_c \quad (3-34)$$

k_t^0 is the rate coefficient for termination of two (hypothetical) coiled radicals of chain length unity whereas $k_t(1,1)$ represents the actual termination coefficient of two (non-coiled) monomeric macroradicals as stated above.

In the short-chain regime, the center-of-mass diffusion velocity of the macroradicals is relatively fast compared to the segmental mobility of the chains. Thus, termination only occurs when the radical sites directly hit each other during collision of the entire macroradicals as the contact time is not sufficiently long to allow for re-orientation of the reactive centers. In this short contact (SC) regime, $k_t(i,i)$ may consequently be described in terms of the Smoluchowski equation (Eq. (3-19)) with a chain-length independent capture radius. Within the composite model, $\alpha_s = 0.5$ has been proposed for dilute solution (low degrees of monomer conversion).^[27] This value is based on measurements of center-of-mass diffusion coefficients of small molecules of various sizes^[115] and on theoretical predictions on the increase of hydrodynamic radius toward higher degrees of polymerization (see Eq. (3-20))^[116-118]. It should, however, be stressed that a value of 0.5 is predicted for flexible chains and $i \rightarrow \infty$, where the macroradical radius is proportional to $i^{0.5}$, i.e. gaussian coils are formed and not rod-like structures. According to the studies of Kirkwood et al.^[116] α_s may be predicted to approach unity for $i \rightarrow 0$, because random coils cannot form in the oligomeric chain-length regime. Moreover, when excluded volume effects are considered, the hydrodynamic radius should be proportional to about $i^{0.6}$ even for long and flexible but self-avoiding chains as derived by Flory.^[119] According to Eq. (3-19), changes in R_C with chain length may additionally contribute to the magnitude of α_s . There is independent experimental evidence that the capture radius slightly decreases toward increasing chain length due to shielding of the radical functionality by polymer segments.^[120] Such decrease in R_C would result in an increase of α_s . Although α_s values close to 0.5 – 0.6 were determined experimentally^[32-34,39,106,121-123] the parameter is yet under debate and may be different for

different monomers. For BA^[37,38] and dodecyl acrylate^[39,124] surprisingly high values, even exceeding unity, were found for α_s .

As detailed above, the center-of-mass diffusion coefficients of macroradicals decrease toward increasing degree of polymerization. Thus, the contact time during collision increases with i as the macroradicals not only approach each other more slowly but also need more time to separate. The contact time may additionally be increased in case the macroradicals entangle. The segmental mobility of the radical chains, however, can be assumed almost independent of i . Consequently, the radical chain-ends may screen their surrounding during such a long contact (LC) which may be expressed in terms of an increase in R_C . Thus, the increase of hydrodynamic radius with chain length is exactly compensated by a growing capture radius and a transition from a normal (center-of-mass) diffusion control in the SC range to so-called mean-field kinetics^[26] in the LC regime occurs at chain length i_c . It needs to be stressed that although contact time strongly increases with i , not every collision of macroradicals is reactive in the LC regime. In fact, a chain-length dependence of k_t for long chains is induced by the shielding of the radical sites by polymer segments which decreases termination probability during coil overlap. An α_l value of 0.16 was theoretically predicted by Khokhlov,^[125] Olaj,^[126] and O'Shaughnessy^[26,127] for chain end-end reaction based on the dynamics of macromolecular coils. In case one or both reactive centers are located in the middle of the chain, power law exponents of 0.27 and 0.43, respectively, are predicted.^[26] This induces additional complexity into the description of the chain-length dependences of k_t^{st} and k_t^{tt} , as the relative position of the radical functionality of an MCR formed by backbiting changes with degree of polymerization. Thus, a gradual decrease of α_l toward increasing MCR chain length (between 0.27 and 0.16 for k_t^{st} and 0.43 and 0.16 for k_t^{tt}) is to be expected and has very recently been verified by Fröhlich et al.^[128,129] The theoretical α_l value of 0.16 has been confirmed in several experiments^[32-34,37-40,121-138] and can be regarded as a good approximation for the long-chain regime of macromolecular coils in which the radical center is located on the terminal chain unit.

The center-of-mass diffusion control of k_t in the SC regime, which is rapidly passed during chain growth, usually not significantly manifests itself in conventional low-conversion FRP. Termination in the the LC regime, however, results in a macroscopical SD control of $\langle k_t \rangle$ (see Figure 3-1).

The discussion above is only valid for low polymer concentrations and good solvents. It is important to emphasize that the center-of-mass diffusion control of $k_t(i,i)$ in the low

conversion SC regime and the TD control of $\langle k_t \rangle$, which may occur at intermediate monomer-to-polymer conversions (see Figure 3-1), are different processes although the notations are sometimes used synonymous. In fact, significantly higher α values (up to 2) may be obtained at high polymer concentrations where all chains are overlapping and $\langle k_t \rangle$ is controlled by TD.^[122,123,137-141] Provided that RD controls k_t , the variation of $k_t(i,i)$ should reflect the chain-length dependence of k_p and C_{RD} under reaction conditions.

The variation of $k_t(i,i)$ with chain length under the assumption of $k_t(1,1) = 10^9 \text{ L}\cdot\text{mol}^{-1}\cdot\text{s}^{-1}$, $\alpha_s = 0.5$, $\alpha_l = 0.16$, and $i_c = 50$ is depicted in Figure 3-2. Indicated are the cross-over chain length, i_c , and k_t^0 which results from back extrapolation of the long-chain regime to the ordinate intercept. This value, which may significantly differ from $k_t(1,1)$, is determined in case the short-chain regime ($i < i_c$) cannot be measured within the experimental technique due to insufficient time resolution.

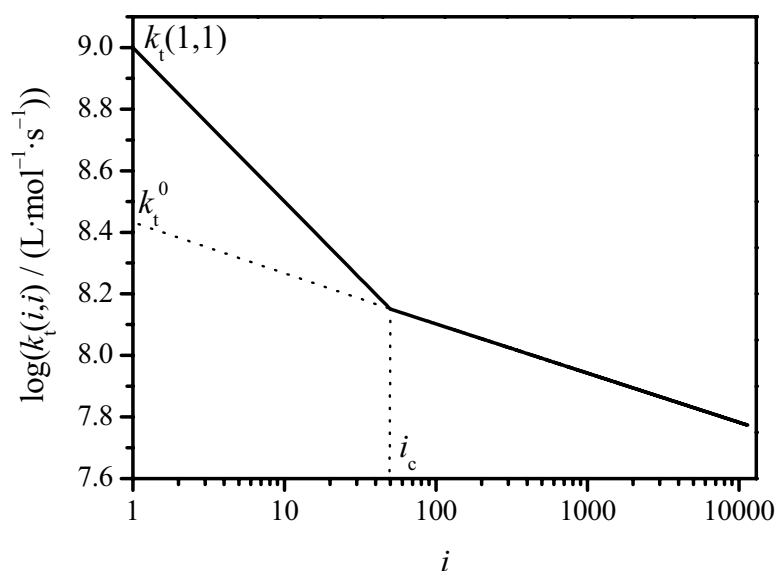


Figure 3-2: Change in k_t as a function of radical chain length as predicted by the *composite model*.

3.4.3 Rate laws for chain-length-dependent k_t

To deduce chain-length-dependent termination rate coefficients from monomer or radical concentration traces recorded after laser pulse initiation, the data have to be transformed from the time domain into the chain-length domain. The kinetic chain length may be estimated

from Eq. (3-8) for any time after laser pulse initiation under the assumption of chain-length independent propagation and the absence of chain transfer. Thus, the average time span required for one propagation step is $(k_p \cdot c_M)^{-1}$ which is also denoted as propagation time, t_p . Applying Eq. (3-8) yields the physically unrealistic result of i being below unity for very short times after laser pulse initiation. This situation can be overcome by adding unity on the right-hand-side of Eq. (3-8).

$$i = \frac{t}{t_p} + 1 \quad (3-35)$$

After the time t_p , a radical of chain length $i = 2$ is formed by monomer addition. Thus, Eq. (3-8) yields the number of propagation steps during a time period t whereas Eq. (3-35) gives the actual chain length. Unfortunately, the implementation of Eq. (3-35) significantly complicates integration of Eqs. (3-4) and (3-5). However, the difference between Eqs. (3-8) and (3-35) is only significant at small chain lengths and short times, respectively, but becomes negligible toward higher i .

In principle, the chain-length dependence of k_t may be determined in a model independent way, that is without assuming a particular k_t vs. i correlation. The rate laws for the change in radical or monomer concentration with time after the laser pulse read:^[97,142]

$$k_t(t) = \frac{-1}{2 \cdot c_R(t)^2} \cdot \frac{dc_R(t)}{dt} \quad (3-36)$$

$$k_t(t) = \frac{k_p}{2} \cdot \left[\frac{c_M(t) \cdot \frac{d^2 c_M(t)}{dt^2}}{\left(\frac{dc_M(t)}{dt} \right)^2} - 1 \right] \quad (3-37)$$

For evaluation of $k_t(i, t)$, the first derivative of $c_R(t)$ or the first and second derivatives of $c_M(t)$ are required. Thus, success or failure of the model independent methods is determined by signal quality. It was demonstrated that the signal-to-noise ratio of $c_M(t)$ traces from SP-PLP-NIR is too low for reasonable application of Eq. (3-37).^[97,142] Junkers showed that sufficiently accurate $c_R(t)$ data for implementation into Eq. (3-36) may be obtained via SP-PLP-ESR.^[33,97] However, even in this case the radical concentration traces had to be fitted by arbitrary functions to obtain a noise-free signal. Thus, also those results cannot be considered totally

model independent as the results for $k_t(i,i)$ dependent to some extent on the choice of the fit function.

As detailed earlier, Eq. (3-6) may be used to evaluate $\langle k_t \rangle$ from SP-PLP-ESR traces, usually in its linearized form:

$$\frac{c_R^0}{c_R(t)} = 1 + 2 \cdot \langle k_t \rangle \cdot c_R^0 \cdot t \quad (3-38)$$

For termination of two macroradicals of identical size, $k_t(i,i)$ may be expressed according to the power-law expression given in Eq. (3-32) with α_s and $k_t(1,1)$ or α_l and k_t^0 , respectively. As i is related to time via Eq. (3-8), Eq. (3-32) has to be inserted into the differential form of the rate law to derive a function for the decay in radical concentration in case of chain-length dependent k_t . Combination of Eqs. (3-5), (3-8), and (3-32) with subsequent integration yields:

$$\frac{c_R(t)}{c_R^0} = \left(\frac{2 \cdot k_t(1,1) \cdot c_R^0 \cdot t_p^{\alpha_s}}{1 - \alpha_s} \cdot t^{1-\alpha_s} + 1 \right)^{-1} \quad t \leq t_c \quad (3-39)$$

$$\frac{c_R(t)}{c_R^0} = \left(\frac{2 \cdot k_t^0 \cdot c_R^0 \cdot t_p^{\alpha_l}}{1 - \alpha_l} \cdot t^{1-\alpha_l} + 1 \right)^{-1} \quad t > t_c \quad (3-40)$$

Logarithmic versions of Eqs. (3-39) and (3-40) may be applied to the data for evaluating the transition between α_s and α_l .

$$\log \left(\frac{c_R^0}{c_R(t)} - 1 \right) = \log \left(\frac{2 \cdot k_t(1,1) \cdot c_R^0 \cdot t_p^{\alpha_s}}{1 - \alpha_s} \right) + (1 - \alpha_s) \cdot \log t \quad t \leq t_c \quad (3-41)$$

$$\log \left(\frac{c_R^0}{c_R(t)} - 1 \right) = \log \left(\frac{2 \cdot k_t^0 \cdot c_R^0 \cdot t_p^{\alpha_l}}{1 - \alpha_l} \right) + (1 - \alpha_l) \cdot \log t \quad t > t_c \quad (3-42)$$

A plot of the left hand sides of Eqs. (3-41) and (3-42) against $\log t$ yields, assuming ideal composite-model behavior, two linear sections with the slopes $(1-\alpha_s)$ and $(1-\alpha_l)$ intersecting at t_c at which time the macroradicals are of chain length i_c . From the corresponding y-axis intercepts, $k_t(1,1)$ and k_t^0 are obtained.

As detailed above, description of chain length by Eq. (3-8) is not absolutely accurate. Smith and Russell^[143] derived the following expressions for $c_R(t)$ in the short-chain and long-chain regime:

$$\frac{c_R^0}{c_R(t)} - 1 = \frac{2 \cdot k_t(1,1) \cdot c_R^0 \cdot \left((k_p \cdot c_M \cdot t + 1)^{1-\alpha_s} - 1 \right)}{k_p \cdot c_M \cdot (1-\alpha_s)} \quad t \leq t_c \quad (3-43)$$

$$\begin{aligned} \frac{c_R^0}{c_R(t)} - 1 = & \frac{2 \cdot k_t(1,1) \cdot c_R^0 \cdot \left((i_c)^{1-\alpha_s} - 1 \right)}{k_p \cdot c_M \cdot (1-\alpha_s)} - \frac{2 \cdot k_t(1,1) \cdot c_R^0 \cdot (i_c)^{1-\alpha_s}}{k_p \cdot c_M \cdot (1-\alpha_1)} \\ & + \frac{2 \cdot k_t^0 \cdot c_R^0 \cdot \left(k_p \cdot c_M \cdot t + 1 \right)^{1-\alpha_1}}{k_p \cdot c_M \cdot (1-\alpha_1)} \quad t > t_c \quad (3-44) \end{aligned}$$

Eqs. (3-43) and (3-44) require non-linear fitting of the radical concentration traces. The more accurate evaluation of the short-chain regime via Eq. (3-43) yields significantly higher α_s values than the linear regression of the same data set according to Eq. (3-41). However, fitting Eq. (3-44) to the long-chain data is not very sensitive and sometimes even results in negative α_1 values. In such cases application of Eq. (3-42) is recommended.^[34]

In SP-PLP-NIR experiments the change in monomer concentration with time is traced from which $\langle k_t \rangle$ may be evaluated according to Eq. (3-7). The implementation of the power-law dependency (Eq. (3-32)) for $k_t(i,i)$ is more complicated for the monomer concentration data due to the required double integration of the differential rate equation. An integral expression of the fit function is given by:^[135]

$$\frac{c_M(t)}{c_M(t=0)} = 1 - c_R^0 \cdot k_p \cdot \int_0^t \left(2 \cdot c_R^0 \cdot k_t^0 \cdot \int_0^{t'} \left(\frac{t_p}{t''} \right)^{\alpha_1} dt'' + 1 \right)^{-1} dt' \quad (3-45)$$

Eq. (3-45) yields k_t^0 , c_R^0 and α_1 for the entire chain-length regime under investigation. In principle, the more complex composite model may also be implemented in a general form of Eq. (3-45). However, the fitting is not very sensitive toward changes in α at short times after laser pulse initiation.^[135,144]

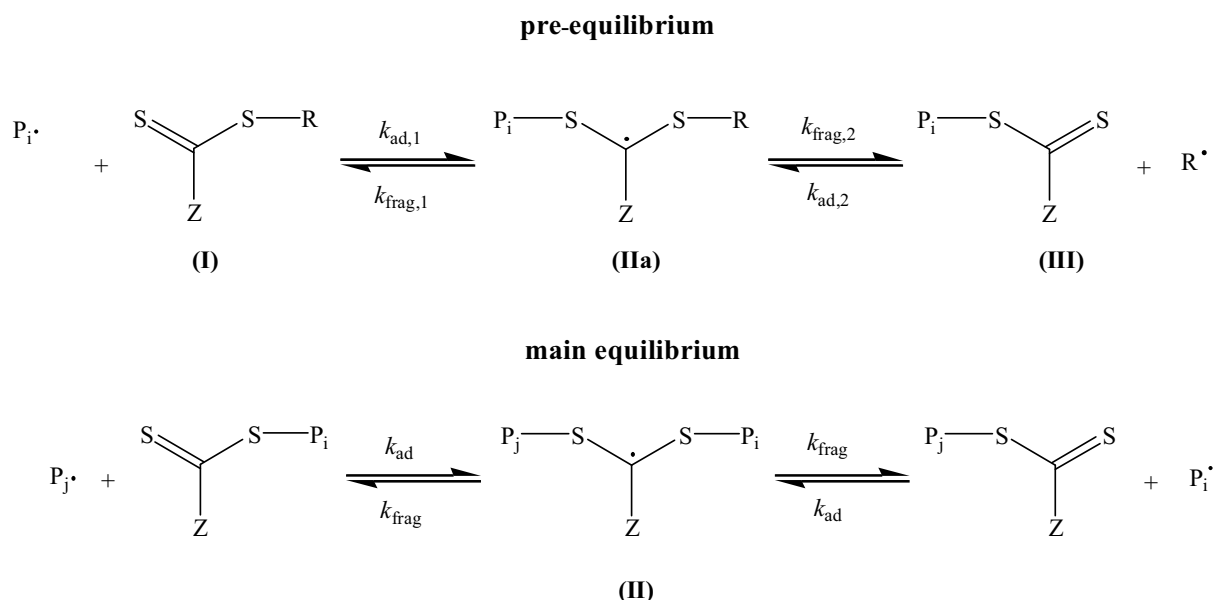
3.5 RAFT-polymerization

The enormous progress in controlled (living) radical polymerization, especially since the middle of the 1990s, has revolutionized polymer synthesis as such techniques allow for the

production of narrowly distributed polymers of defined chain length and macromolecular architecture without losing the robustness and flexibility of conventional FRP.

Most controlled radical polymerization methods (e.g. atom transfer radical polymerization, ATRP^[145,146] and nitroxide-mediated polymerization, NMP^[147]) are based on the persistent radical effect,^[148] i.e. the generation of a dormant species which significantly reduces the concentration of (free-radical) growing chains and thus suppresses the termination reaction. Monomer addition only takes place in the short time spans between the activation and deactivation steps. However, the reversible addition fragmentation chain transfer (RAFT) process^[35,36] relies on degenerative chain-transfer equilibria.

In a typical RAFT process, thiocarbonyl-thio-compounds, so-called RAFT agents, reversibly react with the growing macroradicals. The RAFT mechanism, as depicted in Scheme 3-3, consists of a pre- and a main equilibrium. In the pre-equilibrium, the initial RAFT agent (I) is transformed into a macroRAFT agent (III) via an intermediate radical species (IIa), where P_i is a free radical and R is the so-called leaving group of the RAFT agent. The leaving group R can reinitiate polymerization and is thus converted into a growing chain. After consumption of all initial RAFT agent (I), the molecular weight of all radicals present (and thus the polymer content) is effectively controlled via the main equilibrium by equally distributing the propagation probability over all growing chains.



Scheme 3-3: Pre- and main equilibrium of the reversible addition fragmentation chain transfer (RAFT) process.

The reversible addition fragmentation equilibrium is superimposed on a conventional free-radical polymerization process, which retains all its characteristic kinetic parameters. Ideally, the chain-transfer process should be fast and the intermediate RAFT-adduct radical (II) should be short-lived. Because of the rapid transfer of the growing macroradicals between their free and dormant forms, living characteristics (i.e. a linear increase of molecular weight with monomer-to-polymer conversion) are imparted on the polymerizing system. The pre- and main equilibrium is governed by the addition and fragmentation rate coefficients, $k_{ad,1}$, $k_{frag,1}$, $k_{ad,2}$, $k_{frag,2}$, and k_{ad} , k_{frag} respectively.^[149]

The main equilibrium is usually described by an equilibrium constant K_{eq} , which is a measure for the stability of the intermediate radical:

$$K_{eq} = \frac{k_{ad}}{k_{frag}} \quad (3-46)$$

Rate retardation

In an ideal RAFT process, addition and fragmentation are fast reactions compared to the chain growth and the equilibrium constant should be low. In such cases, the concentration of propagating radicals in the controlled process and in conventional FRP should be close to identical. Thus, no significant differences in polymerization kinetics are to be expected. However, extended induction periods and pronounced rate retardation compared to the conventional FRP are frequently seen, especially when dithiobenzoate-type RAFT agents are used. This observation may be explained by two mechanisms: (i) The rate of fragmentation may be significantly lower than the rate of the addition reaction thus yielding a larger K_{eq} . In case K_{eq} is extremely large, radicals are stored in the intermediate radical species to a significant amount thus reducing the average concentration of free radicals until a steady state has been reached. By that, the overall polymerization rate would be reduced.^[150–152] (ii) Irreversible termination as an additional reaction pathway of the intermediate radical species (II) or (IIa), respectively, leads to deceleration of the polymerization rate as well.^[153–155] Potentially, the intermediate radical can cross-terminate with a propagating radical or self-terminate with a radical of its own species. It should be noted that in case the stabilizing group is an aromatic function where the radical functionality is delocalized, the termination product can also be formed by coupling with the Z-group.^[156]

Both mechanisms may account for the experimentally observed rate retardation, however the proposed high K_{eq} values are in conflict with ESR measurements^[97,154,157,158] and no products of irreversible termination were found in the product of dithiobenzoate mediated polymerization^[159]. This dilemma was recently overcome by identifying a highly efficient “missing step” reaction in which termination products of intermediate radicals are decomposed by reaction with propagating radicals.^[160,161]

Hybrid behavior

If propagation is relatively fast compared to the addition rate of propagating free radicals to the RAFT agent, the RAFT equilibrium is not capable of controlling the molecular weight from chain length unity on. In this case, the radicals undergo a limited number of propagation steps before addition to a RAFT species and thus the linear increase of the molecular weight with monomer conversion starts from a certain degree of polymerization on. This situation is denoted as hybrid behavior.^[162]

3.6 Size-exclusion chromatography

The standard method for determination of polymer MWDs is size-exclusion chromatography (SEC). In SEC, a solution of macromolecules is pressed through columns with highly porous material at constant flow rates. The separation is based on the diffusion of polymer coils between the mobile phase and the pores of the stationary phase. Low molecular weight material, forming coils with small hydrodynamic radius, will spend more time in the pores than polymer of higher molecular weight, therefore eluting more slowly through the column. After separation, the relative concentration of the eluted chains can be detected by measuring changes in, e.g., UV-absorption and refractive index (RI). The retention times are strongly depending on the experimental conditions (polymer type, column packing, eluent). Thus, for concentration-sensitive detectors a calibration curve is required which correlates elution volume with molecular weight. The calibration curve can be constructed using polymeric standard samples of known narrowly distributed molecular weight. However, calibration standards are available only for a limited number of polymers. Without such standards, molecular weight distributions may be estimated via the principle of universal calibration.^[163]

For a given column assembly, a linear correlation between hydrodynamic volume, HV , and molecular weight, M , is assumed to hold:^[164]

$$HV = \frac{[\eta] \cdot M}{2.5 \cdot N_A} \quad (3-47)$$

where $[\eta]$ is the intrinsic viscosity and N_A Avogadro's number. The most frequently used correlation between intrinsic viscosity and molecular weight is given by the Mark-Houwink relation^[165,166] which assumes linearity between $\log([\eta])$ and $\log(M)$ according to:

$$[\eta] = K \cdot M^a \quad (3-48)$$

with K and a being the so-called Mark-Houwink (MH) parameters. For most polymers, the Mark-Houwink parameters are known and may be used for universal calibration.^[163] Combination of Eqs. (3-47) and (3-48) leads to the desired relation:

$$\log M_2 = \frac{1}{1+a_2} \log \frac{K_1}{K_2} + \frac{1+a_1}{1+a_2} \log M_1 \quad (3-49)$$

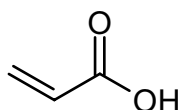
with the index 1 indicating the polymer used for calibration and the index 2 for the polymer of interest. Thus, the calibration curve of $\log(M_1)$ vs. elution volume can be recalculated for polymer 2. In case MH parameters are not available for a certain polymer, alternative methods employing mass sensitive detectors such as on-line viscometry^[167] or light-scattering techniques^[168] may be used to directly determine the molecular weight at a certain elution volume. An SEC setup consisting of both mass sensitive detectors and a concentration detector is often referred to as a triple detector setup by which the need for polymer standards or MH parameters can be overcome.

4 Materials and Instrumentation

4.1 Chemicals

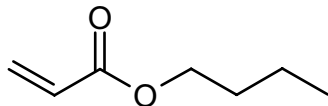
4.1.1 Monomers

acrylic acid



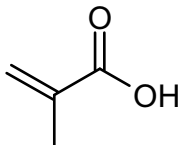
Acrylic acid (AA, $M = 72.06 \text{ g}\cdot\text{mol}^{-1}$, Fluka, purum, > 99 % stabilized by hydroquinone monomethyl ether) was used as received or dehibited by passing the monomer through a column filled with inhibitor remover (Aldrich).

butyl acrylate



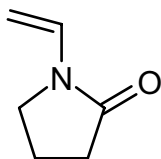
Butyl acrylate (BA, $M = 128.17 \text{ g}\cdot\text{mol}^{-1}$, Fluka, purum, > 99 %, stabilized by hydroquinone monomethyl ether) was dehibited by passing the monomer through a column filled with inhibitor remover (Aldrich).

methacrylic acid



Methacrylic acid (MAA, $M = 100.12 \text{ g}\cdot\text{mol}^{-1}$, Fluka, purum, > 99 %, stabilized by hydroquinone monomethyl ether) was purified by distillation under reduced pressure.

N-vinyl pyrrolidone



N-vinyl pyrrolidone (NVP, $M = 111.16 \text{ g}\cdot\text{mol}^{-1}$, Fluka, purum, > 97 % stabilized with *N,N'*-di-*sec*-butyl-*p*-phenylenediamine) was used as received or purified by distillation under reduced pressure.

4.1.2 Polymers

poly(acrylic acid)

Poly(acrylic acid) sodium salt (poly(NaAA), $M_p = 16\,000 \text{ g}\cdot\text{mol}^{-1}$, $M_w = 18\,100 \text{ g}\cdot\text{mol}^{-1}$, $M_n = 12\,800 \text{ g}\cdot\text{mol}^{-1}$, Polymer Standards Service, Mainz) was dialyzed against an aqueous solution of hydrochloric acid ($\text{pH} \approx 2$) and subsequently against demineralized water to transform poly(NaAA) into poly(AA).

poly(methacrylic acid)

Poly(methacrylic acid) (poly(MAA), $M_p = 170\,000 \text{ g}\cdot\text{mol}^{-1}$, $M_w = 370\,000 \text{ g}\cdot\text{mol}^{-1}$, $M_n = 55\,000 \text{ g}\cdot\text{mol}^{-1}$, Polysciences, Inc, lot# 547 827, 5 % water) was used as received.

poly(N-vinyl pyrrolidone)

Poly(*N*-vinyl pyrrolidone) (poly(NVP), $M_w = 360\,000 \text{ g}\cdot\text{mol}^{-1}$, $M_n = 24\,000 \text{ g}\cdot\text{mol}^{-1}$, Aldrich) was used as received.

4.1.3 Saturated monomer analoga

The saturated monomer analoga have the same chemical structure as the corresponding monomers, however without the olefinic double bond.

propionic acid

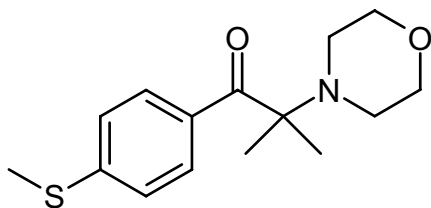
Propionic acid (PA, $M = 74.08 \text{ g}\cdot\text{mol}^{-1}$, Fluka, p.a., > 99.5 %) was used as received.

iso-butyric acid

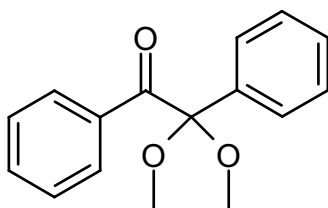
Iso-butyric acid (IBA, $M = 88.11 \text{ g}\cdot\text{mol}^{-1}$, Fluka, p.a., > 99.5 %) was used as received.

N-ethyl pyrrolidone

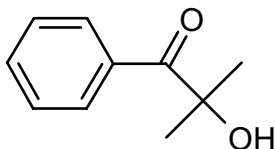
N-ethyl pyrrolidone (NEP, $M = 113.16 \text{ g}\cdot\text{mol}^{-1}$, Aldrich, p.a., > 99.5 %) was used as received.

4.1.4 Initiators***2-methyl-4'-(methylthio)-2-morpholinopropiophenone***

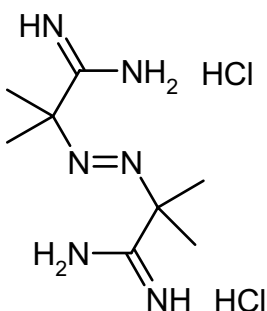
The photoinitiator 2-methyl-4-(methylthio)-2-morpholino-propiophenone (MMMP, $M = 279.40 \text{ g}\cdot\text{mol}^{-1}$, Aldrich, > 98 %) was used without further purification.

2,2-dimethoxy-2-phenyl acetophenone

The photoinitiator 2,2-dimethoxy-2-phenyl acetophenone (DMPA, $M = 256.30 \text{ g}\cdot\text{mol}^{-1}$, Aldrich, > 99 %) was used without further purification.

2-hydroxy-2-methylpropiophenone

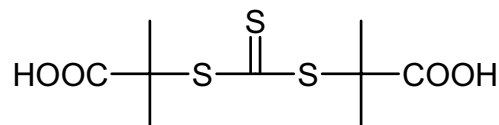
The photoinitiator 2-hydroxy-2-methylpropiophenone (Darocur, $M = 164.2 \text{ g}\cdot\text{mol}^{-1}$, Aldrich, > 97 %) was used without further purification.

2,2'-azobis (2-methylpropionamidine) dihydrochloride

The thermally decomposing initiator 2,2'-azobis (2-methylpropionamidine) dihydrochloride (V50, $M = 271.19 \text{ g}\cdot\text{mol}^{-1}$, Fluka, purum, > 98 %) was used as received.

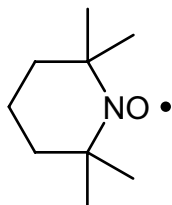
4.1.5 Solvents

Demineralized *water* (taken from internal cycle), *deuterium oxide* (Deutero GmbH, 99.9 %), *toluene* (Fluka, puriss, > 99.7 %), and *tetrahydrofurane* (THF, Roth, p.a., > 99.5 %) were used without further purification.

4.1.6 Miscellaneous***S,S*-bis(α,α' -dimethyl- α'' -acetic acid)-trithiocarbonate**

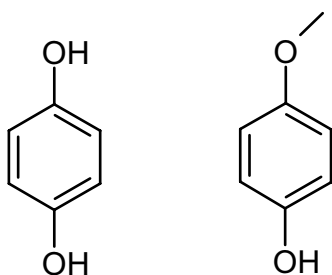
The RAFT agent *S,S*-bis(α,α' -dimethyl- α'' -acetic acid)-trithiocarbonate (TRITT, $M = 282.40 \text{ g}\cdot\text{mol}^{-1}$) was synthesized in accordance to the procedure described in ref.^[169]

2,2,6,6-tetramethyl-1-piperidinyloxy



The stable radical for ESR calibration 2,2,6,6-tetramethyl-1-piperidinyloxy (TEMPO, $M = 156.26 \text{ g}\cdot\text{mol}^{-1}$, Aldrich, > 99 %) was used without further purification.

hydroquinone and hydroquinone monomethyl ether



The inhibitors hydroquinone (HQ, Fluka, > 99 %) and hydroquinone monomethyl ether (MEHQ, Fluka, > 98 %) were used as received.

sodium hydroxide

Sodium hydroxide (Scharlau, p.a., > 99 %) was used as received.

sodium chloride

Sodium chloride (Merck, p.a., > 99.5 %) was used as received.

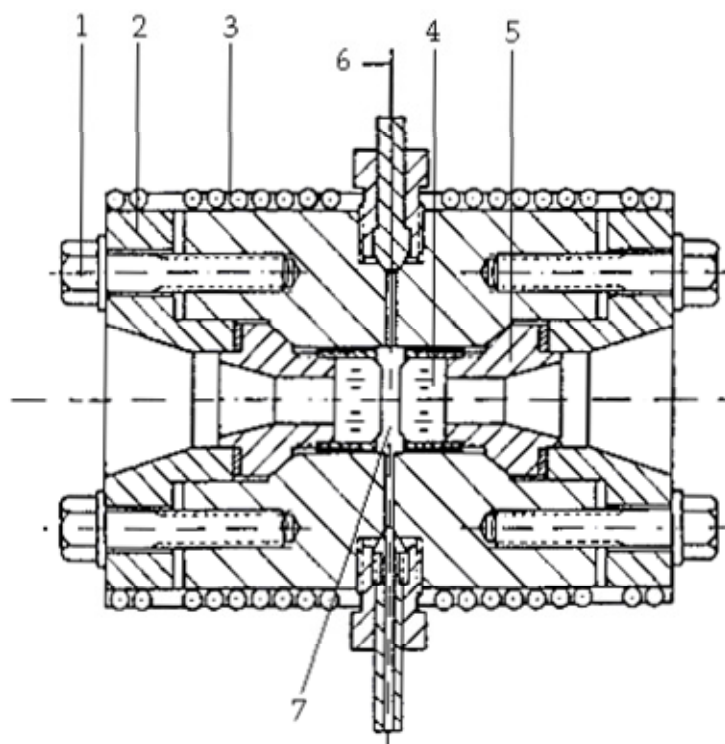
dialyzing tube

The dialyzing tube Spectra/Por® MWCO 2 000 (internal diameter 11.5 mm, Spectrum Laboratories, Inc.) was used for removing small ions from polymer solutions. The membrane was stored at 4 °C in an aqueous solution of 0.1 % sodium azide.

4.2 High-pressure equipment

4.2.1 Optical high-pressure cell

The optical high-pressure cell used for spectroscopic investigations of pulsed-laser induced homo- and copolymerizations under high-pressure conditions is illustrated in Scheme 4-1. The cell is designed for pressures up to 3500 bar and temperatures up to 350 °C. The cylindrical cell body and the sealing flanges are made of a nickel-based alloy of high ultimate tensile strength (RGT 601, material No. 2.4668, Arbed Saarstahl). The length of the cell body is 100 mm and the outer and inner diameters are 80 and 22 mm, respectively. Four borings perpendicular to the cylindrical axis allow for fitting high-pressure capillaries and a sheathed thermocouple (6) directly into the sample volume. The cell is sealed at each end by a conical ram (5) (material No. 2.4668, Arbed Saarstahl). The ram is pressed into the cell cone by the flange (2) (material No. 2.4668, Arbed Saarstahl) which is fixed by six high-pressure bolts (1) (material No. 2.4969). The optical path length may be varied by using different types of rams. The experiments were performed using an internal cell (see Chapter 4.2.2). The rams were chosen such that a path length of approximately 1-2 mm resulted, providing sufficient space for fitting the internal cell between the two high-pressure windows. Each high-pressure window (4) is fitted against the polished surface of a ram and held in place by a stainless steel sealing cap. To compensate for surface area irregularities, about 12 µm thick Teflon foil is placed between the polished surfaces of the window and the ram. This setup is self-sealing under pressure according to the Poulter principle.^[170] The high-pressure optical windows used in this work were made from synthetic sapphire crystals (diameter: 18 mm, height: 10 mm, UV grade, Roditi, Union Carbide) produced by the Czochralski procedure. This material is used because of its high transparency in the wavenumber range from 2 000 to 50 000 cm⁻¹. The optical transmission at the laser wavelength is not affected by laser irradiation or by changing temperature. The optical high-pressure cell is mounted on a metal holder equipped with a wooden grip for easy handling and fitting into the sample compartment of the FT-IR spectrometer.



- | | |
|--------------------------|------------------------------------|
| (1) bolt | (5) ram |
| (2) flange | (6) sheathed thermocouple |
| (3) heating jacket | (7) adjustable optical path length |
| (4) high pressure window | |

Scheme 4-1: Schematic view of the optical high-pressure cell used in the high-pressure experiments.

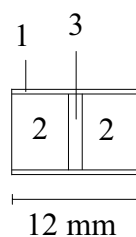
4.2.2 Optical internal cell

The optical internal cell used in the kinetic investigations is depicted in Scheme 4-2. The cell consists of a Teflon tube (1) (outer diameter 10 mm, inner diameter 9 mm, length ~12 mm) which is closed on each side by a quartz window (2) (diameter 10 mm, thickness ~5 mm, Haereus Quarzglas, INFRA-SIL 301). To ensure optimal sealing of the cell, the lateral surfaces of the cylindrical quartz windows were polished using a diamond micrometer suspension (4-8 micron, Mikrodiamant GmbH). Quartz was chosen as the window material because it is transparent in the wavenumber range above 3000 cm^{-1} , thus allowing detection in the desired NIR region. The sample volume (3) is contained between the two windows. The

internal cell is fitted between the sapphire windows of the high-pressure cell and held in place by a Teflon spacer.

To transfer the reaction solution into the internal cell, a quartz window is fitted into one end of the Teflon tube, the mixture is introduced by a pipette before the second quartz window is inserted. Care has to be taken that the cell is well sealed and that no gas bubbles are enclosed.

An excellent survey on the high-pressure techniques described within this section can be found in ref.^[171]



Scheme 4-2: Schematic view of the optical internal cell used for kinetic investigations. (1) Teflon tube; (2) SiO₂ window; (3) sample volume.

4.2.3 Heating and temperature control

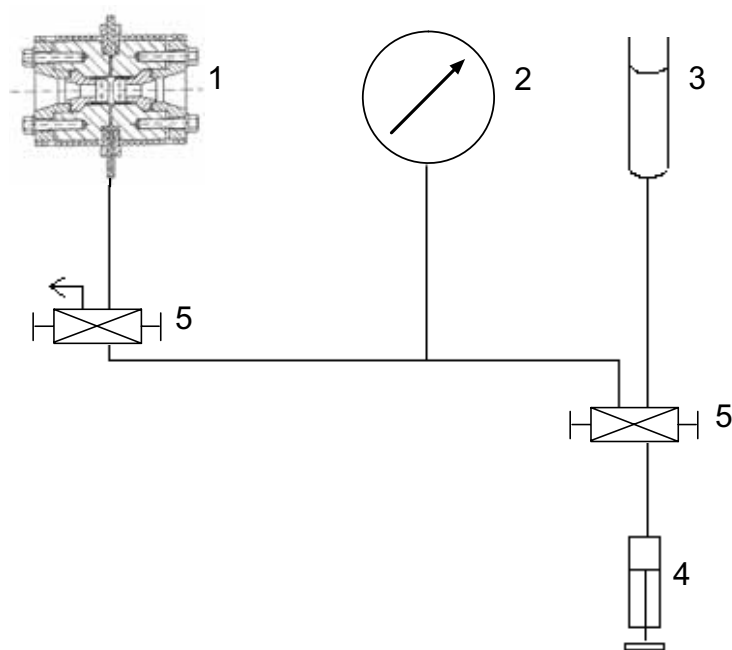
The optical high-pressure cell is brought to temperature by two heating jackets consisting of a brass matrix, into which a sheathed resistance heating wire (CGE-Asthom) is embedded. The closely fitting jackets are mounted on each end of the cell body (see Scheme 4-2 entry (3)). Temperature is measured via a sheathed thermocouple (nickel chromium against nickel, CIA S250, CGE-Alsthom) and regulated by a PID-controller (Eurotherm 815).

For applying temperatures below 25 °C, special brass jackets were used through which cooling liquid provided by a thermostat (Haake 001-4202 or Lauda RCS 6) can be passed.

4.2.4 Pressure generation and control

For the kinetic investigations, *n*-heptane served as the pressure transmitting medium and for providing good heat transfer. The system is pressurized using a manually driven ("syringe"-type) pressure generator (max. volume 12 cm³). Pressure is measured using a high-pressure

precision manometer (Class 0.1, 0-4 kbar, Wiegand). The pressure-generating system is depicted in Scheme 4-3.



- (1) optical high-pressure cell (4) "syringe"-type pressure generator m
(2) manometer (5) valve
(3) pressure medium *n*-heptane

Scheme 4-3: Schematic view of the pressure-generating system.

4.3 FT-IR/NIR spectrometer

Infrared and near infrared spectra were recorded on a Bruker IFS-88 Fourier-Transform spectrometer. To accommodate the heated optical high-pressure cell, the sample chamber of the spectrometer was enlarged (heightened) and fitted into a water-cooled cell holder (to reduce heat transfer to the spectrometer parts). The chamber is permanently purged with compressed water-free air. For the present work the optical configuration consisted of a tungsten-halogen light source, a silicon-coated calcium fluoride beam splitter, and an InSb detector. This configuration allows for optimal recording in the spectral range 4 000 to 10 000 cm^{-1} . Data acquisition and data processing were performed using the software OPUS (Bruker). To allow for quantitative analysis of the spectra, the optical settings were chosen

such that the absorbance did not exceed 0.8 in the wavenumber area of interest, thus ensuring detector linearity.^[172]

4.4 The PLP-SEC setup

4.4.1 Pulsed-laser polymerizations

Pulsed laser polymerizations were performed using an excimer laser with maximum laser pulse repetition rate of 100 Hz (LPX 210i, Lambda Physik) operated on the 351 nm (XeF) line. Incident laser energy was usually around 10 mJ per pulse. The laser beam was widened and focused on the sample by two lenses. The monomer solutions were either charged into QS165 cells (10 mm path length, Hellma-Worldwide) equipped with a jacket for temperature control, QS110 cells (10 mm path length, Hellma-Worldwide), 21/SOG/2 cells (2 mm path length, Starna), or into the internal cell of an optical high-pressure cell.

The *pH* values of the aqueous solutions were measured by a Metrohm 602 *pH*-meter (Switzerland) prior to polymerization. Conductivities were determined by means of a Metrohm Herisau E 527 conductometer.

Details on the experimental procedures used for the different monomer systems are provided in Chapter 5.1.1.

4.4.2 Size-exclusion chromatography

For the thesis in hand, different SEC setups had to be used for measuring the MWDs of the various types of polymer being produced. The THF-soluble polymers poly(BA), poly(MMA) and poly(BMA) were analyzed with setup A in our lab. The MWDs of products from aqueous phase polymerizations were kindly determined by Dr. I. Lacík and co-workers at the Polymer Institute of the Slovak Academy of Science in Bratislava. Poly(AA) and poly(MAA) were analyzed using an aqueous eluent on setup B, whereas poly(NVP) was measured in dimethyl acetamide (DMAc) on setup C.

setup A

The SEC analyses of poly(BA), poly(MMA), and poly(BMA) were performed at 35 °C with THF as the eluent (1 mL·min⁻¹ flow rate) and toluene as flow rate marker on a system composed of a Waters HPLC pump (Model 515), a JASCO AS-2055-plus autosampler, three PSS SDV columns (5 µm particle size; 10⁵, 10³ and 10² Å pore sizes), and a Waters refractive index detector (Model 2410). MWDs of poly(MMA) were determined by direct calibration against narrowly distributed standards ($M_p = 800$ to 2 000 000 g·mol⁻¹, PSS, Mainz). For poly(BA) and poly(BMA), the SEC setup was calibrated with polystyrene (PS) standards of narrow polydispersity ($M_p = 400$ to 2 500 000 g·mol⁻¹, PSS, Mainz). The MWDs are adjusted according to the principle of universal calibration using Mark-Houwink parameters for linear poly(BA) ($K = 1.22 \cdot 10^{-2}$ mL·g⁻¹, $a = 0.700$)^[173] and poly(BMA) ($K = 1.48 \cdot 10^{-2}$ mL·g⁻¹, $a = 0.664$).^[174] Data acquisition and processing were carried out using the WinGPC software (PSS, Mainz).

setup B

The aqueous-phase SEC setup for analyses of poly(AA) and poly(MAA) consisted of a Waters in-line degasser, a Waters pump 515 equipped with a plunger washing kit, a Rheodyne 7725i injector, a guard and three Suprema columns (PSS, Mainz) of particle size 10 µm and pore sizes of 100, 1000 and 3000 Å (positioned in a Waters column heater module), and a differential refractometer (Waters M2410). The measurements were performed at 60 °C using demineralized water as the eluent which contained 0.1 mol·L⁻¹ Na₂HPO₄, to provide a pH value of 9.0, and 200 ppm NaN₃. The poly(AA) and poly(MAA) samples were thus analyzed as the corresponding sodium salts. The eluent was permanently stirred to avoid concentration changes as a consequence of salt sedimentation. Ethylene glycol was used as the flow marker to adjust eluent flow to a rate of 1 mL·min⁻¹. Calibration of the SEC setup was performed with narrowly distributed poly(NaAA) and poly(NaMAA) standards (PSS, Mainz) of peak molecular weights between 1 250 and 1 100 000 and 1 250 to 1 027 000 g·mol⁻¹, respectively. Data acquisition and analysis were performed via the WinGPC[®]7.2 software (PSS, Mainz).

setup C

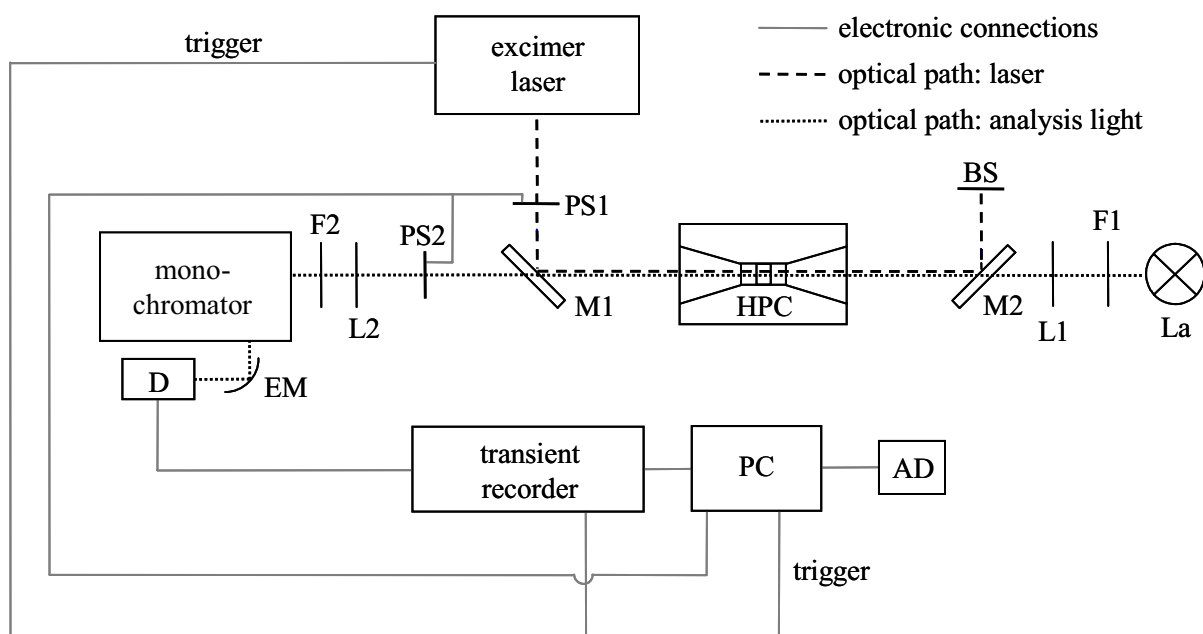
SEC analysis of the poly(NVP) was performed with the eluent dimethyl acetamide (DMAc) containing 0.1 wt.% LiBr pumped through a PSS GRAM 10 µm guard column and three

PSS GRAM 10 μm main columns with pore sizes of 100, 1000 and 3000 \AA at 45 $^{\circ}\text{C}$ (instrumentation otherwise identical to setup B). The flow rate of 0.8 mL/min was controlled by toluene as the flow rate marker. Non-availability of narrow poly(NVP) calibration standards required the use of MALLS–RI (multi-angle laser light scattering–refractive index) detection. A MALLS absolute detector PSS SLD 7000 (PSS, Mainz) in conjunction with the differential refractometer provided absolute molecular weights.^[175] The values of the refractive index increment, dn/dc , were determined on a Brice-Phoenix 2000-V differential refractometer to be 0.093 $\text{ml}\cdot\text{g}^{-1}$ and 0.165 $\text{ml}\cdot\text{g}^{-1}$ for poly(NVP) and PS, respectively. These numbers were estimated,^[176] from the values measured at 436 and 546 nm, for 633 nm which is the wavelength at which the MALLS detector works. A narrow PS calibration standard of $M_p = 67\,500\text{ g}\cdot\text{mol}^{-1}$ (PSS, Mainz) was used as the isorefractive standard. Effective calibration was made using PS standards for the mass range 376 to 2 300 000 $\text{g}\cdot\text{mol}^{-1}$ (PSS, Mainz). The factor which correlates the positions of primary and secondary points of inflection (POI) of the MWDs obtained by absolute (MALLS–RI) detection and by effective (RI detection) calibration was found to be: $M_{i,\text{MALLS-RI}} / M_{i,\text{RI}} = 1.53 \pm 0.10$ in the range of molecular weights of poly(NVP) from 20 000 to 200 000 $\text{g}\cdot\text{mol}^{-1}$. This correction factor was used when the MALLS detector signal was insufficient for precise MWD analysis.

4.5 The SP-PLP-NIR setup

The experimental setup for the SP-PLP-NIR^[31,177] experiments carried out within this work is illustrated in Scheme 4-4. The XeF excimer laser pulses (Lextra 50, Lambda Physik) are reflected by an UV mirror (M1) and passed through the optical axis of the sample cell (HPC). A second UV (M2) mirror redirects the laser light to a beam stop (BS). The UV mirrors are transparent in the infrared region (INFRASIL, ZnSe-coated). A photo-shutter (PS1) (Prontor, magnetic-shutter E/40) can be used to select individual laser pulses. A tungsten-halogen lamp (La) (General electric, 75 W) serves as a source of infrared and near infrared radiation. The lamp is powered by a lead accumulator (12 V, 180 Ah, Varta) to achieve a noise-free signal. A second photo-shutter (PS2), directly in front of the monochromator, is used to block the analysis light for measuring the background detector signal without near infrared radiation. Initiation processes provoked by UV light emitted by the tungsten-halogen lamp are suppressed by a UV cut-off filter (F1) (RG 695). The analysis light is focused by a lens (L1)

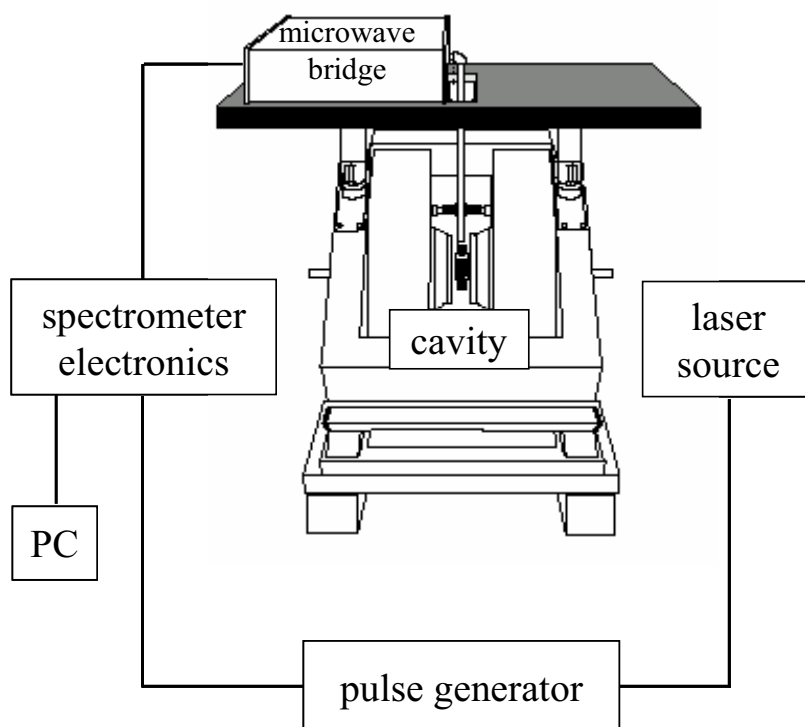
(CaF₂, $f = 100$ mm, $d = 50$ mm) onto the sample contained in the optical high-pressure cell. A second lens (L2) (CaF₂, $f = 100$ mm, $d = 50$ mm) focuses the analysis light onto the lid of a monochromator (B&M Spectronik, BM 50, 0.5 m, $f/6.9$). The light is diffracted by an interference grating (Bausch&Lomb, 76 mm × 76 mm, 600 1/mm, blaze 1.6 mm, $D = 4.1$ nm/mm) and redirected to a fast InAs-NIR-detector (D) (EG&G Judson; cooled by liquid nitrogen) by an ellipsoidal mirror (EM) (Bruker Analytische Meßtechnik GmbH, $f/6$, $f_1 = 200$ mm, $f_2 = 40$ mm). The monochromator is controlled by an Atari computer. A silicon filter (F2) (Oriel, 1 mm, 1.05 μm , transmission in the 5000 to 9000 cm^{-1} range) ensures that only one grating order hits the detector. The detector signal is recorded by a 16-bit transient recorder (TR 1621-4, Fast ComTech) and transferred to a computer (IBM) for further evaluation. For mechanical decoupling from external vibrations, e.g. of the building, the entire setup is placed on a solid granite board, which is supported by rubber tubes. For details to the electronic setup of SP-PLP-NIR are described elsewhere.^[178]



Scheme 4-4: Experimental setup for the single pulse – pulsed laser polymerization – near-infrared (SP-PLP-NIR) technique. The setup is described in detail within the text.

4.6 The PLP-ESR setup

Electron spin resonance spectra were recorded on a Bruker Eleksys E-500 series cw-ESR (continuous wave) spectrometer operating in the X-band (8 to 12 GHz). A field modulation frequency of 100 kHz, modulation amplitudes between 1 and 5 G and microwave powers of 6 to 10 mW were used. Temperature control of the sample is achieved by purging the sample cavity with nitrogen which can be heated to a pre-selected temperature in the range between $-100\text{ }^{\circ}\text{C}$ and $+80\text{ }^{\circ}\text{C}$ by an ER 4131VT (Bruker) unit.



Scheme 4-5: Schematic view of the ESR-spectrometer setup in conjunction with the laser light source for UV irradiation of the samples.

The resonator cavity is equipped with a grid to allow for irradiation of the sample with UV-light at right angle. Recording of the primary data and control of the spectrometer settings was done using the software XEPR (Bruker). The sample was irradiated either with short laser pulses at 351 nm (XeF excimer laser, COMPex 102, Lambda Physik) or with continuous illumination by a 500 W mercury UV-lamp (LAX 1450, Müller Elektronik). The laser source is placed 50 cm and the UV-lamp 20 cm from the cavity, respectively. The laser output energy is typically around 50 mJ per pulse but can be varied from 0 up to 75 mJ per pulse with respect to the particular experiment. The laser source and the spectrometer are

synchronized using a Quantum Composers 9314 pulse generator (Scientific Instruments). The maximum time resolution of data acquisition is 1.28 ms and 500 ns respectively, depending on the type of acquisition board used (ADC signal channel or ADF fast digitizer acquisition board with 12 bit resolution at constant 2 Msamples/s). A schematic view of the cw-ESR spectrometer and the connections to the laser and the spectrometer controlling units is given in Scheme 4-5.

4.7 Simulations

The kinetic model of BA polymerization was implemented into the simulation program PREDICI (**p**olyreaction **d**istributions by **c**ountable system **i**ntegration; CiT), version 6.22p.academic or 6.4.4 (on an Intel Celeron 1.8 GHz or Intel Centrino 1.3 GHz computer), respectively. This program allows for integrating systems of countable differential equations without any assumptions with respect to closure conditions and to calculate full MWDs. Details about the mathematical procedures used in this program are contained in refs.^[179,180] SEC broadening was introduced into the calculated MWD according to the method described in ref.^[181]

ESR spectra were simulated via WINEPR SimFonia Version 1.25 (Bruker Analytische Messtechnik GmbH).

5 Experimental Procedures and Data Evaluation

5.1 The PLP-SEC Technique

The accuracy and reliability of k_p values has considerably improved since the invention of the PLP-SEC technique.^[29] Even though the basic idea is found in earlier references,^[182,183] it was the development and experimental verification by Olaj et al.^[29] that demonstrated the potential of the technique.

In PLP-SEC experiments, a mixture of monomer, photoinitiator and, optionally, a solvent is irradiated at pre-selected temperature and pressure with a sequence of laser pulses being applied at constant laser pulse repetition rate (LPRR) that is with a constant time spacing, t_0 , in between successive pulses. The laser pulse almost instantaneously produces photoinitiator-derived radicals which start chain growth by adding to a monomer molecule. Although termination occurs at any time during the experiment, the large concentration of short radicals produced by each laser pulse induces preferential chain stopping of macroradicals that have started growth by initiation upon applying the preceding pulse(s). In an ideal PLP-SEC experiment, multimodal molecular weight distributions (MWDs) are obtained with the individual maxima resulting from preferential termination of macroradicals after integer multiples of t_0 . The kinetic chain length, i_0 , reached during a growth time t_0 , is usually best identified with the point of inflection on the low-molecular-weight side of the first PLP-induced peak.^[29] For macroradicals which do not experience chain transfer or other side reactions in the dark time period and which are terminated by the successive laser pulse, i_0 is given by

$$i_0 = k_p \cdot c_M \cdot t_0 \quad (5-1)$$

which is directly obtained from Eq. (3-8). The occurrence of additional inflection points in the MWD at integer multiples of i_0 acts as an important internal consistency criterion for reliable k_p evaluation.^[8] Further consistency criteria are that k_p values are independent of initiator concentration, laser pulse energy and LPRR.^[8] the PLP-SEC technique has been successfully applied to many monomers^[16] and benchmark k_p values have been published for styrene,^[8] several alkyl methacrylates,^[9,10,12,15] and butyl acrylate.^[13]

However, for acrylate-type monomers at temperatures above 20 °C and LPRRs of and below 100 Hz no or only broadened PLP structures are obtained.^[13,67–69,142,173,184–193] Intramolecular transfer-to-polymer (see Chapter 3.2.3) is now accepted as the mechanism responsible for this peak broadening.^[13] A detailed discussion of the influence of backbiting on MWDs from PLP is contained in Chapter 10.3.

5.1.1 Experimental procedures

5.1.1.1 PLP-SEC of non-ionized AA, MAA, and NVP in aqueous solution

According to the procedure used for AA,^[67] a stock solution of DMPA or Darocur in monomer was prepared, which was diluted with monomer, water and, optionally, propionic acid (PA), *iso*-butyric acid (IBA) or *N*-ethyl pyrrolidone (NEP) to yield the desired monomer, initiator, and additive concentrations. In case of solutions with pre-mixed poly(AA), poly(MAA) or poly(NVP), the polymers were first dissolved in demineralized water. The molar monomer concentrations at a particular polymerization temperature were calculated from the reported density expressions for AA,^[66] MAA,^[66] NVP,^[194] and water^[195] under the assumption of ideal mixing.

$$\rho_{AA} / \text{g} \cdot \text{cm}^{-3} = 1.0731 - 1.0826 \cdot 10^{-3} \cdot (T / ^\circ\text{C}) - 7.2379 \cdot 10^{-7} \cdot (T / ^\circ\text{C})^2 \quad (5-2)$$

$$\rho_{MAA} / \text{g} \cdot \text{cm}^{-3} = 1.0288 - 5.568 \cdot 10^{-4} \cdot (T / ^\circ\text{C}) - 1.1132 \cdot 10^{-5} \cdot (T / ^\circ\text{C})^2 + 1.0041 \cdot 10^{-7} \cdot (T / ^\circ\text{C})^3 \quad (5-3)$$

$$\rho_{NVP} / \text{g} \cdot \text{cm}^{-3} = 1.0592 - 7.7772 \cdot 10^{-4} \cdot (T / ^\circ\text{C}) - 4.6649 \cdot 10^{-7} \cdot (T / ^\circ\text{C})^2 \quad (5-4)$$

$$\rho_{\text{water}} / \text{g} \cdot \text{cm}^{-3} = 0.9999 + 2.3109 \cdot 10^{-5} \cdot (T / ^\circ\text{C}) - 5.44807 \cdot 10^{-6} \cdot (T / ^\circ\text{C})^2 \quad (5-5)$$

The monomer solution was transferred into a cuvette and purged with nitrogen for 2 to 4 min. In case of high-pressure measurements, the reaction mixture was introduced into an internal cell after deoxygenation. Prior to pulsing, the cuvette or high-pressure cell was thermostated

for about 20 min. The number of pulses was selected such as to reach a monomer conversion below 5 %. Post-polymerization was suppressed by pouring the mixture from PLP into a sample vial containing MEHQ. Water, monomer, and saturated monomer analogs were evaporated under high-vacuum at ambient temperature.

Polymer solutions containing NVP were dried by removal of the majority of water under high vacuum at ambient temperature followed by addition of *n*-hexane to precipitate poly(NVP) and extract residual NVP. After several addition and decanting steps with *n*-hexane, poly(NVP) was dried under vacuum at room temperature to constant weight.

The degree of monomer conversion was determined gravimetrically for all monomer systems.

5.1.1.2 PLP-SEC of ionized MAA in aqueous solution

MAA and DMPA were weighted into a volumetric flask and neutralized under ice cooling using 3 to 8 molar NaOH solutions to the pre-selected degree of ionization, α_D . Subsequently, the flask was filled up with demineralized water. Molar MAA concentrations were obtained from the total mass and the volume of the particular solution. Values of $\alpha_D > 1.0$ are associated with an excess of NaOH with respect to the MAA content, e.g., $\alpha_D = 1.1$ denotes a 10 mol-% excess of NaOH over MAA. The sample preparation and PLP experiments were otherwise identical to the procedure outlined in Chapter 5.1.1.1. However, the treatment of the reaction mixtures after PLP differed in that sodium methacrylate, which would affect the gravimetric conversion detection as well as the determination of the MWDs by SEC, had to be removed by dialysis against demineralized water. It was verified by comparison of the MWDs of dialyzed and non-dialyzed non-ionized poly(MAA) that this procedure leaves the SEC traces unchanged.

5.1.1.3 PLP-SEC of BA

BA was deoxygenized by several freeze-pump and thaw cycles. DMPA or MMMP were added to the monomer at concentrations of 5 to 16 mmol·L⁻¹ under an argon atmosphere and the mixture was transferred to a cuvette. The PLP experiment and sample treatment after PLP was identical to the procedure outlined in Chapter 5.1.1.1 with the exception that high laser

energies (up to 30 mJ) and low pulse numbers were applied to reach monomer conversion of about 0.5 %.

5.1.2 Data evaluation

Figure 5-1 depicts a typical MWD (full line) and the associated first derivate curve (dashed line) as obtained from PLP experiments (20 wt.% MAA in water, $\alpha_D = 0.7$, $c_{\text{DMPA}} = 2.7 \cdot 10^{-3} \text{ mol} \cdot \text{L}^{-1}$, 40 °C, $LPRR = 20 \text{ Hz}$). The MWD is well PLP-structured and exhibits three points of inflection, thus fulfilling the internal consistency criterion for k_p evaluation.^[8]

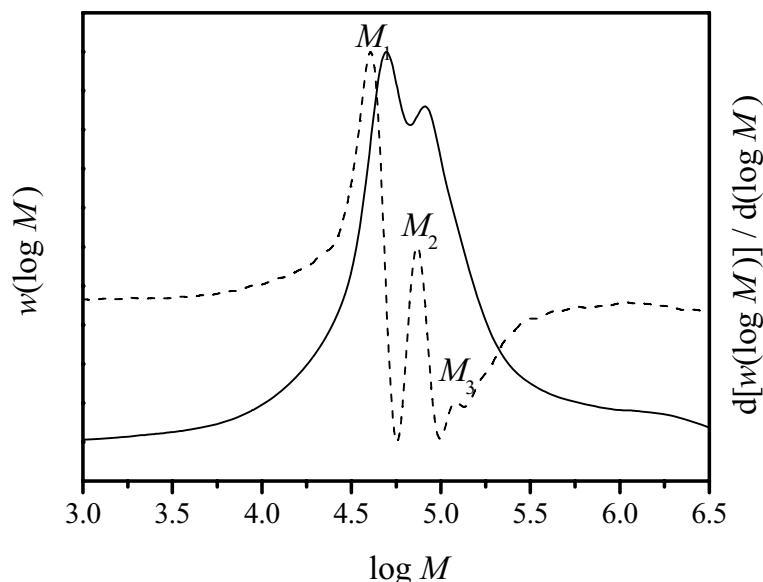


Figure 5-1: MWD (full line) and the associated first derivate curve (dashed line) obtained from PLP-induced polymerizations of 20 wt.% of MAA in water at ambient pressure, 40 °C, a degree of monomer ionization of 0.7, an initiator concentration of $c_{\text{DMPA}} = 2.7 \cdot 10^{-3} \text{ mol} \cdot \text{L}^{-1}$, and a laser pulse repetition rate of 20 Hz.

The kinetic chain length, i_0 , is calculated by M_1 / M_{monomer} (for AA and MAA, the molecular mass of the corresponding sodium salts has to be used) and $t_0 = 1 / LPRR$. Thus, k_p can be assessed from Eq. (5-1) with c_M being the arithmetic mean value of monomer concentration before and after PLP. The treatment of MWDs obtained from PLP on solutions with pre-mixed polymer is detailed in Chapter 6.2.

5.2 Chemically initiated polymerizations

Analysis of the decrease of monomer concentration with time during chemically initiated polymerization, detected e.g. via FT-NIR spectroscopy, allows for the determination of k_t/k_p^2 as a function of conversion according to Eq. (3-10) provided that the reaction obeys ideal kinetics and $k_d \cdot f$ is known. The actual initiator concentration c_I is obtained from the integrated form of the initiator decomposition rate law (Eq. (3-1)). Individual termination rate coefficients may be calculated from combination of k_t/k_p^2 with results from SP-PLP-NIR, yielding k_t/k_p , or by implementing k_p from independent PLP-SEC experiments.

5.2.1 Experimental procedure

Monomer, initiator (V50), and water were mixed in a 5 ml flask and purged with nitrogen under ice cooling for three minutes. The mixture was filled into the internal cell, which is fitted into the stainless steel cell that has been pre-heated to the polymerization temperature. After applying pressure, the stainless steel cell is immediately inserted into the sample chamber of the FT-IR/NIR spectrometer and NIR spectra are taken in most cases every 60 s and until conversion is complete.

5.2.2 Determination of monomer-to-polymer conversion

The decrease of monomer concentration, c_M , toward increasing conversion may be monitored via NIR spectroscopy. It has become standard practice to use the first overtone of the C–H stretching vibration at the olefinic double bond at about $6170 - 6200 \text{ cm}^{-1}$ for quantitative analysis.^[196,197] This band is well suited for the analysis of monomer concentration, because it is in most cases not overlapped by other vibration bands. To deduce overall monomer conversion from the spectra, Beer-Lambert's law (Eq. (5-6)) needs to be valid.

$$A(\tilde{\nu}) = \log\left(\frac{I}{I_0}\right) = \varepsilon(\tilde{\nu}) \cdot c_M \cdot l \quad (5-6)$$

It relates the absorbance A (at a specific wave number, $\tilde{\nu}$) to monomer concentration. In Eq. (5-6), I_0 is the light intensity entering the cell and I is the intensity of NIR light after passing the sample and the optical windows. Monomer conversion, X , at time t is calculated by Eq. (5-8) via the integrated version of Beer-Lambert's law, as given in Eq. (5-7):

$$Int = \int_{\tilde{\nu}_1}^{\tilde{\nu}_2} A(\tilde{\nu}) d\tilde{\nu} = B \cdot c_M \cdot l \quad (5-7)$$

$$X(t) = 1 - \frac{c_M}{c_M^0} = 1 - \frac{Int(t)}{Int_0} \quad (5-8)$$

where B is the integrated molar absorptivity and c_M^0 is the initial monomer concentration.

Figure 5-2 depicts a series of FT-NIR spectra recorded during chemically induced polymerization of 60 wt.% MAA in water at 50 °C and 2000 bar. The arrow indicates the direction of absorbance change during polymerization. The pronounced background absorption, provoked by H₂O combination bands, hampers data evaluation as the baseline is not horizontal. For correctly deducing MAA conversion, the spectrum for complete MAA conversion was subtracted from each spectrum measured during polymerization.^[198] The resulting spectral series (see Figure 5-3) was evaluated by integration of the high-wavenumber half-band between 6178 and 6400 cm⁻¹.

Using D₂O instead of H₂O shifts the stretching modes of the solvent to lower wavenumbers and thus reduces background absorbance which enhances signal-to-noise quality in SP-PLP-NIR experiments.^[198] Shown in Figure 5-4 are FT-NIR spectra recorded during SP-PLP induced polymerization of 60 wt.% NVP in D₂O at 40 °C and 2000 bar. The background absorbance of the solvent is decreased as compared to the spectral series in Figure 5-2. Furthermore, the calculation of monomer concentration is facilitated as subtraction of the full conversion spectrum is not necessary. NVP concentrations were calculated by integration of the high-wavenumber half-band against a horizontal base-line through the absorbance point at 6400 cm⁻¹.

It is assumed that D₂O affects polymerization kinetics of water soluble monomers to the same extent as H₂O and H-D-exchange on the olefinic C-H bond is slow compared to polymerization time.

The rate of polymerization during chemically initiated reaction was estimated from the first-derivative curves of c_M vs. t curves determined via ORIGIN6.1 with subsequent smoothing.

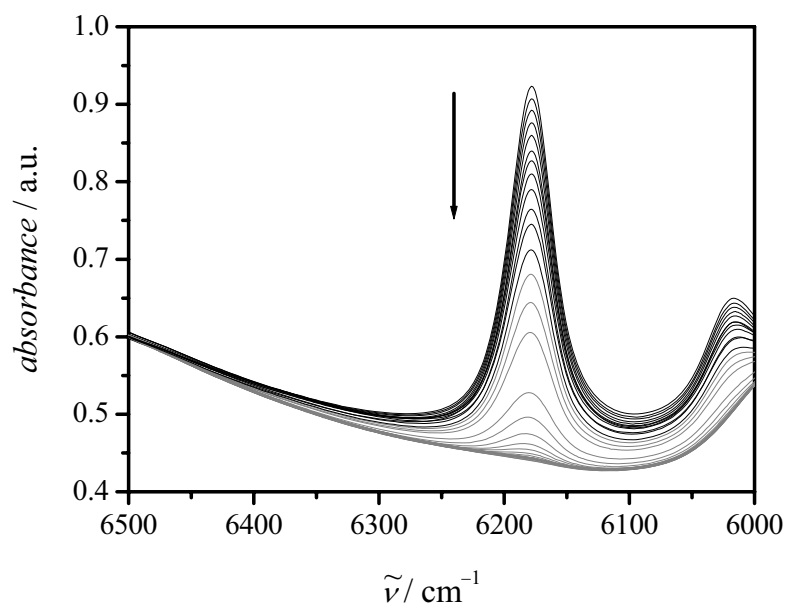


Figure 5-2: Series of FT-NIR spectra recorded during chemically induced polymerization of 60 wt.% MAA in H₂O at 50 °C, 2000 bar and an initiator concentration of $c_{V50} = 2.7 \text{ mmol}\cdot\text{L}^{-1}$. The arrow indicates the direction of absorbance change during polymerization.

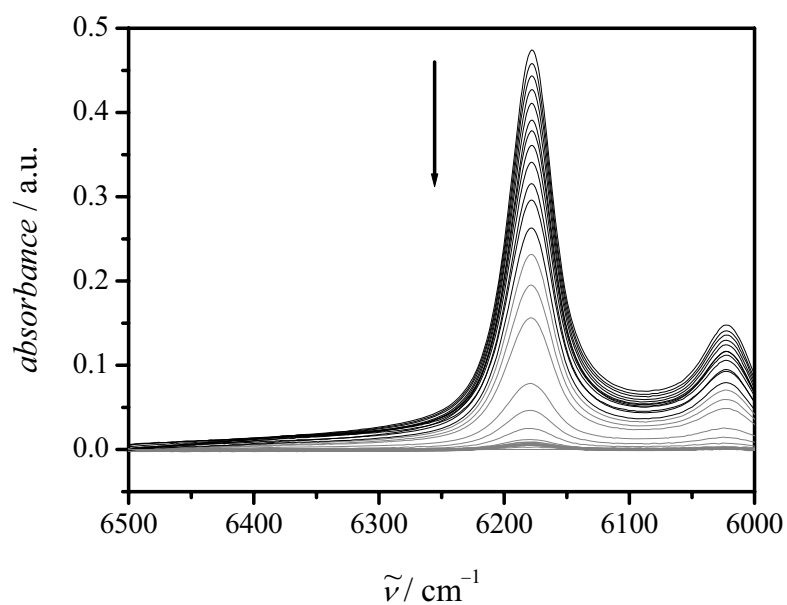


Figure 5-3: FT-NIR spectra deduced from the spectral series shown in Figure 5-2 by subtraction of the spectrum for complete MAA conversion from each of the individual absorbance spectra. The arrow indicates the direction of absorbance change during polymerization.

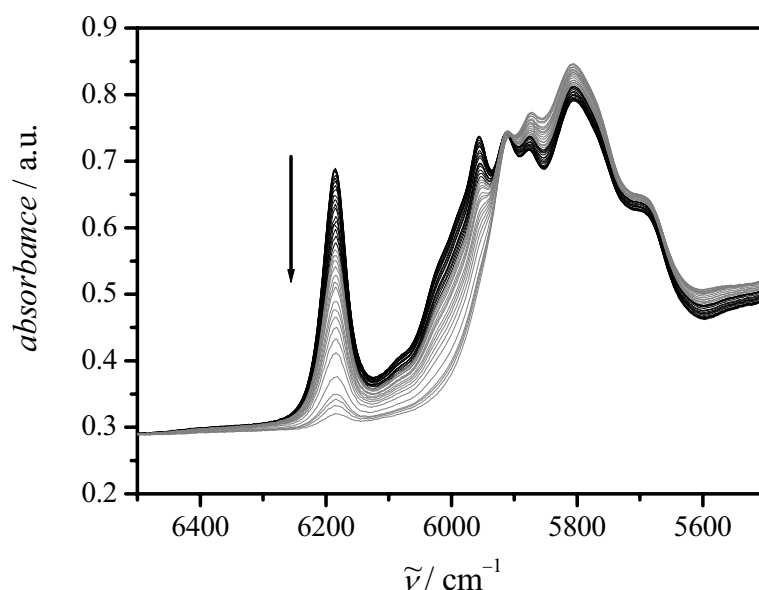


Figure 5-4: Series of FT-NIR spectra recorded during SP-PLP induced polymerization of 60 wt.% NVP in D₂O at 40 °C, 2000 bar and an initiator concentration of $c_{\text{DMPA}} = 1 \text{ mmol}\cdot\text{L}^{-1}$. The arrow indicates the direction of absorbance change during polymerization.

5.3 The SP-PLP-NIR technique

In SP-PLP-NIR, monomer conversion induced by a single laser pulse is monitored via in-line near infrared (NIR) spectroscopy with a time resolution of microseconds.^[31] Among the methods for deducing k_t , the SP-PLP-NIR technique is recommended by the IUPAC Subcommittee on “Modeling polymerization kinetics and mechanism” as the most powerful, although somewhat sophisticated and difficult method.^[14] Eq. (3-7) represents the time evolution of relative monomer concentration within SP-PLP experiments. In the absence of any chain-length dependence of k_t (and of k_p), fitting the experimental monomer concentration vs. time trace to Eq. (3-7) yields k_t/k_p and $k_t \cdot c_R^0$. As c_R^0 is not directly accessible from SP-PLP-NIR measurements, the primary experimental quantity is k_t/k_p . From several successive SP-PLP-NIR experiments carried out during a polymerization up to high degrees of monomer conversion, X , with each of them providing one k_t/k_p value, k_t may be determined as a function of X , provided that k_p is known for this conversion range. As the macroradical chain length varies with time after the laser pulse, the rate coefficient which results from fitting of the

conversion vs. time trace to Eq. (3-7) should be referred to as $\langle k_t \rangle$ (see Chapter 3.4.2). The chain-length dependence of k_t may be evaluated by fitting Eq. (3-45) to the $c_M(t)$ data.

5.3.1 Experimental procedure

The optical high-pressure cell, which at the beginning of an experiment contains an empty internal cell with the quartz windows being in direct contact, is brought to reaction temperature and pressure and a FT-NIR reference spectrum is recorded. Then the high voltage value at the thyatron of the laser is calibrated against a joule meter (Gentec). The reaction mixture containing monomer, photoinitiator, and, optionally, solvent or RAFT agent, is deoxygenized by freeze-thaw and pump cycles or bubbling with nitrogen as detailed in Chapter 5.1.1. Subsequently, the solution is transferred into an internal cell being then fitted into the optical high-pressure cell. The assembly is brought to reaction conditions. An initial FT-NIR spectrum is recorded and the monochromator employed in the SP-PLP-NIR setup is set to the maximum of the absorbance band of the first overtone of the C-H stretching vibration on the C=C bond (see Chapter 5.1.1). The initial intensity at zero per cent monomer conversion, $I_0(X=0)$, is recorded via a custom C++ program.^[144] The same program controls the analog digital converter (ADC) board. In addition, the program records and compensates the output voltage of the InAs detector before and after each series of laser pulses. Further settings, as time resolution, number of signals to be co-added, etc. are controlled by the software SBENCH (v. 4.55, FastComTec). The time resolution may be varied in between 2 μ s and 1 ms. The maximum number of stored data points is 2^{16} . SBENCH records the time-resolved data of the change in light intensity after applying the laser pulse and saves the intensity data averaged over the selected amount of individual signals for further processing. In regular intervals (typically every 5 % monomer conversion), FT-NIR spectra are recorded over an extended wavenumber range to deduce overall monomer conversion. In principle, the overall monomer conversion may be deduced from the NIR data obtained by the SP-PLP-NIR InAs detector. These intensity data may yield X with a relatively large error as the IR-light beam is refracted by the reaction solution to different extents during polymerization. Moreover, with aqueous systems, in which a strong background absorbance of the solvent is observed, conversion detection by SP-PLP-NIR alone is not feasible.^[199,200] Within the FT-NIR spectra a large wavelength region is integrated and background absorbances or baseline

instabilities may be subtracted. Thus, monomer conversion determined from these spectra are used to recalculate virtual $I_0(X=0)$ values for each series of SP-PLP traces to fit absolute monomer conversion. The time-resolved data remain unaffected.^[199,201] More details on the setup and the method are given in the appendix of ref.^[144]

5.3.2 Calculation of monomer concentration traces

In SP-PLP-NIR, the decrease in monomer concentration after single pulse initiation is traced via measurement of NIR intensity at the maximum position of the monomer peak at about 6180 cm^{-1} . However, the analysis light is not monochromatic due to dispersion of the NIR beam at the interference grating. Eq. (5-6) is thus transformed to

$$\Delta c_M(t) = c_M(t) - c_M^0 = -\frac{\log\left(\frac{I(t)}{I_0(X=0)}\right)}{\varepsilon_{\text{eff}}(\Delta\tilde{\nu}) \cdot l} \quad (5-9)$$

where $\varepsilon_{\text{eff}}(\Delta\tilde{\nu})$ is the effective molar absorption coefficient in the wavenumber range $\Delta\tilde{\nu}$ which is calculated from the FT-NIR spectrum recorded at zero per cent conversion according to

$$\varepsilon_{\text{eff}}(\Delta\tilde{\nu}) = \frac{A_{\text{eff}}(\Delta\tilde{\nu})}{c_M^0 \cdot l} \quad (5-10)$$

with $A_{\text{eff}}(\Delta\tilde{\nu})$ being the arithmetic mean absorbance in the corresponding wavenumber range.

5.4 The SP-PLP-ESR technique

Within SP-PLP-ESR, macroradical concentration after single pulse initiation is traced with microsecond time resolution. The termination rate coefficient $\langle k_t \rangle$ may be obtained by fitting Eq. (3-6) or (3-38) to the experimental $c_R(t)$ data. Moreover, SP-PLP-ESR provides more direct and detailed access to $k_t(i,i)$ values, via Eqs. (3-36) or (3-39) to (3-44), than does SP-PLP-NIR (see Chapter 5.3) and allows for tracing of different types of radicals which may

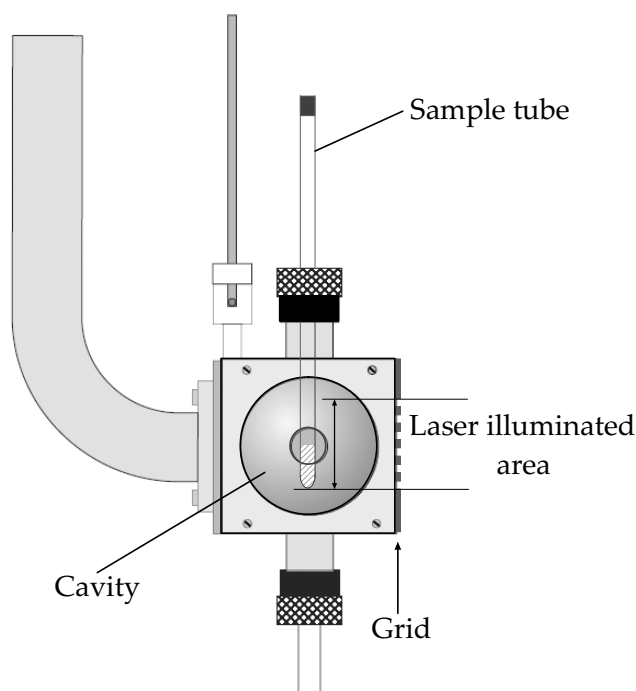
occur during polymerization. Thus, SP-PLP-ESR has to be considered as the more powerful method for kinetic investigations. However, its applicability is limited to measurements on non-polar solutions at ambient pressure without precise detection of monomer-to-polymer conversion so far. The investigations detailed in Chapters 5.4.2 and 5.4.3 have been carried out in cooperation with Johannes Barth. Part of the work already appeared in ref.^[202]

5.4.1 Experimental procedure

The monomer and, if added, the solvent are purified and degassed by several freeze-pump and thaw cycles. The photoinitiator is added under an argon atmosphere in a glove box and the reaction solution (typically 0.1 to 0.2 mL) is filled with a syringe into ESR tubes of 5 mm outer and 4 mm inner diameter. For highly polar solutions (e.g. BMA in bulk) ESR tubes of 3 mm outer and 2 mm inner diameter and sample volumes of 0.05 mL were used to allow for tunability of the ESR spectrometer. The sample tubes are closed with a plastic cap, sealed with PARAFILM, and carefully protected from ambient light to prevent pre-polymerization before laser pulsing.

Calibration solutions of 10^{-4} to 10^{-6} mol·L⁻¹ of TEMPO in the corresponding monomer-solvent-mixtures are prepared by stepwise dilution starting with about 10^{-2} mol·L⁻¹ TEMPO. The spectrometer cavity is brought to reaction conditions and a TEMPO sample is placed into the resonator. The correct alignment of the ESR tube in the cavity is illustrated in Scheme 5-1. The ESR spectra for calibration with TEMPO are recorded at conversion times of 10.24 ms and different receiver attenuations depending on radical concentration. Subsequently, the TEMPO sample is replaced by a monomer-photoinitiator solution and an ESR spectrum under laser pulse initiation of typically 20 Hz repetition rate is recorded with the same spectrometer settings as used for the calibration spectra with the exception of the receiver attenuation. The magnetic field associated with the maximum intensity of a characteristic line in the ESR spectrum is identified for subsequent time-resolved tracing. Whereas full ESR spectra are measured within the *signal channel* (SC), the variation of ESR intensity with time at fixed magnetic field is detected by so called fast-scan coils and recorded with the *fast digitizer* (FD). The laser and the spectrometer are synchronized via the pulse generator with a time delay for firing the laser pulse of about 10 per cent of the entire recording time. To ensure complete decay in radical concentration, a suitable dark time between two laser pulses is

chosen. From the data recorded prior to the laser pulse, the offset in intensity is deduced, as no radicals are present. To improve signal quality, usually 50 to 200 single traces are co-added yielding one $c_R(t)$ curve. Monomer-to-polymer conversion was determined gravimetrically after pouring the sample into a flask with hydroquinone and drying to constant weight.



Scheme 5-1: Schematic view of the ESR cavity with sample tube.

For the purpose of calibration (see Chapter 5.4.2), several full ESR spectra are recorded under laser pulsing at 20 Hz and various laser energy levels. Thus, different amounts of radicals are produced within each experimental run. This data is required to correlate the double integral of signal intensity ($\iint I$) of the full ESR spectrum with signal intensity, I , at a fixed magnetic field.

The ESR intensities of the full spectra and the single pulse traces are finally scaled by the applied scan numbers, accumulations per data point (see Chapter 5.4.3), and receiver gains. Such scaling is required to achieve comparability of the intensity values which are given in arbitrary units.

5.4.2 Determination of radical concentrations

So far, direct determination of radical concentration is only accessible via electron spin resonance spectroscopy. All other methods only yield estimates on c_R mostly on the basis of tracing monomer concentration. Such techniques are thus model dependent and considered being less accurate.

For determination of absolute radical concentrations an individual calibration for each combination of spectroscopical parameters (microwave power, modulation amplitude, time constant, etc.), sample type (monomer-solvent-mixture, sample volume, type of ESR tube), and temperature is required. Calibration with solutions of a stable radical, such as TEMPO, in the corresponding monomer-solvent-mixtures under identical experimental conditions has become standard practice.^[33,97,203,204]

As with NMR spectroscopy, the integral of the ESR absorbance peaks is correlated with the concentration of the traced species. In ESR, a dispersion spectrum, i.e. the first derivative of absorption, is recorded. Thus, from the double integral of the full ESR spectra ($\iint I$) of TEMPO calibration samples with known c_R the radical concentration of any other sample under otherwise identical conditions may be calculated. In SP-PLP-ESR, the change in ESR (dispersion) intensity at fixed magnetic field, H_x , is recorded. Thus, a correlation between $I(H_x)$ and the corresponding $\iint I$ of the full ESR spectrum is required. To determine the concentration of one particular species in a system with several types of radicals (e.g. SPRs and MCRs in acrylate polymerization), additionally the molar fraction of the radical of interest with respect to overall radical concentration needs to be known.

The calibration procedure is detailed below on example of BA polymerization.

By PLP initiation with constant laser pulse repetition rate, a pseudo-stationary radical concentration is created which is proportional to the double integral of its ESR dispersion intensity.

$$c_R = h_1 \cdot \iint I_{SC} \quad (5-11)$$

The constant h_1 is determined from $\iint I_{SC}$ measured via the SC for TEMPO calibration solutions with known radical concentrations.

Depicted in Figure 5-5, by the black line, is an ESR spectrum of TEMPO ($10^{-4} \text{ mol}\cdot\text{L}^{-1}$ in a mixture of $1.52 \text{ mol}\cdot\text{L}^{-1}$ BA in toluene at 233 K) with the corresponding integral (light grey

line) and double integral (dark grey line). The black squares are determined from $\iint I_{SC}$ at different TEMPO concentrations. As is to be expected from Eq. (5-11), the radical concentration is proportional to the double integral of ESR intensity with the slope h_1 .

Peak position and $\iint I_{SC}$ are measured in the SC, $I_{FD}(H_x)$, however, is traced using the FD. Thus, the sensitivities of both detection systems need to be correlated according to:

$$\iint I_{SC} = h_2 \cdot \iint I_{FD} \quad (5-12)$$

with the constant h_2 being determined from measurements of ESR spectra of TEMPO calibration samples via the SC and FD.

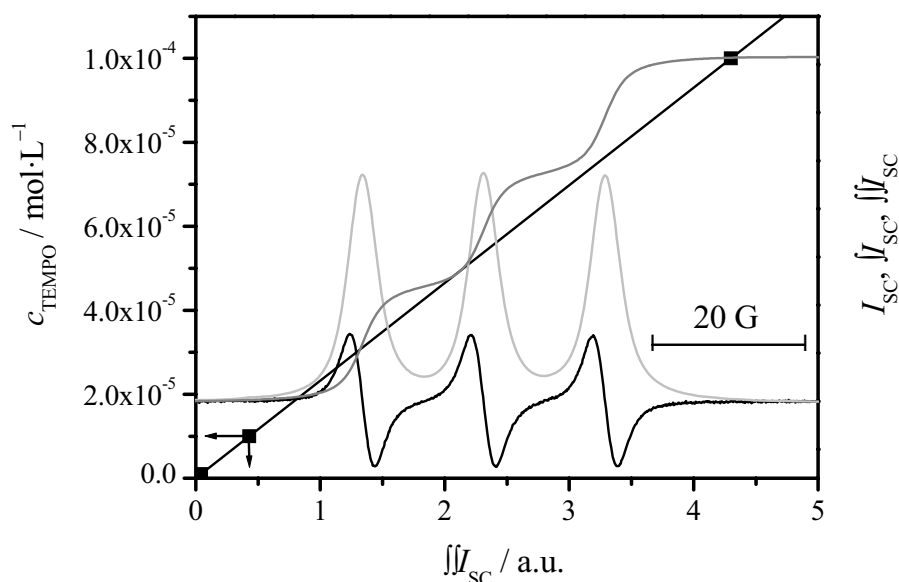


Figure 5-5: Plot of TEMPO concentration in toluene against the corresponding double integral of ESR dispersion intensity measured at 273 K (squares). A typical ESR spectrum of TEMPO (full black line) is shown together with the corresponding integral (light grey line) and double integral (grey line).

Shown in Figure 5-6 are the ESR spectra and the corresponding double integrals of TEMPO ($10^{-5} \text{ mol} \cdot \text{L}^{-1}$ in a mixture of $1.52 \text{ mol} \cdot \text{L}^{-1}$ BA in toluene at 295 K) measured via SC (grey lines) and FD (black lines) detection. Peak positions in SC and FD closely overlap as far as conversion times of and above 10.24 ms are used within the signal channel. Thus, the standard procedure of measuring full ESR spectra for determination of H_x in the SC is feasible. However, the sensitivity, i.e. $\iint I / c_R$, in the SC is by about a factor of 2 above the sensitivity in the FD with the factor being independent of temperature and radical

concentration. The correlation between the double integral for SC and FD measurements, respectively, is shown in Figure 5-7 for different concentrations of TEMPO. According to Eq. (5-12), linear regression of the data in Figure 5-7 yields a straight line through the origin with the slope h_2 .

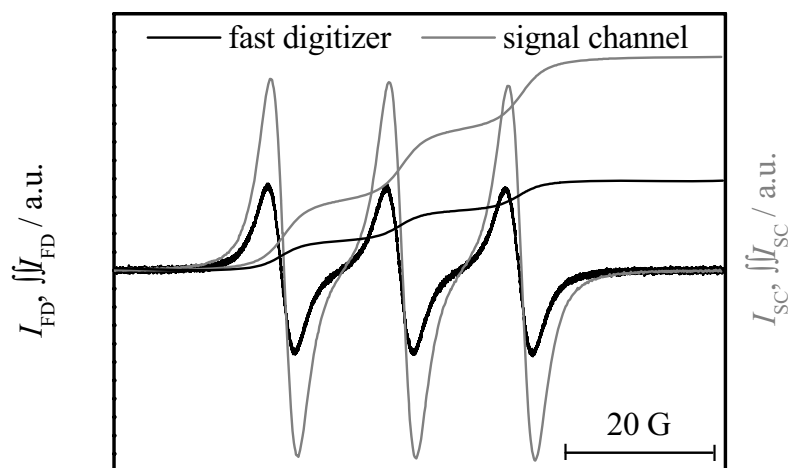


Figure 5-6: ESR spectra and corresponding double integrals measured on a calibration solution of TEMPO in toluene via signal-channel (grey lines) and fast-digitizer (black lines) detection at 295 K.

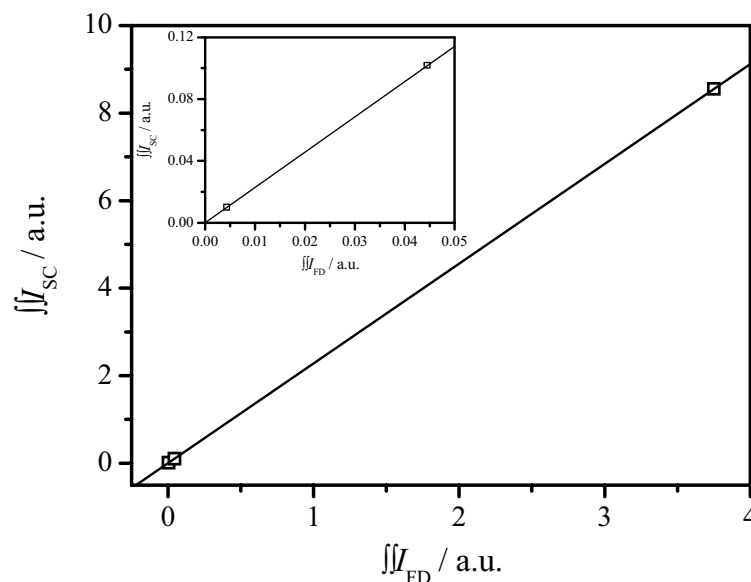


Figure 5-7: Plot of the double integral of ESR spectra measured in the signal channel versus the corresponding double integral determined by the fast digitizer for calibration samples with different TEMPO concentrations in toluene at 295 K. The insert shows an enlargement for the two data points with low double integrals.

Depicted in Figure 5-8 are the temperature dependences of the spectrometer sensitivities of BA in toluene ($1.52 \text{ mol}\cdot\text{L}^{-1}$) and *n*-BMA in bulk, both measured in the SC by means of TEMPO calibration solutions. The sensitivity for the BA in toluene solution (left hand side) decreases toward higher temperatures between 233 K and 263 K, however for higher temperatures, $\iint I_{\text{SC}} / c_{\text{TEMPO}}$ starts to increase again. In fact, the sensitivity at 345 K is above the value at 233 K.

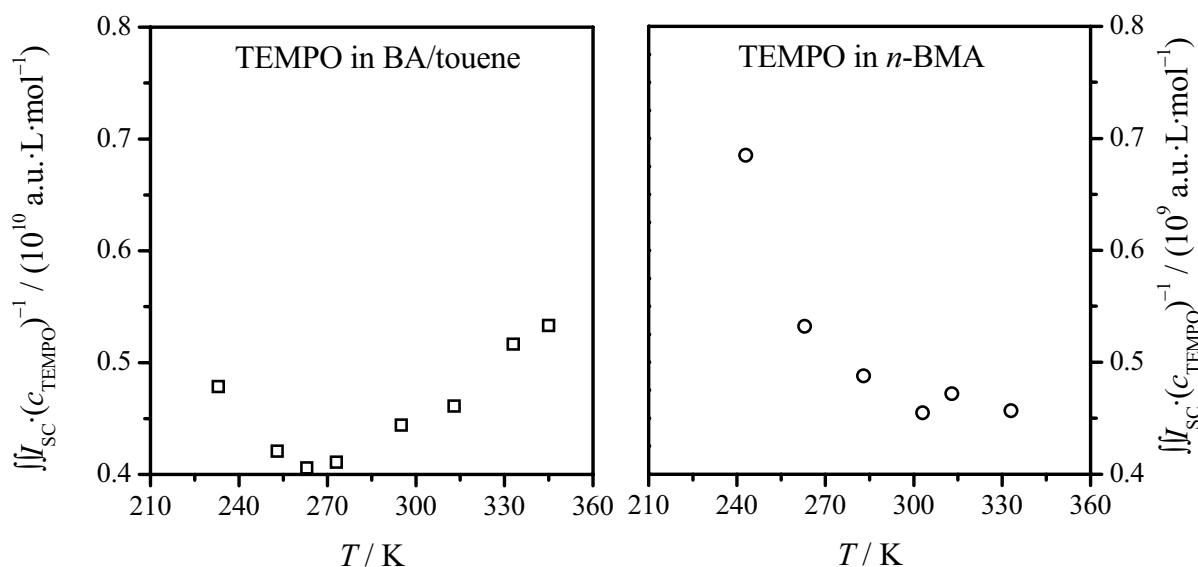


Figure 5-8: Temperature dependence of spectrometer sensitivity determined for TEMPO dissolved in 0.2 mL of a 1.52 molar solution of BA in toluene (left) and TEMPO in 0.05 mL of *n*-BMA in bulk (right).

Such behavior is not expected from theoretical considerations^[205] and also in conflict with the change of sensitivity with temperature observed for TEMPO in *n*-BMA (see Figure 5-8, right hand side) and as well as in pure toluene^[206]. According to the Boltzmann distribution, the spectrometer sensitivity should continuously decrease toward increasing temperature as the population difference between the spin levels in the magnetic field is reduced. In fact, the roughly twofold increase in sensitivity between 333 and 243 K found within the *n*-BMA bulk system is in close agreement with the theoretical expectations based on the applied microwave frequency and the magnetic field at absorption. The origin of the sensitivity minimum observed in the BA-toluene-TEMPO system is not understood so far. This effect may be related to relaxation times^[206] or changes in dielectricity. However, a similar trend has also been seen with vinyl pivalate-heptane-TEMPO mixtures.^[207] The above discussion demonstrates the necessity of careful calibration for all experimental conditions. Finally, it is

to be mentioned that the smaller sensitivity in case of *n*-BMA in bulk compared to BA in toluene is due to the smaller sample volume and the higher polarity of the (solvent free) methacrylate.

In SP-PLP-ESR, the change in ESR dispersion intensity at fixed magnetic field is traced. Thus, a correlation between $\iint I_{\text{FD}}$ and intensity $I_{\text{FD}}(H_x)$ is required. This calibration may be accomplished based on the ESR spectra determined by the SC as the line shape is identical in both detection systems. If the line width is independent of radical concentration, the correlation reads

$$\iint I_{\text{SC}} = h_{3,i} \cdot I_{\text{SC}}(H_{x,i}) \quad (5-13)$$

where $h_{3,i}$ is a constant which is characteristic of the special type of radical and $I_{\text{SC}}(H_{x,i})$ is the ESR dispersion intensity in the maximum of a well separated peak corresponding to radical species *i*.

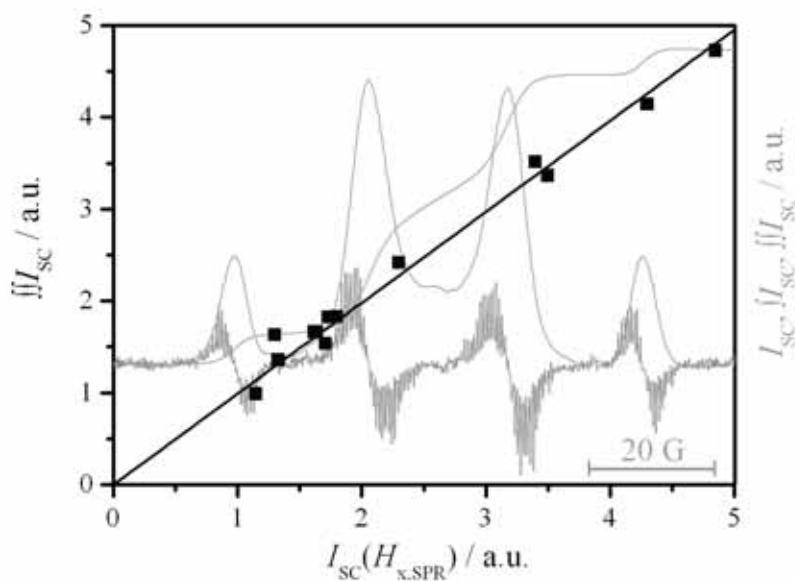


Figure 5-9: Correlation between double integral of the ESR spectrum with intensity in the peak maximum (marked with the arrow) for polymerizations of $1.52 \text{ mol}\cdot\text{L}^{-1}$ of BA in toluene at 233 K initiated by PLP at different laser energies. The grey lines represent a typical ESR spectrum and the corresponding integral and double integral recorded under such conditions.

The value of $h_{3,i}$ is determined from the slope of a plot of $\iint I_{\text{SC}}$ versus $I_{\text{SC}}(H_{x,i})$ as depicted in Figure 5-9 on example of BA polymerization in toluene at 233 K (for illustration I_{SC} , $\iint I_{\text{SC}}$, and

$\int I_{SC}$ are included in grey). The ESR lines in the spectrum show pronounced oscillations which reflect the change in radical concentration with time under pseudo-stationary conditions as will be discussed in detail in Chapter 12.2. Such oscillations, however, hamper the identification of $I_{SC}(H_{x,i})$ for correlation to $\int I_{SC}$ and were thus smoothed by applying a Fourier filter.

ESR spectra recorded during polymerization of acrylate monomers like BA reflect two types of radicals. Hence, the molar fractions of each species at reaction temperature need to be known which may be determined by spectra deconvolution.^[48,97,208,209] For such a procedure, the spectra of the individual species are simulated based on the coupling constants and line widths determined from ESR measurements at high and low temperatures where contributions of the MCR and SPR, respectively, are dominant. The experimental spectrum is subsequently fitted by superposition of different proportions of the simulated SPR and MCR contours. The fractions of the different radical species, x_{MCR} and x_{SPR} , are obtained from the corresponding weighting factors obtained from the fitting. The deconvolution procedure is schematically illustrated in Figure 5-10 on example of a BA polymerization at 313 K. The SPR and MCR simulations were scaled with accordance to the same radical concentration. The concentration of species i may be determined from the overall radical concentration according to:

$$c_i = x_i \cdot c_R \quad (5-14)$$

Shown in Figure 5-11 is the temperature dependence of the fraction of midchain radicals during PLP-initiated polymerization of $1.52 \text{ mol}\cdot\text{L}^{-1}$ of BA in toluene.^[48,97] An increase of x_{MCR} from nearly zero at 223 K to about 0.8 at 343 K is observed. Consequently, the ESR spectrum at low temperatures is almost exclusively due to SPRs whereas at high temperature mainly contributions of the tertiary radical are seen. The kinetic origin of the pronounced decrease of x_{MCR} toward lower polymerization temperatures is detailed in Chapter 12.3.

In systems with two types of radicals it is recommendable to first determine the radical-specific correlation constants for species i and subsequently substitute the radical fractions and introduce the ratios of the particular maximum intensities of the ESR lines to transfer the calibration to species j . According to Eq. (5-13) the following relation is obtained:

$$h_{3,j} = \frac{I_{SC}(H_{x,i})}{I_{SC}(H_{x,j})} \cdot h_{3,i} = h_{4,j} \cdot h_{3,i} \quad (5-15)$$

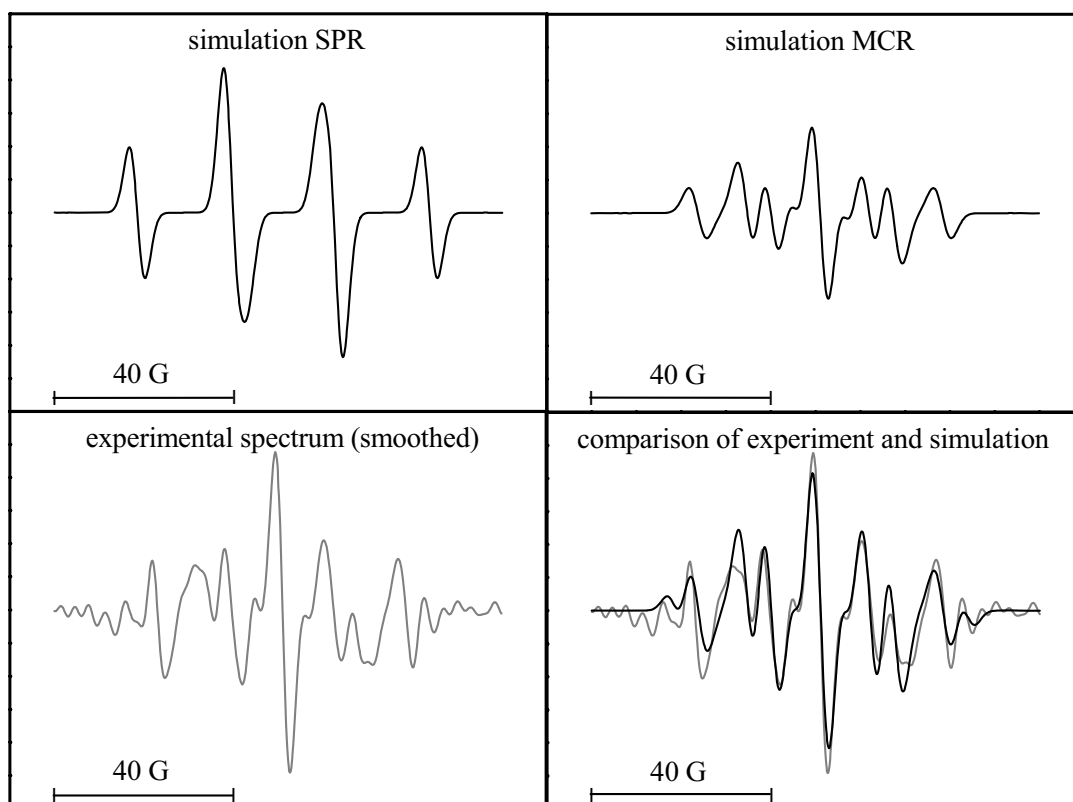


Figure 5-10: Schematic representation of the spectra deconvolution procedure on the example of a polymerization of $1.52 \text{ mol}\cdot\text{L}^{-1}$ of BA in toluene at 313 K. For details see text.

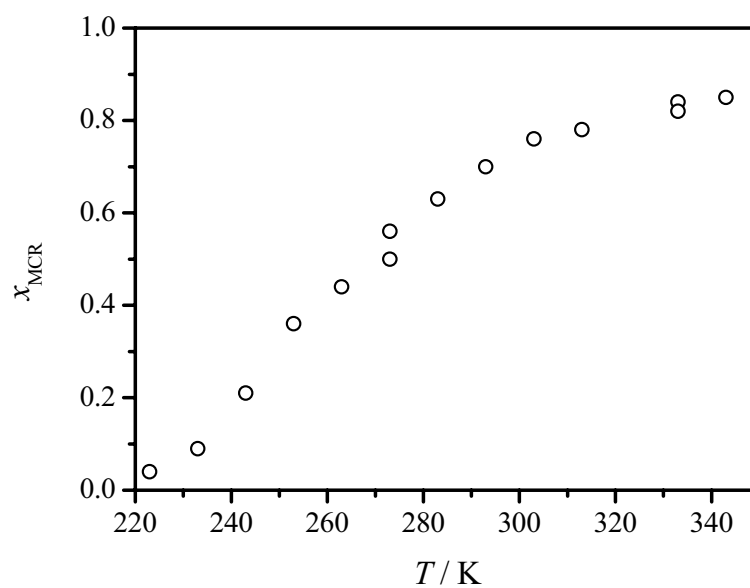


Figure 5-11: Temperature dependence of the fraction of midchain radicals during polymerization of $1.52 \text{ mol}\cdot\text{L}^{-1}$ of BA in toluene. The values are taken from refs.^[48,97]

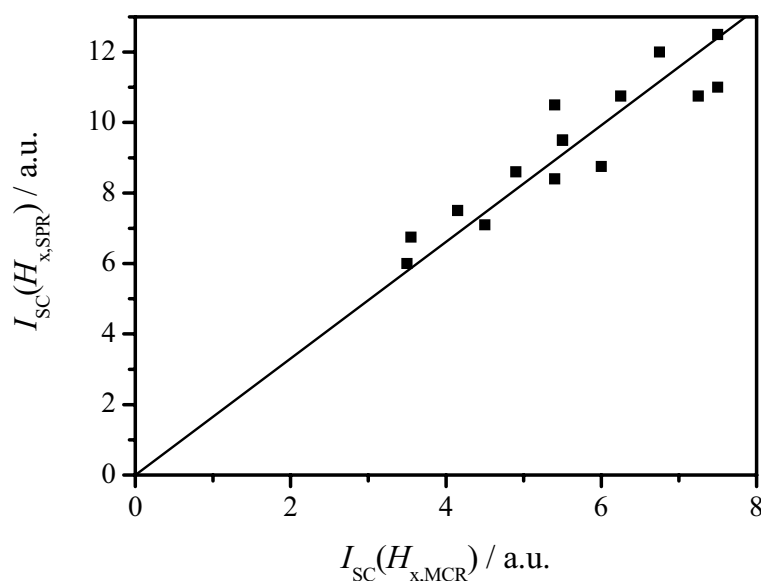


Figure 5-12: Correlation between the ESR dispersion intensities at magnetic field positions characteristic for the SPR and MCR species (polymerization of $1.52 \text{ mol}\cdot\text{L}^{-1}$ of BA in toluene at 295 K). The positions are identical to the ones marked in Figure 5-18.

The correlation between radical concentration and ESR dispersion intensity at the characteristic peak maximum position measured within the FD is obtained by combination of Eqs. (5-11) to (5-15). For systems with one type of radical the correlation reads

$$c_R(t) = h_1 \cdot h_2 \cdot h_3 \cdot I_{\text{FD}}(H_x)(t) \quad (5-16)$$

whereas

$$c_R(t) = h_1 \cdot h_2 \cdot h_{3,i} \cdot x_i \cdot I_{\text{FD}}(H_{x,i})(t) \quad (5-17)$$

$$c_R(t) = h_1 \cdot h_2 \cdot h_{3,j} \cdot x_j \cdot I_{\text{FD}}(H_{x,j})(t) \quad (5-18)$$

is obtained for systems with two types of radicals. The molar fraction of radical j may be calculated according to:

$$x_j = (1 - x_i) \quad (5-19)$$

5.4.3 Interpretation of primary experimental data

It is of fundamental importance for correct kinetic analysis of primary experimental $I_{\text{FD}}(H_x)$ versus t traces to identify potential artefacts. Such artefacts may be related to time resolution, to the influence of the laser pulse on ESR detection, or may result from overlap with other radical species.

The influence of the laser pulse

In SP-PLP, initiator cleavage is induced by high-energy laser pulses which results in a short-time response of the ESR detector as shown in Figure 5-13. The shape and magnitude of this perturbation is independent of magnetic field position however its intensity decreases toward lower laser energies.

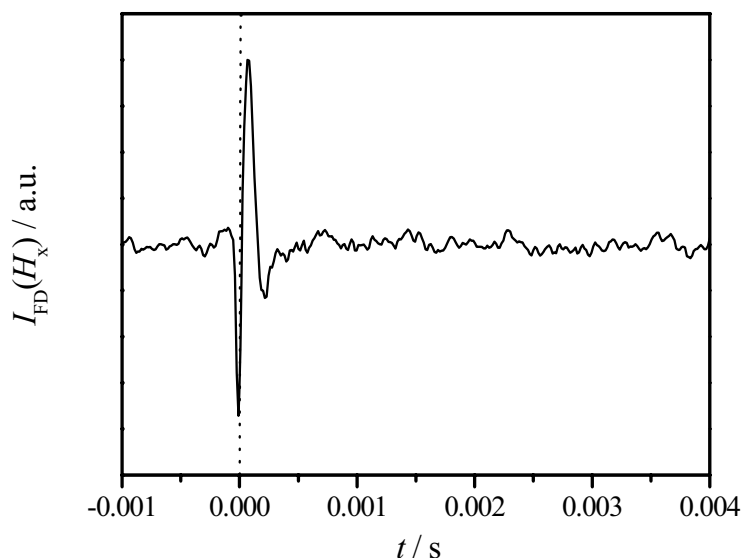


Figure 5-13: Perturbation of the laser pulse hitting the sample at $t = 0$ (indicated by the vertical dotted line) recorded at a magnetic field position beyond the range for carbon centered radicals. Laser pulses were applied to a solution of $1.52 \text{ mol}\cdot\text{L}^{-1}$ of BA in toluene at 295 K with a time resolution of $15 \mu\text{s}$ per data point.

The perturbation of the laser shown in Figure 5-13 was measured at a magnetic field position beyond the absorption range of the different radical species. The laser hits the sample at $t = 0$ which is indicated by the dotted line. The negative amplitude seems to start at $t < 0$. This may be caused by the relatively low time resolution of ESR detection (see Figure 5-14). The time resolution is the same as typically used for tracing SPRs during BA polymerization. Thus, the

laser signal strongly affects the c_R versus t curves at short times after applying the laser pulse. A time resolution being about two orders of magnitude lower was used for tracing the MCR species. In such cases the perturbation of the laser is either not seen at all in the obtained SP-PLP-ESR curves or only occurs as a single data point. Conclusively, for highly time-resolved measurements it is recommended to use high initiator concentrations allowing for relatively low laser energies and to not overinterpret the time range up to 0.5 ms after firing the initiating laser pulse.

The influence of time resolution

Measurements using the FD are carried out with a conversion time of 500 ns, i.e. detection of one intensity value takes 0.5 μ s. In all cases 1024 data points are recorded which would result in an overall recording time of only about 0.5 ms. Thus, n single intensity values were added over the time interval $n \cdot 500$ ns to yield one data point for lower time resolution. If the change in intensity is big compared to the time required for accumulation of one data point, the actual variation of ESR intensity with time is distorted. This effect is illustrated in Figure 5-14 on example of SPR traces of BA measured at different time resolutions (for details see captions). Pronounced intensity changes are induced by the perturbation of the laser, monomer addition to initiator-derived radicals and fast (bimolecular) termination at short times after the laser pulse. The position and magnitude of the maximum in SPR concentration may only be adequately captured by the highest time resolution for which even the disturbance in ESR detection due to the laser pulse is obviously resolved showing up as a negative narrow negative peak at short times. However, it cannot be ruled out that the absolute value in SPR maximum concentration may still be slightly underestimated.

In cases where the changes in ESR intensity are small compared to the recording time, no accumulation artefact should be observed. This is actually observed when tracing intensity for the MCR as shown in Figure 5-15 where identical time resolutions as in Figure 5-14 were used. MCR concentration slowly builds up by backbiting and decreases at much lower rate than does SPR concentration. Thus, no accumulation artefact on $c_{MCR}(t)$ is observed. However, the perturbation of the laser can only be determined at the highest time resolution.

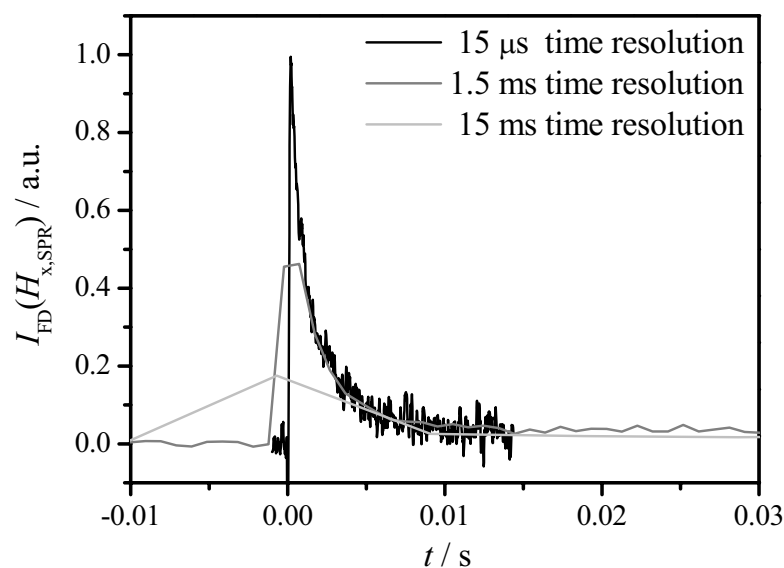


Figure 5-14: Change in ESR intensity after laser pulse initiation at $t = 0$ at the magnetic field position of a characteristic SPR line during polymerization of $1.52 \text{ mol}\cdot\text{L}^{-1}$ of BA in toluene at 295 K. Time resolutions of 15 μs (black line), 1.5 ms (dark grey line) and 15 ms (light grey line) were used.

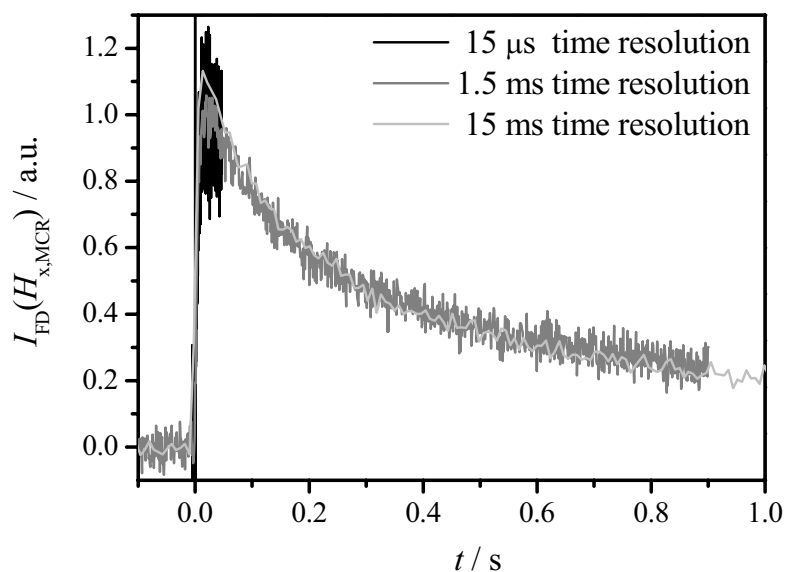


Figure 5-15: Change in ESR intensity after laser pulse initiation at $t = 0$ at the magnetic field position of a characteristic MCR line during polymerization of $1.52 \text{ mol}\cdot\text{L}^{-1}$ of BA in toluene at 295 K. Time resolutions of 15 μs (black line), 1.5 ms (dark grey line) and 15 ms (light grey line) were used.

The influence of primary initiator-derived radicals

Two carbon-centered radicals are formed by decomposition of MMMP (see Scheme 5-2) which is the photoinitiator exclusively used within the ESR experiments of the thesis in hand. In ESR, there is no pronounced chemical shift in between different types of carbon centered radicals as it is observed in NMR techniques. All radicals in the spectrum appear at almost the same magnetic center field but differ in coupling pattern. Thus, the ESR lines of initiator-derived radicals may overlap to some extent with the propagating radical species to be traced. It is to be expected that the influence of primary radicals on the single pulse curves has ceased at 1 ms after the laser pulse as initiator-derived radicals rapidly add to monomer or terminate at high rate.

Figure 5-16 depicts three full ESR spectra measured under PLP-initiation at 295 K by means of single scans of 10.49 s duration. The upper spectrum (Figure 5-16a) was determined for MMMP in toluene and shows two lines marked with X and Y. Line Y strongly oscillates with the applied laser frequency which illustrates that the corresponding species is almost instantaneously formed by the laser pulse however its concentration completely decreases during dark time. For line X, only minor intensity changes upon laser pulsing are seen indicating that there is a second species which is relatively long lived and reaches a pseudo-stationary concentration. The double integral of the initiator-derived radicals in toluene is only 4 % of $\int\int I$ measured during polymerization of BA in toluene under otherwise identical conditions, i.e. temperature, laser energy, and MMMP concentration. The error induced into the calibration procedure should even be smaller than 4 % as the primary radicals may not only be consumed by termination but also by addition to monomer. Thus, the contribution of MMMP derived radicals to $\int\int I$ of ESR spectra of polymerizing systems can be neglected.

To exclude that line X or Y is due to the formation of benzyl radicals, an ESR spectrum of MMMP in benzene under PLP-conditions was recorded (see Figure 5-16b). This spectrum shows two lines at identical magnetic field position as band X and Y within the toluene measurement. Thus, there is no significant formation of benzyl radicals under reaction conditions. Line B, however, is strongly broadened in the spectrum for MMMP in benzene implying that the corresponding radical species is interacting with the solvent. However, it was excluded by recording ESR spectra of pure toluene under PLP-conditions that line X is due to a solvent dependent interaction of the light source with the resonator cavity. The ESR spectrum measured under laser pulsing on a MMMP-BA-toluene mixture is depicted for comparison in Figure 5-16c. It is clearly seen that the spectrum of the initiator-derived

radicals overlaps with the center region of the BA spectrum where the absorbance of the MCR is observed.

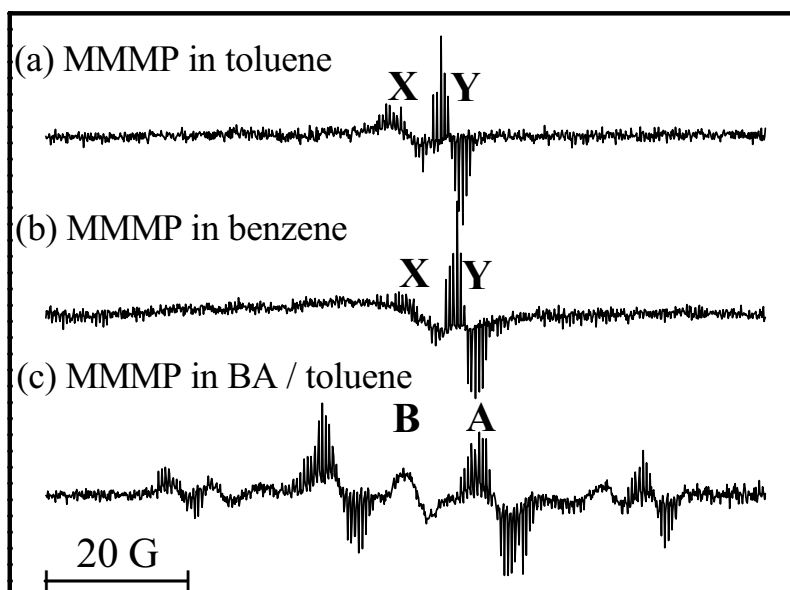


Figure 5-16: ESR spectra recorded during laser pulsing with a pulse separation time of 0.05 s on solutions of MMMP in toluene (a), MMMP in benzene (b), and MMMP in a mixture of $1.52 \text{ mol}\cdot\text{L}^{-1}$ of BA in toluene (c) at 295 K.

The change in ESR intensity with time of lines A and B marked in Figure 5-16c was traced at 295 K in a mixture of MMMP in $1.52 \text{ mol}\cdot\text{L}^{-1}$ of BA in toluene (black lines in Figure 5-17). Those ESR lines are characteristic for the SPR and MCR species, respectively (see below in Figure 5-18). The intensity traces of lines A and B are, however, resulting from an overlap of contributions of the SPR and fragment Y (Figure 5-17A) or of the MCR and fragment X (Figure 5-17B). This is indicated by the grey lines in Figure 5-17 where ESR intensity is recorded at the same magnetic field positions as were the black lines. Thus, the center region of the ESR spectrum where SPR and MCR intensities overlap with fragment Y and X, respectively, should not be used for tracing radical concentrations.

Until now, lines X and Y cannot be assigned to individual fragments of MMMP. Future studies may be devoted to elucidate the different radical structures, e.g. by ESI-MS (electrospray ionization – mass spectrometry) measurements, and to determine the corresponding termination rate coefficients via further SP-PLP-ESR experiments.

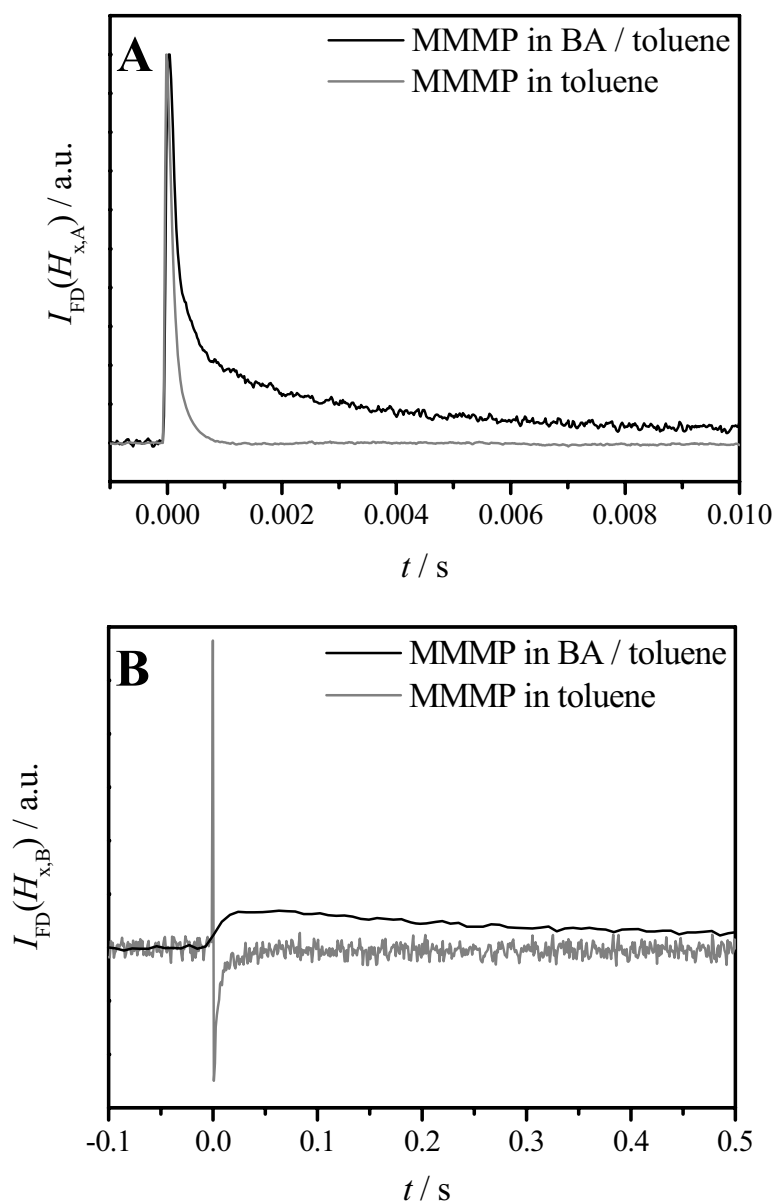


Figure 5-17: Time evolution after single pulse initiation of relative ESR intensity in the maxima of the lines marked with A and B in Figure 5-16c for MMMP in 1.52 mol·L⁻¹ of BA in toluene (black lines) and for MMMP in pure toluene (grey lines) at 295 K.

Identification of suitable ESR lines for SP-PLP-ESR

ESR spectra recorded during BA polymerization consist of an overlap of a SPR and a MCR spectrum. As both radicals show considerably different reactivities, two characteristic ESR lines have to be identified which are not or at least not significantly affected by ESR intensity of the other species.

Figure 5-18 shows simulations of the SPR and MCR spectra. The arrows indicate the magnetic field positions at which single pulse tracing was performed. SPR and MCR concentrations were not measured via lines A and B for reasons detailed above. There is a second well separated ESR line for the SPR at low magnetic field (left). This line was not used for tracing c_{SPR} due to its low intensity which would result in minor signal to noise quality of the single pulse curves.

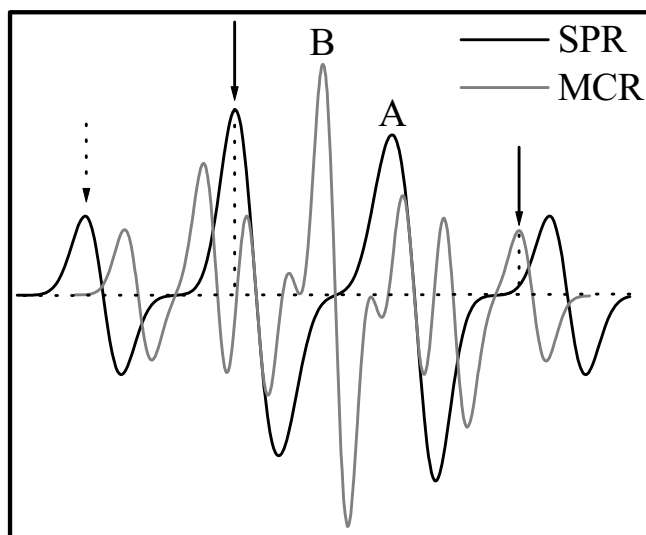


Figure 5-18: Simulated ESR spectra of the SPR (black line) and MCR (grey line) species occurring during acrylate polymerization. The magnetic field positions used for tracing secondary and tertiary radical concentrations, respectively, are indicated with arrows.

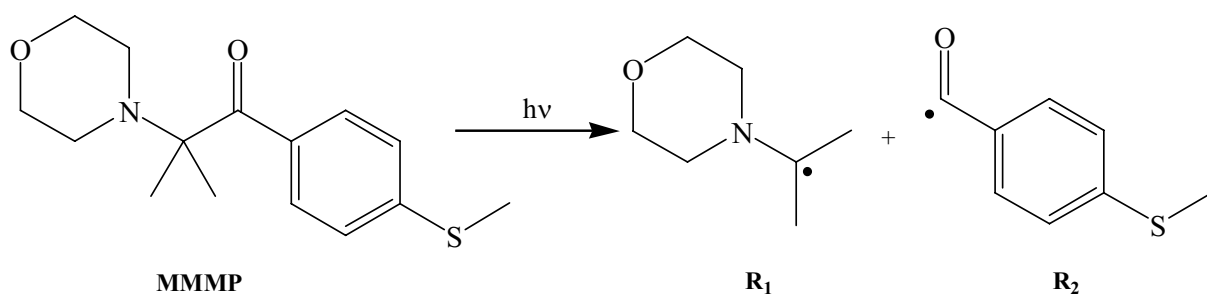
5.5 Selection of experimental conditions

5.5.1 Photoinitiation

The evaluation of the chain-length dependence of the termination reaction by fitting time-resolved data on monomer consumption or on the decay of radical concentration requires accurate knowledge on the chain length of the propagating radicals at a given time after laser initiation. Thus, an ideal photoinitiator for SP-PLP experiments has to fulfill the following criteria:

- The photoinitiator must decompose upon irradiation with excimer laser light. The XeF line of 351nm is preferable, because most monomers do not absorb at this wavelength.
- Laser-induced photoinitiator decomposition must be fast as compared to the subsequent first propagation step (that is below one microsecond).
- The efficiency of the initiator should be high, preferably close to unity, which means that all photoinitiator-derived radicals start chain growth.
- Both radical fragments should be capable of rapidly initiating macromolecular growth at similar rate, which ensures a close-to-monodisperse size distribution of growing radicals unless chain transfer comes into play.

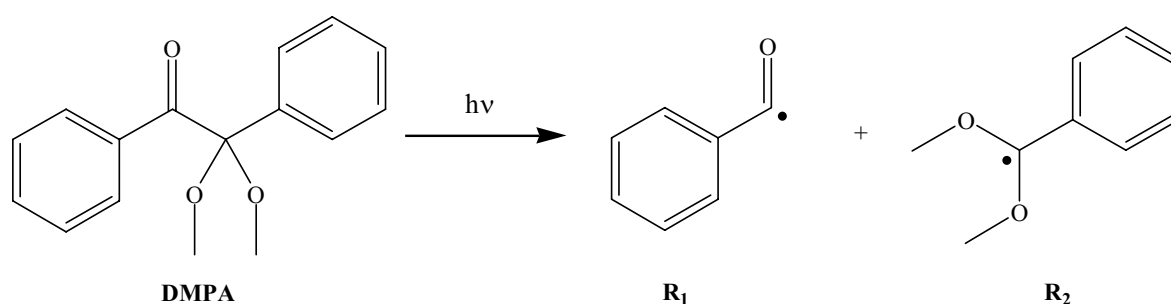
Such an ideal photoinitiator allows for the determination of the CLD of the termination rate coefficient from a single SP-PLP experiment. A good survey on several photoinitiators and their decomposition under UV irradiation has been given by Gruber.^[210] Investigations by Külpmann revealed that 2-methyl-4-(methylthio)-2-morpholino-propiophenone, MMMP, is a close-to-ideal photoinitiator which rapidly decomposes into two propagating free-radical species,^[211,212] as was confirmed by Vana et al. via ESI-MS studies.^[213] The decomposition products of the MMMP decay are shown in Scheme 5-2.



Scheme 5-2: Decomposition reaction of 2-Methyl-4-(methylthio)-2-morpholinopropiophenone (MMMP).

In the present work, MMMP was used within all SP-PLP-ESR experiments, as it allows for close-to-monodisperse growth of radicals, ensuring that termination events take exclusively place between radicals of almost the same size (within Poisson broadening). However, MMMP could not be used for studies into aqueous monomer solutions because of its poor solubility and side-reactions in protic solvents.^[199,214]

In the past, the photoinitiator 2-dimethoxy-2-phenylacetophenone (DMPA) has extensively been used for SP-PLP-experiments,^[144,178] although it does not fully meet the requirements stated above. As depicted in Scheme 5-3, DMPA decomposes into two radical species, R_1 and R_2 (see ref.^[215] for details), which are distinctly different in their characteristics. Whereas the benzoyl radical R_1 is highly efficient in adding to a monomer molecule, the acetyl radical R_2 does not noticeably add to monomer in the dark-time period after the pulse, but may recombine with radicals and thus behaves like an inhibitor. The difference in reactivity of the two fragments originates from the stabilizing effect of the phenyl group, where the radical center is delocalized.



Scheme 5-3: Decomposition reaction of 2-dimethoxy-2-phenylacetophenone (DMPA).

The poor initiating activity of R_2 has first been described by Fischer et al.^[215] and has also been demonstrated via MALDI and ESI experiments by the Davis group.^[216,217] In SP-PLP, the simultaneous initiation and inhibition activity of the DMPA-derived species results in a rather peculiar behavior: The monomer conversion vs. time traces measured at different initial DMPA contents, but otherwise identical reaction conditions, intersect each other. This behavior provides access to measuring the chain-length dependence of the termination rate coefficient.^[134] At low radical concentrations the impact of the poorly initiating primary radicals is, however, negligible and the resulting $\langle k_t \rangle$ values are close to true average termination rate coefficients, although non-ideal initiator behavior is not contained in the kinetic scheme used for data analysis.^[218] DMPA was used for SP-PLP-NIR studies into polymerizations in aqueous solution within the thesis in hand. The required low free-radical concentrations were ensured by suitably selecting initiator concentration and laser pulse energy.

In PLP-SEC, the non-ideality of DMPA does not invalidate the experimental technique, as the inhibiting fragment may only increase the amount of background (non-PLP) polymer.

Nevertheless, mostly MMMP was used for experiments on BA. However, DMPA had to be applied for MAA in water due to the arguments given above. In case of NVP, mostly Darocur was employed because of its better solubility.

5.5.2 Reaction conditions

The SP-PLP-NIR technique allows for measurements in a wide temperature and pressure range up to fairly high degrees of monomer conversion. The signal-to-noise ratio scales with the conversion per pulse. Thus, high propagation rates and low termination rates are preferred. As k_p increases and k_t decreases with pressure, experiments under high pressure conditions allow for higher monomer consumption per pulse and hence for improved S/N quality. In principle, the experimental setup is suitable for measurements in the range from 5 to 3000 bar. A lower limit of 5 bars is required to ensure that the internal cell is properly fixed within the high-pressure cell and to promote heat transfer. Increasing temperature also allows for better S/N ratios in SP-PLP-NIR experiments. Effects as large as the ones induced by pressure variation may however not be achieved. Therefore, most experiments have been performed at 40 to 60 °C. In principle, the lowest feasible temperature is slightly above 0 °C (at even lower temperatures, condensing water on the high-pressure window surface hampers spectroscopic investigations). The upper limit is given by the individual temperature at which the monomer under investigation undergoes self-initiation or the photoinitiator may thermally decompose. To be on the safe side, polymerization temperatures below 80 °C should be used. SP-PLP-NIR experiments were usually carried out up to conversions at which the reaction mixture turns heterogeneous.

The PLP-ESR technique so far only allows for measurements at ambient pressure. The accessible temperature range is from about -100 to 80 °C. The lower limit is given by the melting point of the reaction solution. The S/N ratio is dependent on (i) the amount of radicals and (ii) the sensitivity of the ESR setup (see Chapter 5.4.2). High initial radical quantities are achieved by using photoinitiator concentrations in the range 0.01 to 0.02 mol·L⁻¹ and large sample volumes. The maximum volume is given by the laser-illuminated area as is depicted in Scheme 5-1. However, in most cases, smaller volumes, of 0.05 to 0.2 mL, are used, as the maximum amount of reaction solution is usually determined by sample polarity which affects the resonator quality and thus the tunability of the ESR spectrometer. To reduce sample

polarity, most experiments in this work have been carried out in toluene solution. Furthermore, the pseudo-stationary radical concentration and thus the signal-to-noise quality of the ESR spectra decreases toward increasing k_t .

A temperature range of 2 to 80 °C could be covered in PLP-SEC experiments on aqueous solution polymerizations. Even lower temperatures, down to -10 °C, were accessible within the BA experiments. Temperatures below 25 °C should be used for experiments on AA and BA for reducing transfer-to-polymer reactivity (see Chapter 10.3). Furthermore, high LPRRs (100 Hz) are preferable for obtaining well structured MWDs from experiments on acrylate monomers. However, also low LPRRs were used in some cases with the intention of studying transfer reactions. Experiments on ionized MAA were limited by the solubility of sodium methacrylate being about 45 wt.% in pure water. LPRRs and initiator concentrations (0.1 to 10 mmol·L⁻¹) were chosen such as to obtain well pronounced PLP-structures. Laser pulse repetition rates of 10 to 40 Hz were typically used for experiments on MAA and NVP. A suitable number of pulses had to be selected for each experimental condition to produce an amount of polymer being sufficient for SEC analysis (typically not above 5 % monomer-to-polymer conversion).

More details on the selection of experimental conditions are given together with the experimental results the subsequent chapters.

5.6 Data fitting procedures

To derive kinetic parameters from integrated rate laws, the corresponding equations are fitted to the time-resolved concentration data via non-linear curve fitting procedures by using a numerical iteration algorithm (Levenberg-Marquardt)^[219,220] in which the parameters are refined by a least squares method. Fitting of SP-PLP-NIR traces was performed using the software MATLAB 6.1, Release 12 (Mathworks). Configuration and global data fitting parameters are given in the appendix of the PhD thesis of Junkers.^[97] All other regressions were done using ORIGIN6.1 or ORIGIN7.0 (OriginLab).

5.7 Error estimates

Pressure

The high-pressure precision manometer of class 0.1 offers an accuracy of 0.1 % of the maximum pressure, resulting in an error of ± 3 bar.

Temperature

In experiments using the high-pressure cell, measurement of the reaction temperature in the direct vicinity of the sample volume is achieved via a sheathed thermocouple to better than ± 0.3 K. The PID controller regulates the temperature within ± 0.2 K. This results in an accuracy of ± 0.5 K.

In case cuvettes with a heating jacket are used an error of ± 0.5 K is assumed. Temperature accuracy should be lower when normal rectangular cells are employed. To limit temperature changes during PLP, such cuvettes were only used in cases with short measurement times, i.e. where pulse numbers were small and LPRRs were moderate or high. Temperature accuracy is estimated to be ± 1 K.

Within the ESR technique, the PID controller regulates temperature within ± 0.1 K. Temperature is measured in the nitrogen gas flow with a thermocouple at the lower part of the resonator cavity. To ensure complete temperature equilibration, all samples are positioned into the gas flow up to 10 min prior to recording the spectra. The absolute error is thus estimated to be ± 1 K at most.

Concentrations

For preparing the reaction solutions, an analysis balance (Sartorius) with an accuracy of ± 0.05 mg and volumetric flasks with an uncertainty in volume of 1 % were used. Concentrations were extrapolated to reaction conditions using reported density data. The overall error is estimated to be below 3 %.

Monomer concentration from FT-NIR

The FT-IR/NIR spectrometer used in this work, with the optical configurations detailed in Chapter 4.3, allows for quantitative evaluation of absorbances measured in the range from 0.02 to 0.8 absorbance units. The lower boundary is determined by the S/N ratio and the upper limit by non-linearity of the detector. For absorbance in the above-mentioned range, the

deviation due to non-linearity is less than 3 %.^[221] Further errors are introduced by the apodisation function and the mode of phase correction in the Fourier transformation step. Uncertainties in the determination of the baseline result in an error of less than ± 3 % for the integrated absorbance (which is used for quantitative evaluation). Due to an imperfect determination of the peak maximum, the uncertainty is raised to ± 5 % in the evaluation of half-band integrals.

Error in k_t

The accuracy of k_t deduced from SP-PLP-NIR and SP-PLP-ESR is highly dependent on signal quality, complexity of polymerization scheme, and type of data evaluation. Thus, the corresponding errors are given with the individual results. However, it is expected that the error does not exceed ± 50 % for most polymerizations under investigation in this work.

Error in k_p

The error of the PLP-SEC measurements is composed of several errors: The error in monomer concentration, the error induced by the SEC calibration procedure via Mark-Houwink coefficients, and the errors induced by SEC broadening. These errors add up to a total of ± 15 % for the propagation rate coefficients of this work.

6 Propagation Kinetics in Methacrylic Acid Polymerization

Polymerization in aqueous phase is of enormous technical relevance. Thus, there is an urgent demand for reliable rate coefficients of free-radical polymerizations in aqueous solution. In the past, aqueous-phase PLP-SEC experiments suffered from difficulties associated with accurately measuring the MWD of water-soluble polymers.^[66,70] Further problems resulted from propagation in aqueous solution being very fast which is particularly true for AA.^[67–69] Moreover, transfer-to-polymer reactions may hamper PLP-SEC on AA as well as high sample viscosities at elevated monomer concentrations. Hence, successful PLP-SEC experiments were limited to temperature and monomer concentration ranges of 2 to 25 °C and 1 to 40 wt.% in water, respectively.^[68] Such restrictions are not met with MAA as this monomer is not susceptible to transfer-to-polymer reactions, sample viscosity is no limiting factor and macroradical chain length may be readily controlled by laser pulsing. Thus, k_p for MAA may be studied within wide ranges of both, temperature and monomer concentration. Such investigations may allow for obtaining a fundamental mechanistic understanding of propagation in aqueous phase.

Studies of Kuchta et al.^[66] already revealed a strong acceleration of k_p toward lower c_{MAA} . During polymerization, monomer is continuously transformed into polymer reducing the ratio of monomer to water within the reaction solution. Consequently, the question arises whether k_p for MAA polymerization in water is independent of conversion, as is usually assumed for bulk systems,^[16] or increases toward higher conversion due to changes in solvent composition.

Lacík et al.^[69] showed in their pioneering study that k_p of AA may strongly depend on the degree of monomer ionization, α_D . Thus, k_p of MAA may not only be studied within wide ranges of temperature and monomer concentration but also α_D is of particular interest.

The dependence of k_p on MAA concentration in water and on temperature will be discussed in Chapter 6.1. Subsequently, the variation of k_p with conversion for non-ionized MAA will be outlined (Chapter 6.2). The dependence of k_p on α_D for different monomer concentrations and temperatures is shown and discussed in the last section (Chapter 6.3).

The studies detailed in this chapter were carried out in cooperation with Prof. Sabine Beuermann, Dr. Silvia Kukučková, Dr. Igor Lacík and Lucia Učňová. Part of this work has already been published in refs.^[15,72–74]

6.1 Propagation kinetics of non-ionized MAA at low conversions

PLP-SEC experiments for determination of k_p were carried out at MAA concentrations of $c_{\text{MAA}} = 1, 2, 3, 5, 10, 15, 20, 30, 40, 45, 60,$ and 100 wt.% and at ambient temperature as well as at 40, 60, and 80 °C. That the consistency criteria for reliable PLP-SEC experiments^[8] were met, was verified by using several initiator concentrations and by carrying out part of the PLP experiments under variation of LPRR with all other PLP parameters being kept constant. The number of applied laser pulses was varied such as to keep monomer conversion below 5 %. Only within the PLP experiments at the lowest MAA concentrations, for c_{MAA} between 1 and 3 wt.%, monomer conversion was allowed to be as large as 10 % to provide a sufficient amount of polymer for SEC analysis.

Representative molecular weight distribution (MWD) curves and associated first-derivative curves of poly(MAA) samples from PLP of MAA in aqueous solution are shown in Figure 6-1 and Figure 6-2. The PLP structure is clearly seen which demonstrates that (i) the PLP conditions have been sensibly chosen and (ii) aqueous-phase SEC is obviously capable of resolving the PLP-induced structure of the MWD. Shown in Figure 6-1 are MWDs of poly(MAA) samples obtained by PLP at 25 °C with an LPRR of 20 Hz for aqueous solutions containing 5 and 40 wt.% MAA as well as for bulk MAA polymerization. Primary and secondary POIs on the low molecular weight side of PLP-induced components contributing to the MWD (full lines) are clearly identified from maxima in the associated first-derivative curves (dotted lines). Figure 6-2A presents examples of MWDs measured on PLP-produced poly(MAA) samples prepared at temperatures from 20 to 80 °C. The associated first-derivative curves are plotted in Figure 6-2B. The data in Figure 6-2 refers to $c_{\text{MAA}} = 15$ wt.%, $c_{\text{DMPA}} = 2 \cdot 10^{-3} \text{ mol} \cdot \text{L}^{-1}$ and to an LPRR of 20 Hz. Toward higher MAA concentration (Figure 6-1) and toward higher temperature (Figure 6-2), the amount of high-molecular-weight “back-ground” poly(MAA) increases. For the PLP conditions of Figure 6-1 and Figure 6-2 this high-molecular-weight material, however, does not affect the quality by which the inflection point positions may be determined.

The large body of k_p data for non-ionized MAA in water is not shown for purpose of thesis length but is collated in Tables 1 to 3 in ref.^[72] Within those tables, the excellent reproducibility of k_p measurements is illustrated by the various duplicate experiments. Furthermore, the ratio of the molecular weights at the first and second POI, M_1/M_2 , is always close to 0.5 fulfilling an important consistency criterion for k_p evaluation.^[8]

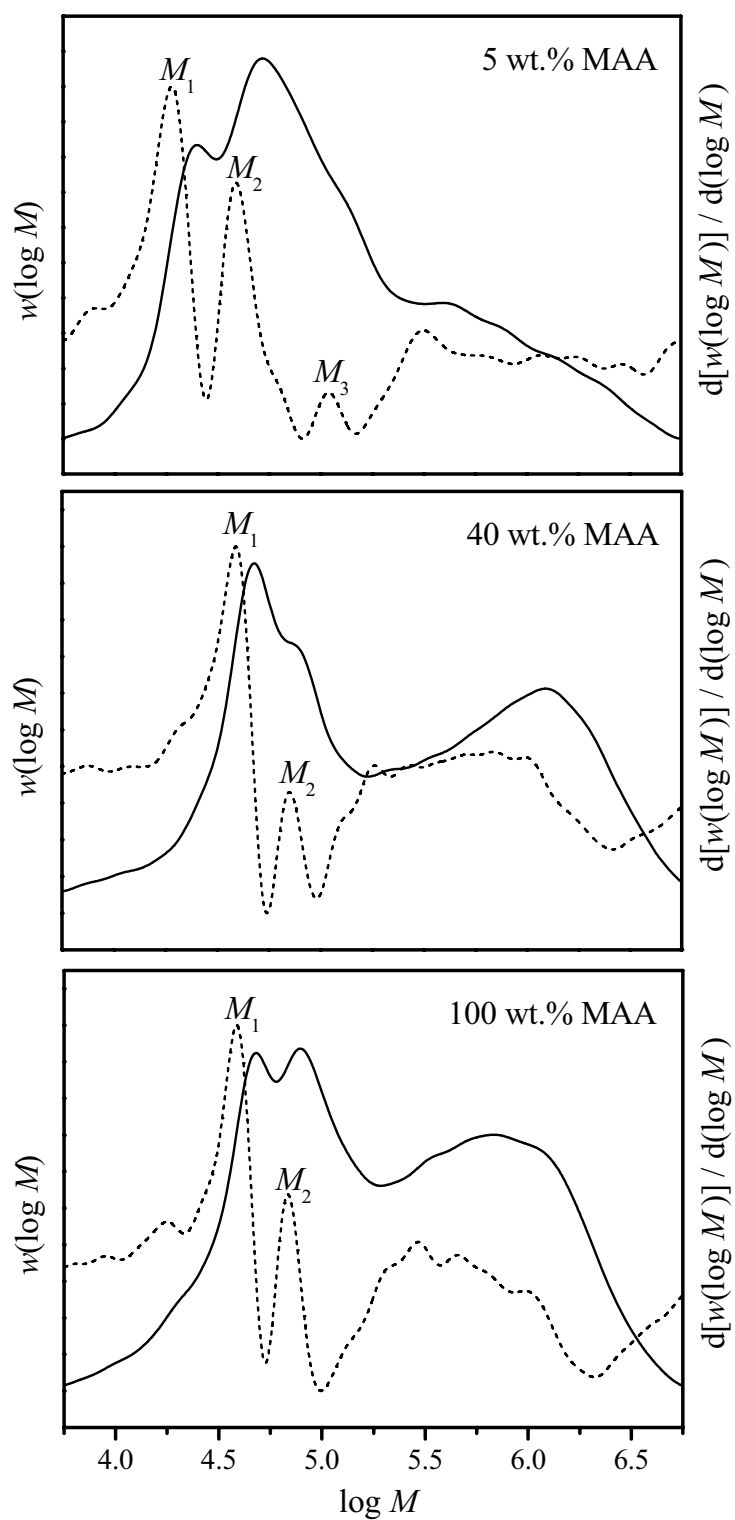


Figure 6-1: MWD (solid lines) and associated first-derivative curves (dashed lines) obtained from polymerizations of MAA dissolved in water at two MAA concentrations and from bulk MAA polymerization at 25 °C and an LPRR of 20 Hz.

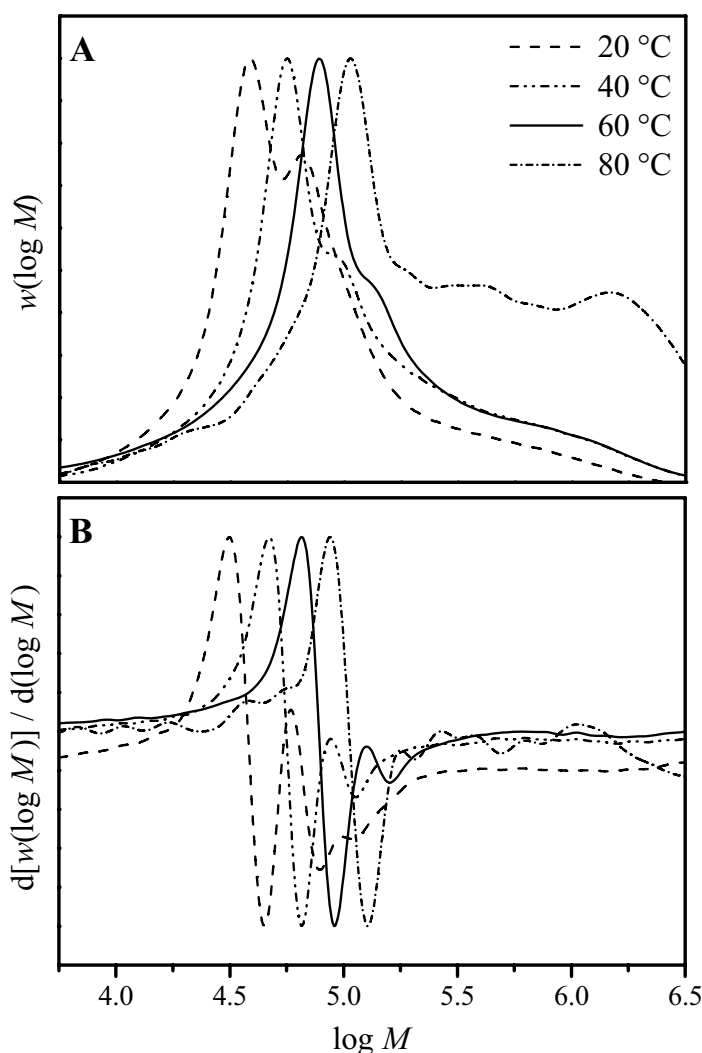


Figure 6-2: Molecular weight distributions (A) and associated first-derivative curves (B) obtained from PLP on 15 wt.% MAA in aqueous solution at various polymerization temperatures ($c_{\text{DMPA}} = 2 \cdot 10^{-3} \text{ mol} \cdot \text{L}^{-1}$, $f_L = 20 \text{ Hz}$)

Plotted in Figure 6-3 is k_p as a function of c_{MAA} for 25 °C. The extended concentration range of the data illustrates the enormous advantage of studying MAA rather than AA propagation. k_p for AA in aqueous solution could only be measured up to about 40 wt.% of monomer in water. The AA literature values^[68] for k_p are plotted in the insert to Figure 6-3. The maximum in apparent k_p which is found with AA aqueous-phase polymerization at monomer concentrations between 1 and 3 wt.% is not seen with MAA. The origin of the peculiar k_p maximum in aqueous-phase polymerization at low AA concentrations is not yet fully understood. It may reflect preferential solvation at low monomer concentrations in systems with strong intermolecular interactions.^[222] The different behavior at low monomer

concentration of apparent k_p for AA and MAA may be due to the fact that water is a better solvent for poly(AA) than for poly(MAA).^[223–225] Thus, an increased local monomer concentration may occur in the vicinity of growing MAA macroradicals. Another explanation for the maximum in apparent k_p of AA may be that AA forms complexes with polymer molecules and macroradicals, thus reducing the AA concentration that is available for propagation, which effect may result in a lowering of apparent k_p . As the amount of such “adsorbed” monomer is small, this effect may only be detected at very small monomer concentrations, as is the case with AA.^[68] MAA may be less efficient in producing such tightly adsorbed monomer layers. Alternative explanations for the k_p maximum assume the formation of self-assembled monomer structures.^[226] None of these “explanations” is fully convincing. The assumption that an “adsorbed” monomer layer is responsible for the “maximum k_p anomaly” at low AA contents, however, appears to be the most likely one. As no maximum in k_p vs. c_M occurs in low-concentration aqueous MAA solutions.

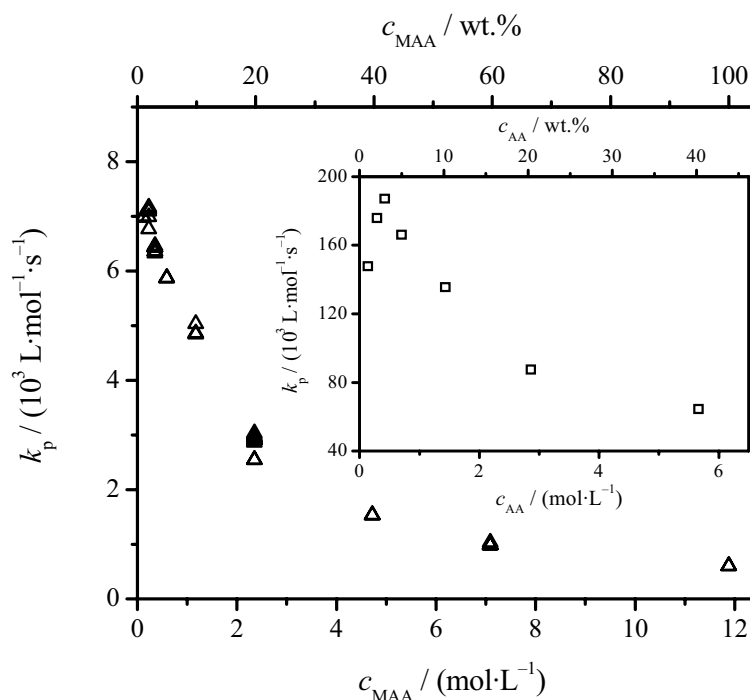


Figure 6-3: Variation of k_p with MAA concentration in aqueous solution at 25 °C. The insert shows k_p values for the aqueous phase polymerization of AA at 25 °C (values taken from ref.^[68]).

Toward higher monomer concentration, both MAA and AA show a pronounced drop in apparent k_p . This strong effect is not or not significantly dependent on the absolute size of k_p ,

which differs for the two monomers by more than one order of magnitude, as can be seen from the ordinate scales in Figure 6-3. The k_p values, e.g., at 25 °C and at a monomer concentration of $1.4 \text{ mol}\cdot\text{L}^{-1}$, are around 4 000 and 140 000 $\text{L}\cdot\text{mol}^{-1}\cdot\text{s}^{-1}$ for MAA and AA, respectively. The resulting ratio of apparent AA and MAA k_p values is 35, which number is close to the ratios observed for k_p at ambient temperature of acrylate and methacrylate monomers (with identical alkyl ester moiety) in the organic bulk phase.^[16]

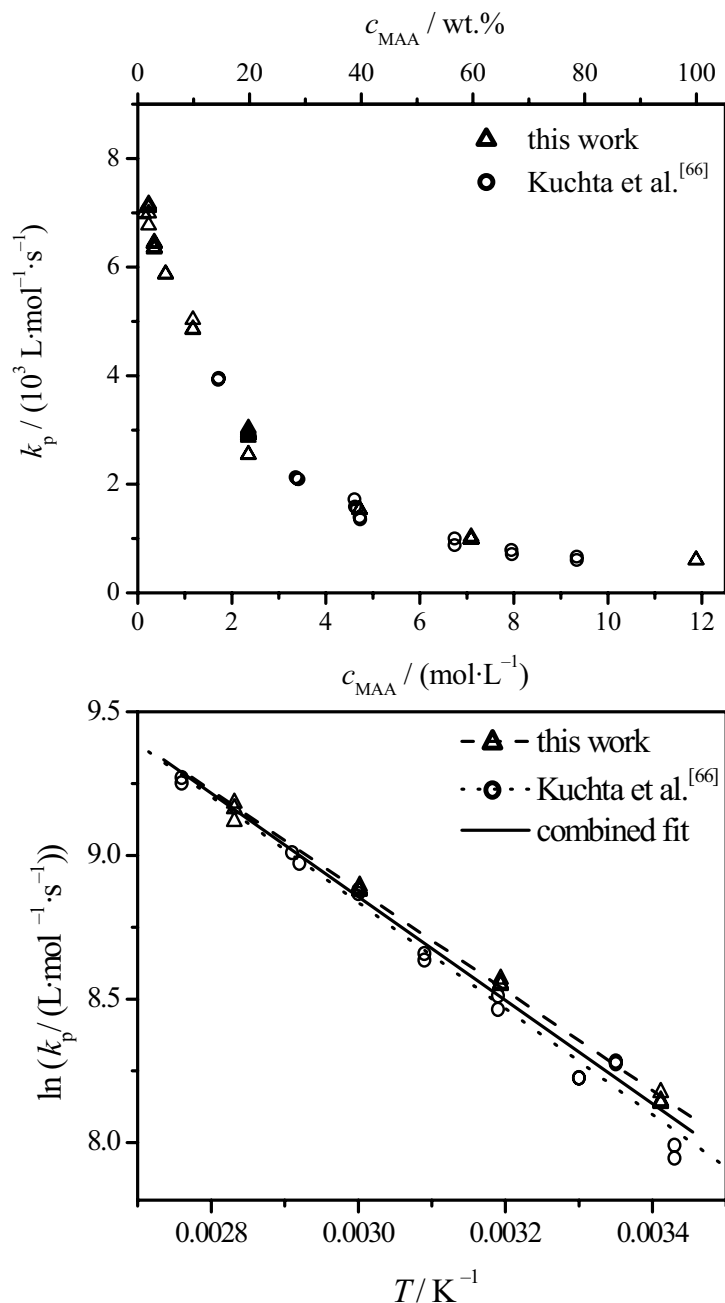


Figure 6-4: Comparison of k_p for MAA polymerization in aqueous phase with data reported by Kuchta et al.^[66] Variation of k_p with MAA concentration at 25 °C (upper figure); temperature dependence of k_p for 15 wt.% MAA (lower figure).

Before discussing the k_p data in more detail, the values determined in this work have to be compared with the earlier results by Kuchta et al.^[66], who reported one data set for both the dependence of k_p on MAA concentration (at 25 °C) and the dependence of k_p on temperature (for $c_{\text{MAA}} = 15$ wt.%). Figure 6-4 illustrates the excellent agreement of k_p data from the two sources, which is particularly pleasing, as Kuchta et al.^[66] employed esterification of poly(MAA) to poly(MMA) with subsequent conventional SEC analysis of the polymer using THF as the eluent, whereas aqueous-phase SEC without preceding polymer modification has been applied in the present study. The almost perfect agreement of the data demonstrates that poly(MAA) esterification does not significantly affect the MWD, whereas changes of the MWD occur in esterifying poly(AA), as has been shown in ref.^[67]. As all k_p values within this chapter have been determined according to the same procedure as used for measuring the data in Figure 6-4, the agreement in Figure 6-4 suggests that the entire set of k_p data may be considered reliable. The full data set will now be discussed with particular emphasis on the dependence of k_p on MAA monomer concentration and on polymerization temperature. One example for each of these dependencies has already been reported in ref.^[66] (see Figure 6-4), where however no attempt was made to provide a detailed kinetic interpretation.

The most striking feature of MAA k_p is the enormous reduction toward high c_{MAA} . Within the preceding study into aqueous-phase k_p of acrylic acid, the range of monomer concentrations was restricted.^[68] It appeared justified to assign the observed variation in apparent k_p up to 40 wt.% AA, by about a factor of three, primarily to changes in “local” monomer concentration. The wide concentration range, from 1 wt.% up to bulk polymerization, that is accessible in aqueous-phase polymerization of MAA, however, demonstrates that the assumption of the “true” propagation rate coefficient, $k_{p,\text{true}}$, being constant would require that “local” monomer concentration differs from overall c_{MAA} by up to a factor of ten. Such enormous differences between “local” and overall monomer concentration are very unlikely, as they would require MAA at low monomer concentrations to be almost exclusively located in the immediate vicinity of polymeric species with these monomer-saturated macromolecules and macroradical coils being contained in almost pure water. No reason is seen for such an effect, as both MAA and water are capable of interacting via hydrogen bonds and thus are too similar as to undergo any such poly(MAA)-induced separation in the liquid state. Specific association of MAA to poly(MAA) would also be in conflict with the good solubility of poly(MAA) in aqueous phase and it is hard to imagine, that any kind of de-mixing would become dominant toward very low c_{MAA} . Moreover, changes of k_p resulting from specific

interactions between poly(MAA) and MAA, which are not or not to a significant extent occurring between poly(MAA) and water molecules, should give rise to differences in the dependence of k_p on c_{MAA} for different temperatures. This is obviously not what the measured data tell, as can be seen from a comparison of apparent k_p values for 25 and 80 °C. In Figure 6-5, reduced propagation rate coefficients, $k_p/k_{p,\text{max}}$, (with $k_{p,\text{max}}$ referring to the k_p value extrapolated for $c_{\text{MAA}} = 0$) are plotted vs. c_{MAA} . Within the region of the steep decrease of k_p , up to 5.11 mol·L⁻¹ (45 wt.% MAA), where data for both temperatures are available, $k_p/k_{p,\text{max}}$ for 25 and 80 °C may be adequately represented by a single line (dotted line in Figure 6-5, which actually is an exponential function). This observation may be taken as a strong argument against the occurrence of any significant selective enhancement of either monomer or water in the immediate vicinity of poly(MAA) molecules or macroradicals. Moreover, this finding is in conflict with assuming special types of association, e.g. dimerization, of MAA molecules being responsible for the dramatic drop in apparent k_p upon enhancing c_{MAA} .

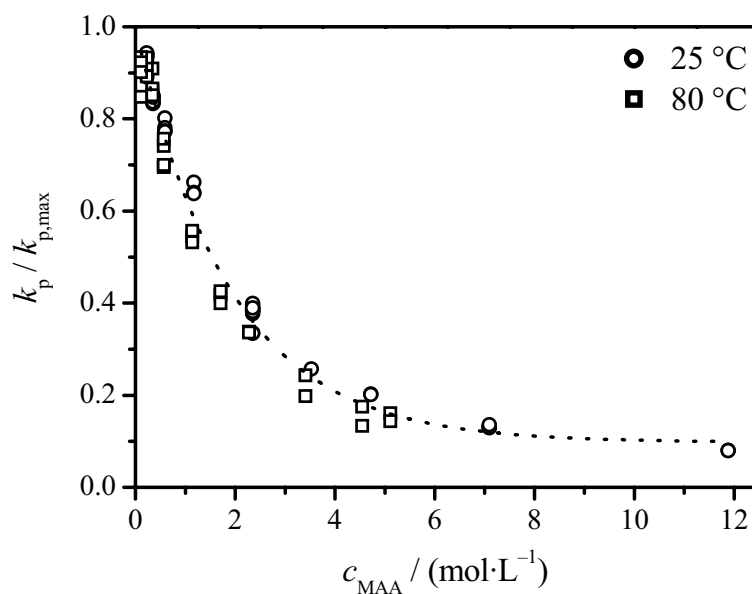


Figure 6-5: Dependence of reduced propagation rate coefficients, $k_p/k_{p,\text{max}}$, (with $k_{p,\text{max}}$ referring to the k_p value extrapolated for a MAA concentration of zero) on overall MAA concentration at 25 and 80 °C for MAA polymerization in aqueous phase ($k_{p,\text{max}}$ values are 7 600 L·mol⁻¹·s⁻¹ at 25 °C and 22 840 L·mol⁻¹·s⁻¹ at 80 °C).

To summarize the discussion on local vs. overall monomer concentration: Both quantities may differ to some extent with this potential difference, however, being far too small to

account for the variation seen with the primary experimental quantity $k_p \cdot c_M$. Thus, to a good approximation, $c_{M,loc}$ may be identified with $c_{M,ov}$ and the propagation rate coefficient is significantly enhanced toward increasing MAA concentration, as a consequence of a genuine kinetic effect.

A kinetic explanation for the dependence of k_p on c_{MAA} may assume, that the activation energy, $E_a(k_p)$, varies as a function of water content. Via quantum-chemical calculations at different levels of theory, Thickett and Gilbert^[19] recently demonstrated that the introduction of a water solvent field lowers the activation energy for addition of AA to an “acrylic acid radical” by about $10 \text{ kJ} \cdot \text{mol}^{-1}$ relative to the associated gas-phase value, whereas $E_a(k_p)$ in a toluene solvent field is not significantly different from the gas-phase value. One might argue, that $E_a(k_p)$ is also varied in MAA polymerizations, with the activation energy being smaller at higher water content, thus enhancing k_p toward lower c_{MAA} . This possibility cannot be tested on the basis of the Thickett and Gilbert paper,^[19] as the solvent field of the acid monomer has not been considered there. Inspection of the activation energies deduced from the apparent k_p data should, however, allow for the detection of a variation of $E_a(k_p)$ with c_{MAA} and thus with water content.

The Arrhenius plots for different monomer concentrations are presented in Figure 6-6. Depicted in the upper part (Figure 6-6A) are the k_p data for MAA concentrations of and below 15 wt.%. Figure 6-6B shows k_p for MAA concentrations of and above 15 wt.% including k_p for bulk MAA polymerization. Also contained in Figure 6-6B are the bulk MAA k_p values reported by Beuermann et al.^[174], which are in close agreement with the data of the present study. The Arrhenius plots for the different MAA concentrations, in particular the ones for c_{MAA} of and above 5 wt.%, are more or less parallel lines, which says that $E_a(k_p)$ is insensitive toward MAA concentration. The observed variation of apparent k_p with c_{MAA} thus results from changes in the pre-exponential factor, $A(k_p)$. Only at the lowest monomer concentrations, below 5 wt.% MAA, the slope of the Arrhenius lines appears to be somewhat steeper. This may indicate, that a weak “low-concentration anomaly”, as with AA, occurs also with MAA. For AA in aqueous phase, the numbers deduced for $E_a(k_p)$ at low monomer concentrations, e.g. below 10 wt.%, are clearly above the activation energies obtained at higher c_{AA} .^[68] The variation with c_{MAA} of $E_a(k_p)$, depicted in Figure 6-6A, is too weak as to allow for deducing any firm conclusion on such a special behavior of apparent k_p for MAA in highly dilute aqueous solution. The subsequent discussion of Arrhenius parameters will be restricted to

MAA concentrations between 5 and 100 wt.%, in which extended region k_p drops by about one order of magnitude.

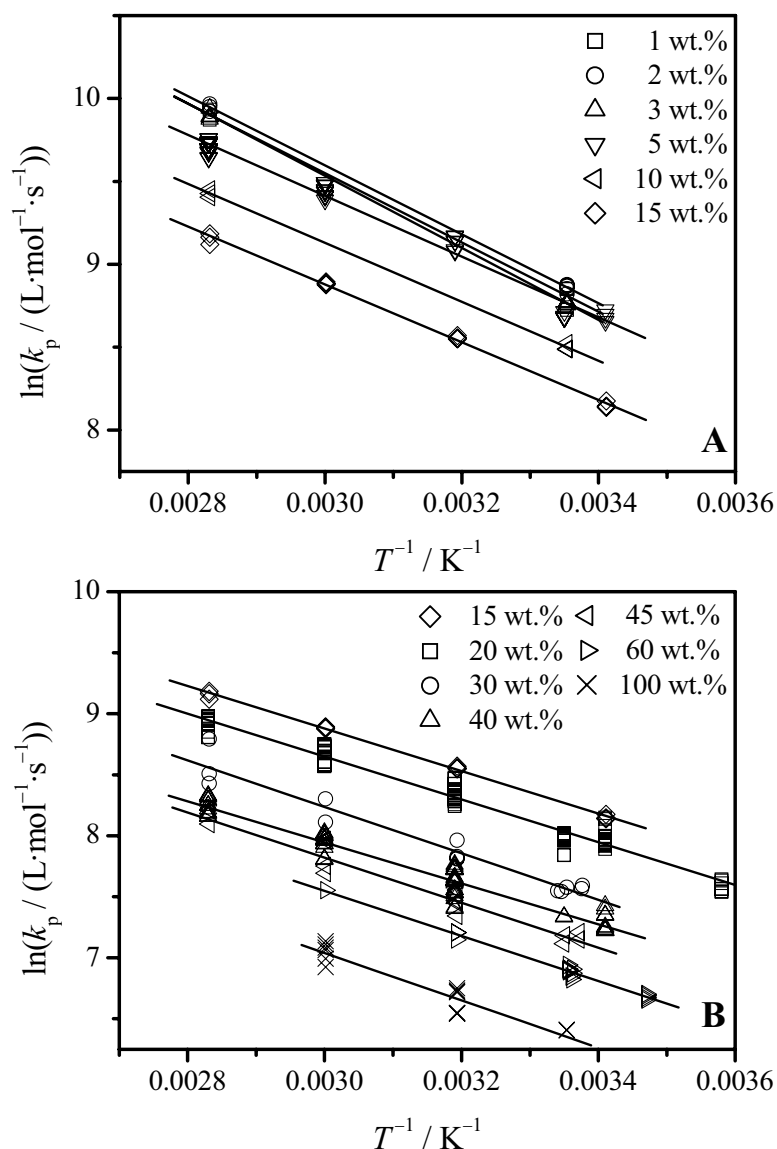


Figure 6-6: Arrhenius plots of k_p for MAA polymerizations in aqueous solution at MAA concentrations from 1 to 15 wt.% (Figure 6-6A) and from 15 to 100 wt.% (Figure 6-6B); bulk polymerization data reported by Beuermann et al.^[174] are included in Figure 6-6B.

Plotted in Figure 6-7 are the 95 % joint confidence intervals (JCIs) associated with the Arrhenius plots in Figure 6-6. The JCIs were estimated according to the procedure suggested by van Herk assuming constant relative uncertainties of the individual data points.^[227] The JCIs for the two correlated Arrhenius parameters, $E_a(k_p)$ and $A(k_p)$, have been constructed for the MAA weight percentages (indicated by the number at each JCI) for which k_p data is

available for at least three temperatures. The size of the individual JCIs reflects the number of underlying k_p data and the scatter of these data points. The JCI for MAA bulk polymerization is rather extended which results from the fact that three types of data contribute to the relatively small overall number of data points: data from PLP experiments at 10 Hz and at 20 Hz carried out within the present study and data from ref.^[174]. Irrespective of the significant extension of some of the JCIs, the data in Figure 6-7 clearly supports the observation from Figure 6-6, that the activation energy is more or less insensitive toward MAA concentration, whereas the Arrhenius pre-exponential factor is strongly diminished toward larger c_{MAA} .

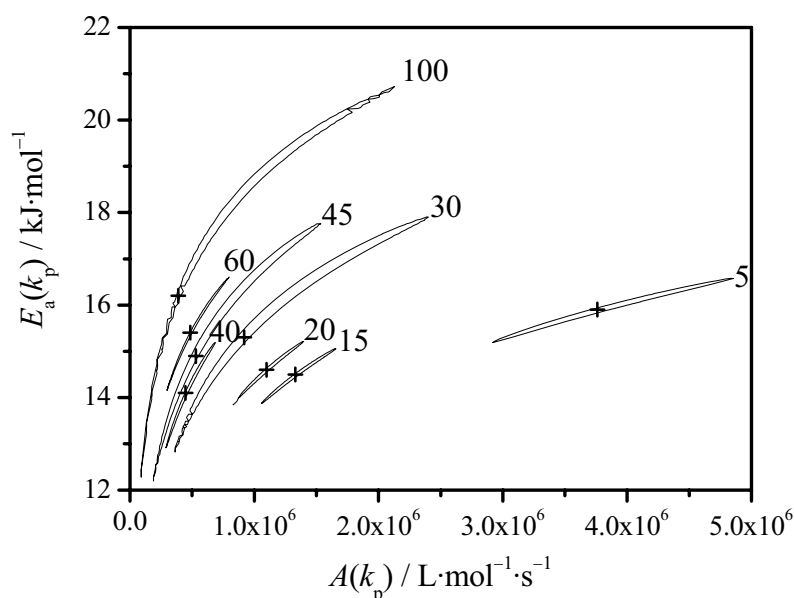


Figure 6-7: 95 % Joint confidence intervals (JCIs) associated with the Arrhenius plots in Figure 6-6 for k_p of MAA in aqueous solution at different MAA weight percentages (indicated by the numbers at the JCIs) and of MAA bulk polymerization. Confidence intervals have been constructed only for MAA concentrations with k_p being available for at least three temperatures.

The activation energies and pre-exponentials listed for the individual MAA concentrations in Table 6-1 were determined from fits to the logarithmic form of the Arrhenius equation. The activation energy shows a minor, but non-systematic variation with MAA concentration. A mean value of $E_a(k_p) = (15.2 \pm 0.8) \text{ kJ}\cdot\text{mol}^{-1}$ encompasses the entire set of individual activation energies obtained in the extended range between dilute aqueous solution containing 5 wt.% MAA and MAA bulk polymerization. Within this range of MAA contents, the pre-exponential, $A(k_p)$, decreases by about one order of magnitude. Only $A(k_p)$ for 40 wt.% MAA

in water seems to not fit in the series of pre-exponential factors. The low frequency factor is, however, associated with a low $E_a(k_p)$ and the joint confidence ellipsoid for 40 wt.% MAA is located between the JCI's for 30 and 45 wt.% of monomer (see Figure 6-7). Thus, the Arrhenius parameters for 40 wt.% of MAA in water are, under consideration of experimental error, in line with the observation of a monomer concentration independent activation energy and a pre-exponential factor which decreases toward higher MAA content.

Table 6-1: Arrhenius parameters, $E_a(k_p)$ and $A(k_p)$, for k_p of MAA in aqueous solution at different concentrations and in bulk.

c_{MAA} (wt.%)	$E_a(k_p)$ (kJ·mol ⁻¹)	$A(k_p)$ (10 ⁶ L·mol ⁻¹ ·s ⁻¹)	temperature interval (°C)
5	15.8 ± 0.3	3.64	20 – 80
15	14.5 ± 0.4	1.33	20 – 90
20	14.6 ± 0.3	1.10	6 – 80
30	15.8 ± 1.1	1.13	23 – 80
40	14.0 ± 0.5	0.43	20 – 80
45	15.3 ± 1.1	0.63	23 – 80
60	15.3 ± 0.5	0.48	15 – 60
100	16.1 ± 1.6	0.38	25 – 60

The results in Figure 6-6 and Figure 6-7 together with the data in Table 6-1 unambiguously show that a variation of $E_a(k_p)$ with MAA content cannot be made responsible for the enormous drop in k_p toward higher c_{MAA} . There is definitely no indication of any lowering in activation energy toward smaller c_{MAA} as would be required for assigning the observed changes in k_p to a variation in $E_a(k_p)$. With reference to the analysis presented by Thickett and Gilbert^[19] (for AA), one would assume very similar effects of MAA and of water solvent fields on the activation energy of the MAA propagation rate coefficient.

The preceding analysis demonstrates that the pronounced changes in k_p which accompany the gradual replacement of an aqueous solvent environment by an MAA one have to be assigned to effects operating on the pre-exponential factor. Although $E_a(k_p)$ and $A(k_p)$ are correlated parameters, due to their simultaneous determination from experimental k_p data measured at various temperatures, they are independent physical quantities, which may be separately accessed by transition state theory, e.g., in conjunction with *ab initio* quantum-chemical calculations, as has been illustrated for propagation reactions in free-radical polymerization by Heuts et al.^[17] The pre-exponential is essentially determined by the geometry of the rotating groups in the reactants and in the transition state (TS) and by the rotational potentials of the relevant internal (hindered) motions in the TS,^[17] as has been demonstrated for $A(k_p)$ by Heuts et al.^[18]

Applying the knowledge from transition state theory to the k_p data of MAA in bulk and in aqueous phase leads to the conclusion, that replacing MAA by H₂O modifies the environment of the transition structure for addition of MAA to a poly(MAA) radical such that the chain-end region experiences a higher degree of rotational freedom. Or, stated otherwise, gradually replacing H₂O by MAA enhances the friction felt by the relevant degrees of freedom of the transition structure for propagation. Along this line of arguments, it appears rewarding to compare the Arrhenius parameters, $E_a(k_p)$ and $A(k_p)$, of MAA and MMA bulk polymerizations:

	$E_a(k_p)$ (kJ·mol ⁻¹)	$A(k_p)$ (10 ⁶ L·mol ⁻¹ ·s ⁻¹)
MAA	16.1	0.38
MMA ^[16]	22.4	2.67

The numbers for $E_a(k_p)$ demonstrate that MAA does not behave like a typical methacrylate monomer, in that the activation energy is clearly below the corresponding MMA value. $E_a(k_p)$ values in the range 21 to 23 kJ·mol⁻¹ are characteristic for the entire family of alkyl methacrylates, but also for several functionalized and cyclic methacrylates.^[16] The lower $E_a(k_p)$ of MAA most likely results from effects of hydrogen-bonded interactions on the reaction barrier of the propagation process. As $E_a(k_p)$ of MAA does not change upon replacing MAA by H₂O (see Table 6-1), hydrogen-bonded interactions with H₂O molecules appear to

have a similar effect on the reaction barrier as have MAA molecules. The change in $E_a(k_p)$ seen in going from non-hydrogen-bonded systems, such as alkyl methacrylates, to a hydrogen-bonded one, such as MAA polymerization, is consistent with the trend described in ref.^[19] for propagation of AA in an H₂O and in a toluene environment.

As an even more remarkable feature, the comparison of Arrhenius parameters for MAA and MMA reveals a large difference in the pre-exponential factors: $A(k_p)$ for MMA exceeds $A(k_p)$ for MAA by about one order of magnitude, which is surprising in view of the fact that the two monomers (and thus also the repeat units of the polymeric species) are of similar size. On the other hand, the $A(k_p)$ values obtained for MAA in dilute aqueous solution, e.g., in the 5 to 15 wt.% MAA region (see Table 6-1), are close to $A(k_p)$ for MMA. According to transition state theory and with special emphasis on the rotational partition function of the TS structure, this observation suggests that the relevant degrees of motion of the TS for MAA propagation experience a reduced barrier to rotation in the dilute aqueous state as compared to bulk MAA polymerization. It is interesting to note, that intermolecular interactions via hydrogen bonds to either H₂O or MAA affect the activation barrier for MAA propagation to approximately the same extent, as is demonstrated by the similarity of $E_a(k_p)$ for polymerization in bulk and in aqueous solution, whereas the relevant rotational potentials of the TS are affected to very different extents by an H₂O and by an MAA environment. A higher barrier to internal rotational motion of the TS structure for MAA propagation in an MAA environment is not unexpected, as carboxylic acid moieties are strongly interacting. The enthalpy of formation of the cyclic dimer of two MAA molecules has been IR-spectroscopically measured^[228] to be as high as 46.7 kJ·mol⁻¹ (in an environment of fluid ethene). This interaction energy exceeds the one between MAA and H₂O molecules. That the difference in interaction energies of the TS structure for MAA propagation with either an H₂O or an MAA environment affects $A(k_p)$ to such an extent, is probably due to the fact that the relevant TS structure may include several units at the macroradical terminus, e.g., penultimate, pen-penultimate and perhaps even further units, which enhances the effect of hydrogen-bonded interactions on the rotational barriers of the TS.

The similarity in $A(k_p)$ for MAA propagation in dilute aqueous solution and for MMA in bulk polymerization ($2.67 \cdot 10^6 \text{ L} \cdot \text{mol}^{-1} \cdot \text{s}^{-1}$), with these two monomers being structurally close to each other, is consistent with the results for AA obtained by Thickett and Gilbert,^[19] if one assumes a similar effect on $A(k_p)$ of the two non hydrogen-bonded environments, toluene and MMA. These authors reported $A(k_p)$ for AA propagation to be more or less the same in a

water and in a toluene environment. The water environment thus appears to offer a similar hindrance to internal rotational motion of the TS as does the MMA environment in MMA bulk polymerization. As compared to bulk MAA polymerization, the water environment provides enhanced internal rotational mobility to the TS structure for MAA propagation.

The number of repeat units at the macroradical terminus that contribute to the effect of molecular environment on $A(k_p)$ is not known. This poses problems toward attempts of quantitatively analyzing the effect of intermolecular interactions on $A(k_p)$ in terms of transition state theory. We will therefore restrict ourselves to the qualitative statement, that the stronger interactions between the TS for MAA propagation with an MAA environment as compared to interactions of the TS with an H₂O environment are the main reason behind the enormous reduction in k_p in moving from MAA polymerization in dilute aqueous solution to MAA bulk polymerization.

Also the weak increase of $A(k_p)$ seen in bulk polymerization of both the acrylate and methacrylate families upon increasing the size of the alkyl ester group may at least partly be assigned to intermolecular interactions and their effect on TS rotational barriers. Longer alkyl groups are capable of more effectively shielding the polar interactions of the carbonyl groups, thereby reducing rotational barriers for the relevant motions of the TS structure for (meth)acrylate propagation.

6.2 Conversion dependence of k_p of non-ionized MAA

Intermolecular interaction of the transition state structure for MAA propagation with the MAA-water solvent environment was shown to be responsible for the strong effects of MAA concentration on k_p . In view of these large changes in k_p with MAA concentration, the question arises whether and to which extent k_p varies during polymerization to higher conversion, which is also associated with large changes in MAA concentration. PLP-SEC studies are restricted to the initial polymerization period up to a very few per cent conversion. As propagation is considered to be chemically controlled, the low-conversion k_p values from PLP-SEC, are assumed to stay constant up to high conversions and viscosities.^[80] Via ESR, this assumption has already been proven for styrene^[81] and methyl methacrylate^[82-84] polymerization in non-polar solutions (see Chapter 3.3.1). Because of the large changes of k_p in aqueous solution of non-ionized MAA, this assumption cannot necessarily be adopted for

MAA-water systems.

Preceding kinetic studies into the polymerization of AA in water-propionic acid mixtures^[68] and into the polymerization of 2-acrylamido-2-methylpropane sulfonic acid (AMPS) up to high degrees of monomer-to-polymer conversion^[198] provided some indication that k_p depends on the total concentration of carboxylic groups, which may be part of the monomer, the polymer, or a carboxylic acid co-solvent, rather than only on monomer concentration. The PLP-SEC-derived k_p values for AA were lowered upon increasing the concentration of propionic acid^[68] and k_p for AMPS, as obtained from a combination of the SP-PLP-NIR technique with chemically initiated polymerization, appeared to be independent of monomer conversion.^[198]

In order to deduce PLP-SEC-based information on the dependence of k_p on monomer conversion, k_p measurements for MAA in the presence of poly(MAA) and of *iso*-butyric acid (IBA) have been carried out. The latter component represents the saturated analogue of MAA and thus may be looked upon as the associated “polymer of chain length unity”. The PLP-SEC experiments were performed at 25 °C and ambient pressure on aqueous MAA solutions to which different amounts of poly(MAA) or of IBA have been added. The mixtures were prepared such that the overall concentration of carboxylic acid, irrespective of the COOH groups being part of the monomer, the polymer, or the *iso*-butyric acid, is fixed at 20 wt.%. Within each PLP-SEC experiment, only a small fraction of the MAA is polymerized, such as to obtain an amount of PLP-induced poly(MAA) which is sufficient for SEC analysis.

Aqueous-phase polymerization of MAA in the presence of IBA

Table 6-2 collates the experimental conditions and k_p values obtained for MAA polymerization in aqueous phase with added IBA. The experiments have been carried out at 25 °C and ambient pressure using an LPRR of 20 Hz, an initiator concentration of $c_{\text{DMPA}} = 2 \text{ mmol}\cdot\text{L}^{-1}$ and a constant overall acid concentration of 20 wt.%. The virtual conversion, X_{virtual} , has been estimated under the assumption that the added saturated acid, IBA, has been produced by preceding polymerization of MAA. The PLP-induced conversion, X_{PLP} (in per cent), is always below 6 %. To account for changes in MAA concentration during laser pulsing, the relevant monomer concentration in Table 6-2, c_{MAA} , is calculated as the arithmetic mean of MAA concentrations before and after PLP. X_{virtual} is determined according to Eq. (6-1):

$$X_{\text{virtual}} = \left(1 - \frac{c_{\text{MAA}}}{c_{\text{MAA}} + c_{\text{IBA}}} \right) + \frac{X_{\text{PLP}}}{2} \cdot \left(\frac{c_{\text{MAA}}}{c_{\text{MAA}} + c_{\text{IBA}}} \right) \quad (6-1)$$

The first term on the r.h.s. of Eq. (6-1) describes the virtual polymerization of MAA to IBA whereas the second addend accounts for actual PLP-induced monomer-to-polymer conversion. The first two entries in Table 6-2 refer to polymerizations without pre-mixed IBA. Thus, X_{virtual} thus is given by 50 per cent of the monomer conversion due to laser pulsing, X_{PLP} . The ratios of the peak positions of the first and second POI, and thus M_1/M_2 in Table 6-2, are mostly close to 0.5, indicating the reliability of k_p determination. Only at the highest virtual conversion, of about 75 %, the M_1/M_2 ratio differs by more than 20 % from 0.5. Within part of these experiments at high IBA content, no second maximum in the first-derivative curve of the MWD is seen, only a shoulder. The first POI of the MWD is significantly reduced toward increasing X_{virtual} , i.e. toward lower MAA concentration. The k_p values are however more or less independent of virtual conversion.

Table 6-2: Experimental details of PLP-induced polymerizations of MAA in aqueous solution with IBA being added. The IBA content is expressed by a virtual conversion, X_{virtual} , which considers the amount of IBA as being produced from MAA by polymerization. The overall concentration of MAA+IBA is 20 wt.% in all these experiments. PLP was performed at 25 °C and ambient pressure using $c_{\text{DMPA}} = 2 \text{ mmol}\cdot\text{L}^{-1}$ and an LPRR of 20 Hz.

X_{virtual} / %	c_{MAA} / mol·L ⁻¹	number of laser pulses	X_{PLP} / %	M_1 / g·mol ⁻¹	M_1/M_2	k_p / L·mol ⁻¹ ·s ⁻¹
2.6	2.29	150	5.2	35 890	0.50	2 903
2.6	2.29	150	5.2	38 370	0.50	3 104
15.1	1.99	150	6.0	33 730	0.50	3 133
15.1	1.99	150	6.0	33 650	0.50	3 126
13.3	2.04	75	1.9	32 810	0.49	2 983
13.3	2.04	75	1.9	34 120	0.49	3 102
13.2	2.04	50	1.6	33 810	0.49	3 070
13.2	2.04	50	1.6	34 120	0.50	3 098
26.9	1.73	100	5.1	29 920	0.50	3 203
26.9	1.73	100	5.1	29 850	0.50	3 195
26.2	1.73	70	3.3	29 040	0.49	3 113
26.2	1.73	70	3.3	30 340	0.51	3 252
26.0	1.73	45	2.6	29 440	0.51	3 144

26.0	1.73	45	2.6	29 040	0.49	3 101
38.0	1.46	40	1.6	25 760	0.49	3 277
38.0	1.46	40	1.6	25 650	0.49	3 262
37.9	1.46	60	1.3	25 820	0.49	3 280
37.9	1.46	60	1.3	25 700	0.49	3 265
50.4	1.17	40	1.4	21 430	0.48	3 400
50.4	1.17	40	1.4	20 510	0.47	3 255
50.6	1.16	60	2.4	20940	0.48	3 339
50.6	1.16	60	2.4	20 650	0.49	3 293
75.7	0.57	50	5.3	10 330	0.41	3 348
75.7	0.57	50	5.3	10 140	0.40	3 287
75.6	0.57	70	4.5	9 860	0.40	3 184
75.6	0.57	70	4.5	10 020	0.39	3 236
75.3	0.59	25	2.6	10 160	SH	3 190
75.3	0.59	25	2.6	10 450	SH	3 279

^{SH} The overtone position only shows up as a shoulder in the first-derivative of the MWD.

Aqueous-phase polymerization of MAA in the presence of poly(MAA)

Within the PLP-SEC experiments on non-ionized MAA in the presence of poly(MAA), the determination of POIs, via the maxima of the associated first-derivative curves of the MWD, is complicated by the pre-mixed polymer which obviously cannot be removed prior to SEC analysis.

Figure 6-8 and Figure 6-9 depict MWDs (A) and the associated first-derivative curves (B) of polymer samples obtained by PLP-induced polymerizations of 15 wt.% MAA dissolved in water containing 5 wt.% of pre-mixed polymer and of 10 wt.% MAA dissolved in water containing 10 wt.% of pre-mixed polymer, respectively. The full lines (a) represent the polymer sample after PLP, whereas the dashed lines (b) are MWDs measured on the commercial (pre-mixed) poly(MAA). Subtraction of MWD (b) from (a), which was carried out via the WinGPC[®]7.20 software employed for SEC data acquisition and evaluation, yields polymer trace (c) as the MWD of the PLP-produced sample. The MWD (c) in Figure 6-8 shows a typical PLP-type structure.

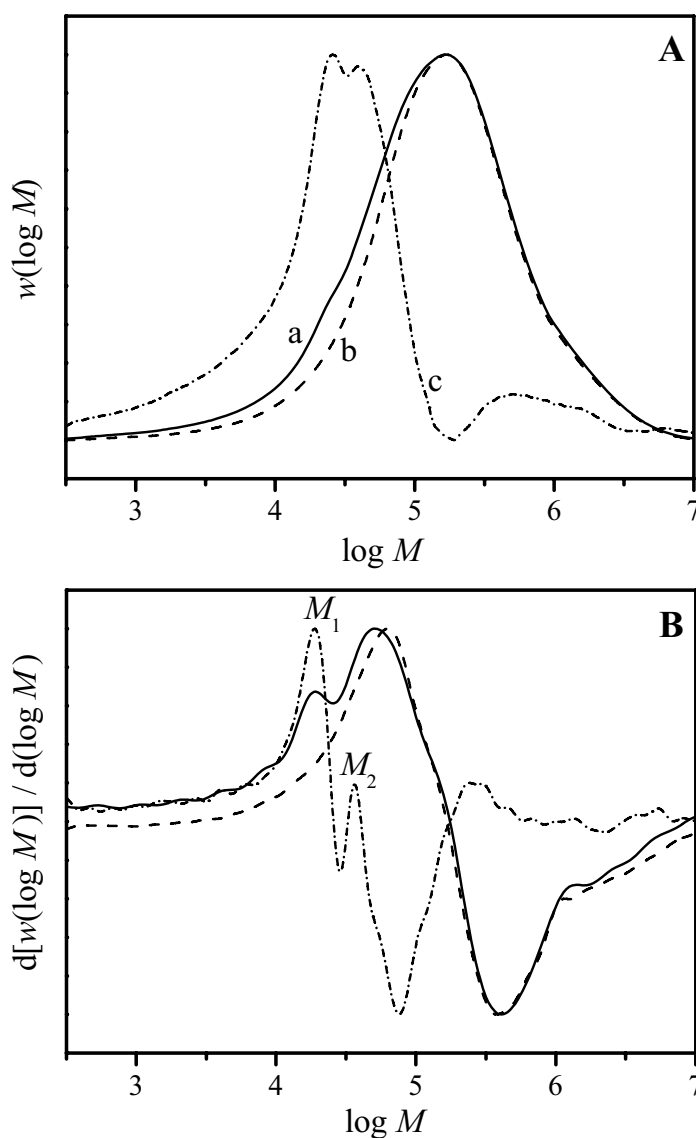


Figure 6-8: Molecular weight distributions (MWD) (A) and associated first-derivative curves (B) for samples from PLP-induced polymerization (at 25 °C and 40 Hz) of 15 wt.% of MAA in aqueous solution containing 5 wt.% poly(MAA). The full line (a) refers to the polymer sample from PLP-SEC, the dashed line (b) represents the pre-mixed poly(MAA), and the dashed-dotted line (c) is obtained by subtracting (b) from (a).

Also with the PLP-SEC data depicted in Figure 6-9, the PLP structure is better seen from curve (c) obtained by the subtraction procedure. The improved detection of PLP-induced structure from MWD curves after applying the subtraction procedure is also evidenced by the first-derivative plots shown in Figure 6-8B and Figure 6-9B. In case of 50 % virtual conversion (Figure 6-9), subtraction of the MWD for the pre-mixed polymer is necessary for identification of the POIs.

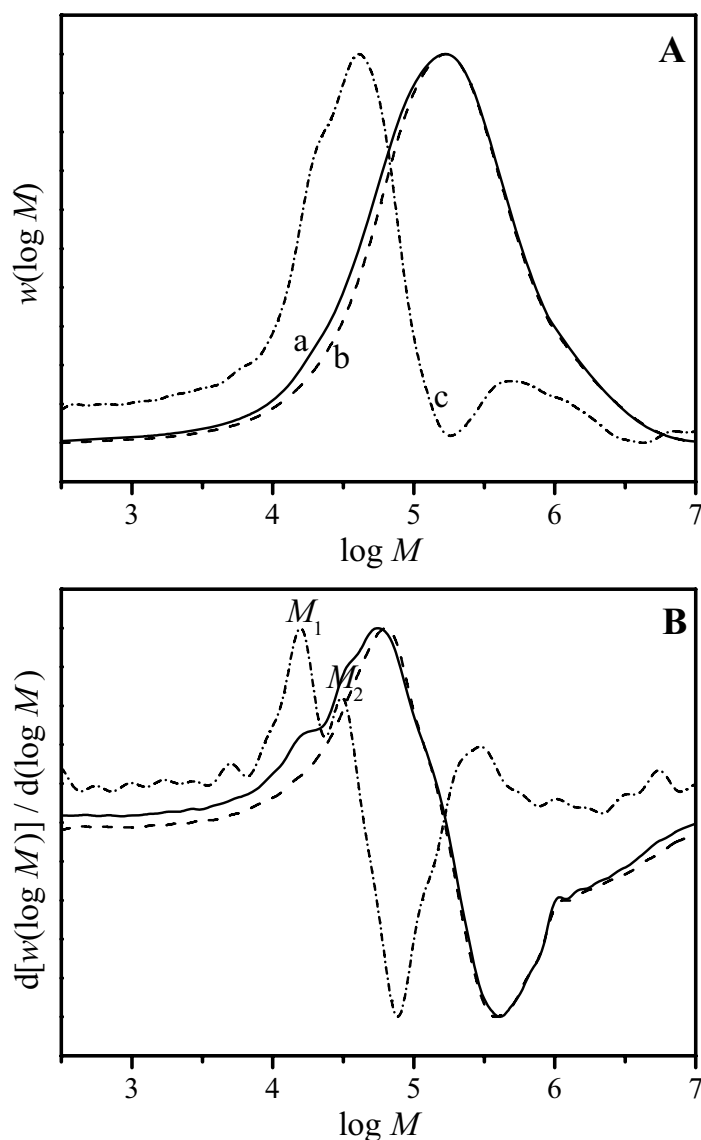


Figure 6-9: Molecular weight distributions (MWD) (A) and associated first-derivative curves (B) for samples from PLP-induced polymerization (at 25 °C and 40 Hz) of 10 wt.% methacrylic acid (MAA) in aqueous solution containing 10 wt.% poly(MAA). The full line (a) refers to the polymer sample from PLP-SEC, the dashed line (b) represents the pre-mixed poly(MAA), and the dashed-dotted line (c) is obtained by subtracting (b) from (a).

Table 6-3 summarizes the experimental results for polymerizations of MAA in the presence of pre-mixed poly(MAA) at 25 °C and ambient pressure, an LPRR of 40 Hz, an initiator concentration of $c_{\text{DMPA}} = 2 \text{ mmol}\cdot\text{L}^{-1}$, and a constant overall acid concentration of 20 wt.%. The LPRR of 40 Hz has been chosen to obtain PLP-produced polymer on the low molecular weight side of the MWD for the pre-mixed poly(MAA). Subtraction of the MWD for the pre-mixed polymer from the overall MWD measured on the sample from PLP allows for precisely

detecting the M_1 and M_2 positions. The propagation rate coefficient clearly increases toward higher degrees of (virtual) monomer conversion, by about a factor of 1.6 in going from 0 to 10 wt.% pre-mixed poly(MAA) at constant overall concentration of MAA units. This behavior is in contrast to what has been observed in the experiments with pre-mixed IBA, where no significant change of k_p was seen.

Table 6-3: Experimental details of PLP-induced polymerizations of MAA in aqueous solution with poly(MAA) being added. The overall concentration of MAA+poly(MAA) is 20 wt.% in all experiments. PLP was performed at 25 °C and ambient pressure using a photoinitiator concentration of $c_{\text{DMPA}} = 2 \text{ mmol}\cdot\text{L}^{-1}$ and an LPRR of 40 Hz.

X_{virtual} / %	c_{MAA} / $\text{mol}\cdot\text{L}^{-1}$	<i>number of laser pulses</i>	M_1 / $\text{g}\cdot\text{mol}^{-1}$	M_1/M_2	k_p / $\text{L}\cdot\text{mol}^{-1}\cdot\text{s}^{-1}$
1.0	2.35	150	19 815	0.52	3 120
1.0	2.35	150	20 370	0.53	3 208
1.7	2.35	300	20 464	0.53	3 223
1.7	2.35	300	20 606	0.53	3 245
26.9	1.76	150	18 967	0.52	3 983
26.9	1.76	150	19 364	0.53	4 066
26.9	1.76	300	18 707	0.51	3 928
27.5	1.76	300	18 793	0.52	3 946
53.2	1.18	150	16 181	0.53	5 096
53.6	1.18	300	15 740	0.51	4 958
53.6	1.18	300	16 144	0.52	5 085

Discussion

The numbers in Table 6-2 and Table 6-3 demonstrate that under conditions of constant overall acid concentration (20 wt.%), which closely corresponds to a constant overall content of (non-ionized) carboxylic acid groups, the replacement of MAA monomer by IBA leaves k_p of MAA constant, whereas the replacement of MAA monomer by poly(MAA) enhances k_p . The latter observation is consistent with the finding from PLP-SEC experiments on aqueous MAA solutions (without any added carboxylic acid groups), that lowering the MAA content results in a higher k_p (see Chapter 6.1). The experimental findings are illustrated in Figure 6-10, where k_p of MAA is plotted vs. virtual MAA conversion for a constant overall acid

concentration of 20 wt.%. This unusual way of representing k_p solution data requires some further explanation. The k_p data for values of X_{virtual} around 2 to 3 per cent (diamonds) are from experiments on aqueous MAA solutions containing 20 wt.% MAA, but no added further carboxylic acid groups (as are contained in IBA or in poly(MAA)). The associated value of X_{virtual} is thus given by 50 per cent of the MAA conversion brought upon by PLP.

The triangles refer to PLP-SEC experiments on aqueous MAA solutions with different amounts of added IBA. The X_{virtual} values around 75 % refer to experiments on 1 : 3 mixtures of MAA : IBA at an overall concentration of 20 wt.% carboxylic acid (MAA + IBA). The virtual conversion thus is made up of a conversion of MAA to an associated “polymer of chain length unity” plus a small poly(MAA) production by PLP. Toward increasing IBA content, k_p slightly increases. This effect however occurs within the accuracy of PLP-SEC measurements which is estimated to be ± 15 per cent for this particular system.

The k_p values of MAA measured in the presence of poly(MAA), indicated by the square symbols, grow significantly with X_{virtual} . Within this series of experiments, conversion during an MAA polymerization in aqueous solution of MAA, is simulated by pre-mixing poly(MAA) and by simultaneously lowering MAA monomer concentration of the solution subjected to PLP such that the overall content of MAA units stays at 20 wt.%.

Also included in Figure 6-10, as circles, are propagation rate coefficients from Chapter 6.1 for aqueous MAA solutions without added acid. These values are truly virtual in that they are estimated for the hypothetical situation that conversion is only reflected in a reduction of MAA monomer concentration without any polymeric MAA units being produced. Virtual conversion was calculated such that the MAA to water ratio is identical to the one of a reference experiment for an initial monomer concentration of 20 wt.% in which MAA is actually transformed into polymeric MAA units. Thus, the virtual conversion for a PLP-SEC experiments on an aqueous solution containing 10 wt.% MAA slightly exceeds 50 per cent, as otherwise the MAA monomer to water weight ratio would be 1 : 9 instead of 1 : 8, which is the ratio for a polymerization to 50 per cent conversion starting from an initial concentration of 20 wt.% MAA. The three types of experiments, indicated by the triangles, squares, and circles, have in common, that identical virtual conversion is associated with the same MAA to water ratio. The circles demonstrate that the reduction in MAA concentration significantly enhances k_p .

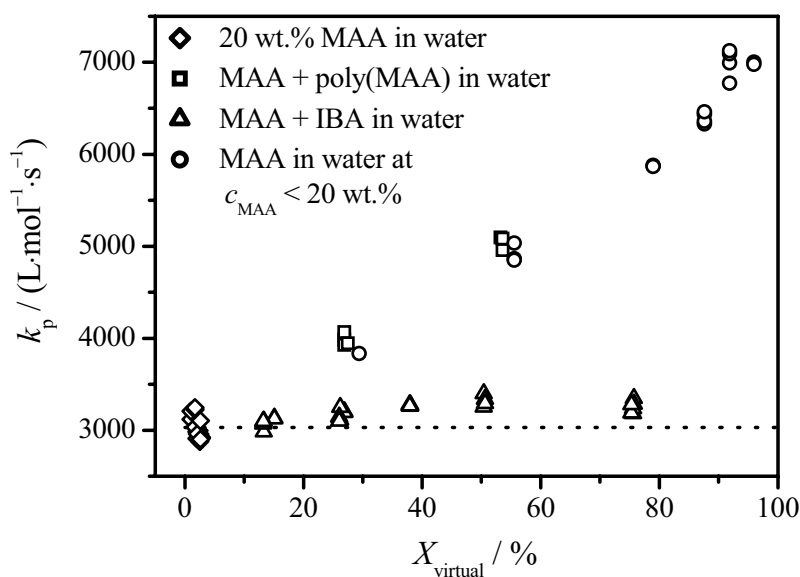


Figure 6-10: Dependence of k_p on X_{virtual} for polymerizations of MAA in water at 25 °C and ambient pressure. The diamond symbols refer to polymerization of MAA (20 wt.%) in aqueous solution without any added carboxylic acid groups. The squares and the triangles represent aqueous-phase polymerizations of MAA in the presence of poly(MAA) and IBA, respectively, at an overall carboxylic acid concentration of 20 wt.%. The k_p values indicated by the circles refer to polymerization of MAA in aqueous solution at concentrations below 20 wt.% (for a more detailed explanation see text). The dotted line indicates the mean value of low conversion k_p at 20 wt.% MAA in aqueous solution.

The close agreement of the MAA k_p values in the presence of poly(MAA) with the ones in aqueous MAA solution of identical monomer concentration (without added carboxylic acid groups, circles in Figure 6-10) indicates that polymeric MAA units do not contribute to changes of k_p . As has been detailed in Chapter 6.1, the propagation rate coefficient of non-ionized MAA in aqueous solution is strongly enhanced toward lower monomer concentration due to weaker intermolecular interactions of the transition state structure with a molecular environment in which carboxylic acid groups are replaced by water molecules. The lower friction of internal rotational motion of the transition state structure in more dilute MAA solution is associated with a higher pre-exponential factor. In an MAA-rich environment, on the other hand, the strong hydrogen-bonded interactions between the carboxylic acid groups lead to significant friction and to a lowering of the pre-exponential factor in the Arrhenius expression for k_p . IBA which is structurally rather close to MAA, obviously has a similar effect on k_p of MAA as has MAA itself. Thus, replacing MAA by IBA at constant overall acid concentration has no significant influence on k_p . That poly(MAA) has not the same effect on

MAA k_p as has IBA indicates that the addition of poly(MAA) is not felt at the reactive site, which is the free-radical functionality of a growing macroradical. The free-radical site is imbedded into the solvent-swollen macroradical coil, which is not or not to a significant extent penetrated by another polymeric coil. Thus the solvent environment of the radical site is not affected by adding polymer. As a consequence, also the effect of solvent friction on the transition structure for propagation remains unchanged. On the other hand, changing the reacting system by adding monomeric carboxylic acid, e.g. MAA or IBA, changes the solvent quality and thus the microscopic environment within the coil. If the two acids are of similar structure, as is the case with MAA and IBA, the k_p value, to a first approximation, depends on overall carboxylic acid concentration, but is insensitive toward the relative amounts of two such acids.

These findings have particularly important consequences for the modeling of polymerization kinetics in aqueous solution, where the concentration dependence of k_p is pronounced. For an estimate of the impact of carboxylic acid concentration on k_p of MAA it needs primarily to be considered whether the carboxylic acid groups (other than of the MAA monomer) are capable of affecting the intra-coil environment of the radical site. Along these lines, k_p of MAA may have a specific chain-length dependence and may be affected by the MWD of produced polymer, in particular by the amount of oligomeric products that may contribute to the intra-coil environment of the growing macroradicals. If an MAA polymerization exclusively produces high molecular weight material, only monomer concentration needs to be taken into account for assessing k_p . However, even long-chain polymer coils penetrate each other when the polymer content in the reaction solution is high. Thus, under such conditions also high-molecular-weight material may affect k_p .

6.3 Dependence of k_p of MAA on monomer concentration and degree of ionization

MAA is a weak acid and therefore practically non-ionized at its natural pH . An increase of pH consequently results in deprotonation of the carboxylic acid group and may strongly influence the rate of propagation and product properties. So far, PLP-SEC studies into k_p of partially or

fully ionized monomers are very limited. Lacík et al.^[69] reported an about ten-fold decrease of k_p from 111 000 L·mol⁻¹·s⁻¹ at $\alpha_D = 0$ to 13 000 L·mol⁻¹·s⁻¹ at $\alpha_D = 1$ for polymerization of 5 wt.% AA in water at 6 °C. This observation was explained by electrostatic repulsion between equally charged monomer molecules and growing macroradicals, which was qualitatively in line with the pioneering kinetic studies for AA^[229] and MAA^[60,229] reporting an around ten-fold decrease in initial rate of polymerization between the non-ionized and completely ionized monomers. The increase in propagation rate upon further addition of NaOH to the solutions of fully ionized AA ($k_p = 57\,000\text{ L}\cdot\text{mol}^{-1}\cdot\text{s}^{-1}$ at $\alpha_D = 1.1$)^[69] was discussed based on the assumption of the “ion-pair concept” which assumes a shielding of electrostatic repulsive interactions by Na⁺ cations from the excess of NaOH.^[229–233] A study into the polymerization kinetics of ionized AA at higher monomer concentrations (up to 37 wt.% AA) indicates that the polymerization rate becomes less dependent on α_D upon increasing c_{AA} .^[234]

It should be noted that the only available k_p values for ionized MAA were 670 and 1 950 L·mol⁻¹·s⁻¹ for pH 8.6 and 13.6 at 23 °C and a monomer concentration of 0.92 mol·L⁻¹ in water determined by the rotating sector technique.^[229]

The goal of this chapter is to show the dependence of k_p on monomer concentration, on temperature and on the degree of ionization of MAA for extending the description of kinetics in aqueous phase by polymerization. The k_p values were determined within the full range of the degree of MAA ionization, for monomer concentrations of 5, 20 and 40 wt.% and in the temperature range of 6 to 80 °C. The effect of added salt (NaCl) was studied for polymerization of 5 wt.% MAA at α_D between 0 and 1.

6.3.1 Specific features of the polymerization system

In this section, the major features of ionized systems and their possible effects on polymerization kinetics are highlighted.

Electrostatic interactions, counterions and ionic strength. With increasing pH, and consequently increasing degree of ionization of weak carboxylic acids, the propagation reaction between monomer and growing radical chain-end is expected to be influenced by electrostatic interactions among the ions in the polymerization system, i.e. carboxylate groups

on ionized monomer and polymer as well as the associated counterions of the carboxylate groups. These counterions screen the charges on the polyelectrolyte chain and reduce the repulsive electrostatic interactions which are also responsible for stiffening and expansion of polyelectrolyte chains.^[235] The ionic strength of the polymerizing solution is predominantly determined by the concentration of ionized monomer. At high ionic strengths, in the range of 10^{-3} to 10^0 mol·L⁻¹, the pronounced screening of charges may lead to similar conformations of polyelectrolyte and neutral polymer chains.^[236,237] Since typical monomer concentrations in FRP are in the range of 10^0 mol·L⁻¹, the polymerization of an ionized monomer at typical degrees of ionization, i.e. $\alpha_D > 0.1$, proceeds at high ionic strengths in view of the chemistry of polyelectrolytes. Consequently, a significant screening of the charges on the polyion chains can be expected. Since monomer is consumed during polymerization, the ionic strength decreases with conversion which may also influence the kinetics. This is, however, not of concern in the low conversion studies of this chapter.

Solvent composition and preferential solvation. The increase in pH for a given monomer concentration leads to an increased content of ionized monomer. The charged groups of polyelectrolyte chains are strongly interacting with water molecules.^[238] Thus, the ionization of polymer leads to changes in the local environment of the polymer chains due to preferential solvation with water molecules. This may affect the composition of the environment of the TS structure and, consequently, the propagation rate in aqueous solutions (see Chapter 6.1).

Electrochemical equilibrium. The acid-base characteristics of polymer and growing radical chain-end may represent another complicating feature. As discussed for polymerization of a partially ionized AA,^[69] there is an exchange of protons and counterions between the carboxylic groups of monomer and growing radical chain-end based on the different pK_a values of these carboxylic groups. The pK_a value of a polymer chain depends on molar mass, degree of ionization and ionic strength^[239] and therefore may change with conversion and even during the growth of a polymer chain.

Conformation. The conformation of ionized poly(MAA) and poly(AA) chains shows different dependencies on α_D .^[240-244] In case of poly(MAA), hydrophobic attractive interactions (causing the lower critical solution temperature behavior of poly(MAA) in aqueous solutions^[245]) compete with repulsive electrostatic interactions at degrees of polymer ionization below 0.2 to 0.3. Thus, hydrophobic interactions may also influence the propagation kinetics and potentially cause differences between polymerization of ionized MAA and AA. Ionic strength (concentration of ionized monomer) and solvent composition

(ratio of non-ionized monomer and water) are additional factors influencing the chain conformation due to changes in solvent quality.

Effective charge of a polymer chain. While for monomer molecules, the degree of ionization equals to the degree of neutralization (monomer is fully dissociated), the effective charge on the ionized poly(MAA) and poly(AA) chains is not identical to α_D . This is not only due to different pK_a values and hence different degrees of ionization at the given pH (see, for example, titration curves in Figure 1 of ref.^[69]) but also due to the counterion condensation, i.e. accumulation of counterions to the carboxylate groups in the vicinity or at the surface of the polyion.^[246–248] For example, the maximum degree of ionization for poly(MAA) is ~ 0.36 in case of monovalent counterions and in the absence of salt.^[249] Thus, poly(MAA) cannot exhibit a higher effective charge and the intra- and intermolecular electrostatic interactions are constant upon further increase of pH .^[249]

In conclusion: The kinetic studies into the polymerization of ionized MAA at different α_D and c_{MAA} are related to the scientific field of polyelectrolyte effects. The factors hampering a more precise specification of the polymerizing system are: (i) The concentration regimes^[235,250] are changing from dilute to even concentrated regimes depending on conversion, initial monomer concentration, degree of monomer ionization and molecular weight of the polymer. (ii) The polymerization does not proceed in a well-defined solvent as used for studies of polyelectrolytes for which usually aqueous solutions of defined ionic strength are applied. The polymerization systems consist of mixtures of water, non-ionized MAA and ionized MAA (determining the ionic strength). Both, the ratio and the amount of non-ionized and ionized MAA, change during polymerization. (iii) The formed polymers are polydisperse while usually the description polyelectrolytes rests on polyelectrolytes with well defined MWD.

The discussion above illustrates that the properties of polyelectrolytes change enormously when investigating the dependence of k_p on c_{MAA} in the range of 5 to 40 wt.% and on α_D in the range of 0 to 1. These factors may strongly influence polymerization kinetics. In the next sections, attempts are made to identify their impact on k_p of ionized MAA.

6.3.2 Propagation kinetics of ionized MAA

MAA allows for k_p measurements within wide ranges of α_D , c_{MAA} , and T without losing PLP structure of the MWDs. A typical MWD from PLP-induced polymerization of partially ionized MAA has already been shown in Figure 5-1. Additional MWDs as well as details on experimental conditions and resulting k_p values for polymerizations of MAA in aqueous solution at monomer concentrations of 5, 20 and 40 wt.%, temperatures of 6 to 80 °C and α_D of 0 to 1 will be provided elsewhere.^[251] Care was taken that the consistency criteria for reliable k_p estimation were fulfilled with respect to the M_1/M_2 ratio being close to 0.5 as well as k_p being independent of photoinitiator concentration, LPRR, number of pulses and laboratory in which PLP was carried out (Göttingen or Bratislava).^[8]

First, the data obtained for 5 wt.% MAA will be discussed in view of the previous work regarding k_p of ionized AA at 6 °C,^[69] where a decrease by a factor of ten was obtained between α_D of 0 and 1. The decrease in k_p between 5 wt.% of non-ionized and fully ionized MAA is also by about one order of magnitude as is illustrated in Figure 6-11. This figure shows the variation of the reduced k_p values, expressed as $k_p / k_p(\alpha_D = 0)$, with α_D at different temperatures. An overlap of the reduced k_p values implies that complications due to the effect of temperature on the various types of interactions (hydrogen-bonding, hydrophobic, electrostatic) are not dominant in the propagation kinetics of MAA. Additionally, this overlap suggests that the activation energy of the propagation rate coefficient, $E_a(k_p)$, does not significantly vary with α_D . The Arrhenius parameters determined for different MAA concentrations and degrees of ionization will be discussed at the end of this chapter.

Figure 6-11 also illustrates the close agreement between the reduced k_p values for AA^[69] and MAA at the common polymerization temperature of 6 °C. This agreement demonstrates that the 35-fold difference between k_p of non-ionized AA and MAA (see ref.^[68] and Chapter 6.1) is maintained also for their ionized forms. Moreover, it is shown that the different conformational behavior of poly(AA) and poly(MAA) upon ionization in aqueous solution^[240–244] does not significantly influence k_p under the applied experimental conditions.

In the preceding paper on ionized AA, the question has been raised whether the time for electrochemical equilibration (the exchange of proton and counterion between monomer and growing polymer chain-end based on their different pK_a values) is shorter than the time required for the propagation step.^[69] If this would be the case for polymerization of AA, the competition between the rates of propagation and of electrochemical equilibration should be

less pronounced for MAA, for which k_p is about 1.5 orders of magnitude lower. The overlap of reduced k_p values for AA and MAA in Figure 6-11 suggests that the electrochemical equilibration is faster than one propagation step in polymerization of both, AA and MAA.

At first sight, the decrease in k_p toward increasing α_D leads to the conclusion that this effect is due to the repulsive electrostatic interactions between the monomer and the radical chain-end as proposed for AA.^[69] Thus, if repulsive interactions were dominant, screening of charges by addition of a low molecular weight electrolyte, e.g. NaCl, should result in increased k_p values for partially and fully ionized MAA. Such experiments were carried out for 5 wt.% MAA polymerized within the entire range of MAA ionization at 40 °C and NaCl concentrations of 0.35 and 0.70 mol·L⁻¹, respectively. Higher NaCl concentrations could not be used since this would lead to phase separation.

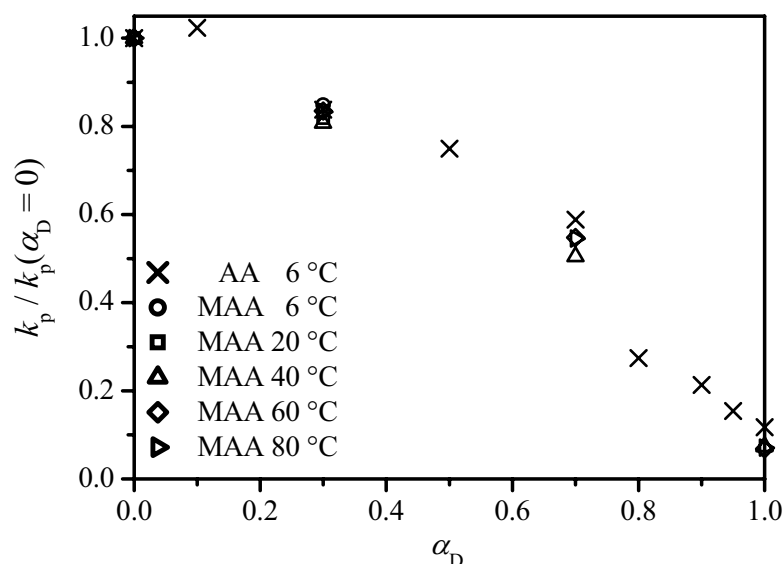


Figure 6-11: Dependence of the reduced propagation rate coefficients, $k_p / k_p(\alpha_D = 0)$ on α_D of MAA and AA (data from ref.^[69]) for aqueous solution polymerizations at monomer concentrations of 5 wt.% and different polymerization temperatures.

Figure 6-12 shows the comparison of the k_p values for solutions containing NaCl with the ones determined without added salt. The increase in ionic strength upon addition of NaCl does not result in a significant effect on k_p for polymerizations carried out at $\alpha_D < 1$. It cannot be judged, based on the available data, whether the almost two-fold higher k_p for $\alpha_D = 1$ and 0.7 mol·L⁻¹ NaCl (1100 L·mol⁻¹·s⁻¹) compared to k_p in the absence of NaCl (680 L·mol⁻¹·s⁻¹) reflects the proposed screening effect of the salt. Nevertheless, this set of experiments indicates that the effect of added NaCl is much weaker than expected under the assumption

that repulsive electrostatic interactions were dominating k_p . This is not that surprising after realizing that already the polymerization of partially ionized MAA, i.e. in the absence of added NaCl, proceeds at ionic strengths in the range of 10^{-1} to $10^0 \text{ mol}\cdot\text{L}^{-1}$, which should effectively screen the charges on a polyelectrolyte chain.^[235–237] This discussion suggests that the classical mechanism^[60,229] proposed for polymerization of ionized AA and MAA in aqueous solution (and adopted in ref.^[69]) should be revised.

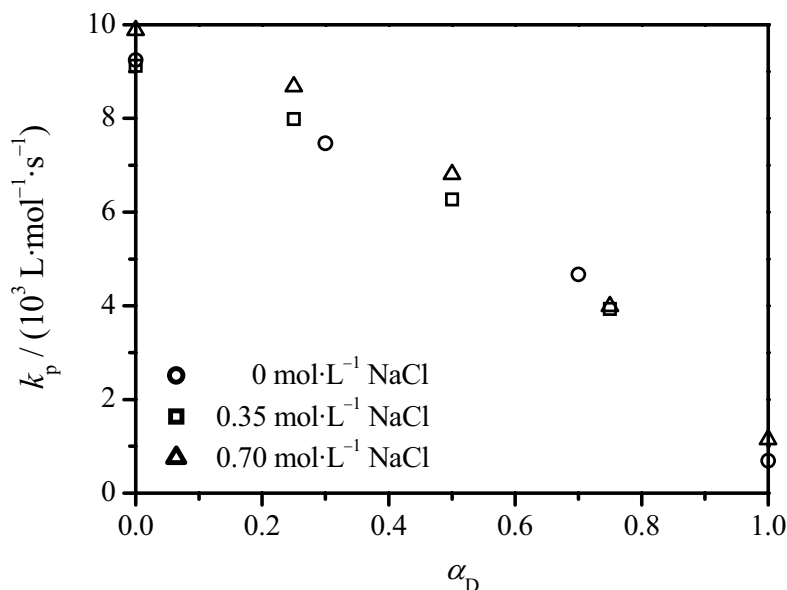


Figure 6-12: Dependence of k_p on α_D for polymerizations of 5 wt.% MAA in water ($0.59 \text{ mol}\cdot\text{L}^{-1}$) at $40 \text{ }^\circ\text{C}$ and in the presence of various concentrations of sodium chloride.

The PLP-SEC experiments into k_p of 5 wt.% of partially and fully ionized MAA were extended to monomer concentrations of 20 and 40 wt.%. Figure 6-13 shows the dependence of the arithmetic mean k_p values on the degree of monomer ionization for polymerizations of 5, 20 and 40 wt.% MAA in aqueous solution at temperatures of 6, 40 and $80 \text{ }^\circ\text{C}$. At each temperature, the same trend was observed for the variation of k_p with α_D at a certain c_{MAA} . As already presented in Figure 6-11, k_p decreases by a factor of ten between non-ionized and fully ionized MAA for 5 wt.% of monomer in water. However, for c_{MAA} of 20 wt.%, the k_p values are almost constant up to $\alpha_D = 0.7$ and drop by a factor of three toward full monomer ionization. Finally, k_p appears to be totally independent of α_D for 40 wt.% MAA. This finding is remarkable in view of the classical picture^[229] of FRP of ionized monomers: Introducing charges on the monomer as well as on the growing radicals does not lower k_p due to repulsive interactions.

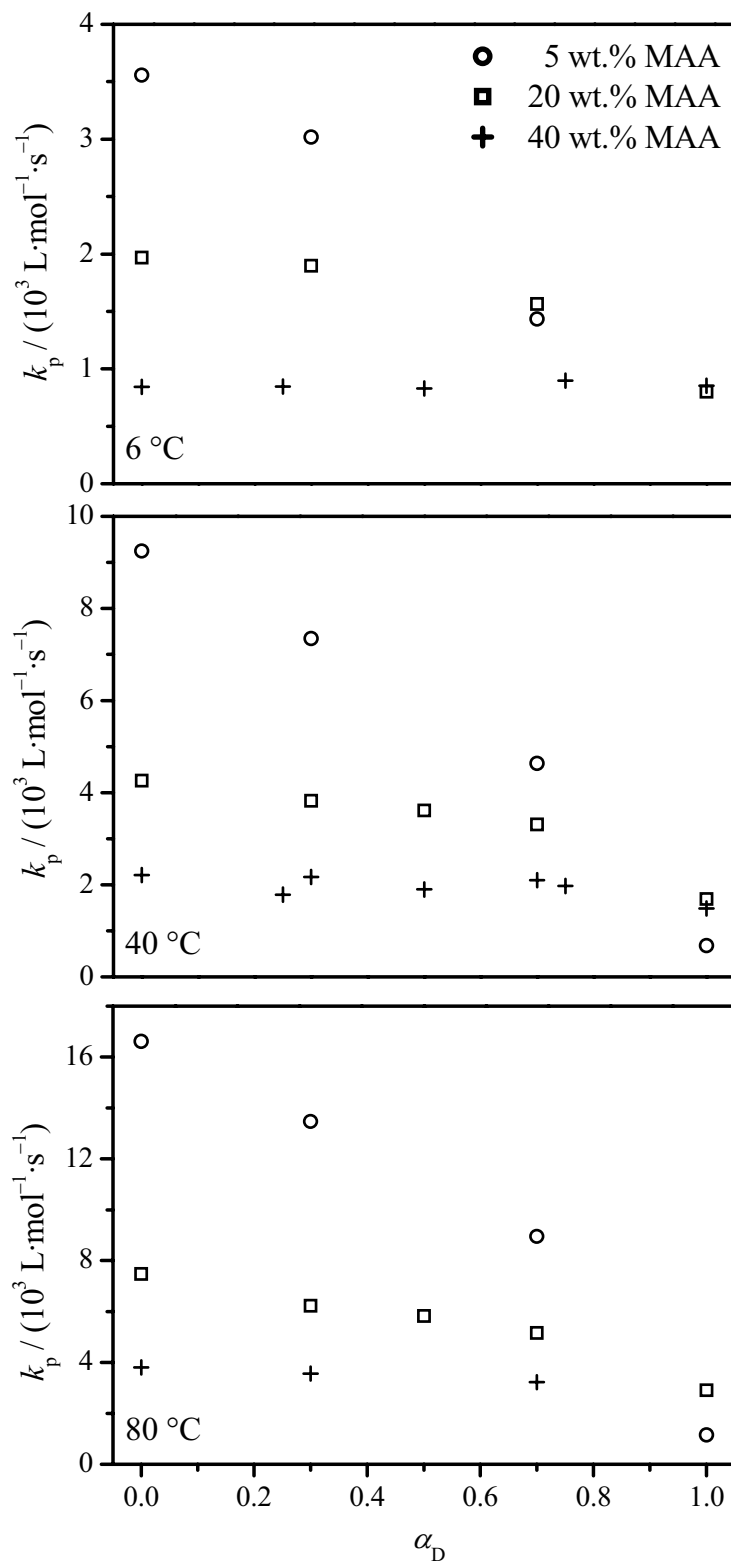


Figure 6-13: Dependence of k_p on α_D for polymerizations of 5 (circles), 20 (squares) and 40 wt.% (crosses) MAA in water at 6, 40 and 80 °C.

The data from Figure 6-13 are re-plotted to Figure 6-14, which is the classical type of figure for illustrating solvent effects in polymerization of water-soluble monomers.^[15,66,68,70-73] Figure 6-14 shows the dependence of k_p on c_{MAA} for different degrees of MAA ionization and temperatures. Two features emerge from Figure 6-14: (1) k_p as a function of c_{MAA} (left-to-right): For the non-ionized form of MAA (see Chapter 6.1), the decrease in k_p toward increasing c_{MAA} is diminished upon rising α_D . Even the reversed case is observed for polymerization of fully ionized MAA where k_p increases toward higher c_{MAA} (2) k_p as a function of α_D (top-to-bottom): While for the low c_{MAA} range (5 wt.% MAA) a pronounced decrease in k_p toward higher α_D is observed, the span between the k_p values narrows upon increasing c_{MAA} until k_p becomes independent of α_D at 40 wt.% of monomer. Figure 6-13 and Figure 6-14 reveal that the mechanism of polymerization of ionized monomers in aqueous solution exhibits special features with respect to the k_p dependence on c_{MAA} and α_D , which have not been reported in any FRP system so far.

Results shown for 5 wt.% of MAA in Figure 6-11 and Figure 6-12 point out that some of the concerns regarding the complexity of the polymerization system do obviously not have a major impact on the propagation kinetics. This holds true for electrostatic repulsive interactions, ionic strength, electrochemical equilibration and hydrophobic interactions. It can be assumed that these factors should not strongly affect k_p also for 20 and 40 wt.% MAA. This simplifies the description of polymerization kinetics as it is hard, if not impossible, to correlate the obtained k_p values to complex acid-base properties, polyelectrolyte effects and electrochemical equilibration. Rather than that, the obtained rate coefficients and will be discussed following genuine kinetics arguments.

After identifying the kinetic reasons of the monomer concentration dependence of k_p for polymerization of non-ionized MAA (see Chapter 6.1), it is straightforward to propose that the same arguments apply to k_p of partially and fully ionized MAA. This appears to be a suitable approach when considering that the decrease in k_p from non-ionized to fully ionized MAA at low c_{MAA} is of the same magnitude as the decrease in k_p of non-ionized MAA between highly diluted and bulk polymerization. The k_p dependence on MAA concentration at $\alpha_D = 0$ has been explained by stronger interactions between the TS for MAA propagation with an MAA environment as compared to interactions of the TS with an H₂O environment. Any contribution to either constraints or degrees of freedom of the TS structure will influence the k_p values of MAA in the partially or fully ionized form. Several mechanisms can be proposed:

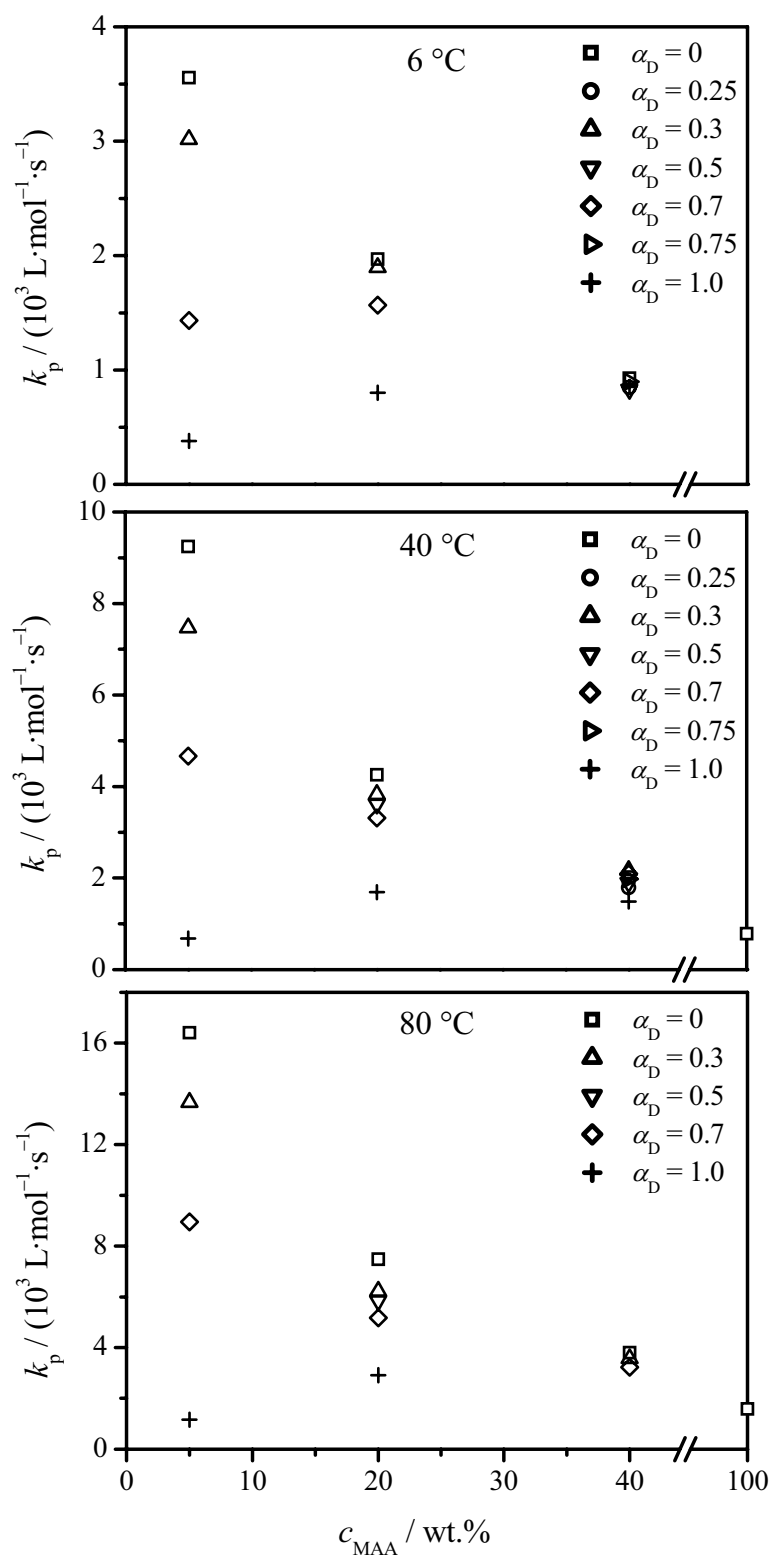


Figure 6-14: Dependence of k_p on MAA concentration in water for polymerizations at different degrees of monomer ionization and temperatures of at 6, 40 and 80 °C.

a) Mechanisms to increase the friction to the internal rotations in the TS:

1. *Electrostatic attractive interactions between charged groups of growing radical chain-end and counterions.* Counterions condensed at the vicinity of a polyion can attractively interact with charged monomer. Thus, the ionized macroradical chain-end may interact with charged monomer through the counterions resulting in changes in chain stiffness. This may result in a hindrance of the transitional modes and consequently in decreased k_p values.^[17]
2. *Electrostatic attractive interactions between growing radicals.* This, at glance, improbable situation can occur via the mechanism of so-called charge inversion by which, polyanions may exhibit cationic character due to the overcharging.^[252,253] This happens when more counterions are attached to the polyion surface (or its vicinity) than are required for compensation of the surface charge. In this case, instead of charge reduction due to shielding, it is possible to observe charge inversion and the attractive interactions between polyions.
3. *Hydrogen-bonded attractive interactions between growing radical chain-end and monomer.* In polymerization of the partially ionized MAA, similar to polymerization of non-ionized MAA, hydrogen-bonded attractive interactions between the growing radical chain-end and monomer occur (in different extent depending on α_D and c_{MAA}). Even stronger hydrogen-bonded interactions between ionized MAA and poly(MAA) chains (and also hydrogen-bonded interactions among partially ionized poly(MAA) chains).^[240]
4. *Electrostatic repulsive interactions between charged polymer chains.* These interactions between the polyions should become important for polymerizations at high monomer concentrations, which lead to poly(MAA) concentrations where the chains come to contact (in and above the semidilute regime) as was recently proposed for polymerization of AMPS in aqueous solution.^[198]
5. *Hydrophobic interactions among methyl groups of poly(MAA).* The hydrophobic interactions are enhanced toward increased ionic strength and charge density on the polymer chain which also should result in an increased friction in the TS.

b) Mechanisms to decrease the friction to the internal rotations in the TS:

1. *Solubilization of polyions.* Charged polymer chains are better solubilized by water molecules than the non-charged ones.^[238] The preferential solvation of polyions by water is expected to enhance the motion of the TS structure. Moreover, a reduced local monomer concentration in the vicinity of the radical chain end may result in a decrease in the (apparent) k_p obtained via PLP-SEC.^[68]
2. *MAA ionization decreases the content of non-ionized MAA.* The increase in α_D at a given c_{MAA} lowers the ratio of non-ionized MAA to water molecules, which should reduce the hindrance to the transitional modes due to interactions of non-ionized MAA with the TS structure.
3. *Flexibility of polyions at increased ionic strength.* The flexibility of the poly(MAA) chains increases toward higher ionic strength^[235] as a result of screened charges.

The individual contribution of the above proposed mechanisms to both, increase and decrease of the constraints to the internal rotations in the TS structure, is impossible to be elaborated based on the presented kinetic data. Assigning the large solvent effects in polymerization of ionized MAA to the hindrance of internal rotational motion in the TS structure is in line with the aqueous solution polymerization of non-ionized MAA (see Chapter 6.1) and NVP (see Chapter 7.1). However, the increased polarity of the environment for the propagation step toward higher α_D may additionally affect the activation energy. In fact, $E_a(k_p)$ is expected to decrease upon introduction of charges to the polymerization system as it was observed in polymerization of methacrylates in solution of ionic liquids.^[254,255] The effect of increased polarity of the environment can additionally lower $E_a(k_p)$, which are already decreased due to hydrogen-bonding interactions as observed experimentally (see Chapter 6.1) and proposed by quantum chemical calculations.^[19] Moreover, changes in the distribution of electron density within the reacting molecules may affect $E_a(k_p)$. Thus, the observed dependence of k_p on c_{MAA} and α_D may possibly be attributed to both $E_a(k_p)$ as well as $A(k_p)$. To discriminate between these effects, the Arrhenius parameters were evaluated from the k_p data at given c_{MAA} and α_D , in case k_p values were available for at least 3 different polymerization temperatures.

The Arrhenius-type plots for aqueous phase polymerizations of MAA at different c_{MAA} and α_D are shown in Figure 6-15 and the resulting Arrhenius parameters are summarized in Table 6-4. Regarding the Arrhenius parameters for partially and fully ionized MAA, these

data suggest that ionization introduces effects responsible for lowering of pre-exponential factor as well as activation energy depending on the composition of the polymerization system. For 5 wt.% MAA, the decrease in k_p between $\alpha_D = 0$ and $\alpha_D = 0.7$ seems to be caused by a lowering of the pre-exponential factor. A decrease in both, $E_a(k_p)$ and mainly $A(k_p)$, leads to the low k_p for $\alpha_D = 1$. However, these Arrhenius parameters are based on relatively few k_p data and $A(k_p)$ seems to be unreasonably low considering the pre-exponential factors for k_p of other monomers.^[16] Thus, the actual $A(k_p)$ and $E_a(k_p)$ values for 5 wt.% of fully ionized MAA in water are probably higher than the ones reported in Table 6-4 (see also the extended JCI in Figure 6-16). For 20 wt.% MAA, in spite of almost constant k_p values between $\alpha_D = 0$ and $\alpha_D = 0.7$ at different temperatures (see Figure 6-13), the Arrhenius parameters exhibit some variation in both values in this α_D range and no strong departure from these parameters is seen for $\alpha_D = 1$. Nevertheless, the data indicates that it is primarily the pre-exponential factor which changes with α_D . For 40 wt.% of MAA, the k_p values are almost independent of α_D at different temperatures. However, both Arrhenius parameters are decreasing toward increasing α_D . Since $E_a(k_p)$ and $A(k_p)$ are correlated quantities with the possibility of a compensation effect, these data should not be overanalyzed and an adequate representation of the k_p data is obtained by a single linear fit (grey line) providing an activation energy of $12.9 \text{ kJ}\cdot\text{mol}^{-1}$. Nevertheless, the properties of the polymerizing system change enormously upon ionization and some impact on the Arrhenius parameters is expected. A slight decrease in $E_a(k_p)$ values by a few $\text{kJ}\cdot\text{mol}^{-1}$ seems to be operative for the polymerization systems with higher ionic strength, which corresponds to either high α_D values at low c_{MAA} ($\alpha_D = 1$ at 5 wt.% MAA gives an ionic strength of $0.59 \text{ mol}\cdot\text{L}^{-1}$) or low α_D value at higher c_{MAA} ($\alpha_D = 0.3$ at 20 wt.% MAA gives an ionic strength of $0.72 \text{ mol}\cdot\text{L}^{-1}$). As discussed above, this reduced $E_a(k_p)$ may result from the effect of increased polarity of the polymerization system on the polarization of the double bond.

The changes in $A(k_p)$ may be due to an increased hindrance to internal rotational motions in the transition state structure toward higher α_D . The $A(k_p)$ values for high levels of MAA ionization reach the range of $\sim 10^5 \text{ L}\cdot\text{mol}^{-1}\cdot\text{s}^{-1}$, which is close to the pre-exponential factor reported for dimethyl itaconate ($\sim 2\cdot 10^5 \text{ L}\cdot\text{mol}^{-1}\cdot\text{s}^{-1}$) where $A(k_p)$ is low most likely due to a strong steric hindrance in the transition state.^[256] However, the k_p values are several orders of magnitude higher for MAA compared to those for dimethyl itaconate due to a significantly lower $E_a(k_p)$.

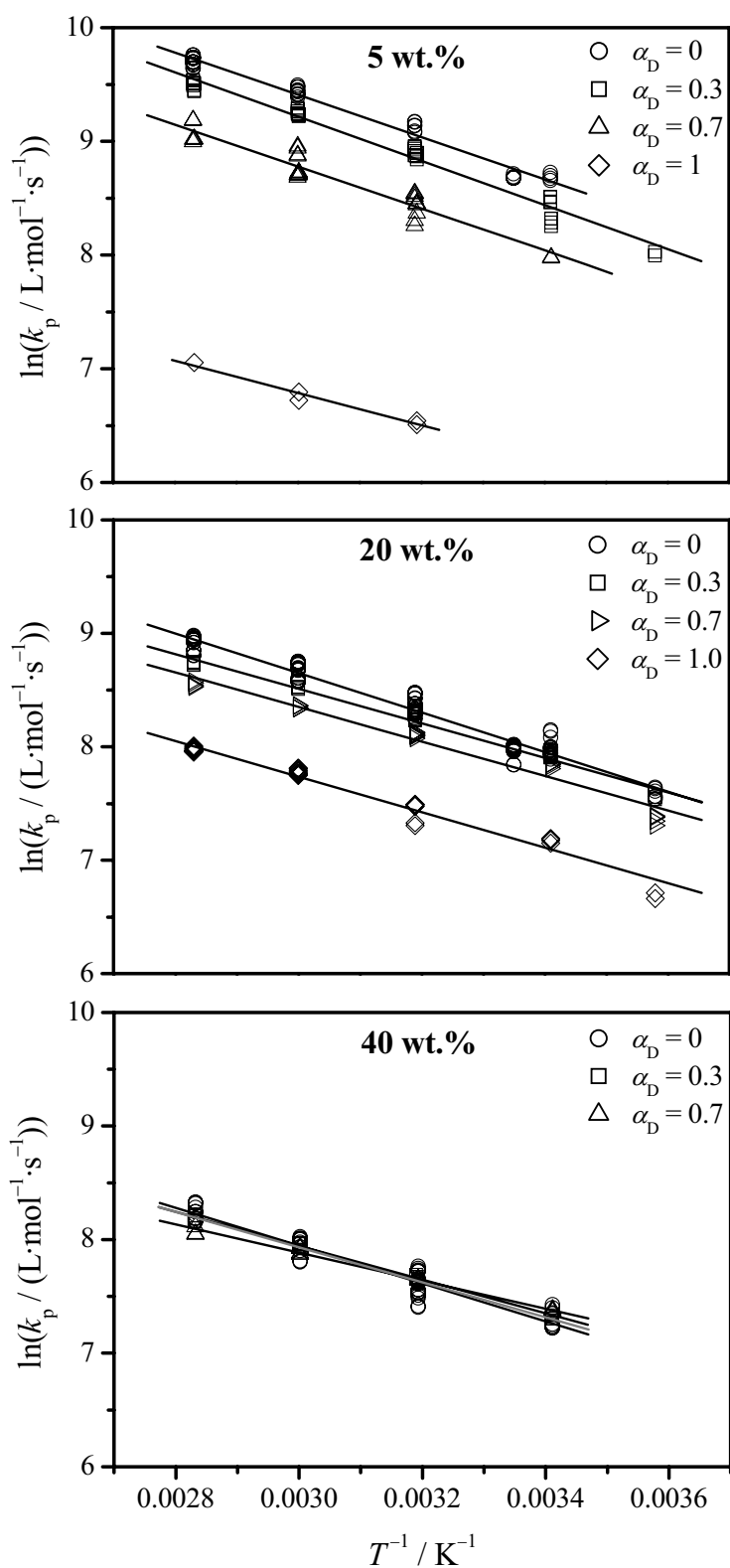


Figure 6-15: Arrhenius representations of k_p for polymerizations of MAA concentration of 5, 20 and 40 wt.% in water at various degrees of monomer ionization. The associated Arrhenius parameters are listed in Table 6-4. The grey line in the lowest figure represents a linear fit to the combined data set.

Table 6-4: Arrhenius parameters E_a and A for k_p of MAA polymerized in aqueous solution at different monomer concentrations and various degrees of MAA ionization.

α_D	5 wt.% MAA		20 wt.% MAA		40 wt.% MAA	
	E_a [kJ·mol ⁻¹]	$A \cdot 10^{-6}$ [L·mol ⁻¹ ·s ⁻¹]	E_a [kJ·mol ⁻¹]	$A \cdot 10^{-6}$ [L·mol ⁻¹ ·s ⁻¹]	E_a [kJ·mol ⁻¹]	$A \cdot 10^{-6}$ [L·mol ⁻¹ ·s ⁻¹]
0	15.8 ± 0.3	3.64	14.6 ± 0.3	1.10	14.0 ± 0.5	0.43
0.3	16.2 ± 0.4	3.45	12.7 ± 0.3	0.48	12.4 ± 0.2	0.25
0.7	15.3 ± 0.9	1.61	12.6 ± 0.5	0.40	10.3 ± 0.3	0.11
1.0	11.8 ± 1.2	0.06	13.0 ± 0.5	0.25	–	–

The statistical significance of the variation of Arrhenius parameters is more appropriately estimated from non-linear least-squares fitting.^[227] The resulting 95 % JCI, obtained assuming constant relative errors in k_p and T , are shown in Figure 6-16. The crosses indicate the associated best estimates for $E_a(k_p)$ and $A(k_p)$. For most of the polymerization conditions, the large data sets allowed for obtaining narrow and well separated JCIs. In principle, a similar conclusion can be drawn from this data evaluation as from the Arrhenius fits. Generally, the JCIs are shifting upon MAA ionization toward lower pre-exponential factors. This is accompanied by some lowering of the activation energy which is particularly pronounced for 5 and 40 wt.% of MAA.

However, compensation effects between $E_a(k_p)$ and $A(k_p)$ may contribute to the observed behavior of the Arrhenius parameters and the interpretation of JCIs should be made with caution in spite of their narrowness. Moreover, it cannot be ruled out that systematic errors, e.g. associated with the calculation of the density of ionized reaction solutions, may partially induce the changes in $E_a(k_p)$ and $A(k_p)$ for different c_{MAA} and α_D . Based on the available kinetic data it would hence be too ambitious to attempt a detailed mechanistic interpretation of the Arrhenius parameters. Further work is required, which may be directed toward studies into dynamics and structure of these complex polymerization systems, to accompany the kinetic analysis. Nevertheless, the information on the dependence of k_p on the polymerization conditions for polymerization of partially and fully ionized MAA provided by this work represents a significant progress. It allows for determination of individual termination rate

coefficients (by decoupling k_t/k_p or k_t/k_p^2) which should allow kinetic modeling also for this polymerization system.

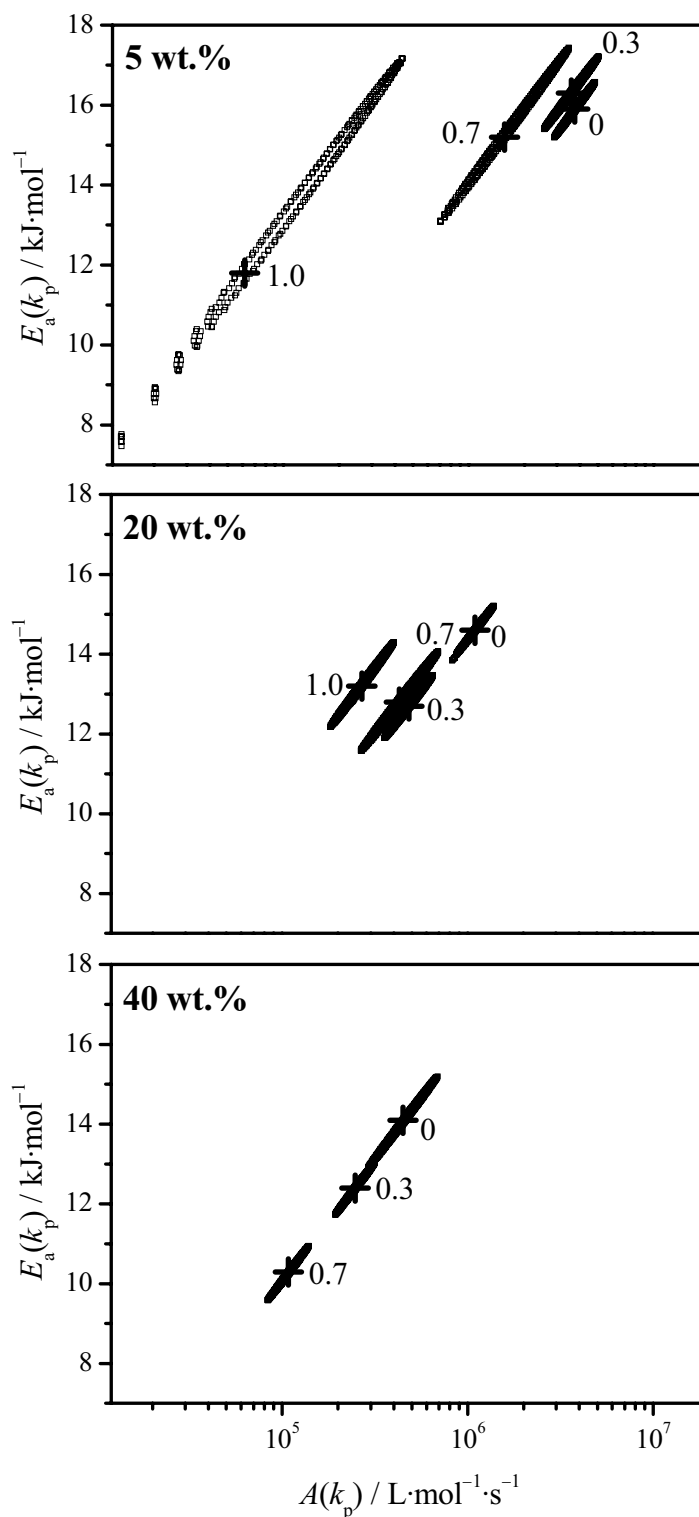


Figure 6-16: 95 % JCIs for aqueous phase polymerization of MAA at different monomer concentrations and degrees of monomer ionization. The crosses represent the Arrhenius parameters from non-linear least squares fitting of the k_p data.

7 Propagation Kinetics in *N*-Vinyl Pyrrolidone Polymerization

The effect of monomer concentration in water, of temperature, of monomer-to-polymer conversion, and of the degree of ionization on k_p for MAA was thoroughly discussed within the previous chapter. It was shown for non-ionized MAA that hydrogen-bonded interactions between the propagating MAA macroradical and an environment which, depending on the particular MAA concentration, consists of different relative amounts of MAA and water molecules, do not significantly affect the activation energy for propagation reaction, $E_a(k_p)$, but largely influence the pre-exponential factor, $A(k_p)$. The observed decrease in $A(k_p)$, by about a factor of 10, in passing from dilute aqueous MAA solution to bulk MAA polymerization, was assigned to the increased friction that the relevant degrees of rotational motion of the transition state structure experience upon replacing H₂O by MAA molecules (Chapter 6.1). Moreover, PLP-SEC experiments on aqueous solutions of non-ionized MAA to which poly(MAA) has been added demonstrated that k_p is determined by the actual monomer concentration and not by the overall content of MAA units (contained in both monomer and polymer). Hence k_p of MAA increases with monomer conversion during polymerization at constant overall content of MAA moieties (Chapter 6.2). Polymerizations of MAA at different degrees of ionic dissociation revealed that ionization also strongly affects k_p (Chapter 6.3).

It appeared to be of interest to see whether the picture that has evolved for MAA also applies to propagation kinetics of other monomers in aqueous phase. NVP should be well suited for this purpose, as the structure is completely different from the one of MAA. NVP bears no hydrogen atom for interaction via hydrogen bonds, but has a large dipole moment, perhaps even exceeding 4 Debye units, which is the dipole moment reported for *N*-methyl pyrrolidone.^[257] Strong dipolar interactions are expected to occur in both pure NVP and in NVP–water mixtures. In aqueous solutions also some hydrogen bonding may contribute to the intermolecular interactions.^[258,259] Moreover, in view of the technical importance of NVP polymerization,^[260] the lack of reliable rate coefficients for this monomer appears to be inadequate. The k_p values which were available so far, have been deduced by combining data from chemically initiated and from photoinitiated polymerization. The resulting k_p values are: $\approx 1\,000\text{ L}\cdot\text{mol}^{-1}\cdot\text{s}^{-1}$ for bulk polymerization at 20 °C^[261] and $\approx 22\,000\text{ L}\cdot\text{mol}^{-1}\cdot\text{s}^{-1}$ for 5.5 wt.% NVP in aqueous solution at 25 °C indicating similar effects of monomer concentration on k_p as observed for non-ionized MAA (see Chapter 6.1).^[262]

The data shown in this chapter results from a collaborative work involving PLP polymerization experiments carried out at the University of Göttingen, at Queen's University Kingston (Canada) and at the Polymer Institute of the Slovak Academy of Sciences in Bratislava accompanied by SEC characterization of poly(NVP) samples in Bratislava. This imparts, at least partially, a benchmark character to the obtained data.

As noted above, this work was carried out within an international cooperation project with contributions from Dr. Dušan Chorvát Jr, Prof. Robin A. Hutchinson, Dr. Igor Lacík, Dr. Marek Stach, and Lina Tang. A manuscript has been prepared for publication.^[263]

7.1 Dependence of k_p of NVP on monomer concentration and temperature

The pulsed-laser polymerizations were carried at NVP concentrations between 1.8 and 100 wt.% and temperatures between 2 and 60 °C using different PLP setups, two types of photoinitiator, different initiator concentrations as well as LPRRs. Moreover, it was checked whether the purity of NVP affects k_p .

Well-structured MWDs were obtained up to temperatures of 60 °C indicating that, unlike with acrylate monomers,^[13] intramolecular hydrogen transfer plays no major role in NVP radical polymerization. As compared to the ester moiety, the amide structure is less capable of activating α -hydrogen atoms on the backbone of NVP macroradicals and of poly(NVP). As a consequence, NVP behaves like the “classical” monomers subjected to PLP-SEC analysis, i.e. like styrene or methacrylates.

The experimental conditions of the large set of PLP-SEC measurements are listed in the upcoming publication.^[263] It was ensured that the IUPAC consistency criteria for reliable k_p measurement are fulfilled, i.e. $M_1/M_2 \approx 0.5$ and k_p is independent of photoinitiator concentration and type, LPRR, and setup used for PLP.^[8] The k_p values obtained for the different grades of NVP are more or less identical, although the different monomer qualities differ in absorption at the laser wavelength. Blank PLP experiments without photoinitiator on non-purified NVP showing significant laser light absorbance due to the stabilizing agent for NVP resulted in no polymer formation even after applying 300 pulses at ambient temperature. Hence, no special precaution needs to be taken for purifying NVP, contrary, e.g., to

polymerization of *N*-vinyl carbazole where significant PLP-induced polymerization occurred in the absence of photoinitiator.^[264]

Plotted in Figure 7-1 are the experimental k_p values (circles) as a function of NVP concentration for 25 °C. The cross symbols in Figure 7-1 represent the arithmetic mean of k_p values determined for each set of independent k_p measurements at a particular NVP content. With the exception of the data for 10 wt.% NVP, the individual k_p values are very close to the arithmetic mean value. Inspection of the data for 10 wt.% NVP reveals no systematic effect on k_p of either photoinitiator concentration, LPRR or the number of applied laser pulses, but indicates an uncertainty of about $\pm 15\%$ for k_p determination. Such an uncertainty is typical for PLP-SEC experiments. As can be seen from the entries in Figure 7-1, k_p varies enormously with the NVP content of the aqueous solution, from about $1\,000\text{ L}\cdot\text{mol}^{-1}\cdot\text{s}^{-1}$ for bulk polymerization up to about $20\,000\text{ L}\cdot\text{mol}^{-1}\cdot\text{s}^{-1}$ for an NVP concentration of 1.8 wt.%. A similar strong effect has been seen with k_p of non-ionized MAA in aqueous solution (see Chapter 6.1). It should be noted that the two literature values ($k_p \approx 1\,000\text{ L}\cdot\text{mol}^{-1}\cdot\text{s}^{-1}$ at 20 °C in bulk and $k_p \approx 22\,000\text{ L}\cdot\text{mol}^{-1}\cdot\text{s}^{-1}$ for $0.5\text{ mol}\cdot\text{L}^{-1}$ NVP)^[261,262] are remarkably close to the PLP-SEC data.

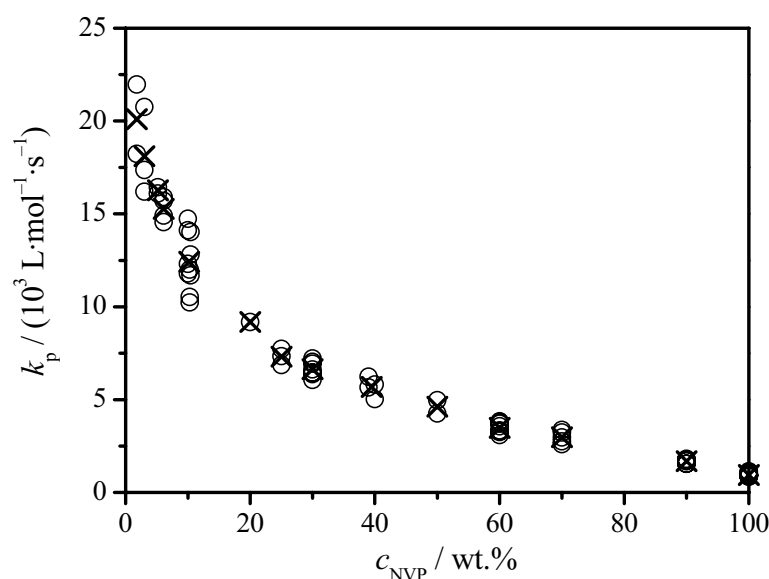


Figure 7-1: Variation of k_p with NVP concentration in aqueous solution at 25 °C (circles). The crosses represent the arithmetic mean k_p value for the individual NVP concentrations under investigation.

Presented in Figure 7-2 are the monomer concentration dependencies of the reduced propagation rate coefficients, $k_p/k_{p,\text{max}}$, for different temperatures. $k_{p,\text{max}}$ refers to the k_p value

obtained from extrapolation of k_p data at identical temperature to zero NVP concentration. The corresponding $k_{p,\max}$ values are $16\,793\text{ L}\cdot\text{mol}^{-1}\cdot\text{s}^{-1}$ at $15\text{ }^\circ\text{C}$, $21\,475\text{ L}\cdot\text{mol}^{-1}\cdot\text{s}^{-1}$ at $25\text{ }^\circ\text{C}$, $30\,154\text{ L}\cdot\text{mol}^{-1}\cdot\text{s}^{-1}$ at $40\text{ }^\circ\text{C}$, and $45\,212\text{ L}\cdot\text{mol}^{-1}\cdot\text{s}^{-1}$ at $60\text{ }^\circ\text{C}$. Within the limits of experimental accuracy, the reduced propagation rate coefficients for the experimental temperatures may be fitted by an expression with an exponential and a linear term in monomer concentration, c_{NVP} :

$$\frac{k_p}{k_{p,\max}} = 0.36 + 0.64 \cdot \exp(-0.092 \cdot (c_{\text{NVP}} / \text{wt.}\%)) - 0.0031 \cdot (c_{\text{NVP}} / \text{wt.}\%) \quad (7-1)$$

Absolute $k_p(c_{\text{NVP}}, T)$ values may be estimated via an Arrhenius expression for $k_{p,\max}$ with activation energy $E_a(k_p) = 17.6\text{ kJ}\cdot\text{mol}^{-1}$ (obtained as the arithmetic mean of the $E_a(k_p)$ values in Table 7-1, see below) and with frequency factor $A(k_p) = 2.57 \cdot 10^7\text{ L}\cdot\text{mol}^{-1}\cdot\text{s}^{-1}$.

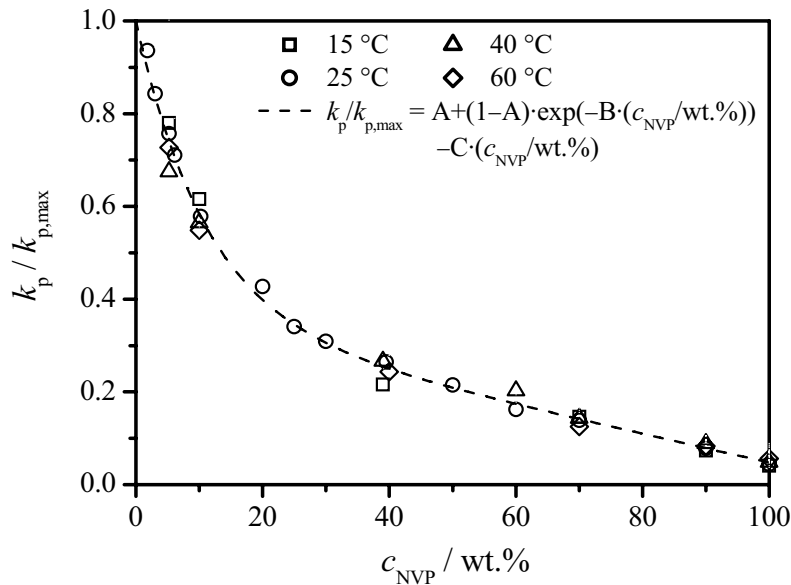


Figure 7-2: Dependence of $k_p/k_{p,\max}$ on c_{NVP} for polymerizations in aqueous solution at 15, 25, 40 and 60 °C. k_p is the arithmetic mean k_p value deduced from experiments at identical NVP concentration and temperature and $k_{p,\max}$ is the k_p value extrapolated toward $c_{\text{NVP}} = 0$ at the same polymerization temperature. The $k_{p,\max}$ values are $16\,793\text{ L}\cdot\text{mol}^{-1}\cdot\text{s}^{-1}$ at $15\text{ }^\circ\text{C}$, $21\,475\text{ L}\cdot\text{mol}^{-1}\cdot\text{s}^{-1}$ at $25\text{ }^\circ\text{C}$, $30\,154\text{ L}\cdot\text{mol}^{-1}\cdot\text{s}^{-1}$ at $40\text{ }^\circ\text{C}$ and $45\,212\text{ L}\cdot\text{mol}^{-1}\cdot\text{s}^{-1}$ at $60\text{ }^\circ\text{C}$. The dashed line represents the fit (to the function given in the figure) of the reduced k_p values. The parameter values of the fitted function are: $A = 0.36$, $B = 0.092$ and $C = 0.0031$.

That $k_p/k_{p,\max}$ may be fitted exclusively as a function of c_{NVP} , irrespective of temperature, is equivalent to saying that $E_a(k_p)$ is insensitive toward NVP concentration. This type of behavior has also been observed for k_p of MAA in aqueous solution. The pronounced

variation of k_p with c_{MAA} has been identified as a genuine kinetic effect that primarily influences the pre-exponential term, whereas attempts to assign the pronounced changes in PLP-SEC-derived k_p of MAA to specific local monomer concentrations at the free-radical site or to monomer association, e.g., to dimer formation, turned out to be not successful (see Chapter 6.1).

Table 7-1: $E_a(k_p)$ and $A(k_p)$ estimated from linear fitting of the logarithm of k_p of NVP in aqueous solutions of different NVP content and in bulk. The indicated uncertainties are standard deviations.

c_{NVP} [wt.%]	$E_a(k_p)$ [kJ·mol ⁻¹]	$A(k_p)$ [L·mol ⁻¹ ·s ⁻¹]	temperature interval [°C]	number of different temperatures	$k_p(25^\circ\text{C})$ extrapolated [L·mol ⁻¹ ·s ⁻¹]
5	16.0 ± 1.4	5.8 < 10.1 < 17.6	15 – 60	4	16 060
10	15.7 ± 0.5	5.9 < 7.0 < 8.4	15 – 60	4	12 662
40	18.3 ± 1.4	4.8 < 8.3 < 14.6	2 – 60	6	5 298
70	17.3 ± 0.6	2.6 < 3.3 < 4.2	10 – 55	5	3 032
90	18.0 ± 1.6	1.3 < 2.5 < 4.8	15 – 60	5	1 768
100	20.1 ± 2.1	1.4 < 3.3 < 7.8	15 – 60	5	1 013

In case of NVP, the limited number of data points, the relatively narrow temperature range, from 15 to 60 °C, and the experimental uncertainty, do not allow for a firm decision whether it is the pre-exponential factor or the activation energy, which changes, or whether both $A(k_p)$ and $E_a(k_p)$ change. Presented in Table 7-1 are the results of linear Arrhenius fitting of k_p values measured on aqueous solutions differing in NVP content and on bulk NVP. The mean values of k_p estimated from each series of individual k_p data obtained at identical c_{NVP} and identical polymerization temperature have been subjected to the fitting procedure. The temperature range and the number of different temperature levels of the underlying experiments are also listed in Table 7-1. The activation energy exhibits no systematic trend toward increasing NVP concentration, although the activation energy for bulk NVP polymerization appears to be slightly above $E_a(k_p)$ for aqueous solution. The two parameters, $E_a(k_p)$ and $A(k_p)$, are correlated by the Arrhenius fitting procedure. Larger uncertainties in

$E_a(k_p)$ are associated with larger uncertainties in $A(k_p)$, as is illustrated by the second and third columns in Table 7-1. The k_p values for 25 °C, as estimated from the mean values of the Arrhenius parameters for each NVP concentration, are given in the last column of Table 7-1. They are in close agreement with the associated experimental values.

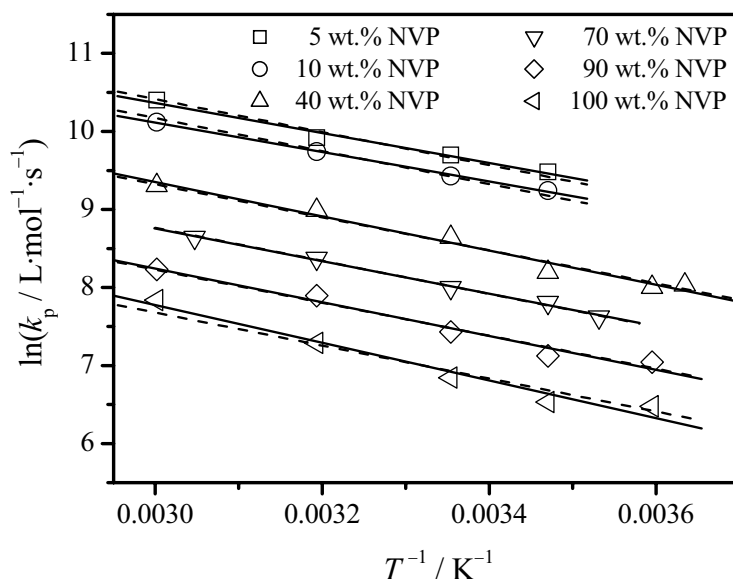


Figure 7-3: Arrhenius fits of the (averaged) propagation rate coefficients for NVP polymerizations in aqueous solution between 5 and 90 wt.% of monomer and for bulk NVP polymerization (full lines). The dashed lines represent Arrhenius fits to the same k_p data set assuming the activation energy to be constant at the mean value of $E_a(k_p) = 17.6 \text{ kJ}\cdot\text{mol}^{-1}$.

Shown in Figure 7-3 are the Arrhenius plots of k_p for NVP in aqueous solution and bulk polymerization. The arithmetic mean values of k_p (deduced from k_p data sets measured at identical NVP concentration and polymerization temperature) were subjected to Arrhenius fitting. The full lines illustrate the resulting fits. The dashed lines are obtained by Arrhenius fitting under the assumption that a single (mean) activation energy, $E_a(k_p) = 17.6 \text{ kJ}\cdot\text{mol}^{-1}$, applies to the entire data, irrespective of NVP concentration. Whether the bulk NVP data also fit into this picture can not be safely established on the basis of the available experimental k_p values. The relatively close comparison of the full and dashed Arrhenius lines for NVP bulk polymerization, however, indicates that using the mean value of activation energy, $E_a(k_p) = 17.6 \text{ kJ}\cdot\text{mol}^{-1}$, allows for reasonable k_p estimates for the entire NVP concentration range, at least at the polymerization temperatures under investigation.

It needs to be mentioned that the alternative procedure of trying to fit measured k_p by adopting a single mean value of $A(k_p)$ and adjusting $E_a(k_p)$ also affords for an adequate representation of k_p values measured in the experimental ranges of temperature and NVP concentration. Plotted in Figure 7-4 are the 95 % JCI^[227] of $E_a(k_p)$ and $A(k_p)$, as obtained from the entire k_p set. The JCIs indicate that both Arrhenius parameters may change with NVP concentration. Even for bulk NVP polymerization, however, where $E_a(k_p)$ appears to be above the activation energy for polymerization in aqueous solution, k_p may be estimated within experimental accuracy from the Arrhenius expression which adopts a single value of activation energy, $E_a(k_p) = 17.6 \text{ kJ}\cdot\text{mol}^{-1}$. Assigning the variations of k_p with NVP concentration entirely to $A(k_p)$ allows for using the same physical concept as with non-ionized MAA to interpret the variation with monomer concentration of k_p in aqueous solution. First experiments on *N*-vinyl formamide suggest that, also with this monomer, the variation of k_p within an extended monomer concentration and temperature range may be interpreted by changes of the pre-exponential rather than of activation energy.^[265]

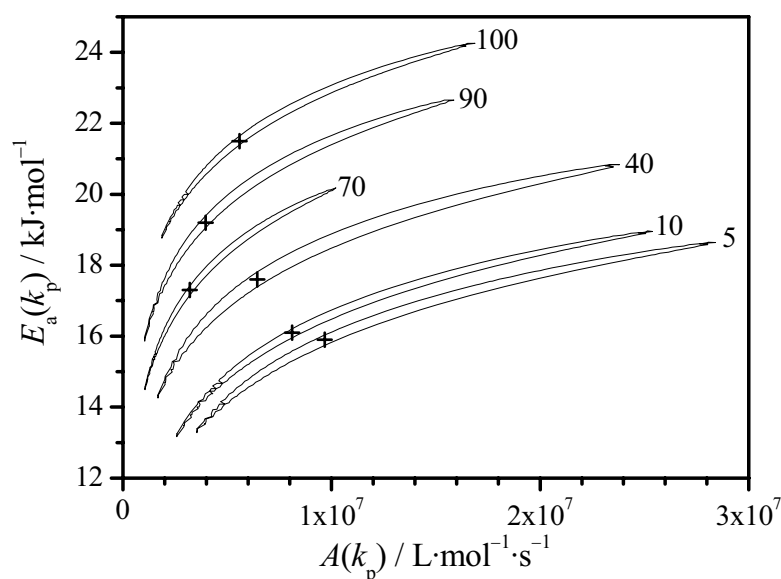


Figure 7-4: 95 % joint confidence intervals (JCIs) for k_p of NVP at different monomer weight concentrations in water (indicated by the numbers at the JCIs) and of NVP in bulk. The crosses represent the Arrhenius parameters from non-linear least squares fitting of the k_p data.

The results of fitting k_p for various NVP concentrations as a function of polymerization temperature may be summarized: Although effects of NVP concentration in aqueous solution on $E_a(k_p)$ may not be ruled out, it is not in conflict with experimental data to assign the

observed large changes of k_p with c_{NVP} entirely to $A(k_p)$. This behavior corresponds to the one observed with non-ionized MAA.

Illustrated in Figure 7-5 is the comparison of the dependence of reduced propagation rate coefficient, $k_p/k_{p,\text{max}}$, on monomer concentration (at low degrees of initial monomer conversion) for NVP and for non-ionized MAA. The dependencies are close to each other and are more or less identical at monomer concentrations up to 20 wt.%. No full agreement is expected, as the intermolecular forces in the NVP and MAA systems are rather different. It should be recalled that even for one and the same monomer, as has been demonstrated for MAA (see Chapter 6.3), variation of pH may completely change the dependence of $k_p/k_{p,\text{max}}$ on monomer concentration and even gives rise to an increase in k_p upon enhancing monomer concentration in aqueous solutions of fully ionized MAA.

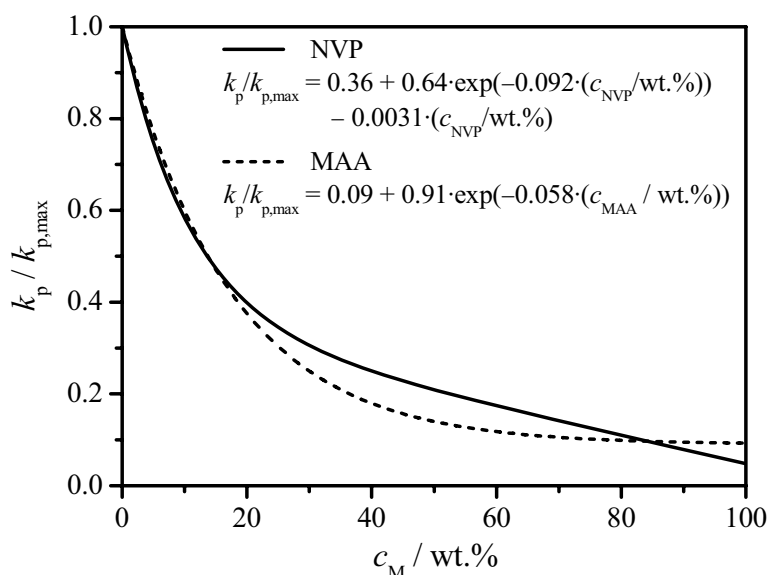
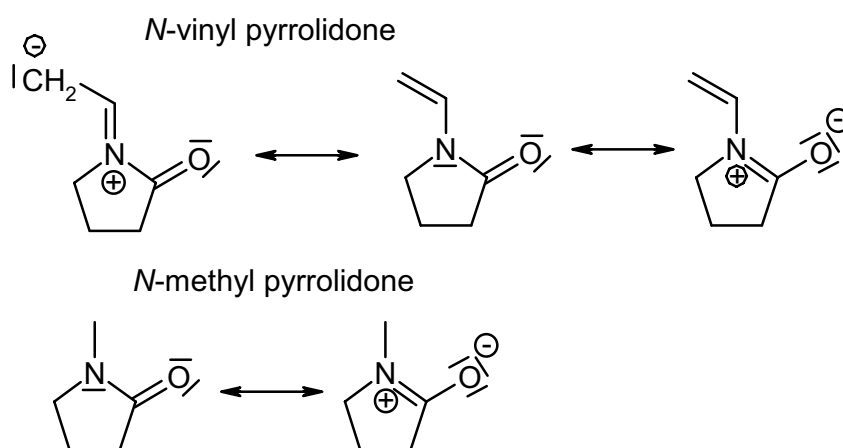


Figure 7-5: Exponential fits of the variation with (initial) monomer concentration of reduced propagation rate coefficient, $k_p/k_{p,\text{max}}$, for polymerization in aqueous solution of NVP and of non-ionized MAA (see Chapter 6.1). The underlying k_p values are deduced from PLP-SEC experiments and thus hold for low degrees of monomer-to-polymer conversion referring to the widely differing initial monomer concentrations plotted on the abscissa.

The similarity of the dependence of k_p on monomer concentration for NVP and for non-ionized MAA provides further support for the same physical effect being operative in both cases. According to transition state theory, the pre-exponential factor is essentially determined by the geometry of the rotating groups in the reactants and by the rotational potentials of the relevant internal (hindered) motions in the TS.^[17] Large hindrance of rotational freedom is

associated with a significant entropy penalty which results in a smaller $A(k_p)$ value and thus in smaller k_p . Applying this knowledge to the k_p data of MAA and NVP measured upon passing from bulk to aqueous solution polymerization, leads to the conclusion that the gradual replacement of monomer molecules by H_2O molecules changes the environment of the TS structure for addition of a monomer molecule to a macroradical such that the chain end experiences a higher degree of rotational freedom. Thus the relevant degrees of freedom in the TS for propagation experience less friction toward increasing water content resulting in an increase of k_p toward lower monomer concentration. Interestingly, the larger hindrance of internal rotational mobility in the propagation TS structure for polymerization at high monomer concentrations, including bulk polymerization, may be brought upon by both hydrogen-bonded interactions, as with non-ionized MAA, and by strong dipolar interactions, as with NVP. That dipolar interactions in NVP can induce an effect similar to the one of hydrogen bonds in MAA is probably due to the size of the NVP dipole moment, μ_{NVP} .^[266] The value μ_{NVP} has not been reported so far. However, it appears likely that μ_{NVP} even exceeds the large dipole moment of *N*-methyl pyrrolidone, (NMP), which is $\mu_{NMP} = 4.06$ D.^[257] The reason behind such large dipole moments is seen in the participation of the nitrogen lone pair electrons to resonance structures for NMP and NVP, as depicted in Scheme 7-1. The assumption of μ_{NVP} being even above μ_{NMP} is based on the fact that the vinyl double bond may enhance the contribution of the resonance structure with a positive charge on the nitrogen and a negative charge on the oxygen atom because of the more extended delocalization associated with these structures. The structures in Scheme 7-1 illustrate that the large dipole moment occurs with NVP, with poly(NVP) and with NVP macroradicals.



Scheme 7-1: Resonance structures of *N*-vinyl pyrrolidone and *N*-methyl pyrrolidone, respectively.

The results for NVP and for MAA suggest that a significant decrease of k_p toward higher monomer concentration seems to be a general phenomenon with non-ionized water-soluble monomers. The reason behind these large solvent effects on k_p with hydrogen-bonded and highly polar monomers in aqueous solution is due to the fact that the intermolecular interactions between functional groups of the monomeric (and polymeric) species and a molecular environment consisting either of monomer or of water are strong, but are different. In principle, solvent effects on k_p are generally occurring. Intermolecular interactions may, however, be too weak as to give rise to easily detectable effects on k_p and mostly the polarities of monomer and solvent will be close to each other, which results in very similar effects on the hindrance to internal friction of the TS structure. It should be noted that, in bulk polymerization, the monomer may be looked upon as a particular solvent. In solution polymerizations, the solvent is frequently chosen such as to be not too dissimilar in polarity from the monomer. Thus the differences in intermolecular interactions of TS structure with molecular environment are not sufficiently pronounced as to give rise to clearly different k_p values. After the safe detection and understanding of the strong k_p solvent effect in MAA aqueous-solution polymerization, closer inspection of acrylate and methacrylate homo- and copolymerizations^[267] has revealed that basically the same entropy-related effects occur with these monomers without water being present. These effects are however less pronounced and require highly accurate PLP-SEC analyses.

7.2 Conversion dependence of k_p for polymerization of NVP in water

The k_p data presented so far refer to polymerization at low degrees of NVP conversion, mostly below 5 %, as is typical for investigations via PLP-SEC. For practical purposes, information on k_p up to much higher monomer conversions is required. For MAA, the situation of higher conversion was simulated by the addition of either poly(MAA) or IBA which may be looked upon as the limiting case of low-molecular-weight “polymer” (see Chapter 6.2). At these virtual conversions to high and to low molecular weight polymer, PLP-SEC experiments were carried out, each of them covering only a small conversion interval as is characteristic for PLP-SEC studies. The results indicate that the effect on k_p is brought upon by low-molecular-weight components containing carboxylic acid moieties. MAA and IBA are part of the intra-coil environment and thus may interact with the radical site embedded in such a coil.

Carboxylic groups on poly(MAA) molecules, on the other hand, do not or not significantly contribute to these interactions unless macroradical and polymeric coils are strongly interpenetrating each other. In essence, the MAA study revealed that k_p in aqueous solution varies with the actual ratio of monomer to water concentrations in the system as far as high-molecular-weight polymer is produced. This ratio depends on both the initial monomer concentration and the monomer-to-polymer conversion.

A corresponding study was carried out for NVP polymerization at 25 °C with *N*-ethyl pyrrolidone, NEP, being the saturated analogue to NVP, and with two commercial poly(NVP) samples of weight average molecular weights of 24 000 and 360 000 g·mol⁻¹ being used for simulating NVP conversion to high-molecular-weight material.

The reference system for the entire data set is the one in which 20 wt.% NVP are dissolved in water without any additive. Different amounts of NEP and poly(NVP) are added to aqueous NVP solutions such that the overall content of pyrrolidone moieties is 20 wt.%. The quantity X_{virtual} has been selected for easier comparison of k_p data determined in aqueous solution without any additive to k_p values measured in aqueous solution in the presence of either NEP or poly(NVP) (see Chapter 6.2).

The resulting dependence of k_p on virtual conversion is depicted in Figure 7-6. A close look at the NVP k_p data measured in the presence of NEP (diamonds) indicates that the k_p values are slightly above the ones measured at the same overall pyrrolidone content, but with only NVP being present (dashed line). This observation might be explained by a smaller dipole moment of NEP as compared to NVP (see the above discussion related to Scheme 7-1), which goes with weaker intermolecular interactions, thus with a lower friction and a slightly higher k_p . Also contained in this figure are a few data points for polymerization in aqueous solution of NVP at concentrations below 20 wt.% (without any additive). Within the concept of virtual conversion, these data are treated as if the lower NVP concentration results from reaction to poly(NVP) with the polymer however being removed from the solution as, e.g., in a precipitation polymerization. The so-obtained k_p vs. X_{virtual} data points (squares) are close to the ones obtained for NVP / poly(NVP) systems (circles and triangles) thus supporting the view that only the pyrrolidone species which may access the interior of macroradical coils are affecting k_p .

With respect to polymerization of NVP in aqueous solution up to high degrees of monomer conversion, the information may be summarized follows: k_p is determined by the actual ratio of NVP to water and thus increases with the degree of NVP conversion. Replacing NVP by

poly(NVP), on the other hand, significantly enhances k_p . The polymer appears to be not available at the site of the growing radical, an observation which is in full agreement with what has been described for MAA within Chapter 6.2.

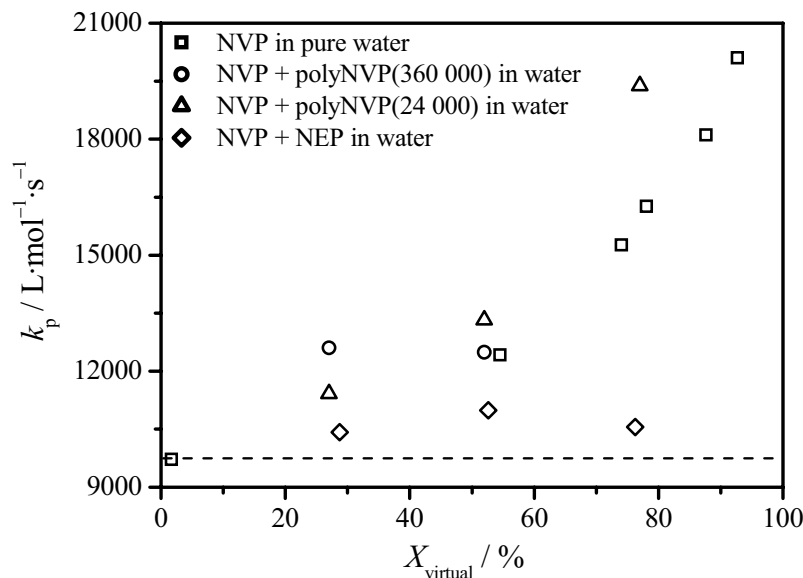


Figure 7-6: Dependence of k_p on X_{virtual} for polymerizations of NVP in water at 25 °C, $c_{\text{Daro-cur}} = 2 \text{ mmol}\cdot\text{L}^{-1}$ and an LPRR of 30 Hz. The squares represent polymerizations of NVP in water at different $c_{\text{NVP}} \leq 20 \text{ wt.}\%$. The k_p values indicated by the circles and triangles refer to polymerizations of NVP in the presence of poly(NVP) of different molecular weight, while the diamonds refer to polymerizations of NVP in the presence of NEP. X_{virtual} was calculated based on the conversion-dependent change in the ratio of NVP to water in polymerizations of an initial monomer concentration (or overall acid concentration) of 20 wt.%. The dashed line indicates the mean value of low conversion k_p .

7.3 Dependence of k_p on pH for polymerization of NVP in aqueous solution

With MAA, the k_p values turned out to be strongly dependent on the pH with this effect being particularly pronounced at low monomer concentrations, where k_p is decreased by about one order of magnitude in passing from non-ionized to fully ionized MAA. This effect becomes very weak at intermediate MAA concentrations and is even reversed at monomer concentrations above 40 wt.% (see Chapter 6.3). Although no significant effect of pH is expected to occur with NVP, as the molecule cannot dissociate, a series of experiments for several NVP concentrations has been carried out to see, whether k_p of NVP exhibits some

sensitivity to *pH*. The early kinetic studies into NVP polymerization rate within the *pH* interval 7 to 10 provided no indication of any *pH* effect.^[262] In the present study, *pH* was varied from 3 to 11. This extended range encompasses *pH* situations as are met in copolymerization reactions of NVP with comonomers exhibiting acid or base properties.

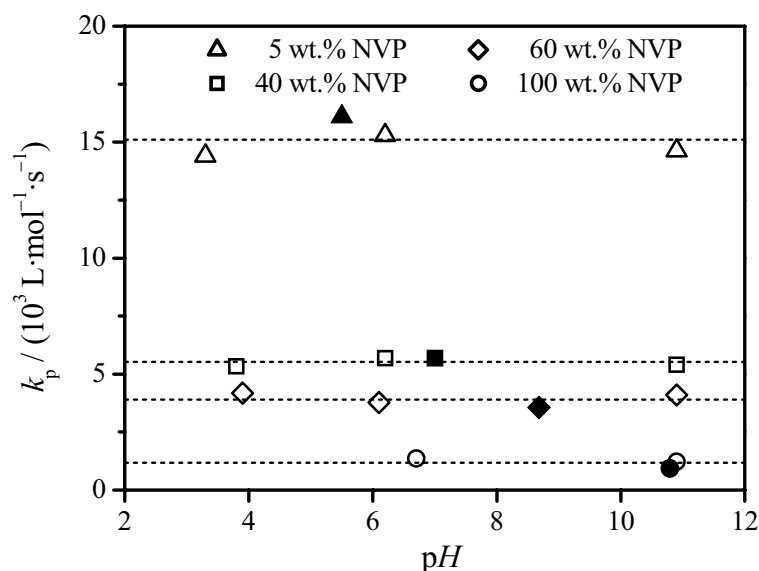


Figure 7-7: k_p as a function of *pH* for polymerizations of NVP at 25 °C in aqueous phase at monomer concentrations of 5, 40, 60 and 100 wt.% (plotted in the figure are the arithmetic mean values deduced from polymerization experiments at identical NVP concentration and temperature). The open symbols refer to polymerizations with the *pH* being adjusted either by NaOH or acetic acid. The filled symbols refer to solutions prepared by using NVP as received (from Fluka stabilized with *N,N'*-di-*sec*-butyl-*p*-phenylenediamine) without additionally adjusted *pH*. The dashed lines indicate the arithmetic mean k_p values for each initial NVP concentration.

The k_p values for 5, 40, 60 and 100 wt.% of NVP in water were measured at 25 °C and different *pH*. The obtained data are plotted in Figure 7-7 as the arithmetic mean of k_p measured at identical NVP concentration. The open symbols refer to aqueous NVP solutions with the *pH* being adjusted by using either sodium hydroxide or acetic acid. The filled symbols represent data taken on solutions without adjusted *pH*. The *pH* of these aqueous NVP solutions increases, between 5 to 100 wt.% from 6 up to 11, because NVP “as supplied” was used which contained *N,N'*-di-*sec*-butyl-*p*-phenylenediamine as the stabilizer. Higher NVP content thus is correlated with a higher amine content which in turn results in a higher *pH*. Figure 7-7 demonstrates that k_p for the aqueous solution polymerizations of NVP is not affected by *pH* in the interval from 3 to 11 over the entire c_{NVP} range examined

experimentally. NVP decomposes at acidic *pH* and higher temperature.^[268] The experimental k_p data for low *pH* in Figure 7-7 may nevertheless be considered reliable, because of the short time interval required for the experiment and the low polymerization temperature of 25 °C.

8 Termination Kinetics in Methacrylic Acid Polymerization

MAA is perfectly suited for studies into the termination kinetics in aqueous solution, as PLP-SEC, SP-PLP-NIR, and chemically initiated experiments may be carried out, which allows for deducing k_t from two independent sources, SP-PLP-NIR and chemically induced polymerization, both in conjunction with literature evidence on k_p . Moreover, MAA polymerization kinetics is much simpler than the one of acrylate-type monomers, such as AA, where inter- and intramolecular chain transfer results in the formation of MCRs which leads to a rather complicated kinetic scheme with additional rate coefficients that are not easily accessible (see Chapters 10 and 13).

SP-PLP-NIR experiments on aqueous MAA solutions with initial monomer concentrations of $3.50 \text{ mol}\cdot\text{L}^{-1}$ and $7.09 \text{ mol}\cdot\text{L}^{-1}$ (30 and 60 wt.% MAA, respectively) were carried out. To obtain reasonable signal-to-noise quality of the SP-PLP-NIR experiment, a reaction pressure of 2000 bar was used. As the compressibility of the polymerizing systems is rather low, there is no reason to assume that high pressure affects the polymerization mechanism. Chemically induced MAA polymerizations were also carried out at this high pressure. In both types of experiments, SP-PLP-NIR and chemically initiated polymerizations, k_t refers to a chain-length-averaged quantity, which is made clear by denoting the primary experimental quantities as $\langle k_t \rangle / k_p$ and $\langle k_t \rangle / k_p^2$, respectively. It needs to be noted that the averaging of k_t occurs over different radical distributions: In the instationary SP-PLP-NIR experiment, termination occurs between radicals of almost identical size which linearly increases with time after applying the laser pulse (unless chain transfer comes into play) whereas, in the stationary chemically initiated polymerizations, termination occurs between radicals of arbitrary size.^[7,11,198,269]

The studies detailed in this chapter were carried out in cooperation with Prof. Sabine Beuermann, Prof. Robin A. Hutchinson, Dr. Silvia Kukučková and Dr. Igor Lacík. Part of this work has already been published in refs.^[75,270]

8.1 Generalized k_p correlation

The primary experimental results of instationary SP-PLP-NIR experiments and stationary chemically induced polymerizations are $\langle k_t \rangle / k_p$ and $\langle k_t \rangle / k_p^2$, respectively. Thus, estimation of $\langle k_t \rangle$ from those coupled parameters requires knowledge of the propagation rate coefficient at reaction conditions, that is temperature, pressure, initial monomer concentration and monomer-to-polymer conversion. To estimate k_p for different experimental conditions, the k_p dependencies need to be fitted to appropriate functional forms. It was shown in Chapter 6.1 that the temperature dependence of k_p is associated with an almost constant activation energy ($15.2 \pm 0.8 \text{ kJ} \cdot \text{mol}^{-1}$) within wide ranges of monomer concentration, from 5 wt.% MAA in water to bulk polymerization, which allows to introduce one single temperature dependent parameter into the data fitting procedure. The propagation rate coefficient which was extrapolated to infinitely low monomer concentrations in water, $k_{p,\text{max}}$, was estimated to be:

$$k_{p,\text{max}}(T) / \text{L} \cdot \text{mol}^{-1} \cdot \text{s}^{-1} = 3.5 \cdot 10^6 \cdot \exp\left(-\frac{1.83 \cdot 10^3}{(T/\text{K})}\right) \quad (8-1)$$

The decrease of k_p toward increasing initial monomer concentration was implemented by fitting the experimental data to an exponential decay function which includes an offset

$$k_p(w_{\text{MAA}}^0, T) = k_{p,\text{max}} \cdot (A + (1 - A) \cdot \exp(-B \cdot w_{\text{MAA}}^0)) \quad (8-2)$$

where w_{MAA}^0 is the initial weight fraction of MAA in water and A and B are fit parameters. The values of A and B were adjusted to match the curvature of the experimental data in a plot of $k_p/k_{p,\text{max}}$ versus w_{MAA}^0 . The best representation of the experimental data was achieved for $A = 0.08$ and $B = 5.3$. The k_p values for ambient-pressure polymerizations of MAA in water at different polymerization temperatures are plotted against monomer weight fraction in Figure 8-1. The lines are estimates according to Eq. (8-2) using the parameters given above. The ordinate is plotted in logarithmic form in order to obtain a good visualization of the excellent agreement of the experimental data with the simple fit function and one single set of parameters A and B.

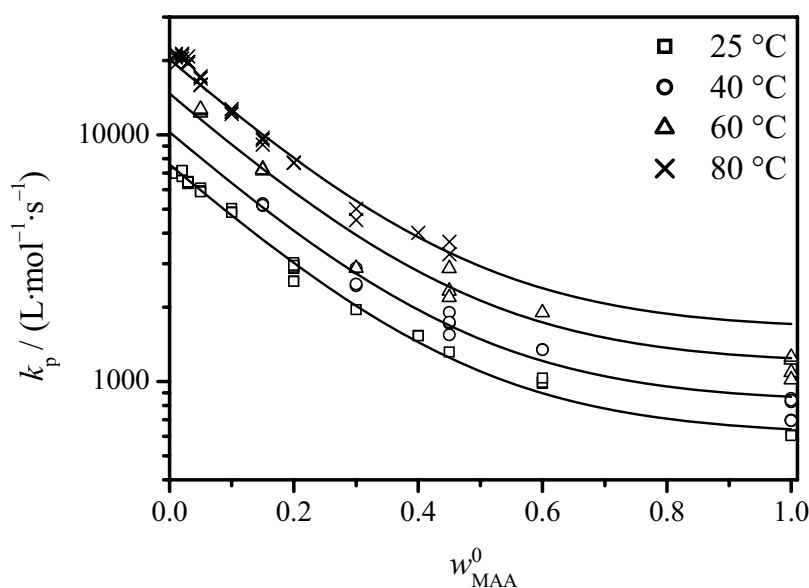


Figure 8-1: Dependence of the k_p on the initial weight fraction of monomer in water, w_{MAA}^0 , for polymerization of MAA in water at ambient pressure and different temperatures (data from Chapter 6.1). The full lines are best fits of the experimental data to Eq. (8-2) with the parameters $A = 0.08$ and $B = 5.3$.

For additional implementation of the pressure dependence of k_p , data collected for polymerizations of 10, 30 and 60 wt.% of MAA carried out at 25 °C and pressures ranging from 1 to 2000 bar^[270,271] were analyzed. Linear regression of the variation of $\ln(k_p)$ with pressure, p , results in a monomer-concentration-dependent activation volume of $\Delta V^\ddagger(k_p) = -(8.0 + 9.0 \cdot w_{\text{MAA}}^0) \text{ cm}^3 \cdot \text{mol}^{-1}$. The extrapolated activation volume of $-17.0 \text{ cm}^3 \cdot \text{mol}^{-1}$ for 100 wt.% MAA ($w_{\text{MAA}}^0 = 1$) is close to $\Delta V^\ddagger(k_p) = -16.7 \text{ cm}^3 \cdot \text{mol}^{-1}$ determined for MMA bulk polymerization at 30 °C.^[272] The origin of the significant reduction in the absolute value of $\Delta V^\ddagger(k_p)$ toward lower MAA concentration in water is not yet clear. The general dependence of k_p on temperature, pressure, and initial weight fraction of monomer in water reads:

$$k_p(w_{\text{MAA}}^0, T, p) / \text{L} \cdot \text{mol}^{-1} \cdot \text{s}^{-1} = \left(2.8 \cdot 10^5 + 3.2 \cdot 10^6 \cdot \exp(-5.3 \cdot w_{\text{MAA}}^0) \right) \cdot \exp\left(-\frac{1.83 \cdot 10^3 - (0.096 + 0.11 \cdot w_{\text{MAA}}^0) \cdot (p/\text{bar})}{(T/\text{K})} \right) \quad (8-3)$$

This k_p correlation refers to the weight fraction of MAA in the initial polymerization period, where PLP-SEC experiments are generally performed. In order to estimate k_p as a function of monomer-to-polymer conversion, a series of PLP-SEC experiments has been carried out on

systems with pre-mixed poly(MAA) (see Chapter 6.2). The resulting data reveals that it is primarily the ratio of monomeric MAA to water which determines k_p . Whether the MAA-in-water concentration is varied by selecting different initial MAA contents or by consuming monomer during polymerization plays no major role. Eq. (8-3) thus appears to be valid for any MAA weight fraction, w_{MAA} . Arbitrary w_{MAA} may be expressed by the initial weight fraction, w_{MAA}^0 , and the degree of monomer conversion, X , according to Eq. (8-4):

$$w_{\text{MAA}} = \frac{w_{\text{MAA}}^0 \cdot (1 - X)}{1 - w_{\text{MAA}}^0 \cdot X} \quad (8-4)$$

It should be noted that the MAA weight fraction, w_{MAA} , in Eq. (8-4) is solely determined by the actual monomer and water concentrations. Poly(MAA) material is not included in the estimate of this weight fraction. As mentioned in Chapter 6.2, poly(MAA) may influence k_p in cases when the molecular weight is small or the polymer contents in the reaction mixture are high. Combination of Eqs. (8-3) and (8-4) yields Eq. (8-5), which may be applied for estimating k_p as a function of initial MAA concentration, of monomer conversion, of temperature and of pressure. The so-obtained k_p data were used to estimate $\langle k_t \rangle$ from the primary experimental quantities, $\langle k_t \rangle / k_p$ and $\langle k_t \rangle / k_p^2$, deduced from instationary SP-PLP-NIR experiments and stationary chemically induced polymerizations, respectively.

$$k_p(w_{\text{MAA}}^0, T, p, X) / \text{L} \cdot \text{mol}^{-1} \cdot \text{s}^{-1} = \left(2.8 \cdot 10^5 + 3.2 \cdot 10^6 \cdot \exp\left(-\frac{5.3 \cdot w_{\text{MAA}}^0 \cdot (1 - X)}{1 - w_{\text{MAA}}^0 \cdot X}\right) \right) \cdot \exp\left(-\frac{1.83 \cdot 10^3 - \left(0.096 + \frac{0.11 \cdot w_{\text{MAA}}^0 \cdot (1 - X)}{1 - w_{\text{MAA}}^0 \cdot X}\right) \cdot (p/\text{bar})}{(T/\text{K})}\right) \quad (8-5)$$

8.2 Determination of $\langle k_t \rangle$ by SP-PLP-NIR

As an example of primary experimental data from SP-PLP-NIR, the upper part of Figure 8-2 shows two MAA concentration vs. time traces obtained during the course of an experiment with an initial MAA concentration of 60 wt.%. Relative monomer concentration is plotted vs.

time t after applying the laser pulse at $t = 0$. Monomer conversion from preceding laser pulsing was 6.1 % and 22.5 %, respectively. The horizontal pre-trigger region in Figure 8-2 demonstrates that polymerization induced by preceding pulses has ceased. At 0.04 s after firing the laser pulse, relative MAA concentration, has decreased by about 0.11 % within the SP-PLP-NIR experiment carried out at $X = 0.061$, that is at a poly(MAA) fraction of 3.7 wt.%. At a later stage during the same polymerization reaction, at a polymer weight fraction of 13.5 wt.% ($X = 0.225$), a single laser pulse induces a change in relative monomer concentration by 0.15 % between $t = 0$ and 0.04 s.

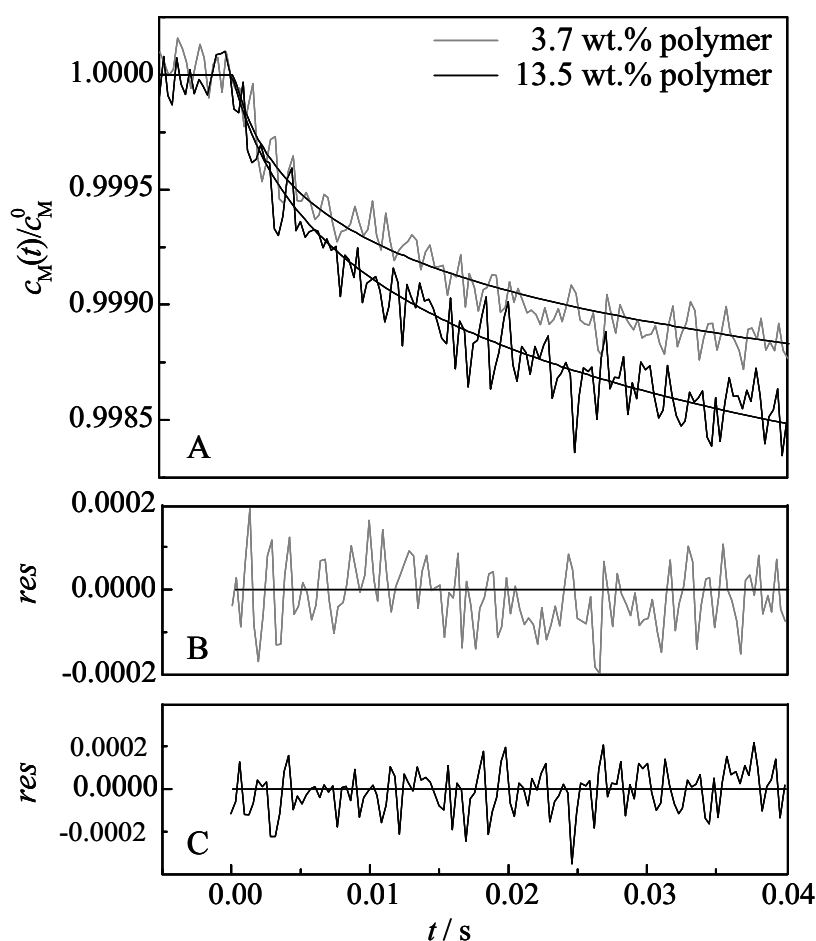


Figure 8-2: Change in relative monomer concentration after applying an excimer laser pulse, at $t = 0$, during a polymerization of 60 wt.% MAA in aqueous solution at 50 °C and 2000 bar (A). At $t = 0$, when the laser pulse is applied, the poly(MAA) content from preceding polymerization is 3.7 wt.% or 13.5 wt.% (6.1 and 22.5 % of monomer-to-polymer conversion, respectively). Differences between measured data and the ones fitted to Eq. (3-7) are illustrated by the plot of residuals (res) in the lower part of the figure, where (B) and (C) refer to experiments carried out at overall MAA conversions of 6.1 and 22.5 %, respectively.

The concentration vs. time traces in Figure 8-2 were fitted to Eq. (3-7) which refers to ideal single pulse kinetics. In systems where chain transfer is negligible, termination in SP-PLP experiments occurs between two radicals of almost identical length i , where i increases linearly with time t after applying the laser pulse at $t = 0$. To indicate that termination kinetics is chain-length dependent (see Chapter 3.4.2), k_t in Eq. (3-7) has been replaced by $\langle k_t \rangle$.

The fits to Eq. (3-7) of the measured MAA conversion vs. time data allow for an excellent representation of the experimental data, as is also demonstrated by the plots of residuals in the lower part of Figure 8-2. The time interval up to 0.04 s refers to the range in which chain length i increases up to approximately 1000.^[97] SP-PLP-NIR traces measured at the lower MAA concentration of 30 wt.% are equally well fitted to Eq. (3-7). Thus, each of the two signals in Figure 8-2A may be adequately represented by one $\langle k_t \rangle$ value, although a wide range of radical chain lengths is covered within both monomer concentration vs. time traces. As discussed elsewhere (see Chapter 5.5.1 and ref.^[198]), the remarkable quality of the data fit to Eq. (3-7) is not indicative of k_t being independent of chain length, but is a specific feature of DMPA acting as the photoinitiator. There is partial compensation of the effects due to chain length dependent k_t and to primary radical termination of the poorly initiating acetal fragment.

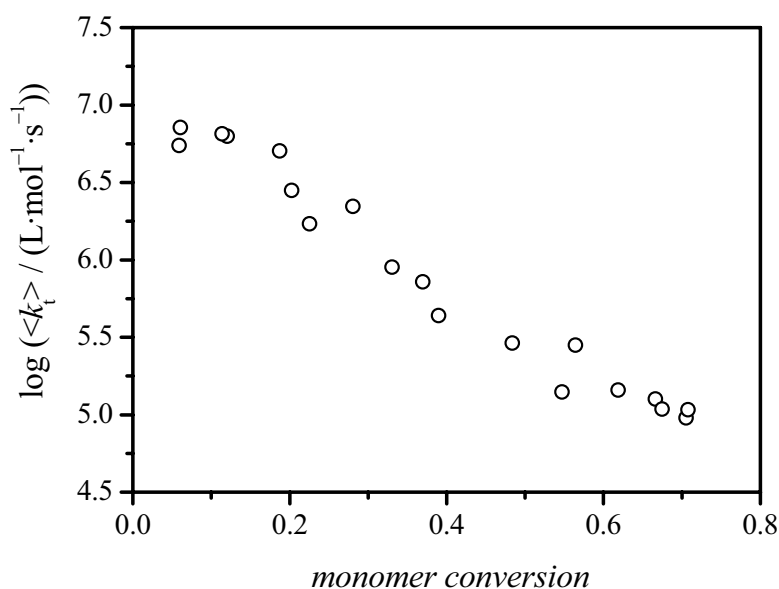


Figure 8-3: Dependence of $\langle k_t \rangle$ on monomer conversion for polymerization of 60 wt.% MAA in aqueous solution at 50 °C, 2000 bar and a photoinitiator concentration of $c_{\text{DMPA}} = 5 \cdot 10^{-3} \text{ mol} \cdot \text{L}^{-1}$. $\langle k_t \rangle$ was calculated from $\langle k_t \rangle / k_p$ by using the k_p expression given in Eq. (8-5).

The variation of $\langle k_t \rangle$ with monomer conversion, as obtained via fitting of SP-PLP-NIR traces to Eq. (3-7) and implementing k_p according to Eq. (8-5), is plotted in Figure 8-3 for an aqueous-phase MAA polymerization at 50 °C and 2000 bar. The initial MAA concentration was 60 wt.%. Data could be measured up to 70 % MAA conversion before the reaction mixture turned heterogeneous. Within the experiment carried out on the solution with an initial concentration of 30 wt.% MAA, even 90 % monomer conversion could be reached. In the initial reaction period an approximately constant value of $\langle k_t \rangle$ is found. Above $X = 0.20$, $\langle k_t \rangle$ decreases significantly, by around one and a half orders of magnitude up to $X = 0.50$. Such significant changes of $\langle k_t \rangle$ are typical for methacrylate monomers with small and medium-size alkyl ester side chain, such as MMA^[16,96,273] and BMA.^[138]

The $\langle k_t \rangle$ vs. X dependence in Figure 8-3 may be understood by assuming control of termination by segmental diffusion (SD), translational diffusion (TD), and reaction diffusion (RD) (see Chapter 3.3.3). At low conversion, $\langle k_t \rangle$ is determined by SD, which refers to the orientational motion of two coiled macroradicals by which the radical functionalities approach each other sufficiently closely to allow for immediate termination. Increasing monomer conversion is associated with an increase in bulk viscosity. As a consequence, translational (center-of-mass) diffusion may become rate determining. The data in Figure 8-3 indicate that $\langle k_t \rangle$ runs under control by TD at about $X = 0.20$. The pronounced decrease in $\langle k_t \rangle$ up to $X = 0.50$ reflects the reduced translational mobility of the macroradicals at significantly increasing bulk viscosity. At even higher degrees of monomer conversion, the lowering of $\langle k_t \rangle$ with X is less pronounced, an observation that indicates that $\langle k_t \rangle$ becomes controlled by reaction diffusion.^[91] Control of $\langle k_t \rangle$ by reaction diffusion suggests that the motion of the radical functionality essentially occurs via propagation steps of the dangling free-radical chain end. Eq. (3-28) was introduced to model $\langle k_t \rangle$ for polymerizations where SD, TD, and RD control are operating (see Chapter 3.3.3).^[22] This expression considers a diffusion control of k_p which may set in at high conversions. Such diffusion limitation is not expected to occur within the solution polymerizations of MAA studied within this work. Thus, the following simplified expression may be used with k_p varying with conversion as described by Eq. (8-5).

$$\langle k_t \rangle = \frac{1}{k_{SD}^{-1} + \eta_t(X)/k_{TD}^0} + C_{RD} \cdot (1 - X) \cdot k_p \quad (8-6)$$

Plotted in Figure 8-4 are the $\langle k_t \rangle$ values for polymerizations of 30 and 60 wt.% MAA in water at 50 °C and 2000 bar which are obtained from $\langle k_t \rangle/k_p$ using the k_p correlation given in

Eq. (8-5). For 30 wt.% MAA, the initial plateau value of $\langle k_t \rangle$ is slightly above the one for 60 wt.% and extends up to higher degrees of monomer conversion. After passing the initial plateau region, $\langle k_t \rangle$ decreases significantly, by about 1.5 orders of magnitude between 20 and 50 % conversion with the 60 wt.% MAA system and by about 1 order of magnitude between 30 and 60 % conversion with the 30 wt.% MAA system. Toward even higher degrees of monomer conversion, the decrease in $\langle k_t \rangle$ becomes less pronounced. This effect is clearly seen with the polymerization of the 60 wt.% MAA solution.

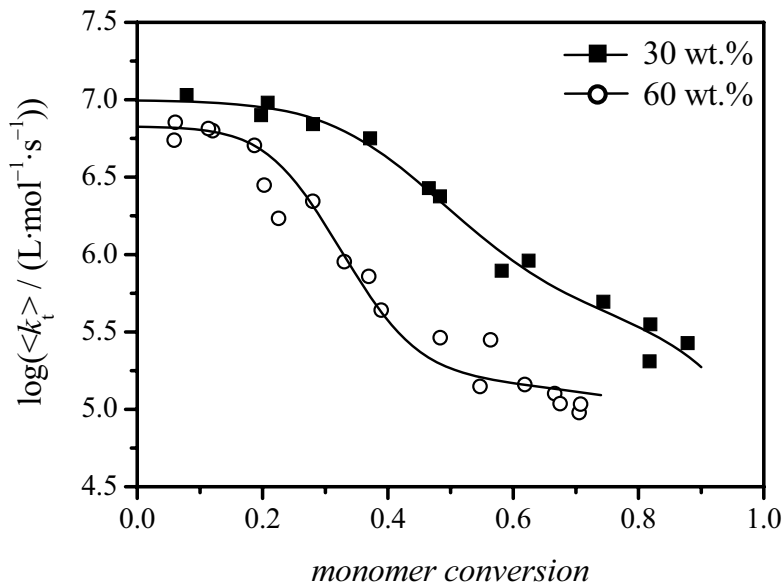


Figure 8-4: Conversion dependence of $\langle k_t \rangle$ for polymerizations at 50 °C, 2000 bar and initial MAA concentrations of 30 and 60 wt.% in water, respectively. $\langle k_t \rangle$ was calculated from $\langle k_t \rangle/k_p$ by using the k_p expression given in Eq. (8-5). The lines are fits of the experimental data to Eq. (8-6). The associated parameter values are listed in Table 8-1.

Table 8-1: Model parameters used for fitting the experimental data in Figure 8-4 to Eq. (8-6). The parameter values refer to MAA polymerization at 50 °C and 2000 bar. For further details see text.

$c_{\text{MAA}} / \text{wt.}\%$	30	60
$k_{\text{SD}} / \text{L}\cdot\text{mol}^{-1}\cdot\text{s}^{-1}$	$(9.3 \pm 0.2) \cdot 10^6$	$(6.5 \pm 0.2) \cdot 10^6$
C_η	12.8 ± 0.4	21.2 ± 0.7
$k_{\text{TD}}^0 / \text{L}\cdot\text{mol}^{-1}\cdot\text{s}^{-1}$	$1.0 \cdot 10^9$	$1.0 \cdot 10^9$
C_{RD}	94 ± 11	61 ± 7

The lines in Figure 8-4 are representations of the experimental data by Eq. (8-6). The associated parameter values are listed in Table 8-1. k_{SD} is obtained as the value of experimental $\langle k_t \rangle$ in the very initial polymerization period. $k_{TD}^0 = 1.0 \cdot 10^9 \text{ L} \cdot \text{mol}^{-1} \cdot \text{s}^{-1}$ has been adopted from studies into alkyl methacrylate termination rate which report monomer concentration independent k_{TD}^0 values of this order of magnitude.^[96] The rate coefficient of translation diffusion during polymerization, k_{TD} , is given by Eq. (3-25). Bulk viscosity depends on the characteristics of each individual polymerization reaction, in particular on the polymer content, that is on the degree of monomer conversion and on the type of polymer produced, e.g., whether low-molecular or high-molecular weight material is formed. For most polymerization systems information on relative viscosity, $\eta_r(X)$, is not available. Within preceding studies into bulk (meth)acrylate^[22] and MMA solution polymerizations,^[96] as a rough approximation for modeling the conversion dependence of $\eta_r(X)$, Eq. (8-7) has been used:

$$\ln \eta_r = C_\eta \cdot X \quad (8-7)$$

The parameter C_η may be looked upon as an adjustable parameter, which essentially determines the conversion dependence of $\langle k_t \rangle$ under conditions where k_{TD} controls termination rate. The C_η parameters in Table 8-1 may be found from the slope of the straight line which intersects the ordinate at $\log(k_{TD}^0)$ and passes through the inflection point of the sigmoidal $\log(\langle k_t \rangle)$ vs. X curve, that is in the region where k_{TD} controls termination rate but was simultaneously determined with C_{RD} via fitting of $\langle k_t \rangle$ data according to Eq. (8-6). The so-obtained C_η values are 12.8 and 21.2 for the polymerizations of 30 and 60 wt.% MAA, respectively. The roughly twofold higher value of C_η at 60 wt.% MAA as compared to the system with 30 wt.% MAA may be understood as being due to twice the amount of polymer being present at identical monomer conversion. Linear extrapolation of C_η toward $w_{MAA}^0 = 0$ yields a C_η value close to zero which corresponds to constant $\eta_r(X)$ as is to be expected in the hypothetical case of no monomer being present and thus no polymerization taking place. The clear trend of decreasing C_η toward lower monomer concentration has also been seen with MMA solution polymerizations.^[96] Extrapolation of C_η from this earlier study to zero monomer content however does not yield C_η close to zero, which may be due to the rather weak decrease of $\langle k_t \rangle$ in the TD-controlled regime with MMA solution polymerizations and

the associated significant error in deducing C_η . For bulk MAA polymerization a C_η value of about 35 is estimated from the 30 and 60 wt.% data. This value is significantly above $C_\eta = 21$ as obtained for MMA bulk polymerization.^[96] The very pronounced increase of η_r with conversion for MAA bulk polymerization may be due to the action of strong hydrogen bonds which are absent with MMA. Moreover, differences in molecular weight distribution of the background polymer matrix may affect C_η . It goes without saying that one individual C_η value cannot fully take into account both polymer content and polymer size distribution of the reacting systems. It should further be noted that the size of C_η is affected by the selection of k_{TD}^0 . E.g., assuming k_{TD}^0 at 60 wt.% MAA to differ from the associated value for 30 wt.% MAA by the same factor as do the associated k_{SD} values, yields an optimum fit of the $\langle k_t \rangle$ vs. X data with $C_\eta = 20.0$ rather than with $C_\eta = 21.2$, as listed in Table 8-1.

The second adjustable parameter in the fitting procedure, the reaction diffusion constant, is listed as the last entry in Table 8-1. For 60 wt.% MAA, C_{RD} is obtained with a better accuracy, as the reaction diffusion controlled region is more pronounced than for 30 wt.% MAA. The C_{RD} values in Table 8-1 are close to the numbers reported for MMA bulk polymerization at 60 °C: $C_{RD} = 76$ at 1000 bar and $C_{RD} = 50$ at 2000 bar.^[274] That C_{RD} for polymerization of MAA in aqueous solution slightly decreases with increasing MAA concentration is in line with the argument used to describe the dependence of k_p on MAA content (see Chapter 6.1). The stronger intermolecular hydrogen-bonded interactions at higher MAA content should enhance both the friction experienced by the transition state for propagation, which effect reduces k_p , and the friction which the free-radical chain ends experience during the reaction-diffusion process. A lower mobility of the macroradical chain-end should result in a lower C_{RD} .^[23,198]

The parameters in Table 8-1 afford for an excellent representation of the experimental $\langle k_t \rangle$ over a wide range of MAA conversion (Figure 8-4). This finding suggests that Eq. (8-6), which has been used for fitting $\langle k_t \rangle$ of various monomers in both bulk and in organic solvents,^[16,22,23,138] is applicable also toward radical polymerizations in aqueous solution. The variation of the parameters k_{SD} and C_η with solvent content seen in aqueous solution of MAA is consistent with what has been observed, e.g., for MMA polymerized in solution of toluene. The initial k_{SD} plateau value is slightly enhanced toward lower monomer content whereas, within the range of translational diffusion control, the $\langle k_t \rangle$ vs. X correlation is strongly affected by the solvent content.^[96]

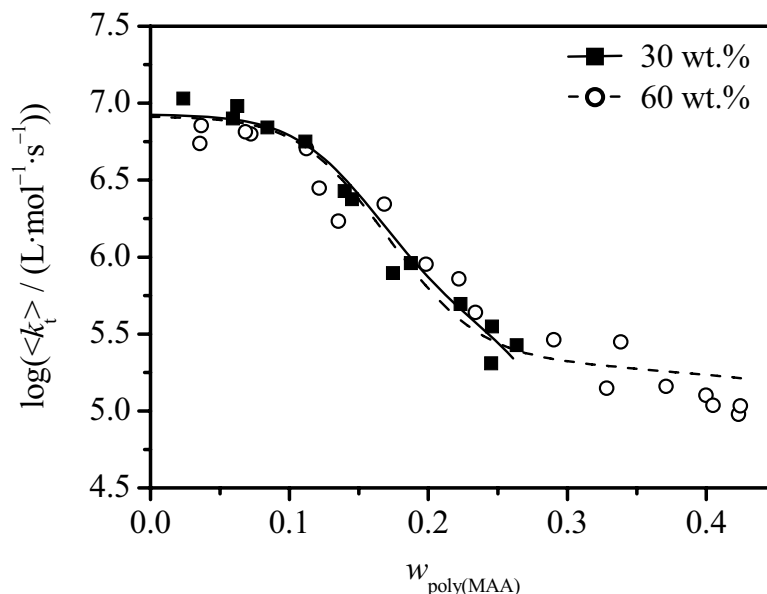


Figure 8-5: Dependence of $\langle k_t \rangle$ on weight fraction of polymer, $w_{\text{poly(MAA)}}$, for MAA polymerizations at 50 °C, 2000 bar and initial monomer concentrations of 30 and 60 wt.%, respectively. The lines are representations of the experimental data via Eq. (8-8) (full line for 30 wt.% MAA and dashed line for 60 wt.% MAA). The associated parameter values are listed in the text.

As mentioned above, the increase of C_η toward higher initial monomer concentration may be due to higher amounts of polymer being present at a given conversion. The approximately twofold increase of C_η between 30 and 60 wt.% MAA implies that, for estimating the viscosity change during polymerization, a parameter C_η^* should be used which scales with polymer weight fraction $w_{\text{poly(MAA)}} = w_{\text{MAA}}^0 \cdot X$. Thus a modified expression (Eq. (8-8)) may be used for fitting the experimental $\langle k_t \rangle$ data measured on 30 and 60 wt.% MAA in aqueous solution. As the variation of both k_{SD} and C_{RD} is minor as compared to the differences in translational diffusion behavior, expressed by C_η , for both MAA contents a single mean value of k_{SD}^* and of C_{RD}^* has been used within the fitting procedure. Eq. (8-8) reads:

$$\langle k_t \rangle = \frac{1}{1/k_{\text{SD}}^* + \exp(C_\eta^* \cdot w_{\text{MAA}}^0 \cdot X)/k_{\text{TD}}^0} + C_{\text{RD}}^* \cdot (1-X) \cdot k_p \quad (8-8)$$

with the mean values: $k_{\text{SD}}^* = 7.9 \cdot 10^6 \text{ L} \cdot \text{mol}^{-1} \cdot \text{s}^{-1}$, $C_{\text{RD}}^* = 77.5$ and $C_\eta^* = 39$. The remarkably good representation of the experimental $\langle k_t \rangle$ data (full line for 30 wt.% and dashed line for 60 wt.%) by Eq. (8-8) is illustrated by the plot of $\log \langle k_t \rangle$ vs. polymer weight fraction in Figure 8-5. The data from experiments at initial MAA concentrations of 30 and 60 wt.%

almost sit on top of each other, which indicates the general type of $\langle k_t \rangle$ behavior. For an even more accurate representation of $\langle k_t \rangle$ within extended ranges of MAA concentration, the experimental k_{SD} and C_{RD} values may be used for interpolation and extrapolation of k_{SD} and C_{RD} data for a given MAA weight fraction.

8.3 Determination of $\langle k_t \rangle$ by chemically initiated polymerizations

Chemically initiated (CI) polymerization under steady-state conditions provides access to $\langle k_t \rangle / k_p^2$ in case that the initiator decomposition rate coefficient, k_d , and initiator efficiency, f , or the product of both quantities, $k_d f$, are known. Carrying out both CI and SP-PLP experiments, with k_p being available from PLP-SEC, allows for estimating $\langle k_t \rangle$ as a function of monomer conversion from the two independent experiments. The CI polymerizations for MAA were performed at 50 °C, 2000 bar and at MAA contents of 30 and 60 wt.% in water as were the SP-PLP-NIR experiments. Monomer conversion vs. reaction time, t , profiles deduced from FT-NIR are depicted in Figure 8-6A for 30 wt.% MAA and in Figure 8-6B for 60 wt.% of monomer.

In most cases, duplicate experiments have been carried out. The agreement of polymerization data from measurements under ostensibly the same conditions is rather satisfactory, in particular in case of higher MAA concentration (Figure 8-6B) and of higher initiator concentration. The reasons behind these observations are the better quality of NIR analysis at higher MAA content and the lower impact of impurities at high levels of radical concentration, respectively. A significant increase of the rate of polymerization, R_p , is seen toward higher initiator concentration.

The kinetic data in Figure 8-6 were analyzed via the expression for steady-state polymerization (Eq. (3-10)). The reported ambient-pressure decomposition rate coefficient of V50 in aqueous solution at 50 °C, $k_d = 8.14 \cdot 10^{-6} \text{ s}^{-1}$, has been adopted to hold for 2000 bar, as has been the reported ambient-pressure initiator efficiency, $f = 1$.^[275] Polymerization rate, $R_p = -dc_M/dt$, was estimated from first-derivative curves of c_M vs. t traces determined via ORIGIN 6.1 with subsequent smoothing. Plotted in Figure 8-7 are the $\langle k_t \rangle / k_p^2$ vs. X values obtained, via Eq. (3-10), from R_p of the chemically initiated polymerizations at 30 and 60 wt.% MAA in aqueous solution for 50 °C / 2000 bar and from the known values of f , k_d , c_I and c_M . The data is plotted only up to 80 % monomer conversion, as the minor changes of

c_{MAA} with time at higher conversions induce a significant scatter for $\langle k_t \rangle / k_p^2$. As inhibition may significantly affect $\langle k_t \rangle / k_p^2$ in the early polymerization period, values for conversions below 10 % were also ignored; the initiator consumed during this period is taken into account in the estimation of $\langle k_t \rangle / k_p^2$ by Eq. (3-10).

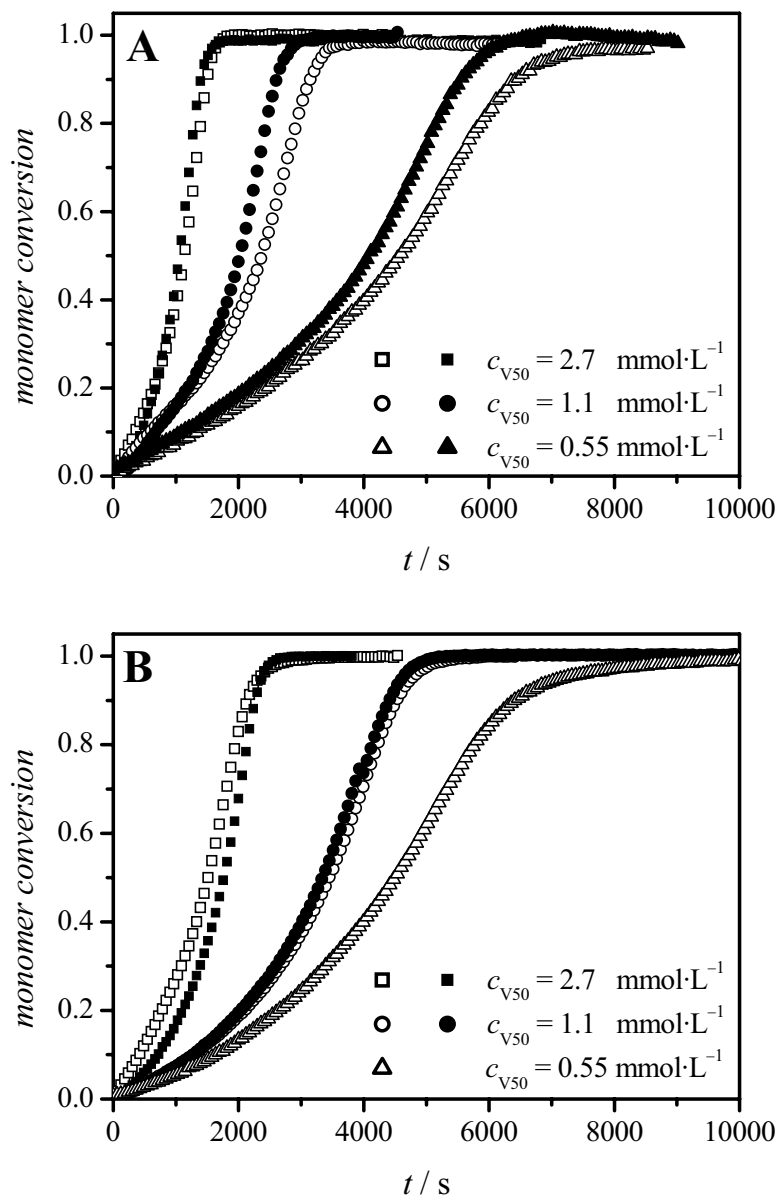


Figure 8-6: Monomer conversion vs. time plots for a chemically initiated polymerizations of 30 wt.% (A) and 60 wt.% (B) of MAA in aqueous solution at 50 °C and 2000 bar. The primary initiator concentrations were 2.7, 1.1, and 0.55 $\text{mmol}\cdot\text{L}^{-1}$ of V50, respectively. Open and filled symbols refer to repeat experiments under ostensibly the same conditions.

A close overlap of the entire data set for polymerizations at 60 wt.% initial MAA concentration is seen, whereas $\langle k_t \rangle / k_p^2$ for 30 wt.% MAA slightly increases toward lower

V50 concentration. The origin of the increase in $\langle k_t \rangle / k_p^2$, by about half an order of magnitude in passing from 2.7 to 0.55 $\text{mmol}\cdot\text{L}^{-1}$ initiator, is not clear. Probably, a loss of initiator-derived radicals due to inhibition results in a lower than expected radical concentration which, by the evaluation procedure, translates into termination rate coefficients that are too large. For both 30 and 60 wt.% MAA in aqueous solution, a pronounced decrease of the coupled parameter $\langle k_t \rangle / k_p^2$ is seen toward higher conversions.

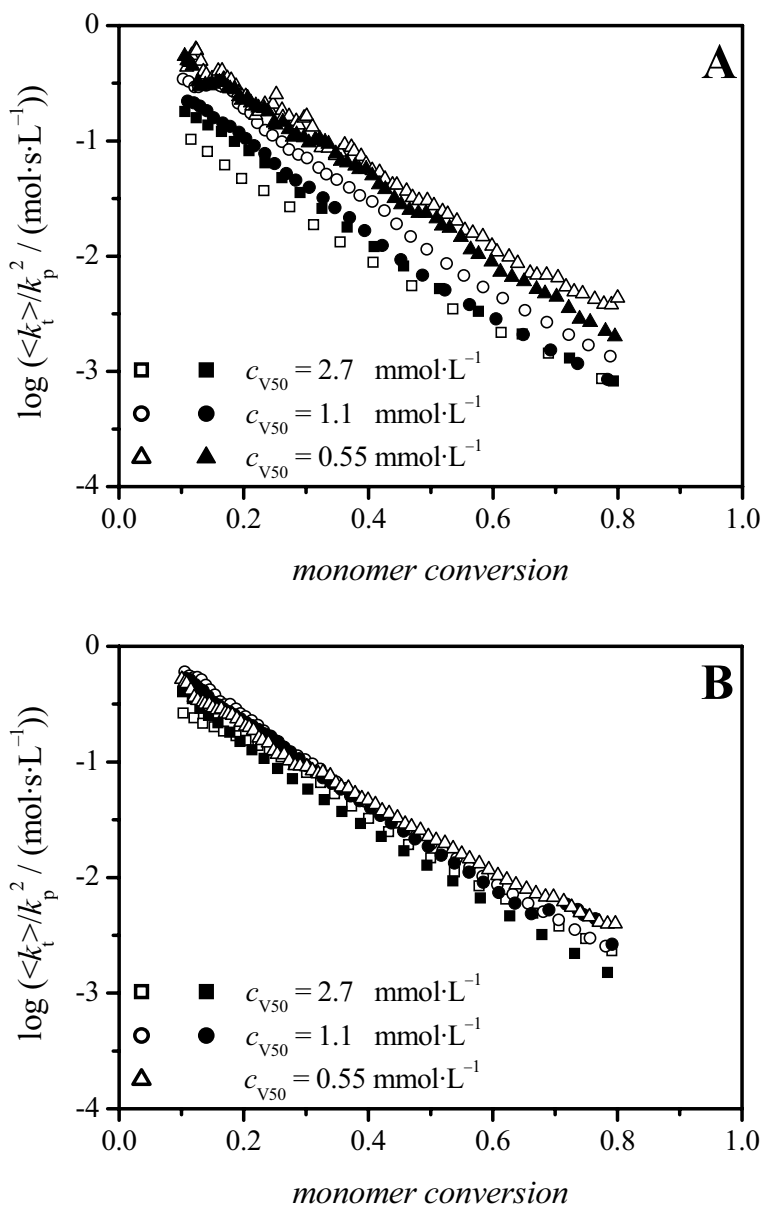


Figure 8-7: Conversion dependence of $\langle k_t \rangle / k_p^2$ derived from chemically initiated polymerizations of 30 wt.% (A) and 60 wt.% (B) MAA in aqueous solution at 50 °C, 2000 bar and with primary initiator concentrations of $c_{V50} = 2.7$, 1.1, and 0.55 $\text{mmol}\cdot\text{L}^{-1}$.

Figure 8-8 shows a comparison of $\langle k_t \rangle$ values for 30 wt.% (A) and 60 wt.% (B) MAA in aqueous solution at 50 °C and 2000 bar as obtained from both stationary (open symbols) and instationary (filled symbols) experiments. $\langle k_t \rangle$ was extracted from the two types of coupled parameters via k_p values estimated from Eq. (8-5). For 30 wt.% MAA, the $\langle k_t \rangle$ data from SP-PLP-NIR fit into the range of $\langle k_t \rangle$ values provided by the data from CI polymerizations performed at different initiator concentrations. The $\langle k_t \rangle$ data for aqueous solutions with an initial MAA content of 60 wt.% demonstrate the satisfactory agreement of $\langle k_t \rangle$ data from SP-PLP and from CI polymerization. A sigmoidal curvature cannot be clearly detected from the $\langle k_t \rangle$ vs. monomer conversion data obtained by CI polymerization. There is, however, a weak indication with some of the 60 wt.% MAA data that the decrease of $\langle k_t \rangle$ with conversion appears to be somewhat weaker in both the low and high conversion regions. The comparison of stationary and instationary experiments suggests that the SP-PLP-NIR experiments allow for a more detailed and accurate study into the termination kinetics than do the CI polymerization experiments, e.g., the sigmoidal $\langle k_t \rangle$ vs. X curvature, which is what one expects from a comparison with MMA polymerization data, can be clearly seen from SP-PLP experiments. The enhanced scattering and the systematic shift with initiator concentration of the $\langle k_t \rangle$ data from CI polymerization may be due to an impact of inhibition and thus of impurities on the kinetic data, which is not easily avoidable in CI polymerization, but can be overcome by the intense laser pulsing where the first few pulses may have some cleaning effect on the system. The chain-length distribution being broader in CI polymerizations may give rise to some smoothing of $\langle k_t \rangle$ vs. X data. With the SP-PLP experiments, on the other hand, the chain-length distribution is very narrow, which facilitates detection of conversion-related effects on $\langle k_t \rangle$.

In view of the various sources of error that should primarily effect CI polymerizations rather than SP-PLP experiments, the agreement of absolute $\langle k_t \rangle$ values obtained by the two methods must be considered as very satisfactory. For an inspection of detailed effects associated with the mode of diffusion control of k_t , it appears recommendable to apply the SP-PLP-NIR method rather than carrying out stationary CI polymerization experiments.

The satisfactory agreement of $\langle k_t \rangle$ values derived from chemically initiated polymerizations and SP-PLP-NIR further indicates that combination of experimental $\langle k_t \rangle/k_p$ and $\langle k_t \rangle/k_p^2$ values should yield reliable individual rate coefficients of propagation and termination for MAA in aqueous solution. This is also illustrated by the $\langle k_t \rangle$ data plotted as black and grey symbols in Figure 8-9.

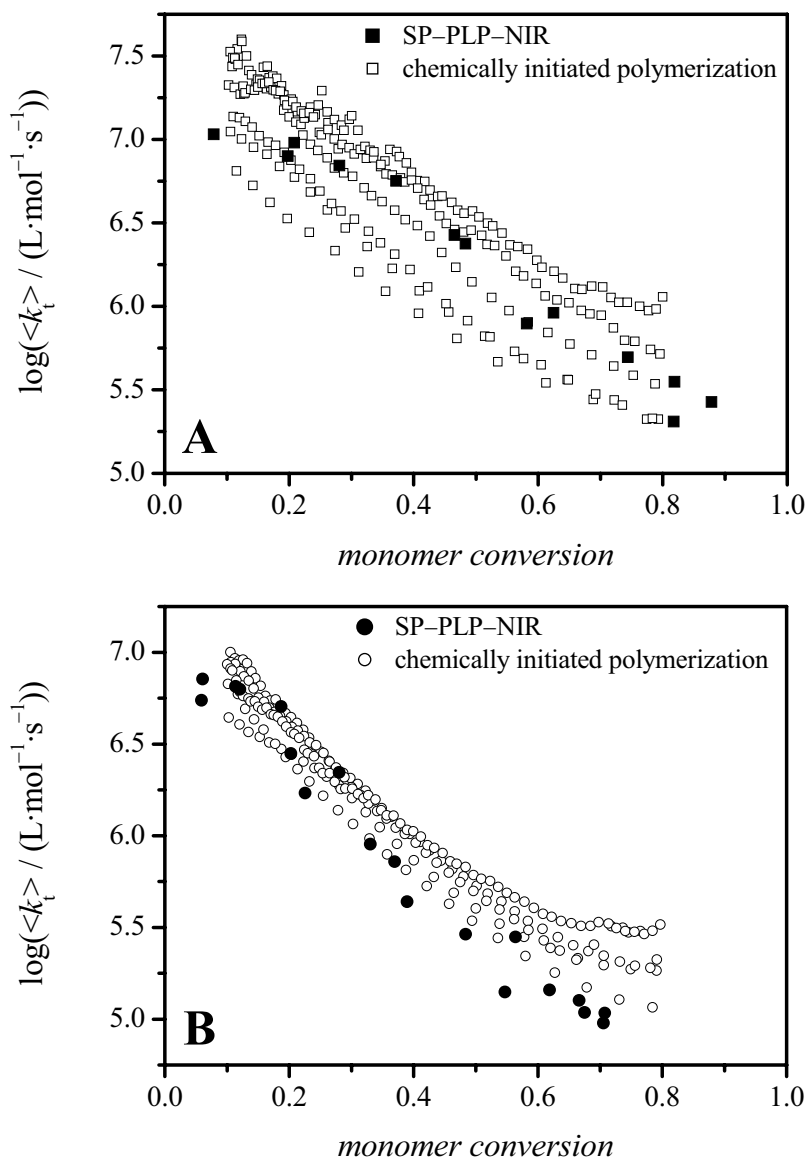


Figure 8-8: Conversion dependence of $\langle k_t \rangle$ derived from chemically initiated polymerizations of 30 wt.% (A) and 60 wt.% (B) MAA in aqueous solution at 50 °C, 2000 bar and with V50 concentrations of 2.7, 1.1 and 0.55 $\text{mmol} \cdot \text{L}^{-1}$ (open symbols). The $\langle k_t \rangle$ data from SP-PLP-NIR at identical monomer concentration are given as filled symbols. $\langle k_t \rangle$ values are calculated from $\langle k_t \rangle / k_p^2$ or $\langle k_t \rangle / k_p$ using the general k_p expression given by Eq. (8-5).

The values indicated in grey were calculated from $\langle k_t \rangle / k_p$ via combination with the $\langle k_t \rangle / k_p^2$ data from Figure 8-7 (conversion interval of 10 to 80 %). The agreement with the $\langle k_t \rangle$ values which were evaluated by means of k_p from Eq. (8-5) (black symbols) is adequate which in turn also demonstrates the validity of the generalized k_p correlation even for high monomer-

to-polymer conversions. The procedure of combining $\langle k_t \rangle / k_p$ and $\langle k_t \rangle / k_p^2$ has already been used within a recent study into aqueous-solution polymerization of AMPS.^[198]

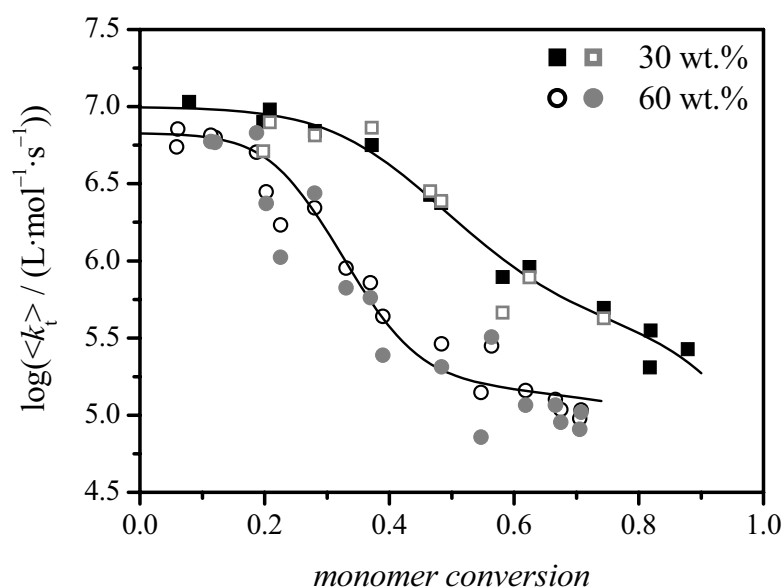


Figure 8-9: Conversion dependence of $\langle k_t \rangle$ for polymerizations at 50 °C, 2000 bar and initial MAA concentrations of 30 and 60 wt.% in water, respectively. $\langle k_t \rangle$ was calculated from $\langle k_t \rangle / k_p$ by using the k_p expression given in Eq. (8-5) (black symbols) or from combination with the $\langle k_t \rangle / k_p^2$ data from Figure 8-7 (grey symbols). The lines are representations of the experimental data according to Eq. (8-6) with parameter values listed in Table 8-1.

9 Termination Kinetics in *N*-Vinyl Pyrrolidone Polymerization

It was shown in the previous chapter that non-ionized MAA behaves similar to MMA concerning its termination reactivity with $\langle k_t \rangle$ being controlled by SD, TD and, at high conversions, by RD. However, the range of experimental conditions for $\langle k_t \rangle$ measurements via SP-PLP-NIR were rather limited.

NVP is a suitable candidate for further studies into the termination kinetics of water-soluble monomers as poly(NVP) is well soluble in both, monomer and water. Thus, broad ranges of monomer-to-polymer conversion may be covered even for bulk polymerizations of NVP. NVP propagates faster than MAA at identical monomer concentration and temperature (see Figure 6-3 and Figure 7-1) which is beneficial for the signal-to-noise quality of SP-PLP-NIR experiments. Moreover, the observation of a PLP structure within MWDs obtained from PLP experiments at temperatures of 60 °C and LPRRs of 20 Hz indicates that MCR formation during NVP polymerization does not occur or only to a minor extent.

The conversion dependence of the chain-length-averaged termination rate coefficient $\langle k_t \rangle$ at 40 °C and 2000 bar was measured for polymerizations of NVP in solution of D₂O and monomer concentrations of 20, 40, 60, and 80 wt.% as well as for NVP in bulk. Additional experiments were carried out for NVP bulk polymerization at 40 °C and pressures of 1500, 1000 and 500 bars. High-pressure conditions were chosen to increase the monomer conversion induced per pulse. Moreover, up to 40 single monomer concentration curves were coadded to reduce scatter within the SP-PLP-NIR traces. As detailed earlier (see Chapter 5.2.1), using D₂O instead of H₂O reduces the background absorbance in the region of the first overtone of the C–H stretching vibration at the olefinic double bond which enhances signal-to-noise quality. It was shown in previous studies that neither k_p (from PLP-SEC of MAA)^[271] nor $\langle k_t \rangle / k_p$ (from SP-PLP-NIR of AMPS)^[198] were significantly different for polymerizations in H₂O and D₂O, respectively.

9.1 Generalized k_p correlation

For decoupling of $\langle k_t \rangle$ from $\langle k_t \rangle / k_p$, knowledge of the propagation rate coefficient at identical reaction conditions is required. Figure 9-1 shows the variation of k_p with initial NVP

weight fraction for polymerizations of NVP in D₂O at 40 °C and 2000 bar determined via PLP-SEC. The data show an acceleration of k_p toward lower NVP content as has already been observed for ambient pressure conditions (see Figure 7-1). The k_p values are well represented by an expression of the same functional form as Eq. (7-1):

$$k_p / \text{L} \cdot \text{mol}^{-1} \cdot \text{s}^{-1} = 64000 \cdot (0.33 + 0.67 \cdot \exp(-7.7 \cdot w_{\text{NVP}}) - 0.27 \cdot w_{\text{NVP}}) \quad (9-1)$$

It was shown in Chapter 7.2 that k_p increases toward higher monomer conversion for polymerization of NVP in water. Implementing Eq. (8-4) yields the dependence of k_p on initial monomer weight fraction, w_{NVP}^0 , and conversion for polymerizations of NVP in D₂O at 40 °C and 2000 bar:

$$k_p / \text{L} \cdot \text{mol}^{-1} \cdot \text{s}^{-1} = 64000 \cdot \left(0.33 + 0.67 \cdot \exp\left(-7.7 \cdot \left(\frac{w_{\text{NVP}}^0 \cdot (1-X)}{1 - w_{\text{NVP}}^0 \cdot X}\right)\right) - 0.27 \cdot \left(\frac{w_{\text{NVP}}^0 \cdot (1-X)}{1 - w_{\text{NVP}}^0 \cdot X}\right) \right) \quad (9-2)$$

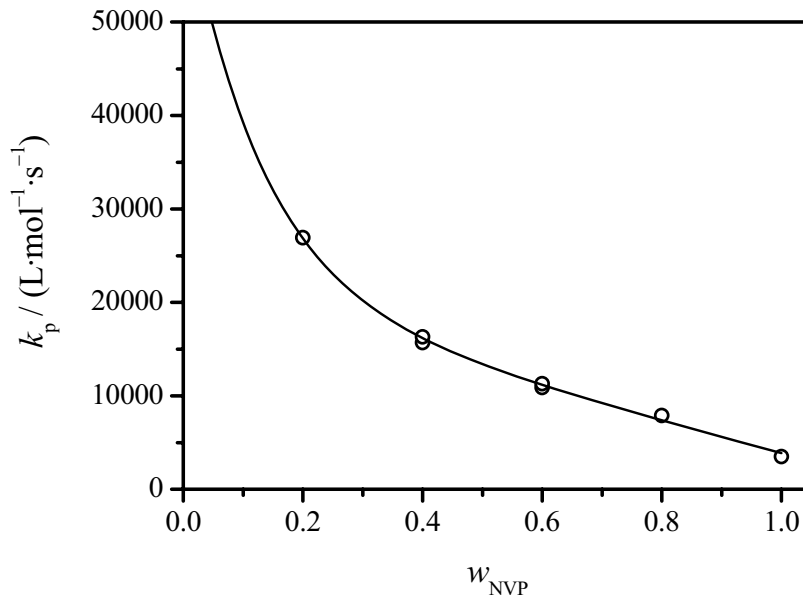


Figure 9-1: Dependence of k_p on c_{NVP} for polymerizations of NVP in D₂O at 40 °C and 2000 bar. The line represents the best fit of the experimental data by Eq. (9-1).

9.2 Dependence of $\langle k_t \rangle$ on initial monomer concentration, monomer-to-polymer conversion and pressure for polymerizations of NVP in D₂O

Chain-length-averaged termination rate coefficients were obtained via fitting of SP-PLP-NIR traces to Eq. (3-7) and implementing k_p according to Eq. (9-2). The so-obtained variation of $\langle k_t \rangle$ with monomer-to-polymer conversion at 40 °C and 2000 bar for different initial concentrations of NVP in D₂O is plotted in Figure 9-2. Duplicate experiments were carried out for each initial monomer concentration. There is a good reproducibility of the $\langle k_t \rangle$ vs. X data for all initial NVP contents as is illustrated by open and filled symbols of the same style. Whereas DMPA had to be employed for polymerizations of NVP in solution of D₂O (see Chapter 5.5.1), the absence of acidic protons in NVP allows for using the ideal photoinitiator MMMP under bulk conditions.^[214] The good agreement between the $\langle k_t \rangle$ data obtained from the DMPA and MMMP measurements (open and filled diamonds) illustrates that DMPA concentration and laser energies were chosen sufficiently low to circumvent the non-ideality effects of DMPA. Thus, the $\langle k_t \rangle$ values for polymerizations of NVP in D₂O are also not expected to be artificially increased by the use of DMPA.

The variation of $\langle k_t \rangle$ with conversion for different initial NVP contents is very similar to the one of non-ionized MAA in water (compare Figure 8-4 and Figure 9-2). At low conversions, $\langle k_t \rangle$ appears to be controlled by SD. This mechanism is associated with an almost constant termination rate coefficient until TD control of $\langle k_t \rangle$ sets in. The monomer-to-polymer conversion at which the decrease in $\langle k_t \rangle$ occurs is shifted to higher values toward lower initial NVP concentration. The plateau range of $\langle k_t \rangle$ expands between zero and 10 % conversion for the bulk system. However, $\langle k_t \rangle$ remains constant until $X = 20$ % for polymerization of 60 wt.% of NVP in D₂O. Toward even lower initial monomer concentrations, a TD control of $\langle k_t \rangle$ cannot be safely assigned to the data though there is an indication of a slight decrease in $\langle k_t \rangle$ for 40 wt.% of NVP in D₂O from $X = 30$ % on. The deceleration of $\langle k_t \rangle$ in the TD controlled regime is more pronounced for the higher initial NVP contents as more polymeric material is present at a given conversion. An indication of an RD control of $\langle k_t \rangle$ is observed with the 60 and 80 wt.% data for which SP-PLP-NIR traces could be measured up to 80 % monomer-to-polymer conversion.

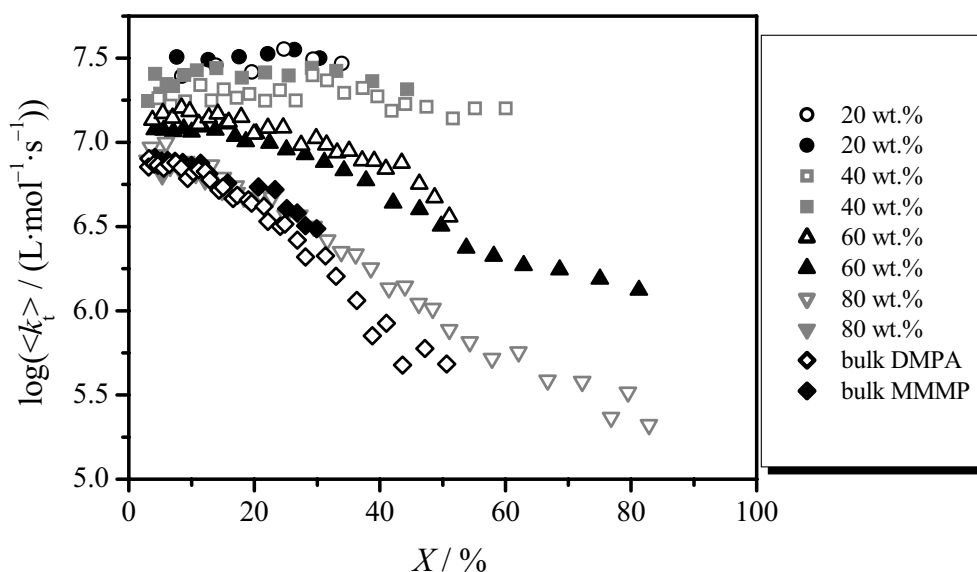


Figure 9-2: Variation of $\langle k_t \rangle$ with monomer-to-polymer conversion for polymerizations of NVP in D_2O at $40\text{ }^\circ\text{C}$, 2000 bar and different initial monomer concentrations (indicated in the figure). $\langle k_t \rangle$ was obtained by fitting of SP-PLP-NIR traces to Eq. (3-7) and implementing k_p according to Eq. (9-2).

The average low conversion $\langle k_t \rangle$, denoted as $\langle k_{SD} \rangle$, increases toward lower initial NVP concentration as is illustrated in Figure 9-3. $\langle k_{SD} \rangle$ for polymerization of 20 wt.% of NVP is about 4 times higher than for the bulk system. The acceleration is slightly more pronounced compared to solution polymerizations of MAA and MMA and may be explained by the higher mobility of the macroradical chain ends in dilute aqueous solution which facilitates termination via the segmental diffusion mechanism. This argumentation is similar to the explanation for the acceleration of k_p toward lower c_{NVP} (see Chapter 7.1). $\langle k_{SD} \rangle$ is almost identical for polymerizations of 80 wt.% of NVP in D_2O and NVP in bulk. However, the decrease of $\langle k_{SD} \rangle$ toward very high monomer contents has to level off, as linear extrapolation of the $\langle k_{SD} \rangle$ data from low c_{NVP} would yield negative termination rate coefficients.

Plotted in Figure 9-4 are the $\langle k_t \rangle$ values for polymerizations of 40, 60 and 80 wt.% of NVP in D_2O and for polymerization of NVP in bulk at $40\text{ }^\circ\text{C}$ and 2000 bar. The lines represent fits of the experimental data to Eq. (8-6). The conversion dependence at an initial monomer content of 20 wt.% was not evaluated by Eq. (8-6), as $\langle k_t \rangle$ does not significantly change within the experimentally accessible conversion interval. The entire $\langle k_t \rangle$ data set for 20 wt.% of NVP in D_2O is adequately described by an average termination rate coefficient of $(3.1 \pm 0.1) \cdot 10^7\text{ L}\cdot\text{mol}^{-1}\cdot\text{s}^{-1}$. For polymerizations of 40 wt.% NVP in D_2O the reaction

diffusion constant C_{RD} was not adjusted as the RD controlled conversion regime was obviously not reached.

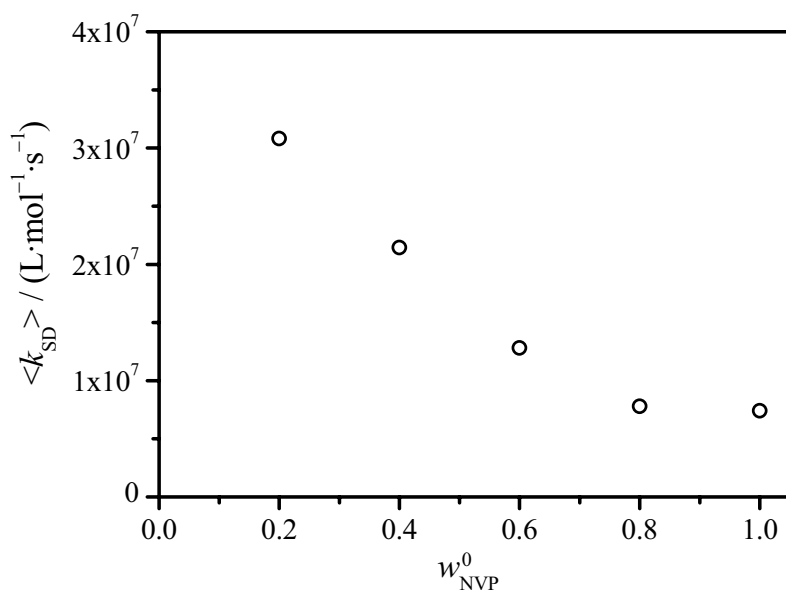


Figure 9-3: Variation of the arithmetic mean $\langle k_t \rangle$ value in the low conversion plateau range, $\langle k_{SD} \rangle$, with initial monomer weight fraction for polymerizations of NVP in D_2O and in bulk at 40 °C and 2000 bar.

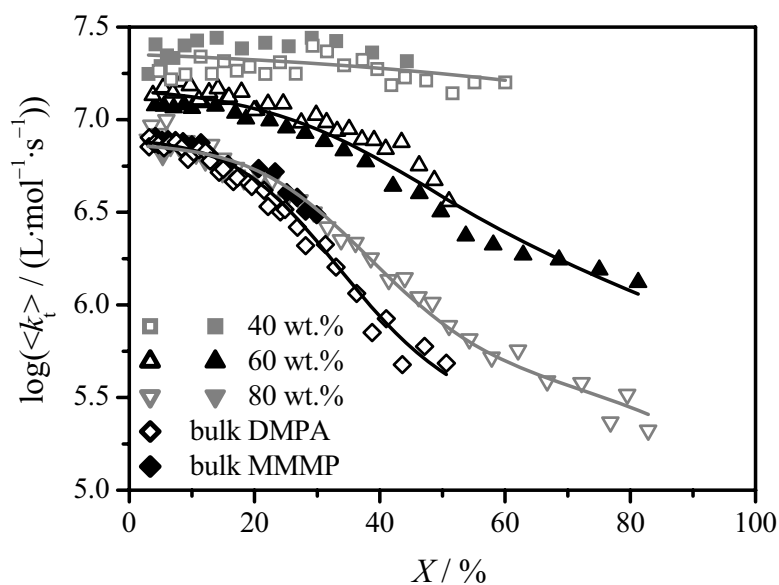


Figure 9-4: Conversion dependence of $\langle k_t \rangle$ for NVP polymerizations in D_2O and in bulk at 40 °C, 2000 bar and different initial monomer concentrations (indicated in the figure). The lines are fits of the experimental data to Eq. (8-6). The associated parameter values are listed in Table 9-1.

It turned out that the $\langle k_t \rangle$ vs. X dependencies could not be adequately represented by $k_{TD}^0 = 10^9 \text{ L}\cdot\text{mol}^{-1}\cdot\text{s}^{-1}$ as has been used with MAA in Chapter 8.2. A significantly lower value of $2\cdot 10^8 \text{ L}\cdot\text{mol}^{-1}\cdot\text{s}^{-1}$ was chosen in order to adequately describe the experimental data. The origin of this difference is not yet clear. k_{TD}^0 results from back extrapolation to zero conversion of the TD-controlled regime where polymer and macroradical chains are overlapping. Thus, k_{TD}^0 cannot be simply related to solution viscosity at $X=0$ and macroradical size as is implied by Eqs. (3-19) and (3-20). Actually, the termination mechanism in the TD controlled conversion range is not well understood until now and object of current investigations.^[122,123]

The parameter values obtained from fitting the experimental data in Figure 9-4 to Eq. (8-6) are listed in Table 9-1. As outlined above, there is a weak increase of k_{SD} toward lower concentration of NVP in water. A pronounced RD controlled regime is only observed within the 80 wt.% data (see Figure 9-4) for which high monomer-to-polymer conversions and, more importantly, also high polymer contents were reached. Thus, the associated C_{RD} value of 91 is more reliable than the results for the 60 wt.% and 100 wt.% systems as is indicated by the error margins. The reaction diffusion constant for 80 wt.% of NVP is in the same range, i.e. between 50 and 100, as has been observed for MAA (see Table 8-1) and MMA^[274] polymerization at 2000 bar. An increase of C_{RD} toward lower monomer concentration in water was seen for MAA and AMPS^[198]. Such a clear trend cannot be observed with the NVP data which may be due the above-mentioned low sensitivities of the experimental $\langle k_t \rangle$ vs. X dependencies toward C_{RD} . Of particular interest is the dependence of C_η on initial monomer concentration as discussed in Chapter 8.2 for aqueous solution polymerizations of MAA. C_η is about 15 for NVP bulk polymerization, which is well below $C_\eta \approx 35$ extrapolated for the MAA bulk system (see Chapter 8.2). This observation may be mainly due to the absence of an α -methyl group in NVP, as acrylic acid esters usually exhibit much weaker variations of k_t with conversion than the associated methacrylates.^[16] Moreover, NVP is solely a hydrogen-bond acceptor^[258,259] whereas the carboxylic acid group of MAA acts as both, donor and acceptor. The C_η value for MMA bulk polymerization of 21^[96] is much closer to the one for NVP bulk polymerization. Strong influences of ester chain length on the extent of the k_t decrease in the TD-controlled regime have been observed for acrylate- and methacrylate-type monomers. A long side chain acts as an internal solvent for the polymer backbone. Thus, pronounced decelerations of k_t with conversion are observed for MA and MMA whereas for DA and DMA only minor variations are seen.^[96,98,276] However, it needs to be stressed that

the C_η data for NVP should not be overinterpreted as C_η and k_{TD}^0 are to some extent correlated quantities (see discussion to Table 8-1) reducing the accuracy and comparability of the results. Moreover, the magnitude of C_η strongly depends on the MWD of the background polymer. Relatively small C_η values may be found when low molecular weight material is formed during the polymerization process.

Table 9-1: Model parameters used for fitting the experimental data in Figure 9-4 to Eq. (8-6). The parameter values refer to NVP polymerization at 40 °C and 2000 bar.

w_{NVP}^0	0.4	0.6	0.8	1.0
$k_{SD} / L \cdot mol^{-1} \cdot s^{-1}$	$(2.6 \pm 0.1) \cdot 10^7$	$(1.3 \pm 0.1) \cdot 10^7$	$(6.8 \pm 0.2) \cdot 10^6$	$(7.3 \pm 0.3) \cdot 10^6$
C_η	2.5 ± 0.5	8.5 ± 0.5	12.6 ± 0.3	14.9 ± 0.4
$k_{TD}^0 / L \cdot mol^{-1} \cdot s^{-1}$	$2.0 \cdot 10^8$	$2.0 \cdot 10^8$	$2.0 \cdot 10^8$	$2.0 \cdot 10^8$
C_{RD}	0	200 ± 44	91 ± 6	166 ± 29

The dependence of the C_η values on initial NVP weight fraction in D₂O (see Table 9-1) is depicted in Figure 9-5. In agreement with the studies on MMA and MAA solution polymerizations, a pronounced decrease of C_η toward lower monomer concentration is observed. C_η is assumed to approach zero for infinite monomer dilution as detailed in Chapter 8.2. The data at initial monomer concentrations of and above 60 wt.% in D₂O are well represented by a linear fit through the origin as illustrated by the dashed line in Figure 9-5. Such direct proportionality between C_η and initial monomer content has already been assumed for deriving the generalized k_t correlation for MAA (Eq. (8-8)). However, C_η for $w_{NVP}^0 = 0.4$ significantly deviates from the full line in Figure 9-5. This discrepancy indicates a sigmoidal decrease of C_η toward increasing solvent content as illustrated by the full line which represents a fit to the C_η data according to Eq. (9-3).

$$C_\eta(w_{NVP}^0) = \exp\left(A + B \cdot w_{NVP}^0 + C \cdot (w_{NVP}^0)^2 + D \cdot (w_{NVP}^0)^3\right) \quad (9-3)$$

The resulting parameter values are $A = -6.438$, $B = 29.59$, $C = -33.03$, $D = 12.59$.

In fact, recent studies into chemically initiated polymerizations of non-ionized MAA at monomer concentrations of 30 to 10 wt.% in water revealed that the $\langle k_t \rangle$ vs. X profile is almost independent of w_{MAA}^0 at those rather low monomer contents and, consequently, C_η is constant.^[277]

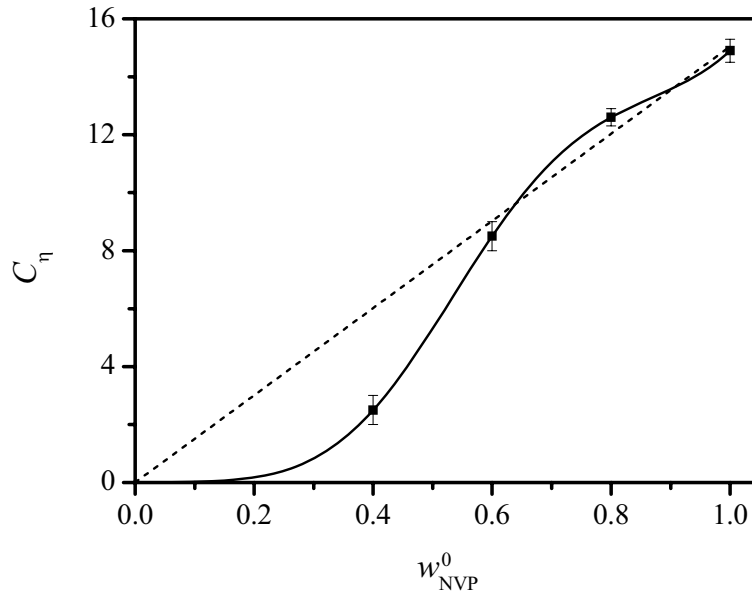


Figure 9-5: Dependence of the viscosity parameter C_η (see Eq. (8-7)) on initial NVP weight fraction for polymerizations of NVP in bulk and solution of D_2O at 40 °C and 2000 bar. The associated values are contained in Table 9-1. The dashed line represents a linear fit to the C_η values for w_{NVP}^0 of 0.6 to 1 whereas the full line was obtained from regression of the entire C_η data (see Eq. (9-3)). In both cases, the fit was imposed to pass the origin.

The proportionality between C_η and w_{NVP}^0 for high w_{NVP}^0 indicates that the $\langle k_t \rangle$ dependencies for different initial monomer concentrations should converge when plotted against the weight fraction of polymer which is produced by monomer conversion, $w_{\text{poly(NVP)}}$. However, the $\langle k_t \rangle$ vs. $w_{\text{poly(NVP)}}$ data shown in Figure 9-6 are not overlapping in contrast to the corresponding values for MAA depicted in Figure 8-5. This discrepancy is caused by the relatively strong dependence of $\langle k_{\text{SD}} \rangle$ on w_{NVP}^0 . However, an almost perfect match of the $\langle k_t \rangle$ data is obtained when plotting reduced termination rate coefficients, i.e. $\langle k_t \rangle / \langle k_{\text{SD}} \rangle$, against $w_{\text{poly(NVP)}}$ as is shown in Figure 9-7. The close overlap indicates that a generalized $\langle k_t \rangle$ correlation may be used to describe the entire set of termination rate coefficients contained in Figure 9-2. The associated correlation (Eq. (9-4)) is analogous to Eq. (8-8) however a dependence of k_{SD} on w_{NVP}^0 according to the data in Table 9-1 has to be implemented.

$$\langle k_t \rangle = \frac{1}{1/k_{SD}(w_{NVP}^0) + \exp(C_{\eta}^* \cdot w_{NVP}^0 \cdot X)/k_{TD}^0} + C_{RD}^* \cdot (1-X) \cdot k_p \quad (9-4)$$

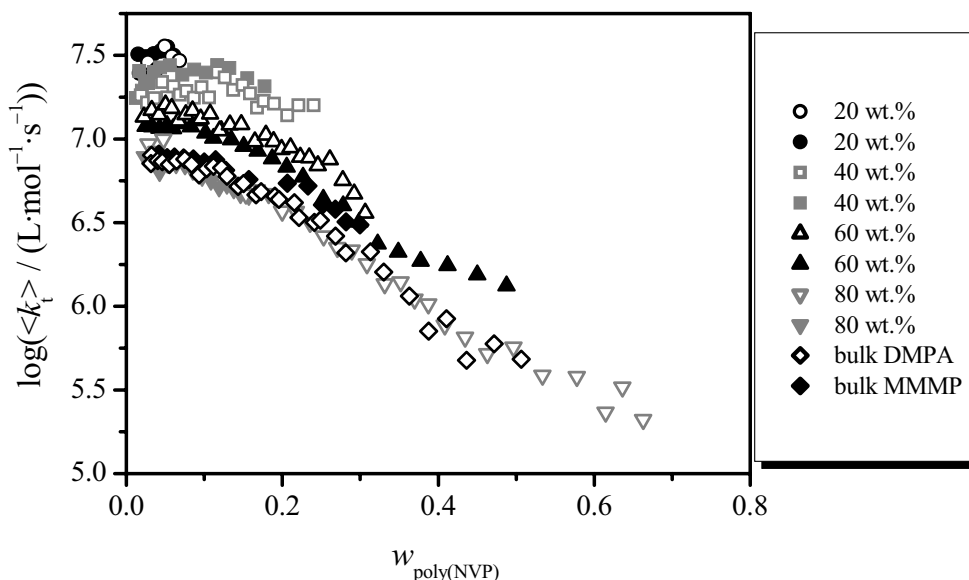


Figure 9-6: Dependence of the $\langle k_t \rangle$ on weight fraction of polymer, $w_{\text{poly(NVP)}}$, for NVP polymerizations in D₂O and in bulk at 40 °C, 2000 bar and different initial monomer concentrations (indicated in the figure).

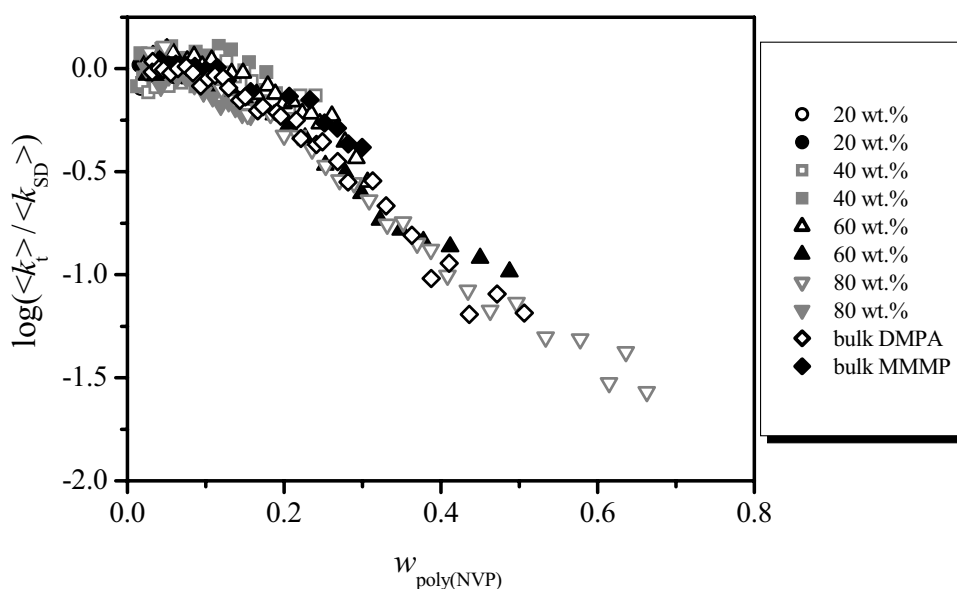


Figure 9-7: Dependence of the reduced termination rate coefficient, $\langle k_t \rangle / \langle k_{SD} \rangle$, on weight fraction of polymer, $w_{\text{poly(NVP)}}$, for NVP polymerizations in D₂O and in bulk at 40 °C, 2000 bar and different initial monomer concentrations (indicated in the figure).

Within Eq. (9-4), k_p changes with w_{NVP}^0 and X according to Eq. (9-2) and k_{TD}^0 is constant at a value of $2 \cdot 10^8 \text{ L} \cdot \text{mol}^{-1} \cdot \text{s}^{-1}$. As the variation of C_{RD} in Table 9-1 follows no systematic trend, a constant C_{RD}^* of 100 is used. $C_{\eta}^* = 15$ is determined from the data for w_{NVP}^0 of 0.6, 0.8 and 1.0. The change in $k_{\text{SD}}(w_{\text{NVP}}^0)$ as contained in Table 9-1 was fitted to a second order polynomial:

$$k_{\text{SD}}(w_{\text{NVP}}^0) = 6.27 \cdot 10^7 - 1.23 \cdot 10^8 \cdot w_{\text{NVP}}^0 + 6.75 \cdot 10^7 \cdot (w_{\text{NVP}}^0)^2 \quad (9-5)$$

Figure 9-8A illustrates the good representation of the experimental $\langle k_t \rangle$ vs. X data for high w_{NVP}^0 by Eq. (9-4) with the parameters given above. However, pronounced discrepancies are seen for $w_{\text{NVP}}^0 = 0.4$, as in this case the actual C_{η} strongly deviates from $C_{\eta}^* \cdot w_{\text{NVP}}^0$ (see Figure 9-5). An adequate representation of the entire $\langle k_t \rangle$ is obtained when $C_{\eta}^* \cdot w_{\text{NVP}}^0$ in Eq. (9-4) is replaced by Eq. (9-3) which has been used for non-linear fitting of the C_{η} values in Figure 9-5. The good representation of the entire $\langle k_t \rangle$ collected in this work by Eqs. (9-3) to (9-5) is shown in Figure 9-8B.

The generalized k_p and $\langle k_t \rangle$ correlations given in Eqs. (8-5) and (8-8) for MAA as well as (9-2) and (9-4) for NVP are valuable modeling tools as they allow for easy estimation of kinetic coefficients within the corresponding ranges of validity. Moreover, Eqs. (8-8) and (9-4) are based on a meaningful physical model. These correlations thus not only allow for estimating $\langle k_t \rangle$ by interpolation but may also give reasonable results for extrapolation beyond the experimentally covered range. This is the major advantage compared to empirical surface functions which may better match the experimental $\langle k_t \rangle$ data however at the expense of predictive power.

In industry, the radical polymerization of NVP is carried out under ambient pressure conditions as the costs of using high pressure cannot be compensated by the increase in turnover rate. Thus, knowledge of the activation volume of $\langle k_t \rangle$ is required for modeling industrial processes. The pressure dependence of the coupled parameter $\langle k_{\text{SD}} \rangle / k_p$ for bulk polymerization of NVP at 40 °C is depicted in Figure 9-9. Mean values of $\langle k_t \rangle / k_p$ values for the low-conversion plateau range of each SP-PLP-NIR measurement are given as circles. Though the experimental data shows pronounced scatter, especially for the lower pressures, the corresponding averages are highly reproducible.

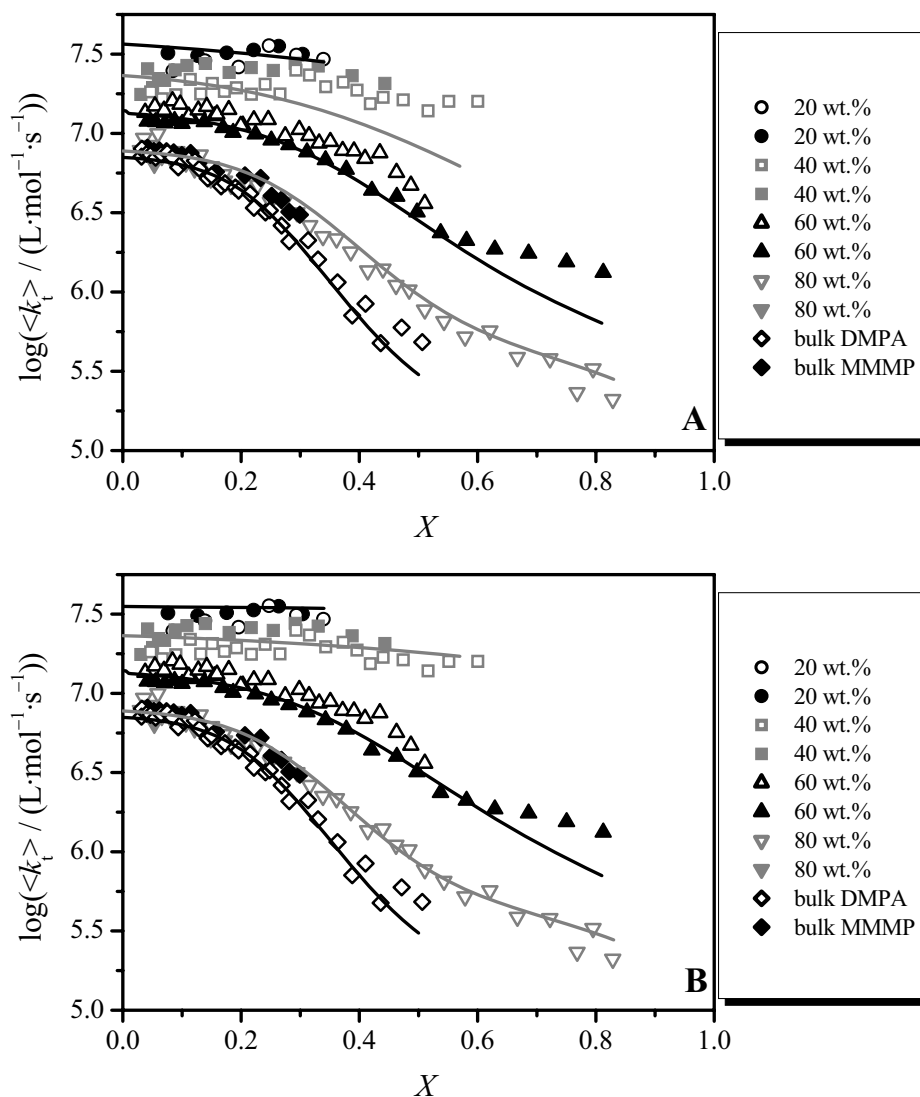


Figure 9-8: Dependence of $\langle k_t \rangle$ on fractional conversion, X , for NVP polymerizations in D₂O and in bulk at 40 °C, 2000 bar and initial monomer concentrations as indicated in the figure. The lines are representations of the experimental data via Eq. (9-4). The associated parameter values are listed in the text.

The $\log(\langle k_{SD} \rangle / k_p)$ vs. p data are well represented by a linear fit providing an activation volume of $\Delta V^\ddagger(\langle k_{SD} \rangle / k_p) = 25.9 \text{ cm}^3 \cdot \text{mol}^{-1}$. The k_p data for NVP bulk polymerization is so far limited to pressures of 1 and 2000 bar from which $\Delta V^\ddagger(k_p) = -11.3 \text{ cm}^3 \cdot \text{mol}^{-1}$ is estimated. This value is in the same activation volume range as measured during polymerization of styrene, vinyl esters and acrylic acid esters.^[16] $\Delta V^\ddagger(\langle k_{SD} \rangle) = 14.6 \text{ cm}^3 \cdot \text{mol}^{-1}$ is obtained from combination of $\Delta V^\ddagger(\langle k_{SD} \rangle / k_p)$ and $\Delta V^\ddagger(k_p)$. The result for $\Delta V^\ddagger(\langle k_{SD} \rangle)$ of NVP is close to previously determined activation volumes of styrene ($14 \text{ cm}^3 \cdot \text{mol}^{-1}$), BA ($16 \text{ cm}^3 \cdot \text{mol}^{-1}$) and MMA ($15 \text{ cm}^3 \cdot \text{mol}^{-1}$).^[16] It goes without

saying that the individual activation volumes are attributed by relatively high error margins as they are based on k_p data for only 2 pressures. Moreover, $\Delta V^\ddagger(k_p)$ and $\Delta V^\ddagger(\langle k_{SD} \rangle)$ may vary with initial NVP content in aqueous solution. The pressure dependence of $\langle k_{SD} \rangle$ was, however, not studied for polymerizations of NVP in dilute solution due to the low signal-to-noise quality at low p .

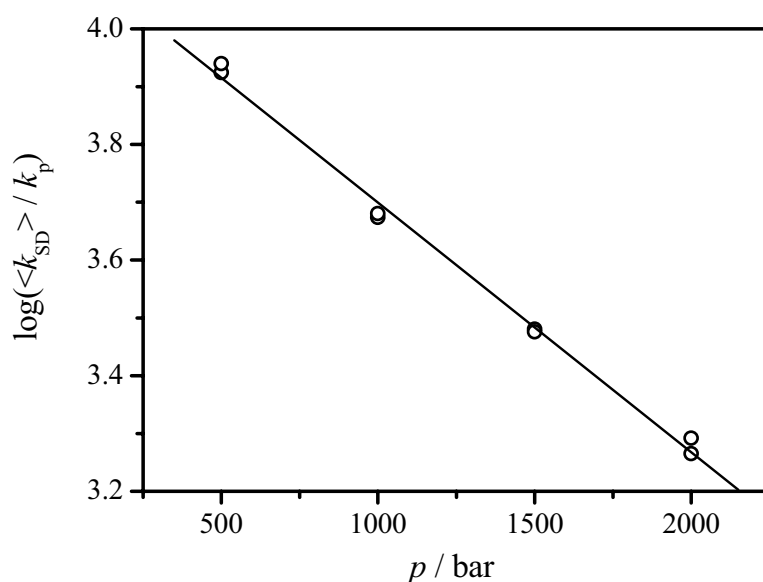


Figure 9-9: Pressure dependence of the coupled parameter, $\langle k_{SD} \rangle / k_p$, for bulk polymerization of NVP at 40 °C.

10 Midchain Radicals in Acrylate Polymerization

The influence of midchain radical formation on the polymerization kinetics, especially of acrylate-type monomers, is currently a topic of eminent scientific interest as is evident from the numerous studies published during recent years. A short introduction into this topic has already been provided within the Theoretical Background section (see Chapter 3.2.3).

In this chapter, the impact of midchain radical formation on stationary, pseudo-stationary and instationary polymerization will be detailed. Special emphasis will be devoted to the influence of MCR build-up on the methods for k_p and k_t determination.

The studies into the influence of MCR build-up on the kinetics of pseudo-stationary polymerization were partially carried out in cooperation with Prof. Robin A. Hutchinson and Dr. Anatoly N. Nikitin. Aspects of this work already appeared in refs.^[52,53]

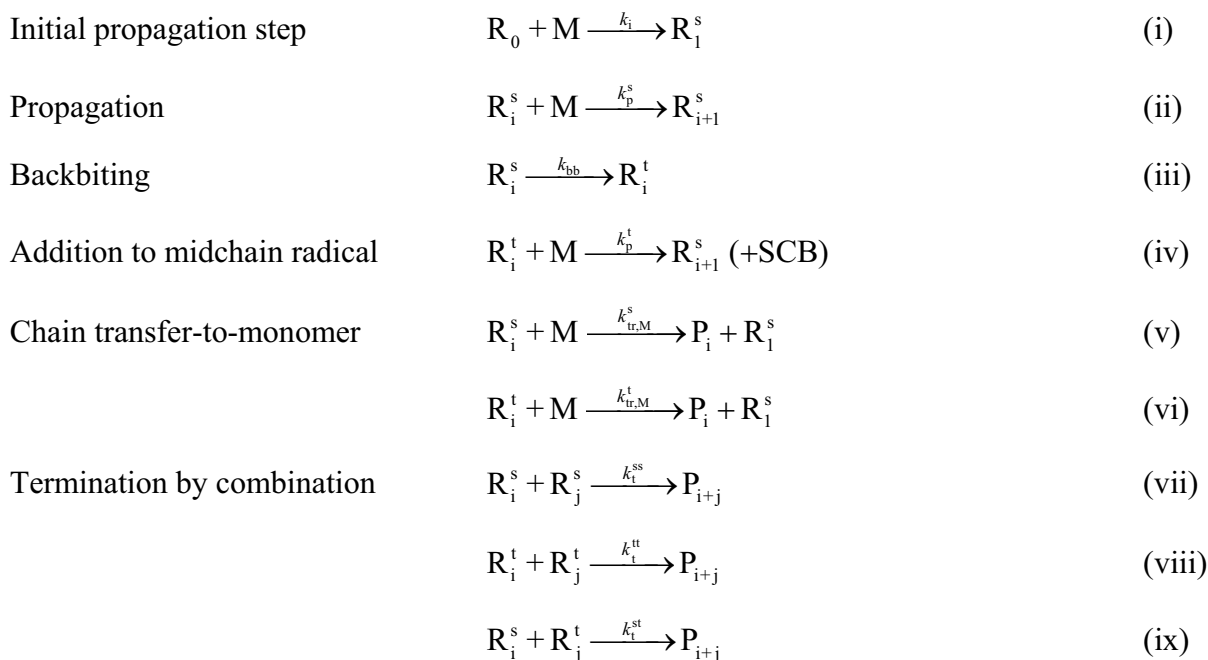
10.1 Acrylate polymerization scheme and basic kinetic equations

The basic mechanistic model of acrylate polymerization at temperatures below 80 °C is given in Scheme 10-1. As the model is used to analyze low-conversion kinetic data, intermolecular chain transfer-to-polymer is not included, nor is β -scission of tertiary radicals since the mechanism has been found to be of negligible importance in this temperature regime.^[45,46] The different reactivity of midchain (R_i^t) and chain-end (R_i^s) radicals toward propagation and termination is explicitly considered, and termination is assumed to take place exclusively by combination.

As two types of radicals occur within acrylate polymerization, the differential rate law given in Eq. (3-5) has to be subdivided into the individual SPR and MCR contributions:

$$\begin{aligned} \frac{dc_{\text{SPR}}}{dt} = & v_1 + k_p^t \cdot c_M \cdot c_{\text{MCR}} + k_{\text{tr},M}^t \cdot c_M \cdot c_{\text{MCR}} \\ & - 2 \cdot k_t^{\text{ss}} \cdot (c_{\text{SPR}})^2 - 2 \cdot k_t^{\text{st}} \cdot c_{\text{SPR}} \cdot c_{\text{MCR}} - k_{\text{bb}} \cdot c_{\text{SPR}} \end{aligned} \quad (10-1)$$

$$\begin{aligned} \frac{dc_{\text{MCR}}}{dt} = & k_{\text{bb}} \cdot c_{\text{SPR}} \\ & - 2 \cdot k_t^{\text{st}} \cdot c_{\text{SPR}} \cdot c_{\text{MCR}} - 2 \cdot k_t^{\text{tt}} \cdot (c_{\text{MCR}})^2 - k_p^t \cdot c_M \cdot c_{\text{MCR}} - k_{\text{tr},M}^t \cdot c_M \cdot c_{\text{MCR}} \end{aligned} \quad (10-2)$$



Scheme 10-1: Acrylate polymerization scheme for low monomer-to-polymer conversions and temperatures below 80 °C.

The initiation rate, v_i , equals $2 \cdot k_d \cdot f \cdot c_I$ for chemically induced polymerizations. Including SPR-MCR termination with the term $2 \cdot k_t^{st} \cdot c_{SPR} \cdot c_{MCR}$ in Eqs. (10-1) and (10-2) is not straight forward. This notation has been chosen to provide comparability with the work of Nikitin and Hutchinson. The change in overall radical concentration, i.e. of $dc_{SPR}/dt + dc_{MCR}/dt$, is given by:

$$\frac{dc_R}{dt} = v_i - 2 \cdot k_t^{ss} \cdot (c_{SPR})^2 - 4 \cdot k_t^{st} \cdot c_{SPR} \cdot c_{MCR} - 2 \cdot k_t^{tt} \cdot (c_{MCR})^2 \quad (10-3)$$

As $c_R = c_{MCR} + c_{SPR}$, $x_{MCR} = c_{MCR} / (c_{SPR} + c_{MCR})$, and $x_{SPR} = (1 - x_{MCR})$, Eq. (10-3) may be transformed to:

$$\frac{dc_R}{dt} = v_i - 2 \cdot (c_R)^2 \cdot \left(k_t^{ss} \cdot (1 - x_{MCR})^2 + k_t^{st} \cdot 2 \cdot (1 - x_{MCR}) \cdot x_{MCR} + k_t^{tt} \cdot (x_{MCR})^2 \right) \quad (10-4)$$

This relation shows strong analogy to the differential rate law in Eq. (3-5). The termination rate coefficient in acrylate polymerization may consequently be expressed in terms of an effective k_t value (k_t^{eff}) which is weighted over the fractions of the reacting radical species according to:

$$k_t^{\text{eff}} = k_t^{\text{ss}} \cdot (1 - x_{\text{MCR}})^2 + k_t^{\text{st}} \cdot 2 \cdot (1 - x_{\text{MCR}}) \cdot x_{\text{MCR}} + k_t^{\text{tt}} \cdot (x_{\text{MCR}})^2 \quad (10-5)$$

Strictly speaking, the propagation rate coefficient should be expressed in an analogous manner by:

$$k_p^{\text{eff}} = k_p^{\text{s}} \cdot (1 - x_{\text{MCR}}) + k_p^{\text{t}} \cdot x_{\text{MCR}} \quad (10-6)$$

However, the second addend on the right hand side of Eq. (10-6) may be neglected in case of $k_p^{\text{s}} \gg k_p^{\text{t}}$ and x_{MCR} being well below unity. The obtained result has already been derived mathematically in Chapter 3.2.3 (see Eq. (3-18)).

10.2 Impact of midchain radical formation on the kinetics of stationary polymerization

A comprehensive description of stationary acrylate polymerization kinetics is contained in the work of Nikitin and Hutchinson.^[28,51] This chapter briefly presents this topic in an intuitively understandable way.

In a stationary radical polymerization, the rate of radical formation by initiation equals the rate of radical loss by termination. Under such conditions, the rate of polymerization (compare with Eq. (3-10)) may be expressed in terms of effective propagation and termination rate coefficients according to:

$$R_p = -\frac{dc_M}{dt} = c_M \cdot \frac{k_p^{\text{eff}}}{\sqrt{k_t^{\text{eff}}}} \cdot \sqrt{f \cdot k_d \cdot c_I} \quad (10-7)$$

The midchain radical fraction required for calculating k_p^{eff} and k_t^{eff} from Eqs. (10-5) and (10-6) may be estimated by Eq. (3-14), assuming $dc_{\text{MCR}}/dt = 0$, i.e. MCR concentration reaches stationarity. Upon additionally including transfer-to-monomer reactions, the relation reads:

$$x_{\text{MCR}} = \frac{k_{\text{bb}}}{k_p^{\text{t}} \cdot c_M + k_{\text{tr,M}}^{\text{t}} \cdot c_M + 2 \cdot k_t^{\text{tt}} \cdot c_{\text{MCR}} + 2 \cdot k_t^{\text{st}} \cdot c_{\text{SPR}} + k_{\text{bb}}} \quad (10-8)$$

Due to the two monomer-concentration dependent terms in the denominator of Eq. (10-8), x_{MCR} increases toward lower c_{M} . This introduces an inherent dependence of $k_{\text{p}}^{\text{eff}}$ and $k_{\text{t}}^{\text{eff}}$ on monomer concentration and thus on conversion as far as the individual k_{p} and k_{t} values, respectively, are not identical.

Significant simplifications are possible when the so-called long-chain hypothesis holds true, i.e. that it is much more probable for an MCR to add to a monomer molecule than to terminate or undergo transfer reactions:

$$k_{\text{p}}^{\text{t}} \cdot c_{\text{M}} \gg k_{\text{tr,M}}^{\text{t}} \cdot c_{\text{M}} + 2 \cdot k_{\text{t}}^{\text{tt}} \cdot c_{\text{MCR}} + 2 \cdot k_{\text{t}}^{\text{st}} \cdot c_{\text{SPR}} \quad (10-9)$$

Combination of Eq. (10-8) and inequality (10-9) yields:

$$x_{\text{MCR}} = \frac{k_{\text{bb}}}{k_{\text{p}}^{\text{t}} \cdot c_{\text{M}} + k_{\text{bb}}} \quad (10-10)$$

Under the assumption that k_{t}^{st} is the geometric mean of k_{t}^{ss} and k_{t}^{tt} , i.e. $k_{\text{t}}^{\text{st}} = (k_{\text{t}}^{\text{ss}} \cdot k_{\text{t}}^{\text{tt}})^{0.5}$, the following expression for $k_{\text{t}}^{\text{eff}}$ is obtained from Eq. (10-5):

$$\sqrt{k_{\text{t}}^{\text{eff}}} = \sqrt{k_{\text{t}}^{\text{ss}}} \cdot (1 - x_{\text{MCR}}) + \sqrt{k_{\text{t}}^{\text{tt}}} \cdot x_{\text{MCR}} \quad (10-11)$$

Implementing Eqs. (3-18), (10-10), and (10-11) into Eq. (10-7) yields:

$$R_{\text{p}} = -\frac{dc_{\text{M}}}{dt} = c_{\text{M}} \cdot \frac{k_{\text{p}}^{\text{s}}}{\sqrt{k_{\text{t}}^{\text{ss}}}} \cdot \sqrt{f \cdot k_{\text{d}} \cdot c_{\text{I}}} \cdot \left(\frac{c_{\text{M}}}{c_{\text{M}} + \frac{\sqrt{k_{\text{t}}^{\text{tt}}}}{\sqrt{k_{\text{t}}^{\text{ss}}}} \cdot \frac{k_{\text{bb}}}{k_{\text{p}}^{\text{t}}}} \right) \quad (10-12)$$

a relation previously derived by Nikitin and Hutchinson.^[28] Eq. (10-12) illustrates the kinetic origin behind the experimental observation of reaction orders in monomer concentration exceeding unity in stationary acrylate polymerization (with the upper boundary value of two reached for $(k_{\text{t}}^{\text{tt}}/k_{\text{t}}^{\text{ss}})^{0.5} \cdot (k_{\text{bb}}/k_{\text{p}}^{\text{t}}) \gg c_{\text{M}}$). Nikitin and Hutchinson also derived more general expressions removing e.g. the restrictions in terms of the mathematical relation between the individual k_{t} values. Those relations were used to estimate k_{t}^{ss} , k_{t}^{st} , and k_{t}^{tt} values from R_{p} data measured at different concentrations of BA in benzene.^[51]

10.3 Impact of midchain radical formation on the kinetics of pseudo-stationary polymerization

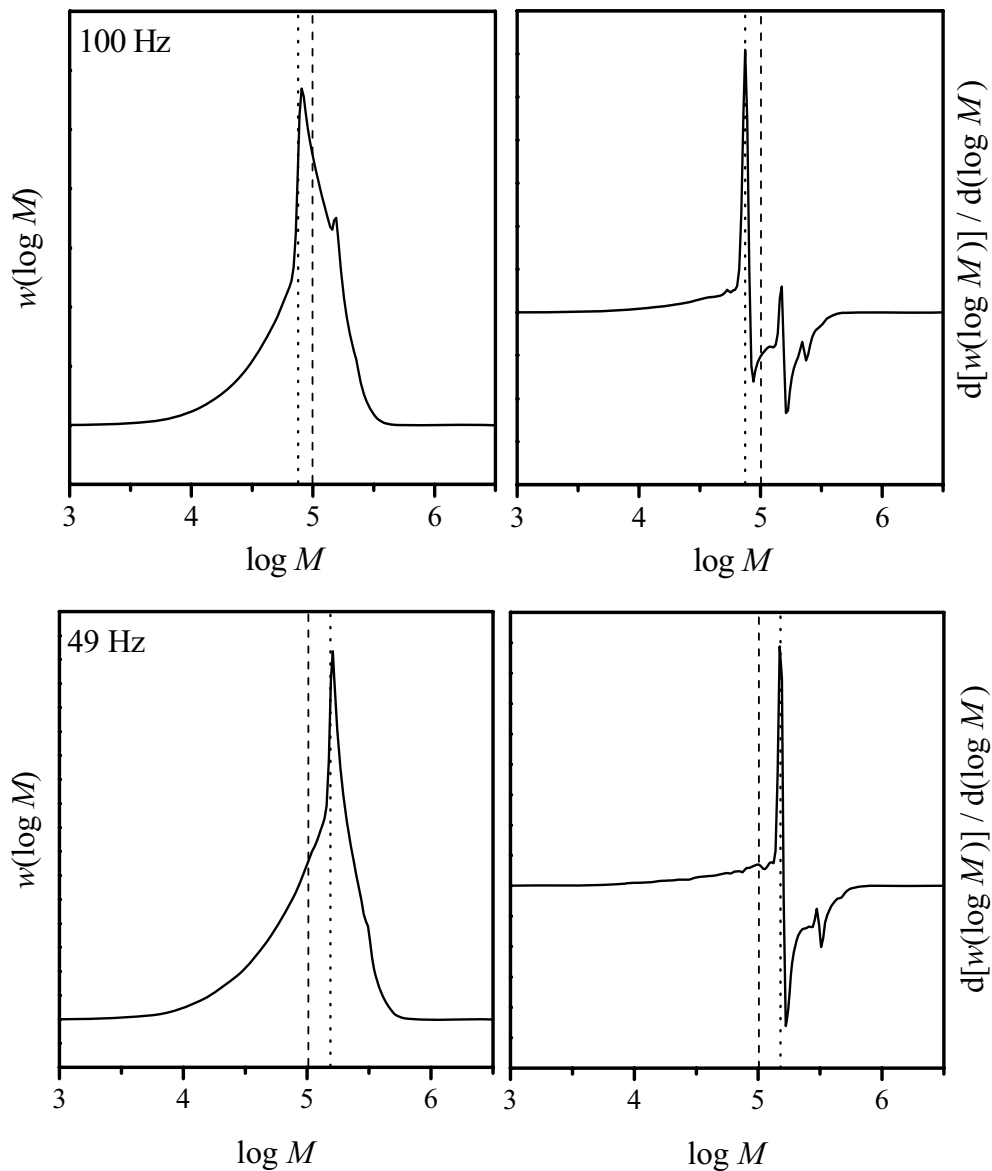
The PLP-SEC technique introduced in Chapter 5.1 is a powerful experimental method for determination of the propagation rate coefficient k_p . Within this technique, a pseudo-stationary radical concentration is produced by laser pulsing on the reaction solutions at constant LPRR, f_L . Significant difficulties arise when PLP-SEC is applied to acrylate-type monomers at temperatures above 20 °C and LPRRs of and below 100 Hz. At such conditions no or only broadened PLP structures are obtained.^[13,67–69,142,173,184–193] This broadening has been attributed to the action of intramolecular transfer to polymer.^[13,55,56,57]

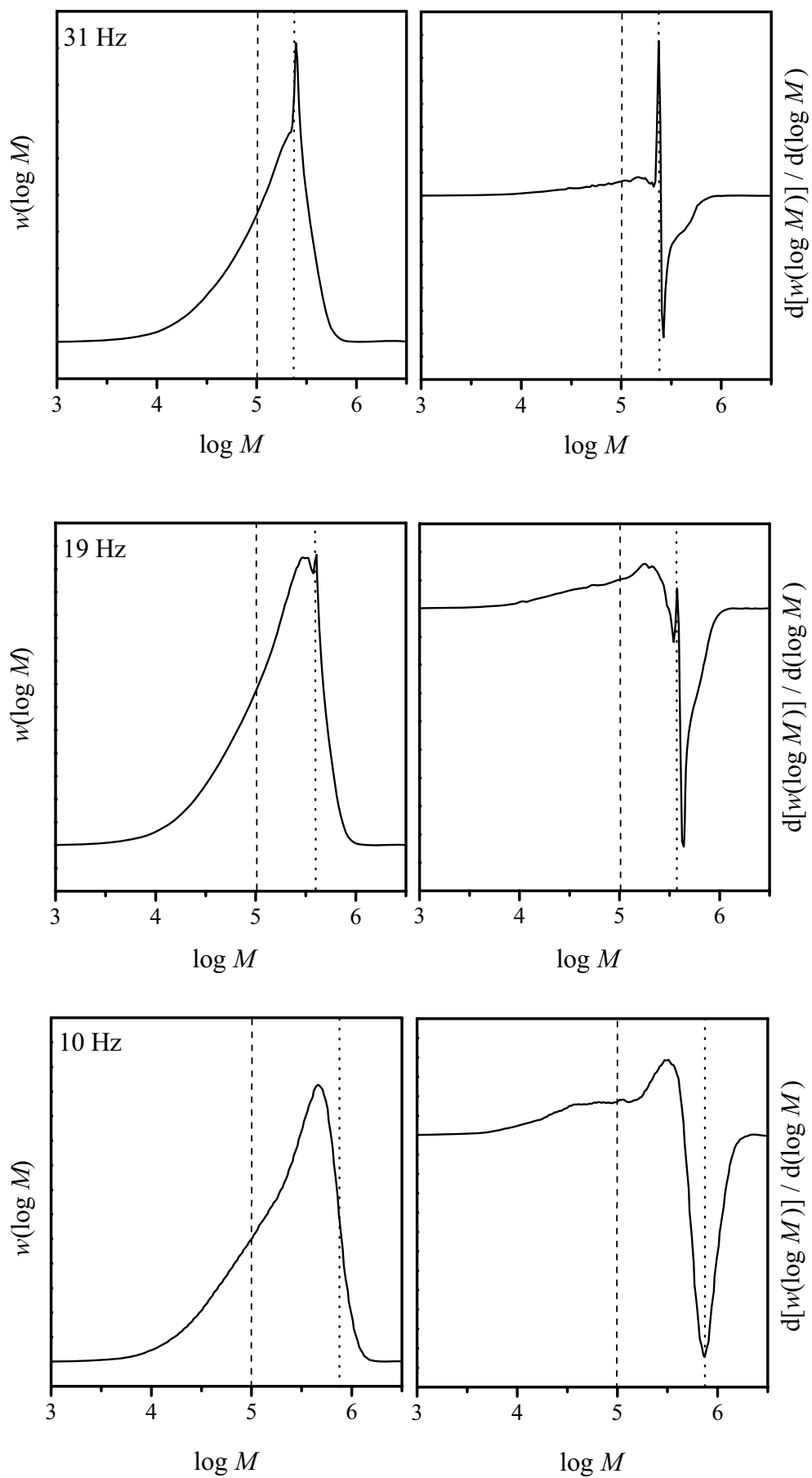
The influence of MCR formation on the MWDs of polymer produced by PLP has been studied via PREDICI simulations on the basis of the reaction steps collected in Scheme 10-1. The frequency factors and activation energies of the corresponding rate coefficients for BA are listed in Table 10-1.

Table 10-1: Arrhenius parameters of the rate coefficients used for simulation of BA polymerization

	pre-exponential factor $\text{L}\cdot\text{mol}^{-1}\cdot\text{s}^{-1}$ or s^{-1}	activation energy $\text{kJ}\cdot\text{mol}^{-1}$	references
k_p^s	$2.21\cdot 10^7$	17.9	[13]
k_{bb}	$4.84\cdot 10^7$	31.7	this work
k_p^t	$1.52\cdot 10^6$	28.9	this work
$k_{tr,M}^s$	$2.9\cdot 10^5$	32.6	[278]
k_t^{ss}	$6.70\cdot 10^8$	5.6	[16], [51]
k_t^{st}	$1.37\cdot 10^8$	5.6	this work, [16], [51]
k_t^{tt}	$9.0\cdot 10^6$	5.6	this work, [16], [51]
$k_{tr,M}^t$	$2.0\cdot 10^5$	46.1	[56],[278]

The complexity of chain-length-dependent termination is not considered, as it should have negligible effect on the position and breadth of the main MWD peak which is controlled by termination of radicals with lifetime t_0 by newly generated short-chain radicals. The Arrhenius parameters for the rate coefficients of backbiting and monomer addition to midchain radical are determined in this work by means of PLP-SEC measurements, as presented in Chapter 11. The activation energies for the termination rate coefficients k_t^{ss} , k_t^{st} , and k_t^{tt} are chosen to be the same as in ref.^[16], and the pre-exponential factors are calculated from the lumped rate coefficients $2 \cdot k_t^{ss} \cdot (k_p^s)^{-2}$, $\theta_1 = 2 \cdot (k_t^{st}/k_t^{ss}) \cdot (k_{bb}/k_p^t)$, and $\theta_2 = (k_t^{tt}/k_t^{ss}) \cdot (k_{bb}/k_p^t)^2$ reported in ref.^[51] from analysis of stationary R_p data at 50 °C.





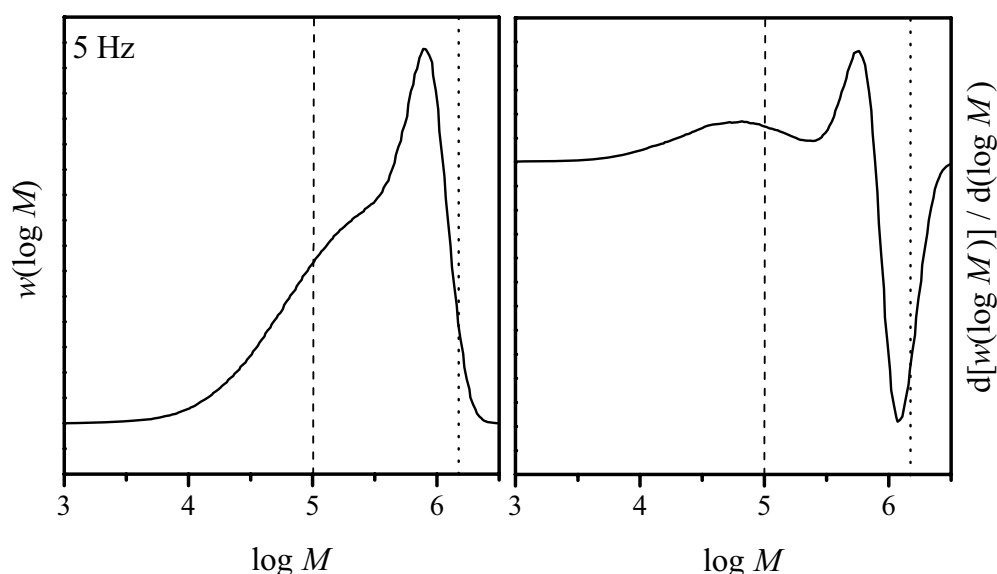


Figure 10-1: Simulated MWDs (left) and associated first-derivative curves (right) for PLP of BA in bulk at 0 °C, $c_R^0 = 5 \cdot 10^{-6} \text{ mol} \cdot \text{L}^{-1}$, and different laser pulse repetition rates (indicated in the figures). The dashed lines are for $\log M = 5$. The vertical dotted lines have been estimated according to Eq. (5-1) with k_p^s from Table 10-1. Additional SEC broadening has not been introduced. Rate coefficients for modeling are either identical or close to the ones collated in Table 10-1.

Figure 10-1 presents simulated MWDs (l.h.s) and their associated first-derivative curves (r.h.s.) for PLP of BA in bulk at 0 °C and different LPRRs. The rate coefficients used for modeling are either identical to the literature values or close to the final values being determined in the thesis in hand (see Table 10-1). Slight discrepancies are, however, not of concern, as only general trends are discussed with Figure 10-1. Additional SEC broadening was not introduced to allow for clear detection of the effects examined below.

For 100 Hz, a perfectly PLP-structured MWD is obtained, as is indicated by the three maxima in the associated first-derivative curve. Thus, the important consistency criterion for k_p evaluation is fulfilled.^[8] The position of the first POI is close to the $\log M$ value estimated according to Eq. (5-1) with k_p^s from Table 10-1 (indicated by the vertical dotted line). Hence, the first maximum in the derivative curve of the MWD seems characteristic for propagation of SPRs with chain growth not being affected by MCR formation. At a lower LPRR of 49 Hz, the position of the narrow peak in the MWD is shifted to higher molecular weight as expected from Eq. (5-1). However, more material evolves on the low molecular weight side of the PLP peak. The intensities of the overtones decrease and only one overtone maximum is observed

in the first-derivative curve of the MWD. The distribution simulated for a LPRR of 31 Hz shows that the narrow PLP peak, though decreasing in intensity, still provides precise access to k_p^s . As inspection of the first-derivative curve tells, there is no longer clear evidence of an overtone maximum on the high molecular weight side of the narrow PLP peak to prove consistency. However an additional broad maximum evolves on the low-molecular-weight side. This maximum is due to the high amount of PLP-controlled polymer chains which underwent backbiting and eventually re-initiation reactions, i.e. monomer addition to a MCR, during dark time. The backbiting step itself may happen at any time between two laser pulses and the resulting MCR formation decelerates chain growth as k_p^t is lower than k_p^s . Thus, the emerging maximum in the first-derivative curve is broad and of lower molecular weight than the narrow one being characteristic for k_p^s . At a LPRR of 19 Hz, the MWD peak for SPR propagation is of very small intensity and disappears toward even higher pulse-separation times. The broad maximum at low molecular weight in the first-derivative curve is, however, well pronounced. Inspection of the simulations for 10 and 5 Hz tells that the position of the broad maximum shifts to higher molecular weights as LPRR is decreased. This shows that molecular weight is controlled by laser pulsing even though the distributions are significantly broadened not fulfilling the overtone criterion. However, such distributions must not be considered meaningless as they contain valuable information about the transfer kinetics. Finally, it is to be mentioned that the very broad maximum in the first-derivative curve of the MWD simulated for 5 Hz is due to the high termination probability of radical chains in the dark time period at low LPRRs. Hence, the position of this maximum is not controlled by laser pulsing and k_p values must not be evaluated from such peak.

Careful analysis of an entire set of MWDs obtained from PLP of acrylate-type monomers at different LPRRs is required to correctly assign the observed maxima in the first-derivative curves. At intermediate LPRRs (see Figure 10-1, 31 Hz and 19 Hz) two k_p values may be estimated from one single MWD. Whereas the narrow peak allows for estimating k_p^s , the broad one at lower molecular weight provides access to an apparent k_p value (k_p^{app}) being affected by transfer reaction. In their pioneering theoretical study, Nikitin et al.^[55] simulated MWDs from PLP of BA at 20 °C and different LPRRs. They observed similar trends as discussed above, i.e. a significant broadening of the MWD toward lower LPRR but without loss of chain-length control by laser pulsing. However, no situations were mentioned in their work where two k_p values, k_p^s and a lower k_p^{app} , were evaluated from one MWD. This may be

due to the choice of kinetic parameters (see Chapter 11) and the introduction of SEC broadening.

The resulting dependency of k_p^{app} on LPRR is depicted in Figure 10-2 (values taken from ref.^[55]). The k_p^{app} values show a sigmoidal decrease toward lower LPRRs. For high LPRRs, k_p^s is asymptotically reached as is to be expected from the discussion to Figure 10-1. A pronounced drop of k_p^{app} sets in at a LPRR of about 100 Hz. The limiting value approached for low LPRRs is k_p^{eff} .

In PLP, SPRs are formed by monomer addition to initiator-derived radicals shortly after laser pulse application. Such SPR has an average lifetime of τ_{SPR} until it undergoes backbiting:

$$\tau_{\text{SPR}} = \frac{1}{k_{\text{bb}}} \quad (10-13)$$

The lifetime of the thereby formed MCR is

$$\tau_{\text{MCR}} = \frac{1}{k_p^t \cdot c_M} \quad (10-14)$$

until it is re-transformed into a SPR by monomer addition. The average number of backbiting and re-initiation cycles during one dark-time period, n_c , is thus.^[57]

$$n_c = \left(\frac{f_L}{k_{\text{bb}}} + \frac{f_L}{k_p^t \cdot c_M} \right)^{-1} = \frac{1}{f_L \cdot (\tau_{\text{SPR}} + \tau_{\text{MCR}})} \quad (10-15)$$

The n_c values calculated on the basis of the k_{bb} and k_p^t values given in ref.^[55] are plotted together with k_p^{app} in Figure 10-2 (full line). Comparison of n_c and k_p^{app} shows that for LPRRs of 30 Hz and below, for which k_p^{app} is close to k_p^{eff} , the average number of backbiting and re-initiation cycles is 3.5 and above. Consequently, sufficient frequency is reached that the k_p^{app} value accounts for the slow-down of chain growth due to formation of the poorly propagating MCRs. At the LPRR value where the pronounced drop of k_p^{app} sets in (100 Hz), n_c is around unity. Such value is insufficient to provide a reasonable estimate of k_p^{eff} as a big fraction of the chains which form the broad PLP peak did not undergo MCR propagation so far.

The situation shown in Figure 10-2 opens up the possibility to estimate k_p^s and k_p^{eff} values from experimental dependencies of k_p^{app} on LPRR. Moreover, implementation of k_p^s and k_p^{eff} into Eq. (3-18) provides access to x_{MCR} . Provided that k_{bb} is known, k_p^t may then be estimated

from Eq. (10-10). PLP-controlled peaks are corresponding to radicals which are formed by laser pulse initiation, survived the dark time period(s) and are terminated by a burst of new radicals generated at a subsequent laser pulse. Radicals which terminate during the pulse-separation time or which are formed by intermolecular transfer reactions only occur as background polymer below the actual PLP peak. Thus, description of x_{MCR} by Eq. (10-10) is valid for k_p^{eff} from PLP-SEC experiments as the long-chain hypothesis cannot be violated by termination or intermolecular transfer reactions.

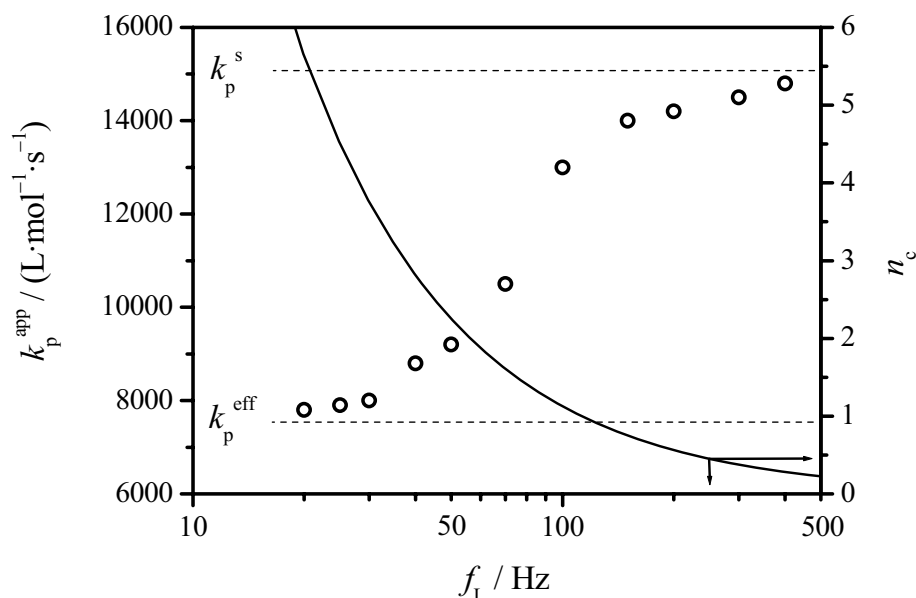
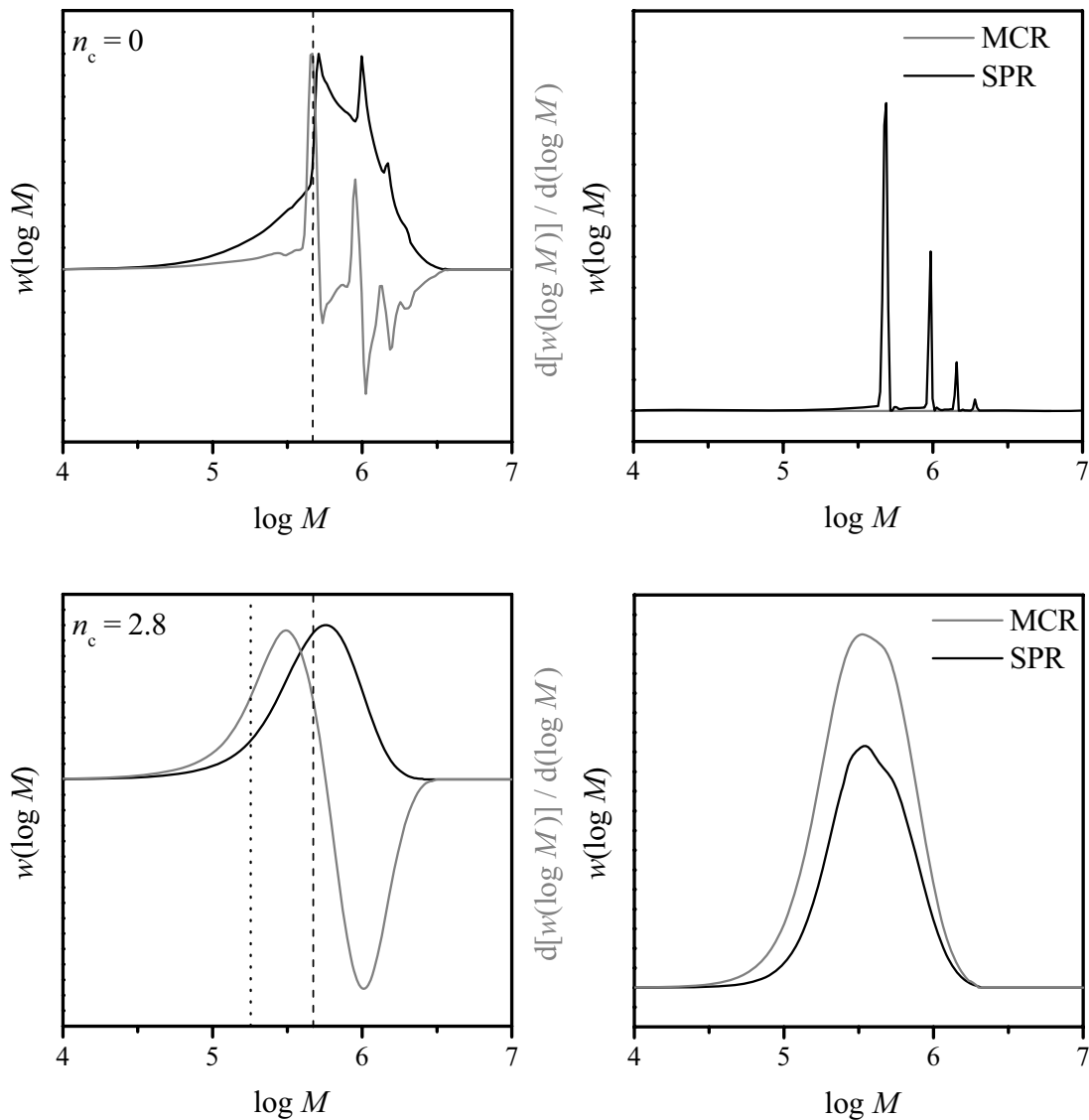


Figure 10-2: Dependence of the apparent propagation rate coefficient on LPRR determined from simulated MWDs for PLP of BA at 20 °C as reported in ref.^[55] Horizontal dashed lines indicate the k_p^s and k_p^{eff} values. The full line indicates the associated average number of backbiting and re-initiation cycles during one dark time period determined from Eq. (10-15).

PLP-SEC experiments under wide variation of LPRR are strongly recommended as they contain valuable kinetic information. This approach has been experimentally explored by Castignolles^[279] for BA polymerization initiated by pulsed UV lamp radiation at 15 °C, under which conditions k_p^{eff} was estimated to be about 4800 L·mol⁻¹·s⁻¹. However, the k_p^{app} variation with LPRR was found to be not reproducible, as the pulse energy of the lamp was not well stabilized. Thus Castignolles recommended application of the PLP technique. PLP-SEC experiments under wide variation of LPRRs are detailed in Chapter 11 for BA and in Chapter 13 for AA polymerization.

As detailed above, MCR formation has been identified as the origin of the loss in PLP structuring for MWDs obtained from PLP of acrylate-type monomers at elevated temperatures. However, the dependence of the extent of peak broadening on k_{bb} and k_p^{\dagger} has not been properly described so far. Nikitin et al.^[55] pointed out that weakly PLP-structured MWDs may be obtained from PLP at low LPRRs (providing access to k_p^{eff}) when monomer addition to the MCR is fast. However, simulations with the parameter set collated in Table 10-1 do not show formation of an overtone for PLP of BA at 20 °C and low LPRRs. A particularly useful quantity for describing the effect of peak broadening during PLP of acrylate monomers is n_c .



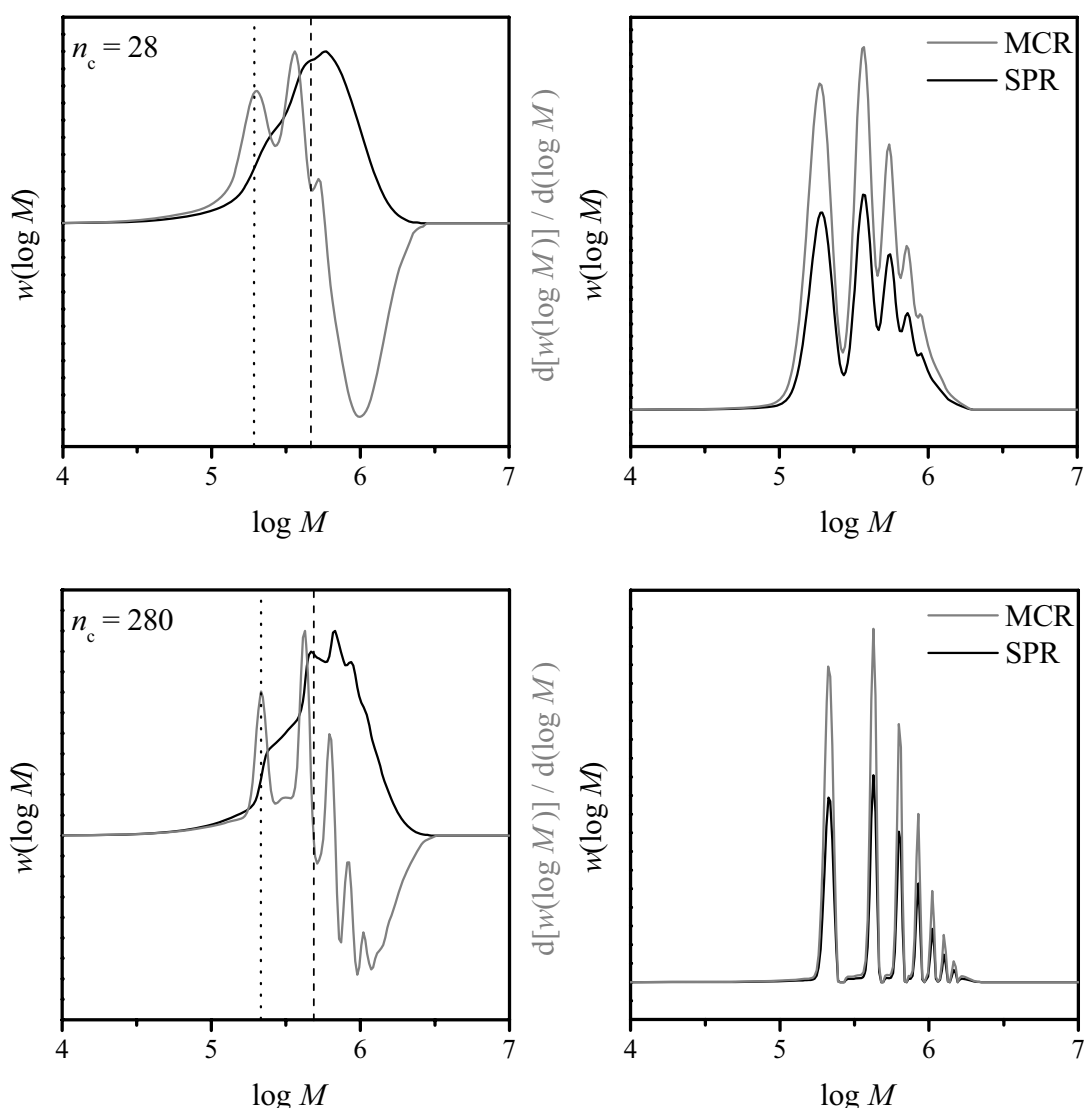


Figure 10-3: Simulated MWDs (left, black lines) and associated first-derivative curves (left, grey lines) for PLP of BA in bulk at 50 °C, a LPRR of 50 Hz, 50 pulses, a primary radical concentration of $1 \cdot 10^{-6} \text{ mol} \cdot \text{L}^{-1}$, and different numbers of backbiting and re-initiation cycles during one dark-time period (indicated in the Figures). Other rate coefficients are chosen according to Table 10-1 (k_{bb} and k_{p}^{t} are varied). The vertical dashed and dotted lines have been estimated according to Eq. (5-1) with k_{p}^{s} and $k_{\text{p}}^{\text{eff}}$, respectively. The $k_{\text{p}}^{\text{eff}}$ values were determined from Eq. (10-6) in combination with Eq. (10-10). On the right hand side, the SPR (black lines) and MCR (grey lines) MWDs at 0.02 s after application of the last laser pulse are shown. Additional SEC broadening has not been introduced.

The left hand side of Figure 10-3 depicts simulated MWDs (black lines) and the associated first-derivative curves (grey lines) for PLP of BA in bulk at 50 °C, a LPRR of 50 Hz, and different magnitudes of n_{c} (for details see caption to Figure 10-3). The right hand side of the figure shows SPR (black lines) and MCR (grey lines) MWDs at 0.02 s after application of the

last laser pulse. The rate coefficients for modeling are chosen according to Table 10-1 with k_{bb} and k_p^t being systematically varied. A n_c value of zero denotes the situation of $k_{bb} = 0$ where no MCRs are formed and k_p^s equals k_p^{eff} . In such case a PLP-structured MWD is obtained as is indicated by the three supporting overtones in the first-derivative curve. The MWD of the SPRs at 0.02 s after the last laser pulse shows 4 narrow and well separated peaks which correspond to macroradicals which started chain growth 0.02, 0.04, 0.06, and 0.08 s (t_0 , $2 \cdot t_0$, $3 \cdot t_0$, $4 \cdot t_0$) ago. A well structured MWD is obtained from termination of such narrowly distributed SPR peaks with small radicals providing access to $k_p^s (= k_p^{eff})$ as is indicated by the vertical dashed line on the left hand side of the figure. With the normal k_{bb} and k_p^t values of Table 10-1, n_c of about 2.8 results from Eq. (10-15). The corresponding MWD is broad and structureless as is the associated first-derivative curve. Such shape is in agreement with experimental experience for PLP-SEC under such conditions. The point of inflection is neither providing direct access to k_p^s (dashed line) nor to k_p^{eff} (dotted line) being estimated according to Eq. (10-6) in combination with Eq. (10-10). The MCR and SPR distributions only show a weak shoulder being insufficient for producing a PLP-structured MWD. From the integrals over the simulated MWDs of the secondary and tertiary radicals, $x_{MCR} \approx 0.62$ can be estimated matching the value determined by Eq. (10-10). When both, k_{bb} and k_p^t , are increased by a factor of 10, n_c is also raised by one order of magnitude to 28. However, x_{MCR} stays the same as the rates of MCR formation by backbiting and MCR loss by monomer addition are increased to the same extent. The constancy of x_{MCR} is also reflected by the integrals over the SPR and MCR distributions in Figure 10-3. Furthermore, k_p^{eff} is only slightly increased compared to the case of $n_c = 2.8$ as monomer addition to tertiary radicals is still rather slow compared to SPR propagation. However, what has been changed is the back and forth transformation velocity in the dynamic equilibrium between the SPR and MCR species. The MCR is thus a relatively short lived species which, although being formed at high rate, rapidly adds to a monomer. Chain growth between initiating and terminating pulses by SPR propagation is therefore only shortly interrupted in a frequent and periodical way by backbiting and re-initiation steps. This induces sufficient statistic frequency into the backbiting and monomer addition cycles during the dark time period(s) to produce narrow and thus structured SPR and MCR distributions. The k_p value obtained from the associated MWD is consequently close to k_p^{eff} as overlap of the dotted line with the first POI illustrates. The SPR and MCR distributions are similarly narrow as for the case without MCR formation when n_c is further raised to about 280 representing a polymerization to highly short-chain-

branched polymer. Even 5 maxima are observed in the first-derivative curve of the MWD being more than for $n_c = 0$. This results from the smaller termination reactivity of MCRs compared to SPRs which decreases termination probability between macroradicals and short initiator-derived radicals being formed by laser pulsing. Consequently, it is more likely for a macroradical to pass several laser pulses before termination which generates high overtone numbers. Even for such extremely increased k_p^t value used for simulating the last pair of figures, propagation of SPRs is about tenfold faster than propagation of MCRs and the error of expressing k_p^{eff} by Eq. (3-18) rather than the using correct expression (Eq. (10-6)) is only about 15 %.

The preceding discussion illustrates that there are two strategies for obtaining structured MWDs from PLP of acrylate-type monomers.

(i) The typically applied approach is to suppress MCR formation in the dark time period(s) by using high LPRRs and low temperatures. The probability of a SPR chain to escape backbiting during a time interval t can be derived from the corresponding integrated first order rate law.

$$\frac{c_{\text{SPR}}(t)}{c_{\text{SPR}}(t=0)} = \exp(-k_{\text{bb}} \cdot t) \quad (10-16)$$

Eq. (10-16) is based upon the neglect of termination reactions and SPR formation by MCR propagation or transfer-to-monomer of tertiary radicals. In principle, those prerequisites strongly restrict the applicability of Eq. (10-16). When $c_{\text{SPR}}(t=0)$ is the primary radical concentration formed by laser-pulse initiation (c_{R}^0), $c_{\text{SPR}}(t)$ describes the residual concentration of growing macroradicals at time t after the initiating laser pulse which escaped backbiting reactions, c_{SPR}' . Assuming that both, SPRs and MCRs, are affected to the same extent by termination, the fraction of radicals which survived one pulse-separation time without undergoing backbiting compared to the overall radical concentration after t_0 , c_{R}^{ov} , is thus given by:

$$\frac{c_{\text{SPR}}'}{c_{\text{R}}^{\text{ov}}} = \exp(-k_{\text{bb}} \cdot t_0) = \exp\left(-\frac{k_{\text{bb}}}{f_{\text{L}}}\right) \quad (10-17)$$

PLP-SEC experiments of BA at 0 °C and a LPRR of 100 Hz typically yield PLP-structured MWDs allowing for k_p^s estimation.^[13] According to Eq. (10-17), 66 % of the radicals pass t_0 without suffering to backbiting; 44 % and 28 % even pass $2 \cdot t_0$ and $3 \cdot t_0$, respectively, without undergoing intramolecular transfer. Such high fractions of SPRs are sufficient to allow for

forming a PLP structure on top of a background of non-PLP-controlled polymer and chains which suffered to backbiting. When increasing temperature to 50 °C, $c_{\text{SPR}}' / c_{\text{R}}^{\text{ov}}$ drops to 2.6 and 0.07 % after t_0 and $2 \cdot t_0$, respectively, which is obviously too low to be detected within the MWD.

(ii) Another approach for obtaining PLP-structured MWDs is to select experimental conditions which facilitate backbiting and monomer addition to the MCR during t_0 ; a strategy which, to the best of my knowledge, has not been suggested so far. Toward increasing temperature, k_{bb} and k_{p}^{\dagger} grow significantly due to their relatively high activation energies. The n_{c} value may be furthermore increased by selecting low LPRRs.

Systematic simulations were carried to identify experimental conditions being suitable for testing approach (ii).

Figure 10-4 shows simulated MWDs (left) and their associated first-derivative curves (right) for PLP of BA at 100 °C, a primary radical concentrations of $10^{-6} \text{ mol} \cdot \text{L}^{-1}$, and 9 pulses being applied with different LPRRs (indicated in the figure). The average molecular weight increases toward higher pulse-separation times indicating chain-length control by laser pulsing; the MWDs and first-derivative curves are, however, rather broad and structureless. The first POI for 50 and 20 Hz is well representing $k_{\text{p}}^{\text{eff}}$ (see captions to Figure 10-4) as overlap of the maxima in the first-derivative curves with the corresponding vertical lines shows (see caption to Figure 10-4). The $k_{\text{p}}^{\text{eff}}$ value estimated from the MWD simulated for 100 Hz would, however, be by a factor of 1.6 too high. The discrepancy may be overcome by using higher primary radical concentrations and thus selecting so-called high-termination-limit conditions.^[280] At a c_{R}^0 value of $10^{-5} \text{ mol} \cdot \text{L}^{-1}$, a good representation of the molecular weight at the first POI in the MWD simulated for a LPRR of 100 Hz by $k_{\text{p}}^{\text{eff}}$ is achieved which is, however, on cost of the possibility to obtain the desired overtones (not shown for the purpose of thesis length).

The SPR and MCR distributions at time t_0 after the last laser pulse (not depicted) only show slight structuring being insufficient to provoke PLP structures in the MWDs in Figure 10-4 though the corresponding n_{c} values are 6, 12, and 30 for the LPRRs of 100, 50, and 20 Hz, respectively. The increasing importance of transfer-to-monomer reactions is most likely an important factor contributing to additional broadening at high temperatures.

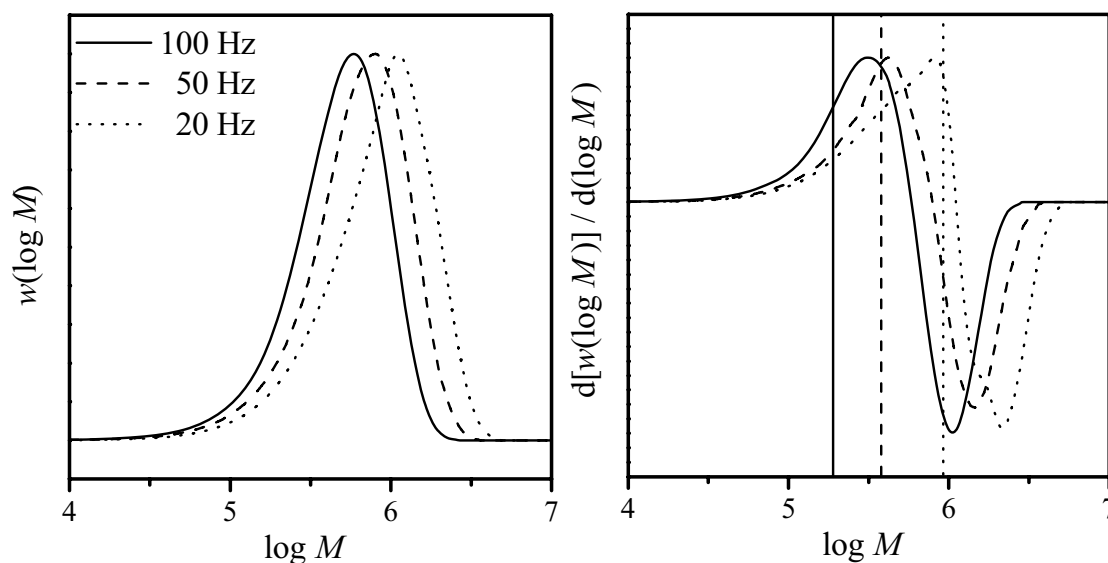


Figure 10-4: Simulated MWDs (left) and associated first-derivative curves (right) for PLP of BA in bulk at 100 °C, 9 pulses, a primary radical concentration of $1 \cdot 10^{-6} \text{ mol} \cdot \text{L}^{-1}$, and different LPRRs (indicated in the figure). Rate coefficients are chosen according to Table 10-1. The vertical lines have been estimated according to Eq. (5-1) with k_p^{eff} determined from Eq. (10-6) in combination with Eq. (10-10).

Depicted in Figure 10-5 are simulated MWDs and associated first-derivative curves (left) for PLP of BA at 120 °C, an LPRR of 50 Hz, 19 pulses, and a primary radical concentration of $10^{-6} \text{ mol} \cdot \text{L}^{-1}$. The upper figure (A) was simulated using the full kinetic scheme and figure B was modeled upon the neglect of transfer-to-monomer reactions. The MWD in figure A is broad and only a weak shoulder occurs at the high molecular weight side of the maximum in the derivative curve. However, the MWD shown in figure B is PLP-structured as indicated by the two POIs which appear as maxima in the first derivative curve. Inspection of the SPR and MCR distributions at 0.02 s after application of the last laser pulse (see right hand side of Figure 10-5) tells that two (figure A) or even three (figure B) maxima can be observed corresponding to growth times of t_0 , $2 \cdot t_0$, and $3 \cdot t_0$, respectively. However, the individual peaks are broad and overlap to high extent. Nevertheless, the basis for obtaining PLP-structured MWDs is significantly improved compared to the polymerization at 50 °C under otherwise identical conditions (see Figure 10-3, $n_c = 2.8$). This indicates that at least the concept of approach (ii) is valid though PLP-structured MWDs are probably not easily obtained from experiments at high temperatures due to transfer-to-monomer reactions. Moreover, side reactions which are not captured by the kinetic scheme used for simulating the MWDs in

Figure 10-5 (β -scission of MCRs or self initiation reactions) may additionally hamper PLP-SEC experiments at high temperatures.

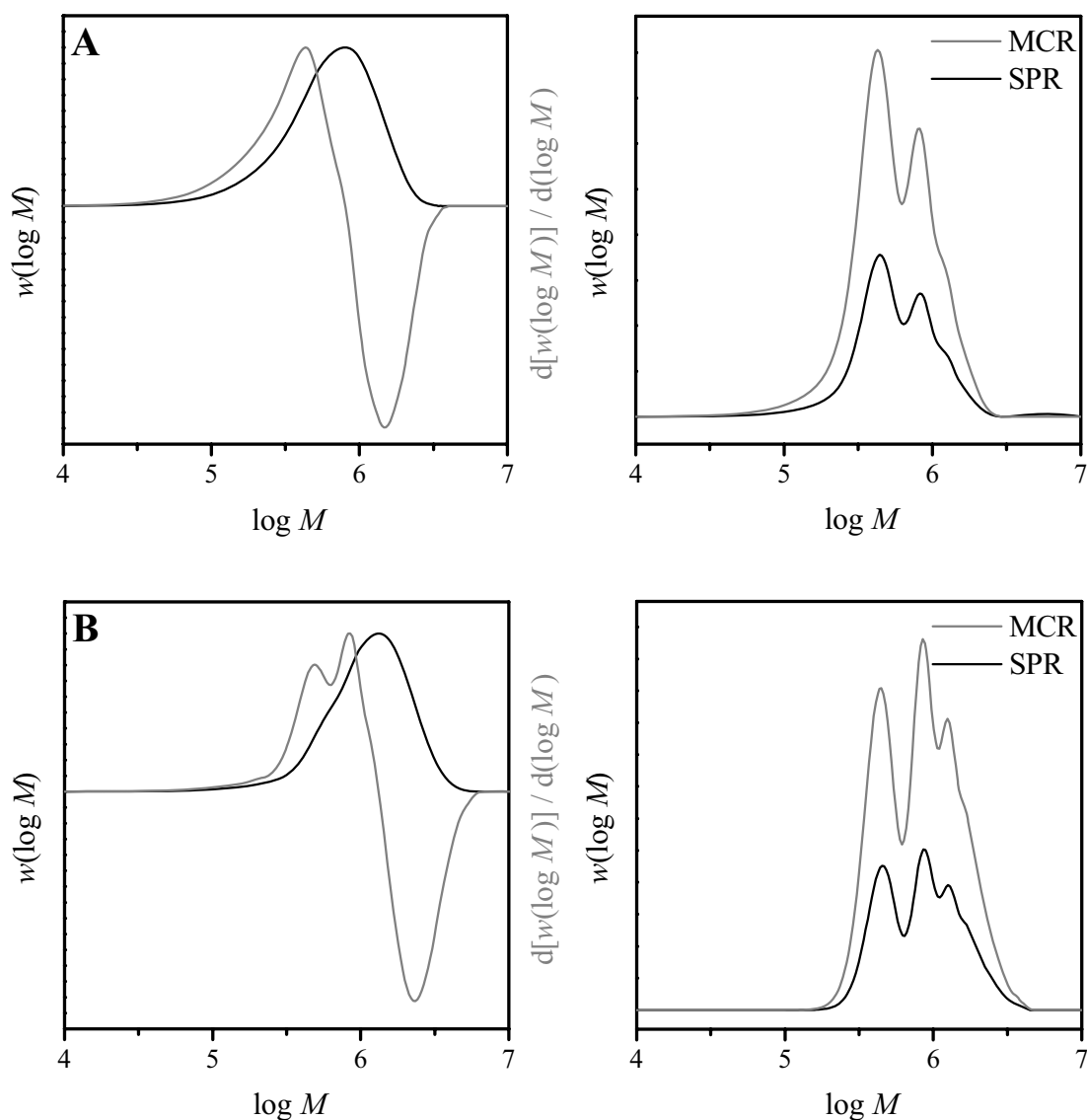


Figure 10-5: Simulated MWDs and their associated first-derivative curves (left) for PLP of BA in bulk at 120 °C, a LPRR of 50 Hz, 19 pulses, and a primary radical concentration of $1 \cdot 10^{-6} \text{ mol} \cdot \text{L}^{-1}$. Rate coefficients are chosen according to Table 10-1. Figure A was simulated with the full kinetic scheme whereas in figure B transfer-to-monomer was neglected. Shown on the right hand side are the corresponding MCR and SPR distributions at 0.02 s after application of the last laser pulse.

Figure 10-6 shows an experimental MWD (black line) and the associated first-derivative curve (grey line) obtained from PLP-induced polymerization of BA in bulk at 100 °C, ambient pressure, an MMMP concentration of $5 \text{ mmol} \cdot \text{L}^{-1}$, an LPRR of 100 Hz, and 40

applied laser pulses. The POI on the low molecular weight side of the MWD is well representing the molecular weight estimated from Eq. (5-1) with k_p^{eff} determined from Eq. (10-6) in combination with Eq. (10-10), as is demonstrated by the agreement between the maximum of the first-derivative curve and the vertical dashed line. Moreover, there is a shoulder at about twice the molecular weight of the maximum (indicated by an asterisk). This shoulder may indicate an overtone which corresponds to a macroradical growth time of $2 \cdot t_0$. However, comparison with MWDs obtained from PLP-induced polymerization at different LPRRs but under ostensibly the same conditions (Figure 10-7) tells that chain length is not efficiently controlled by laser pulsing as no or no significant shift of the MWD to higher molecular weight is seen when LPRR is reduced. Thus, the MWD shown in Figure 10-6 cannot be used for k_p^{eff} evaluation as the consistency criterion of k_p being independent of LPRR is not met. For acrylate-type monomers, this consistency criterion can only be applied within the limits of the characteristic frequency ranges for k_p^s and k_p^{eff} , respectively.

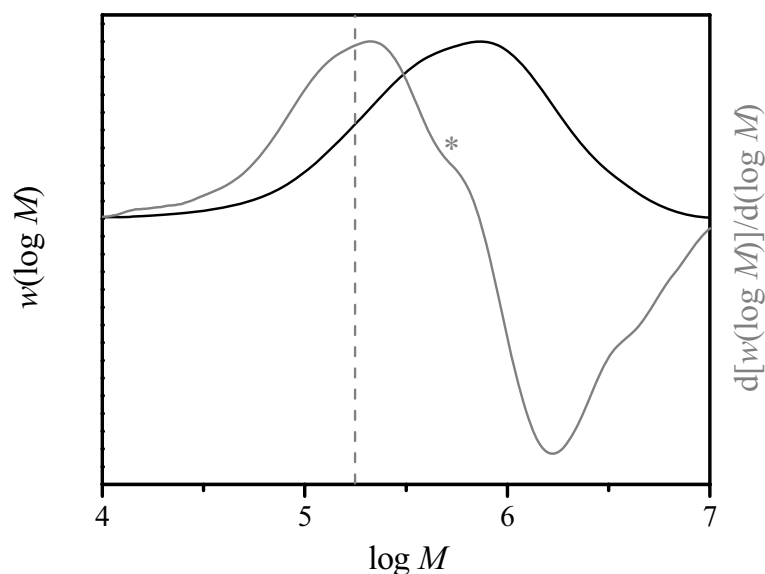


Figure 10-6: MWD (black line) and associated first-derivative curve (grey line) obtained from PLP of BA in bulk at 100 °C, ambient pressure, a LPRR of 100 Hz, an initiator concentration of $c_{\text{MMMP}} = 5 \text{ mmol} \cdot \text{L}^{-1}$, and with 40 pulses being applied. The vertical line has been estimated according to Eq. (5-1) with k_p^{eff} determined from Eq. (10-6) in combination with Eq. (10-10).

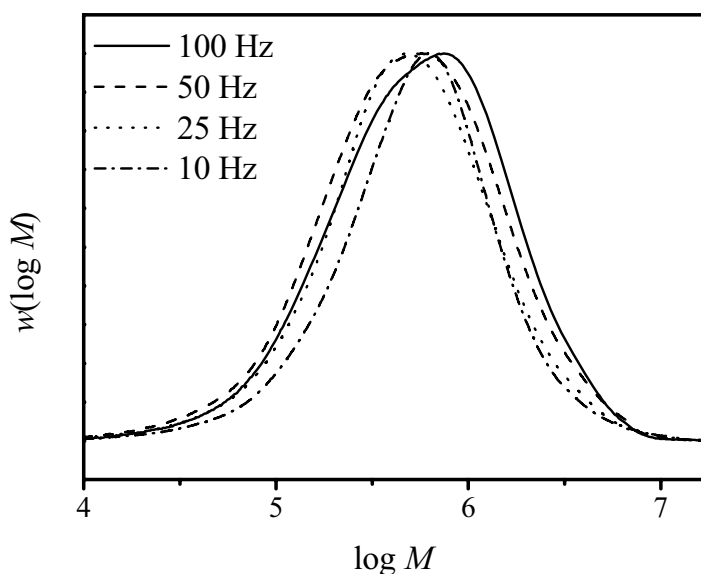


Figure 10-7: MWDs obtained from PLP-induced polymerization of BA in bulk at 100 °C, ambient pressure, an initiator concentration of $c_{\text{MMMP}} = 5 \text{ mmol}\cdot\text{L}^{-1}$, 40 pulses, and different LPRRs as indicated in the figure.

It has already been pointed out in the discussion of Figure 10-4 and Figure 10-5 that PLP-structured MWDs may not be easily obtained from PLP of BA at high temperatures. Propagation rate coefficients are usually featured by negative activation volumes.^[16] It is thus expected that k_p^\ddagger increases toward higher pressure which should, in principle, result in more narrow SPR and MCR distributions as n_c increases. Hence, some additional PLP-SEC experiments were carried out under high-pressure conditions. As an example, MWDs obtained from PLP-induced polymerizations of BA at 80 °C, 2000 bar, an LPRR of 100 Hz and different initiator types and concentrations (indicated in the figure) are depicted in Figure 10-8. The relatively low temperature and high LPRR were chosen to suppress intermolecular transfer and β -scission reactions. All distributions show a pronounced high-molecular-weight peak or shoulder which is, however, not due to a real kinetic effect but caused by the exclusion limit of the SEC setup. The low molecular weight part of the MWD is broad and structureless as are the distributions from experiments at 1000 bar (not shown for purpose of thesis length). Consequently, the MWDs obtained from PLP at high pressure do not afford for reliable k_p^{eff} evaluation.

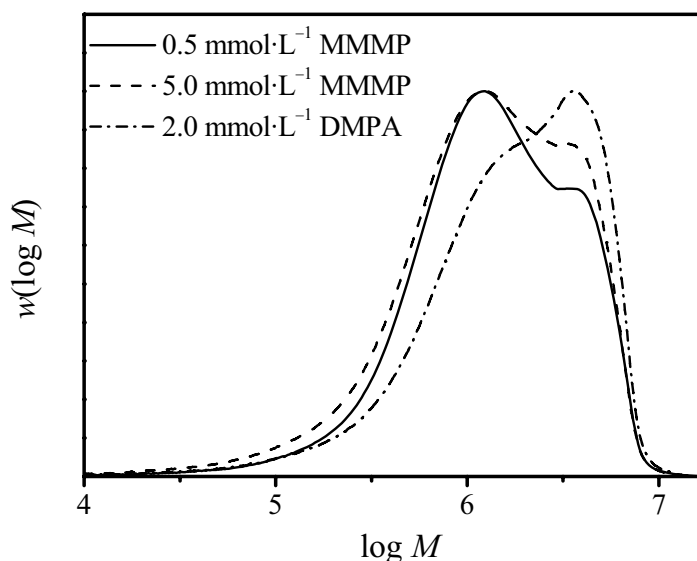


Figure 10-8: MWDs obtained from PLP-induced polymerization of BA in bulk at 80 °C, 2000 bar, a LPRR of 100 Hz, pulse numbers between 20 and 7 and different initiator types and concentrations as indicated in the figure.

The loss of chain-length control within the experiments at high temperature may be associated with SEC broadening, transfer-to-monomer reactions, and additional reaction pathways not being included in the kinetic scheme used for simulation. Such side reactions are self-initiation of the monomer, thermal or photochemical (by ambient light) decomposition of initiator, and β -cleavage of MCRs.

10.4 Impact of midchain radical formation on the kinetics of instationary polymerization

Instationary radical concentrations are created in SP-PLP-NIR and SP-PLP-ESR by applying short laser single pulses to the reaction solution. From those methods, $\langle k_t \rangle$ or even $k_t(i,i)$ values may be determined. However, significant difficulties are introduced when acrylate-type monomers are studied by single pulse techniques as will be shown below.

In SP-PLP, a laser pulse creates a high concentration of initiator-derived radicals which rapidly add to monomer and thereby form SPRs. Those secondary radicals may subsequently undergo backbiting eventually followed by re-initiation reactions establishing a certain MCR

fraction. The advantage of highly time resolved instationary methods is thus that the relaxation into the equilibrium ratio between SPR and MCR concentrations may be detected which should allow for estimating individual k_{bb} and k_p^t values. When radical concentrations are stationary, as e.g. during chemically induced polymerization after passing the initial transient period, x_{MCR} values are reached which can be expressed by Eq. (10-8). Plotting $(1-x_{MCR})/x_{MCR}$ vs. c_M yields only the lumped parameter k_p^t/k_{bb} as does the analysis of R_p measured at different c_M (see discussion to Table 10-1).

Integrated rate laws describing the change in SPR and MCR concentration after single pulse initiation may only be derived from a very simplified model for acrylate polymerization.^[281] The following restrictions have to be made: (i) chain-length dependencies of the kinetic coefficients are ignored, (ii) transfer-to-monomer and intermolecular transfer-to-polymer reactions are neglected, and (iii) k_t^{ss} , k_t^{st} and k_t^{tt} are chosen to be identical (denoted as k_t). The corresponding differential equations for the change in SPR and MCR concentration read:

$$\frac{dc_{SPR}}{dt} = v_i + k_p^t \cdot c_M \cdot c_{MCR} - 2 \cdot k_t \cdot (c_{SPR})^2 - k_t \cdot c_{SPR} \cdot c_{MCR} - k_{bb} \cdot c_{SPR} \quad (10-18)$$

$$\frac{dc_{MCR}}{dt} = k_{bb} \cdot c_{SPR} - k_t \cdot c_{SPR} \cdot c_{MCR} - 2 \cdot k_t \cdot (c_{MCR})^2 - k_p^t \cdot c_M \cdot c_{MCR} \quad (10-19)$$

The sum of the radical concentrations at time t after the initiating laser pulse is given by an expression being analogous to Eq. (3-6):

$$c_{SPR} + c_{MCR} = \frac{c_R^0}{1 + 2 \cdot k_t \cdot c_R^0 \cdot t} \quad (10-20)$$

According to Eqs. (10-18) to (10-20), integrated rate laws for the variation in SPR and MCR concentration after single pulse initiation can be derived as:^[281]

$$c_{SPR} = \frac{c_R^0}{(1 + 2 \cdot k_t \cdot c_R^0 \cdot t)} \cdot \frac{k_{bb}}{(k_{bb} + k_p^t \cdot c_M)} \cdot \left[\frac{k_p^t \cdot c_M}{k_{bb}} + \exp(-(k_{bb} + k_p^t \cdot c_M) \cdot t) \right] \quad (10-21)$$

$$c_{MCR} = \frac{c_R^0}{(1 + 2 \cdot k_t \cdot c_R^0 \cdot t)} \cdot \frac{k_{bb}}{(k_{bb} + k_p^t \cdot c_M)} \cdot [1 - \exp(-(k_{bb} + k_p^t \cdot c_M) \cdot t)] \quad (10-22)$$

Though expressions (10-21) and (10-22) are rather simple and may be used for non-linear curve fitting of experimental c_{SPR} and c_{MCR} traces, restriction (iii) is definitely not valid as will be shown in the following chapters and is already contained in Table 10-1.

A more reasonable simplification of the acrylate model would be to assume that termination takes place exclusively between secondary radicals. This restriction should not induce major errors unless x_{MCR} is high. However, the simple expression (10-20) cannot be easily used to account for selective SPR-SPR termination. Implementation of an effective termination rate coefficient $k_t^{\text{eff}} = k_t^{\text{ss}} \cdot (1 - x_{\text{MCR}})^2$ into Eq. (10-20) is not feasible as k_t^{eff} changes with time after the laser pulse as does x_{MCR} . Thus, integration over radical concentration and time of complicated differential rate laws is required which is not easily processed. Moreover, implementation of, at least, a composite power law model for $k_t(i,i)$ (see Chapter 3.4.2) is hence required to adequately describe the experimental SPR and MCR curves as $k_t(i,i)$ largely depends on chain length. Due to the enormous complexity of the system, kinetic parameters may only be extracted from SPR and MCR concentration traces by iterative parameter refinement of a comprehensive simulation model aimed at overlapping experimental and simulated data. This approach will be detailed in Chapter 12 on hand of SP-PLP-ESR traces recorded during polymerization of BA in toluene.

Conclusively, secondary and tertiary radical concentration versus time traces measured under single pulse conditions contain a wealth of kinetic information including k_{bb} and k_{p}^{t} values and may moreover provide access to individual $k_t(i,i)$ values, at least for SPR-SPR and SPR-MCR termination (MCR-MCR termination is negligible unless x_{MCR} is close to unity). This information, however, may not easily be extracted from the experimental data.

There are no previous SP-PLP-ESR investigations into the polymerization kinetics of acrylate-type monomers with the exception of a single MCR trace being depicted in the closing remarks section of the PhD thesis of Junkers.^[97] However, SP-PLP-NIR has been used for extensive studies into the homo- and copolymerization kinetics of AA^[270] and alkyl acrylates (see e.g. ref.^[16] and the citations therein) in bulk or solution. Within those studies, only an overall k_t value was determined without splitting into k_t^{ss} , k_t^{st} and k_t^{tt} . The k_t values were usually estimated as chain-length averaged quantities from the exponent k_t/k_p of Eq. (3-7) via implementing k_p from separate PLP-SEC experiments. However, those k_p values were exclusively determined at low temperatures and high LPRRs thus reflecting k_p^{s} and not k_p^{eff} . To account at least for the conversion induced decrease of k_p^{eff} , in recent studies the following relation for k_p was used:^[38,39,97,98,270]

$$k_p = k_p^s \cdot (1 - X)^{\omega-1} \quad (10-23)$$

where ω is the reaction order in monomer concentration determined from stationary polymerization methods. It has already pointed out by Junkers^[97] that an additional term should be included in Eq. (10-23) accounting for the differences between k_p^s and k_p^{eff} at low conversion. During polymerization of acrylate-type monomers, ω may exceed unity as is evident from the last factor on the right hand side of Eq. (10-12). However, the non-ideality of acrylate polymerization is not expressed in a mathematically correct way by a reaction order in c_M as Eq. (10-12) shows, i.e. ω is expected to change with c_M . Furthermore, the reaction order in c_M not only accounts for changes in k_p^{eff} but also in k_t^{eff} , as ω is a mathematical tool for linearizing R_p vs. c_M dependencies providing access to a constant $k_p^s \cdot (k_t^{\text{ss}})^{-0.5}$. Actually, treating SP-PLP-NIR data with k_p from Eq. (10-23) is not valid as ω was calculated for $k_p \cdot (k_t)^{-0.5}$ and not for $k_p \cdot (k_t)^{-1}$. Moreover, ω is determined from low conversion experiments. Hence, a conversion dependence of $k_p^s \cdot (k_t^{\text{ss}})^{-0.5}$ is not even directly accessible from R_p vs. X data determined via chemically induced polymerization, as a dependence of the individual k_t values on X induces changes in ω .

To summarize, implementing k_p^s into the primary experimental data from SP-PLP-NIR leads to k_t values with unclear physical meaning. Treating the data with k_p from Eq. (10-23) is preferable, as conversion induced changes in k_p^{eff} are at least to some extent considered. However, using ω for instationary experiments is not fully correct and the resulting k_t vs. X dependencies get distorted. Moreover, additional complications may arise from the finite time required for equilibration between the SPR and MCR species especially at low c_M where the re-initiation frequency is small as will be detailed below.

An extreme acceleration of k_t from SP-PLP-NIR toward lower monomer concentration was observed for AA polymerization in aqueous solution.^[270] The $\langle k_t \rangle$ values for 5 wt.% of AA in D₂O at 25 °C and 2000 bar are about $2 \cdot 10^9 \text{ L} \cdot \text{mol}^{-1} \cdot \text{s}^{-1}$ being higher than typical values for $k_t(1,1)$ of alkyl acrylates under ostensibly the same conditions.^[38,39] The AA k_t data were thus not considered reliable. PREDICI simulations of SP-PLP-NIR traces were carried out on the basis of the chemical reaction steps collated in Scheme 10-1 with the rate coefficients of Table 10-1. Chain-length dependent termination was not included to prevent superposition with the effects arising from MCR formation. Most simulations were carried out for 25 °C,

ambient pressure and different monomer concentrations to match the conditions where most of the AA k_t data was collected. A time interval of $0 \leq t \leq 0.1$ s being typical for SP-PLP-NIR experiments was chosen for the simulations.

Figure 10-9 depicts simulated SP-PLP-NIR traces for BA polymerization at various monomer concentrations (indicated in the figure). In case k_{bb} equals zero (full black line), the change in relative monomer concentration with time after single pulse initiation is independent of initial BA content. This is agreement with Eq. (3-7) which was derived based on ideal polymerization kinetics. According to this expression, the shape of the $c_M(t) / c_M(t = 0)$ traces only depends on k_t , k_p , and c_R^0 . The traces simulated for different monomer concentrations under consideration of MCR formation strongly deviate from each other from 0.01 s on. The monomer conversions reached after passing 0.1 s increase toward higher monomer concentration. This is easily understood based on the fact that chain growth primarily proceeds via propagation of SPRs and, according to Eq. (10-10), the SPR content increases toward higher MCR propagation frequency ($k_p^t \cdot c_M$) which is proportional to c_M . The differences in curvature become significant only after a certain MCR concentration has been formed by backbiting, i.e. after passing the first 0.01 s. It is, however, at first glance, puzzling that even higher final conversions (after e.g. 1 s; not shown in Figure 10-9) may be reached for simulations including intramolecular transfer as compared to estimates for $k_{bb} = 0$. It is thus worth to study the corresponding changes in SPR (upper figure) and MCR (lower figure) concentrations being depicted in Figure 10-10. The upper figure shows that for short times after the laser pulse the decrease in SPR concentration is more pronounced in case of MCR build up, as backbiting, in addition to termination, provides another source of SPR loss. At longer times, however, the curves may intersect with the simulation of the transfer-free system. The origin behind this observation is that the radical functionality is protected from fast bimolecular SPR-SPR termination when stored in MCR position. Those MCRs may subsequently provide a certain flux of SPRs formed by monomer addition. The final monomer-to-polymer conversions are thus governed by the complex counterplay between reduction of termination rate and deceleration of chain growth which are dependent on c_M , c_R^0 , k_p^s , k_p^t , k_{bb} , k_t^{ss} , k_t^{st} , and k_t^{tt} . In the hypothetical case, where k_t^{st} and k_t^{tt} are zero, k_{bb} is high, and $k_p^t \cdot c_M$ is low, enormous final monomer conversions, easily exceeding 10 %, may be induced by a single laser pulse due to the low but steady flux of SPRs. This is in strong analogy to simulations of RAFT polymerizations for SP conditions under consideration of slow fragmentation (see Chapter 3.5).^[97]

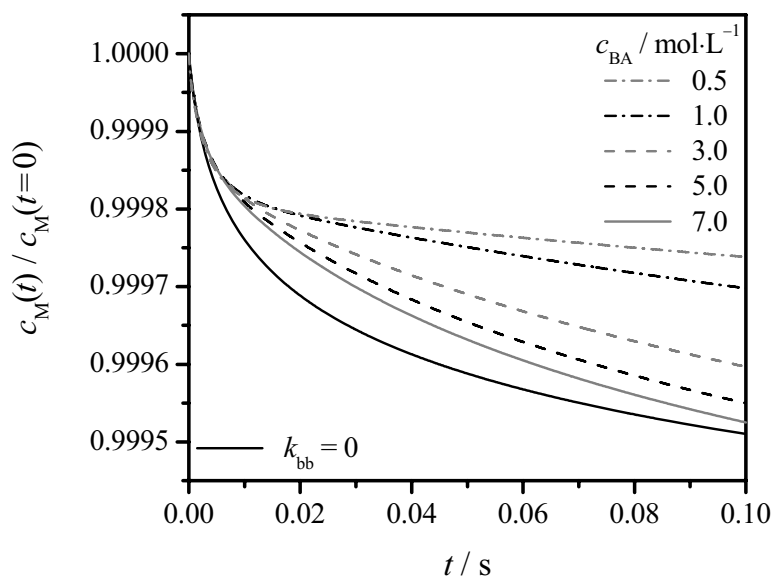


Figure 10-9: Simulated variation of relative monomer concentration after applying a single laser pulse, at $t = 0$, for different BA concentrations at 25 °C and ambient pressure with a primary radical concentration of $5 \cdot 10^{-6} \text{ mol}\cdot\text{L}^{-1}$. The rate coefficients are chosen according to Table 10-1. The shape of the traces simulated for $k_{\text{bb}} = 0$ is independent of BA concentration.

All MCR concentration curves simulated for different c_{M} (see lower part of Figure 10-10) increase with time at a similar slope which is governed by $c_{\text{SPR}} \cdot k_{\text{bb}}$. At longer times after the pulse they start to deviate from each other primarily due to the different re-initiation frequencies. The maximum in c_{MCR} is formed when the rate of MCR formation by backbiting equals the sum of the rates of MCR loss by termination and propagation to SPRs. The corresponding MCR fraction at the position of the maximum may be expressed by Eq. (10-8) as the restriction $dc_{\text{MCR}}/dt = 0$ fulfilled. At long times after the laser pulse, when c_{MCR} and c_{SPR} are low, the impact of termination on x_{MCR} can be neglected and the midchain radical fraction reaches the value predicted by Eq. (10-10). The differences in the slopes of the decrease in c_{MCR} are due to different amounts of SPR being formed by MCR propagation. Toward higher SPR concentrations, not only the rate of cross termination increases but also the rate of SPR-SPR termination. This causes an indirect loss of tertiary radical concentration as the MCR back-formation by intramolecular transfer is reduced.

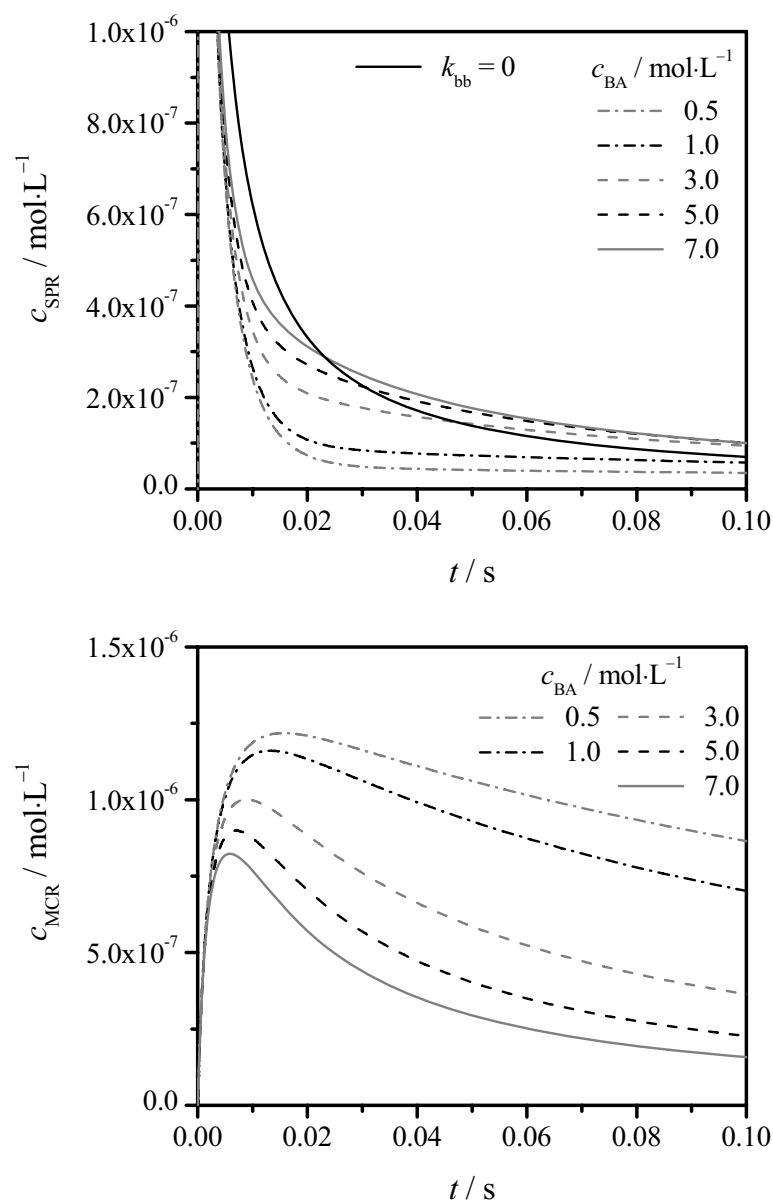


Figure 10-10: Simulated variation of SPR (upper figure) and MCR (lower figure) concentration after applying a single laser pulse, at $t = 0$, for different BA concentrations (indicated in the figures) at 25 °C and ambient pressure with a primary radical concentration of $5 \cdot 10^{-6} \text{ mol}\cdot\text{L}^{-1}$. The rate coefficients are chosen according to Table 10-1. The shape of the SPR traces simulated for $k_{\text{bb}} = 0$ is independent of BA concentration.

In the next step, the monomer concentration traces shown in Figure 10-9 were fitted to Eq. (3-7). The input value of k_{t}^{ss} was perfectly retrieved from the simulations for $k_{\text{bb}} = 0$ when k_{p}^{s} is used to decouple $k_{\text{t}}/k_{\text{p}}$. However, a strong increase of $k_{\text{t}}/k_{\text{p}}$ toward lower c_{M} is obtained from the simulations which include transfer. The resulting dependences of the apparent termination rate coefficient, $k_{\text{t}}^{\text{app}}$, on c_{M} are plotted in Figure 10-11 where the circles were

determined by decoupling via k_p^s and for the triangles k_p^{eff} was used. The full line is representing k_t^{eff} being estimated according to Eqs. (10-5) and (10-10). x_{MCR} at 7 mol·L⁻¹ of BA is about 60 % resulting in a k_t^{eff} value being close to k_t^{st} . Toward lower monomer concentration, k_t^{eff} decreases to k_t^{tt} as x_{MCR} grows to unity. It goes without saying that changing monomer concentration between 7 mol·L⁻¹ and zero reflects a bulk polymerization to complete conversion. The k_t^{app} values determined via k_p^s are close to k_t^{ss} at monomer concentrations of and above 3 mol·L⁻¹ whereas a pronounced increase of k_t^{app} is seen toward lower c_M . These k_t^{app} values for low c_M differ from k_t^{eff} by more than two orders of magnitude for BA concentrations below 1 mol·L⁻¹. The close agreement between k_t^{app} and k_t^{eff} at high c_M must be considered coincidental. In case k_t^{app} is evaluated using k_p^{eff} , the resulting k_t^{app} values are close to k_t^{eff} at high c_M and decrease toward lower monomer concentrations. At very low BA concentrations, however, still a discrepancy of almost one order of magnitude is seen between k_t^{app} and k_p^{eff} .

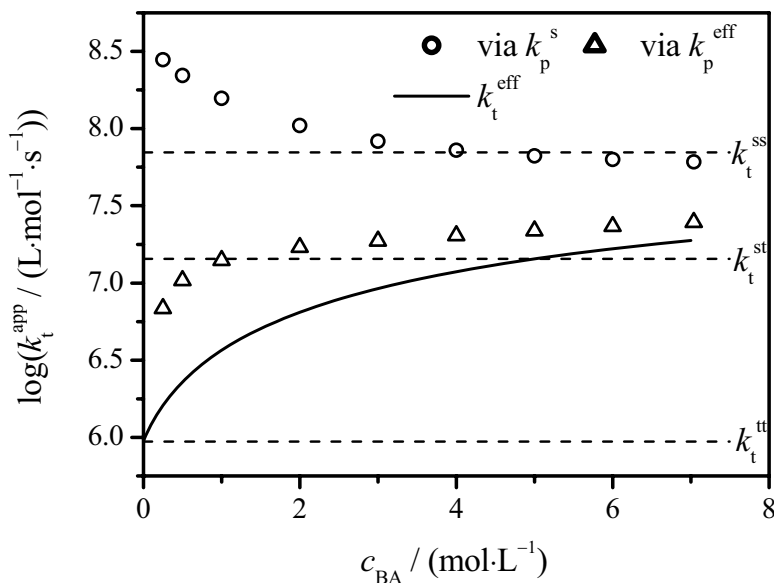


Figure 10-11: Variation of k_t^{app} with BA concentration obtained from fitting the monomer concentration traces shown in Figure 10-9 to Eq. (3-7). k_t^{app} was calculated from k_t/k_p by implementing k_p^s (squares) or k_p^{eff} (triangles) from Eqs. (10-6) and (10-10). The full line representing k_t^{eff} was estimated according to Eqs. (10-5) and (10-10). The dashed lines are indicating k_t^{ss} , k_t^{st} , and k_t^{tt} .

It was thoroughly discussed for pseudo-stationary polymerization that not only the ratio of k_{bb} to $k_p^t \cdot c_M$ (and thus x_{MCR}) may be of relevance, but also the equilibration velocity between SPR and MCR. As can be clearly seen, especially for the traces at low monomer concentration in

Figure 10-9, a slow backbiting rate induces a kink in the monomer concentration traces which separates the non-equilibrated regime at short times from the equilibrated range at longer times after the pulse. The influence of the non-equilibrated regime on the monomer concentration traces may, however, be reduced by significantly increasing k_{bb} and k_p^t . Figure 10-12 shows the simulated change in relative monomer concentration with time after single pulse initiation with both, k_{bb} and k_p^t , being increased by a factor of 100 but with ostensibly the same parameters as used for the traces in Figure 10-9. It is clearly seen that the $c_M(t) / c_M(t=0)$ curves deviate from each other from short times on as is to be expected for high equilibration velocities. Higher final conversions than for the $k_{bb} = 0$ case are reached for all initial BA concentrations. This is caused by a very efficient protection of radicals, by MCR formation, from fast SPR-SPR termination which is particularly pronounced at short time after the pulse due to its bimolecular nature (see upper part of Figure 10-10).

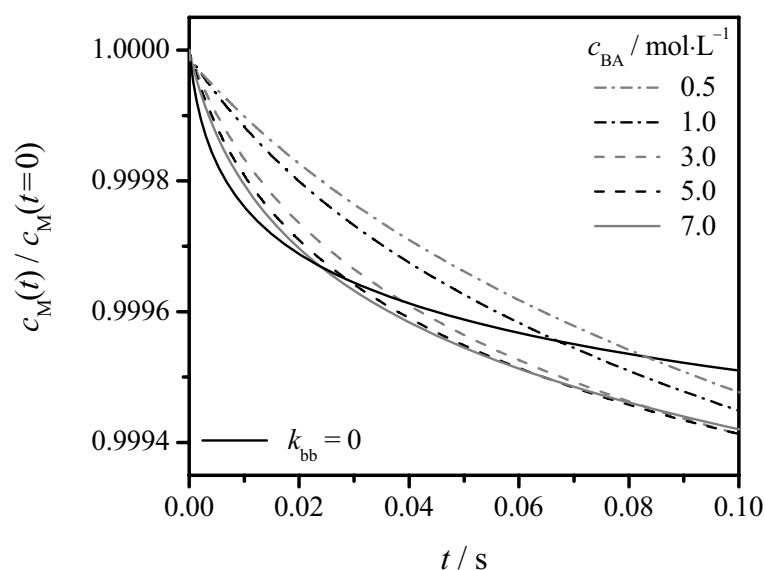


Figure 10-12: Simulated variation of relative monomer concentration after applying a single laser pulse, at $t = 0$, for different BA concentrations at 25 °C and ambient pressure with a primary radical concentration of $5 \cdot 10^{-6} \text{ mol} \cdot \text{L}^{-1}$. The rate coefficients are chosen according to Table 10-1 with exception that k_{bb} and k_p^t are increased by a factor of 100.

The traces depicted in Figure 10-12 were fitted to Eq. (3-7) for obtaining k_t/k_p as a function of monomer concentration. The agreement between the experimental curves and their representations by Eq. (3-7) is largely improved compared to the traces shown in Figure 10-9 as the influence of the non-equilibrated section is almost absent. The results for k_t^{app} evaluated by decoupling k_t/k_p with k_p^s (circles) and k_p^{eff} (triangles), respectively, are shown in

Figure 10-13 together with the predicted change of k_t^{eff} (black full line). The k_t^{app} values evaluated using k_p^{eff} perfectly match the k_t^{eff} curve at high c_M and only minor deviations are seen for low c_M . This observation also results from fast equilibration which allows for describing the curves with effective propagation and termination rate coefficients from times shortly after the initiating pulse on. Moreover, it is more likely for an MCR to propagate than to terminate due to the relatively high re-initiation frequency. Thus, x_{MCR} may be well expressed by Eq. (10-10) even at rather high radical concentrations (the long-chain hypothesis is fulfilled). Although the k_t^{app} values evaluated via k_p^s show only minor variations toward lower c_M , they cannot be attributed to an individual termination rate coefficient, such as e.g. k_t^{ss} .

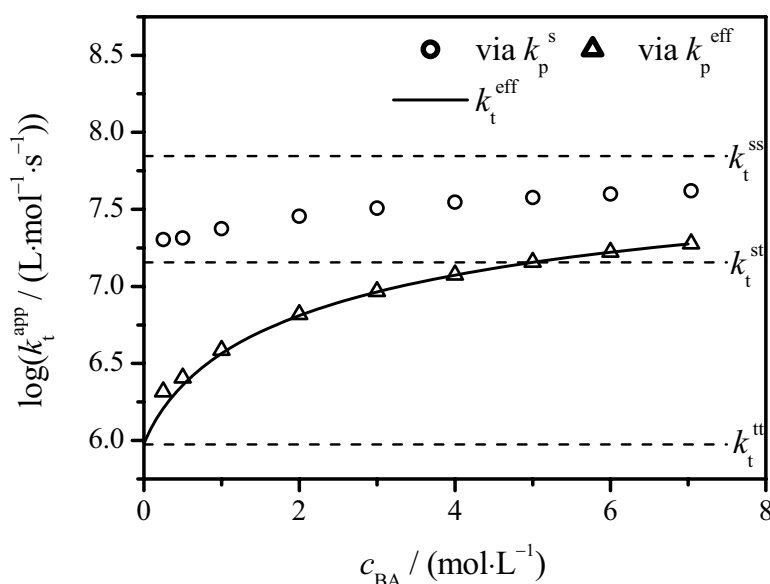


Figure 10-13: Variation of k_t^{app} with BA concentration obtained from fitting the monomer concentration traces shown in Figure 10-12 to Eq. (3-7). k_t^{app} was calculated from k_t/k_p by implementing k_p^s (squares) or k_p^{eff} (triangles) from Eqs. (10-6) and (10-10). The full line representing k_t^{eff} was estimated according to Eqs. (10-5) and (10-10). The dashed lines are indicating k_t^{ss} , k_t^{st} , and k_t^{tt} .

It was shown above that equilibration velocity between SPR and MCR species plays a crucial role for evaluating k_t^{eff} especially at low c_M and high conversions, respectively. It is thus recommendable to perform SP-PLP-NIR experiments under conditions where k_{bb} and $k_p^{\text{t}}\cdot c_M$ are high, i.e. at high temperatures and monomer concentrations. Moreover, k_p^{t} may be significantly increased by applying high pressure conditions whereas no strong influence of

pressure on the unimolecular backbiting step is expected. Fortunately, most SP-PLP-NIR experiments on alkyl acrylates were conducted as bulk polymerizations at temperatures between 40 and 60 °C and pressures of 1000 to 2000 bar. Nevertheless, a strong discrepancy between k_t^{eff} and k_t^{app} (evaluated using k_p^{eff}) may persist at low monomer concentrations in the system. This is illustrated in Figure 10-14 showing the variation of k_t^{app} with monomer concentration as being evaluated from $c_M(t) / c_M(t=0)$ curves which were simulated for 50 °C using the rate coefficients collated in Table 10-1. Though SPR-MCR equilibration should be faster as compared to the simulations for 25 °C, the disagreement between k_t^{app} evaluated via k_p^{eff} and the prediction for k_t^{eff} is even more pronounced at low monomer concentrations (compare to Figure 10-13). This illustrates the enormous kinetic complexity of the acrylate polymerization systems.

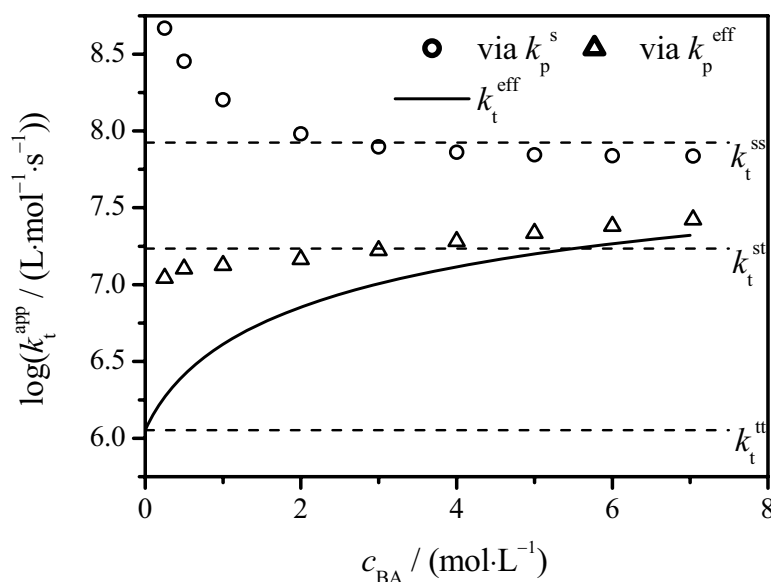


Figure 10-14: Variation of k_t^{app} with BA concentration obtained from fitting simulated monomer concentration vs. time traces for BA polymerization at 50 °C ($c_R^0 = 5 \cdot 10^{-6} \text{ mol}\cdot\text{L}^{-1}$, other coefficients chosen according to Table 10-1) to Eq. (3-7). k_t^{app} was calculated from k_t/k_p by implementing k_p^s (squares) or k_p^{eff} (triangles) from Eqs. (10-6) and (10-10). The full line representing k_t^{eff} was estimated according to Eqs. (10-5) and (10-10). The dashed lines are indicating k_t^{ss} , k_t^{st} , and k_t^{tt} .

Even in case precise $k_t^{\text{eff}}(X)$ values are determined from SP-PLP-NIR, it will be rather difficult to discriminate between effects which are due to conversion induced changes in the (diffusion controlled) individual k_t values (see Chapter 3.3.3) and changes in k_t^{eff} caused by a different weighting of k_t^{ss} , k_t^{st} and k_t^{tt} (see Eq. (10-5)). Nevertheless, inspection of

Figure 10-14 tells that k_t^{eff} changes by less than a factor of 3 between 0 and 70 % monomer-to-polymer conversion when starting under bulk conditions; a decrease easily being hidden below the orders of magnitude changes k_t which in may occur in the TD-controlled regime (compare to Figure 3-1). Moreover, the difference between k_t^{eff} and k_t^{app} (using k_p^{s}) determined in previous SP-PLP-NIR studies on bulk polymerizations of alkyl acrylates at low conversions is assumed to be about a factor of 3 or below.

Individual k_t values, at least k_t^{ss} and k_t^{st} , may be estimated from analysis of well resolved SP-PLP-NIR traces measured under slow equilibration conditions. However, such analysis requires knowledge of k_{bb} and k_p^{l} for reduction of fit parameters and may be further complicated by superposition of effects arising from backbiting and the chain-length dependence of each termination rate coefficient, respectively.

It was discussed that intramolecular transfer-to-polymer may strongly distort SP-PLP-NIR traces. However, in previous studies^[135,144] Eq. (3-45) was used to evaluate k_t^0 and α_1 from single $c_M(t) / c_M(t=0)$ curves (see Chapter 3.4.3). Junkers^[97] already pointed out that problems may arise when applying this procedure to acrylate-type monomers. Unexpected high values of α_1 in the range of 0.4 were experimentally found for DA polymerization already at low monomer- to-polymer conversions.^[135] The variation of α_1 and k_t^0 obtained from fitting the simulated SP-PLP-NIR traces depicted in Figure 10-9 to Eq. (3-45) is shown in Figure 10-15. The parameters were evaluated using k_p^{s} (A) or k_p^{eff} (B). In both cases, α_1 is about 0.3 at high c_M and slightly decreases toward lower monomer content. It is to be stressed that those α_1 values do not reflect an actual chain-length dependence of k_t as only chain-length independent k_t values were implemented in the model. In fact they are fully artificial results of MCR formation. Moreover, the slight decrease of α_1 toward lower monomer concentration does not indicate that the single pulse traces are more ideal but is associated with a strongly reduced quality of the fits under such conditions. Actually, for BA concentrations below $2 \text{ mol}\cdot\text{L}^{-1}$ the fitting procedure fails at all. Whereas α_1 is almost insensitive toward using k_p^{s} or k_p^{eff} , k_t^0 strongly depends on the choice of the propagation rate coefficient. The effect is similar as discussed for k_t^{app} on hand of Figure 10-11. However, the k_t^0 values are higher than the corresponding k_t^{app} data. This is caused by the applied back-extrapolation to $t = 0$, i.e. into the non-equilibrated range where k_t^{app} (via k_p^{s}) is even higher than k_t^{ss} due to mutual action of SPR-SPR termination and backbiting.

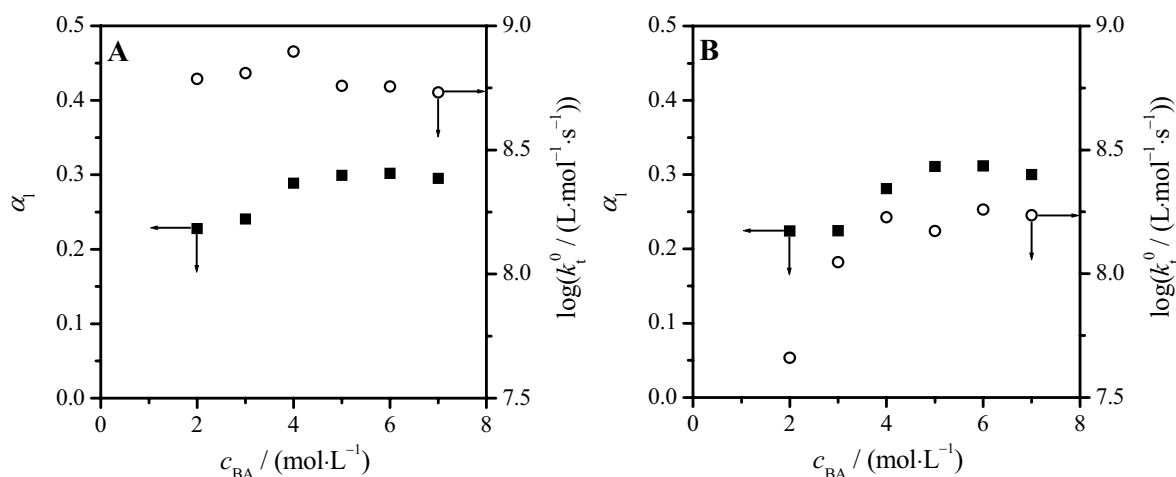


Figure 10-15: Dependence of apparent power-law parameters α_1 (squares) and k_t^0 (circles) on BA concentration obtained from fitting the monomer concentration traces shown in Figure 10-9 to Eq. (3-45) using k_p^s (A) or k_p^{eff} (B) from Eqs. (10-6) and (10-10).

As k_t may only change at short times after the pulse, where k_t^{eff} is not yet established, α_1 should be close to zero in case of fast equilibration. This result is indeed obtained when fitting the simulated traces shown in Figure 10-12 to Eq. (3-45). The corresponding monomer concentration dependences of α_1 and k_t^0 are shown in Figure 10-16. The power-law exponent α_1 is well below 0.1 for monomer concentrations higher than $2 \text{ mol}\cdot\text{L}^{-1}$ and very close to zero for bulk conditions. A pronounced acceleration of α_1 is only seen for very low c_M . Whereas α_1 is almost insensitive toward the choice of k_p^s (A) or k_p^{eff} (B), k_t^0 closely resembles the associated monomer concentration dependencies of k_t^{app} depicted in Figure 10-13.

As already mentioned above, particularly high α_1 values determined by analysis of SP-PLP-NIR traces were found for DA whereas the low conversion data of MA and BA closely resemble the theoretical expectations and results determined by other techniques.^[135] This implies that the DA data is strongly affected by the non-equilibrated range which may be due to its relatively low monomer concentration even in case of bulk polymerizations. Moreover, the pronounced acceleration of k_t provoked by dilution of DA with supercritical carbon dioxide^[16] may at least partially be caused by the influence of MCR build up. It is likely that a concentration range was reached in which k_t^{app} evaluated via k_p^s even increases toward lower c_M though the actual k_t^{eff} decreases (see circles in Figure 10-11 and Figure 10-14). A potential conversion dependence of the individual k_t values may also be masked by such effects.

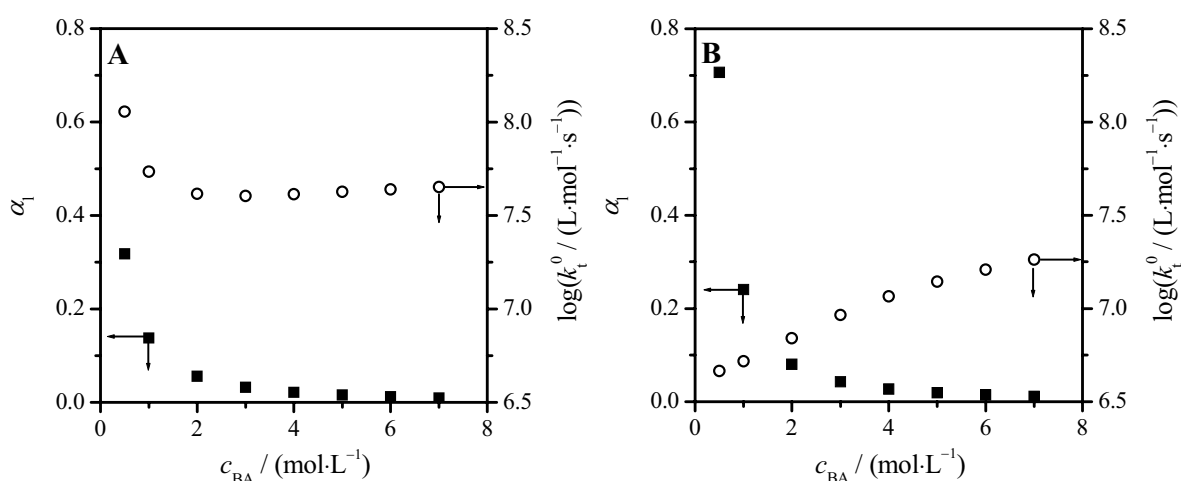


Figure 10-16: Dependence of apparent power-law parameters α_1 (squares) and k_t^0 (circles) on BA concentration obtained from fitting the monomer concentration traces shown in Figure 10-12 to Eq. (3-45) using k_p^s (A) or k_p^{eff} (B) from Eqs. (10-6) and (10-10).

The investigations detailed in this section illustrate that MCR formation strongly hampers the analysis of SP-PLP-NIR traces measured during polymerization of acrylate-type monomers. In particular a slow equilibration of SPRs and MCRs at short times after application of the laser pulse may result in a pronounced overestimation of k_t . It is thus recommended to select experimental conditions such that a constant x_{MCR} is rapidly established, i.e. conditions where both, k_{bb} and $k_p^{\text{t}}c_{\text{M}}$, are high. Consequently, SP-PLP-NIR experiments for acrylate-type monomers should be carried out at high temperatures, pressures and monomer concentrations. However, the last restriction is not only violated for polymerizations in dilute solution (see Chapter 13.2 and the discussion therein) but also for acrylic acid esters with long side chains (like DA) and for all acrylates at high monomer-to-polymer conversions. As illustrated in Figure 10-13, a good estimate for k_t^{eff} may be obtained from SP-PLP-NIR traces in case the SPR-MCR equilibration is fast and k_p^{eff} is known. Thus, literature data for k_t from SP-PLP-NIR experiments conducted under the above suggested reaction conditions can be easily re-evaluated by multiplication with k_p^{eff}/k_p^s .

Although a refined evaluation of the SP-PLP-NIR data is possible, even the so-obtained effective termination rate coefficients are highly system specific, as k_t^{eff} is governed by x_{MCR} (see Eq. (10-5)) which itself depends on radical concentration (see Eq. (10-8)). Thus, it is recommended to use the SP-PLP-ESR technique for studies into acrylate type monomers as with this experimental approach SPR and MCR concentration traces after single pulse

initiation become available providing access to chain-length-dependent individual termination rate coefficients as well as detailed insights into the transfer kinetics (see Chapter 12).

11 Determination of Rate Coefficients for Acrylate Systems by PLP-SEC

It was shown in the previous chapter that polymerization of acrylate-type monomers may be strongly affected by MCR formation. It was illustrated that not only the ratio of k_{bb} to $c_M \cdot k_p^t$ is of concern but also the magnitude of the individual rate coefficients. Some previous efforts have been made toward the evaluation of k_{bb} and k_p^t for BA. Firstly, a measure of quaternary carbons via ^{13}C -NMR has been used to determine k_{bb} applying the expression for branching level (BL):^[47]

$$BL = \frac{k_{bb}}{k_p^s \cdot c_M + k_{bb}} \quad (11-1)$$

The so-obtained Arrhenius parameters are: $E_a(k_{bb}) = 29.8 \text{ kJ}\cdot\text{mol}^{-1}$ and $A(k_{bb}) = 4.31 \cdot 10^7 \text{ s}^{-1}$ (The values reported here are recalculated from the BL data in ref.^[47] using the IUPAC values^[13] for k_p^s in Eq. (11-1)). x_{MCR} in the BA system has been measured by ESR under PLP conditions by Willemse et al.,^[49] with the difference in activation energies between backbiting and monomer addition to the MCR estimated as $\Delta E_a = E_a(k_{bb}) - E_a(k_p^t) = 18.8 \text{ kJ}\cdot\text{mol}^{-1}$. This value is surprising, as it suggests, in conjunction with the above-mentioned value of $E_a(k_{bb}) = 29.8 \text{ kJ}\cdot\text{mol}^{-1}$, that the activation energy for monomer addition to MCRs, $E_a(k_p^t)$, is only $11 \text{ kJ}\cdot\text{mol}^{-1}$, a value much lower than the $34 \text{ kJ}\cdot\text{mol}^{-1}$ measured for polymerization of the butyl acrylate dimer (BAD).^[282] The origin behind these contradictory observations will be detailed in Chapter 12.3. Ref.^[49] provides an upper bound estimate of $68 \text{ L}\cdot\text{mol}^{-1}\cdot\text{s}^{-1}$ for k_p^t at $50 \text{ }^\circ\text{C}$, about 400 times lower than the value of k_p^s .^[51]

The simulations detailed in Chapter 10.3 as well as the work of Nikitin et al.^[55,57] show that the MWDs from PLP may yield valuable information, even if the growing radicals are subjected to backbiting events during the dark-time period. The apparent propagation rate coefficient, k_p^{app} , varies with LPRR between two limiting values. At high repetition rate, k_p^{app} provides a measure for k_p^s , as the chains associated with the inflection point do not undergo any backbiting events between pulses.^[13] As LPRR is decreased, a greater fraction of chains undergo backbiting in the time between pulses; the slow re-initiation of these MCRs back to SPRs by monomer addition shifts the inflection point to a lower value ($k_p^{\text{app}} < k_p^s$). As LPRR

is decreased even further, a chain has the opportunity to undergo several backbiting and re-initiation cycles in the dark time, such that k_p^{app} provides a measure of k_p^{eff} , defined by Eq. (10-6) in combination with Eq. (10-10).

In this chapter, a novel experimental technique for determination of k_{bb} and k_p^{t} will be introduced and applied to BA polymerization. This method is based on PLP-SEC experiments conducted under wide variation of LPRR. The work presented in this chapter was carried out in cooperation with Dr. Anatoly N. Nikitin and Prof. Robin A. Hutchinson. Part of these investigations have already been published in ref.^[53]

11.1 Experimental and simulated MWDs for PLP of BA

Though the simulations indicate the above described variation of k_p^{app} with LPRR, it is not trivial to reproduce this experimentally.^[279] With the exception of the BA data shown below, such sigmoidal decrease in k_p^{app} toward lower LPRR was only reported for polymerization of 9.6 wt.% of non-ionized AA in water at 6 °C (see ref.^[52] and Chapter 13). The kinetics of AA polymerization in the aqueous solution is complicated by the variation of rate coefficients with AA concentration^[67–69,270] and the non-availability of estimates on individual k_t values. Therefore, the BA system was chosen for investigating the feasibility of determining kinetic coefficients from the variation in k_p^{app} with LPRR.

Experimental conditions had to be carefully selected for obtaining successful PLP-SEC experiments:

- a low number of pulses was used to reduce broadening of the MWD due to initiator consumption (changes in initial radical concentration) and monomer conversion (changes in monomer concentration)
- a large sample volume was chosen to produce an amount of polymer being sufficient for SEC analysis even at rather low monomer-to-polymer conversions
- the reaction mixture was protected from ambient light to minimize formation of background polymer not produced by PLP
- the optical setup was carefully aligned to minimize non-uniform irradiation of the sample cell

- high initiator concentrations and laser energies were used, to approach the high termination rate conditions^[280] and to ensure chain-length control by laser pulsing

The MWDs obtained from PLP-SEC experiments of BA in bulk at 20 °C and various LPRRs are shown in Figure 11-1A together with the associated first-derivative curves (Figure 11-1B).

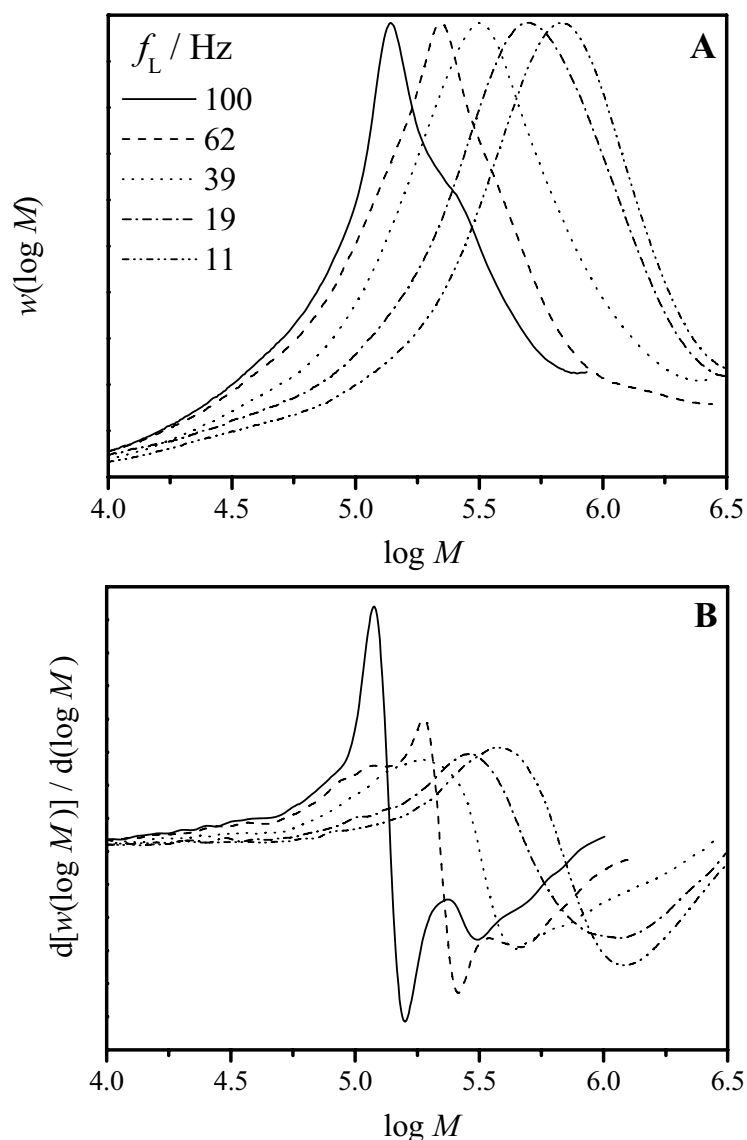


Figure 11-1: Experimental MWDs (A) and associated first-derivative curves (B) produced by PLP of BA at 20 °C and different LPRRs, f_L (as indicated in the figure).

The features of the distributions and their derivative curves are in accord with earlier experimental observations.^[186,188] For the higher LPRRs ($f_L = 100$ and 62 Hz), the MWDs satisfy the main criterion of the PLP-SEC method for determining k_p^s : second inflection points

are clearly observed in the first-derivative plots.^[8] Further lowering of LPRR results in MWDs without clear PLP structure. The experimental MWDs perfectly reflect the effects discussed by means of Figure 10-1. The sharp peak observed in the MWDs generated at LPRRs of 100 and 62 Hz is the result of termination of secondary radicals that have survived t_0 (0.01 or 0.016 s). A fraction of the radicals undergoes intramolecular transfer-to-polymer during this time interval. However, a sufficient fraction of radicals grow exclusively by chain-end propagation without undergoing backbiting during t_0 , thus producing a characteristic PLP structure. Lowering LPRR to 39 Hz and below results in a greater fraction of radicals which undergo backbiting prior to the arrival of the subsequent laser pulse. As monomer addition to these MCRs is slow, the linear relationship between chain length and pulse separation time (see Eq. (5-1)) is lost. The MWDs are broadened and contain no PLP structure. Thus, the IUPAC consistency criteria for determination of k_p by PLP-SEC is not met. Nevertheless, these MWDs should not be considered meaningless, as has been shown in Chapter 10.3.

Figure 11-2 presents the MWDs simulated for bulk BA polymerizations at 20 °C, with LPRRs chosen to be identical to the ones of the experiments given in Figure 11-1 and the rate coefficients being the ones specified in Table 10-1. The additional parameters required for simulation are the concentration of radicals produced per laser pulse, $c_R^0 = 6.5 \cdot 10^{-6} \text{ mol} \cdot \text{L}^{-1}$, and the dispersion parameter used to represent SEC broadening of the MWD, $b\sigma = 0.04$. The evaluation of these parameters is described below. The calculated distributions in Figure 11-2 capture the features of the experimental distributions and their first-derivative curves very well. As observed experimentally, the simulated distributions exhibit no PLP structure at repetition rates of 39 Hz and below. At the same time, these distributions still shift to higher MWs with the increase of pulse separation time. The peak provides a measure of k_p^{app} evaluated by applying the standard PLP-SEC methodology, i.e. by using the inflection point on the low-molecular weight side of the peak.

Close examination of Figure 11-1 and Figure 11-2 reveals that the first-derivative curve obtained at 62 Hz contains a broader maximum followed by a sharper peak. Another experimental example is shown in Figure 11-3, where both experimental (full line) and simulated (dashed line) MWDs (A) of BA polymerization at 20 °C with a LPRR of 49 Hz show two peaks in the first-derivative curves (B). The origin of this observation has already been discussed by means of Figure 10-1. The broad maximum arises from the termination of radicals that have undergone backbiting and the narrow one results from termination of SPRs that have escaped backbiting. The POI at higher molecular weight provides access to k_p^s

whereas the k_p^{app} value calculated from the broad POI accounts for the slowing down of chain growth by MCR formation. Thus, even such subtle effects which are hardly detectable in the simulated distribution can be reproduced experimentally. However, the situation of simultaneous occurrence of a broad and a narrow maximum is only seen at intermediate LPRRs; higher LPRRs give distributions that have a sharper primary inflection point (and sometimes also a secondary inflection point), and lower LPRRs give distributions with broader first-derivative curves having a single inflection point.

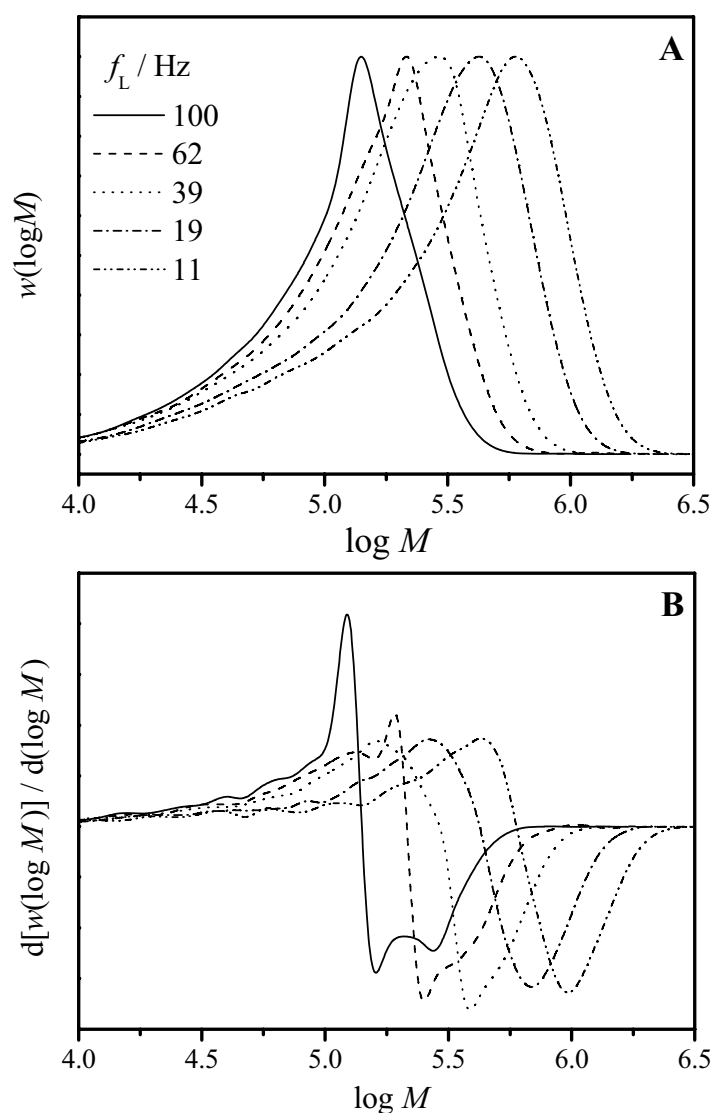


Figure 11-2: Simulated MWDs (A) and associated first-derivative curves (B) produced by PLP of BA at 20 °C and different LPRRs, f_L . The MWDs are calculated for $c_M = 7.02 \text{ mol}\cdot\text{L}^{-1}$, $c_R^0 = 6.5\cdot 10^{-6} \text{ mol}\cdot\text{L}^{-1}$ and $b\sigma = 0.04$. Other rate coefficients are chosen according to Table 10-1.

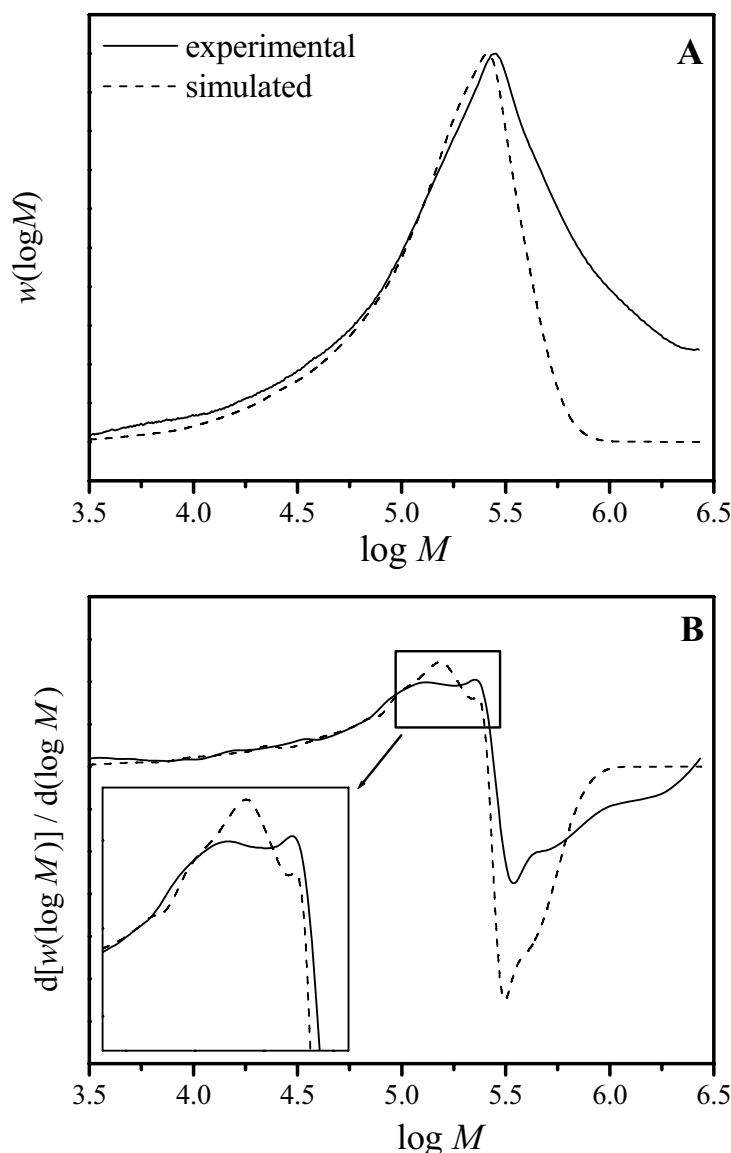


Figure 11-3: Experimental (full line) and simulated (dashed line) MWDs (A) and associated first-derivative curves (B) produced by PLP of BA at 20 °C at a LPRR of 49 Hz. The simulated MWD has been calculated for $c_M = 7.02 \text{ mol}\cdot\text{L}^{-1}$, $c_R^0 = 6.5 \cdot 10^{-6} \text{ mol}\cdot\text{L}^{-1}$ and $b\sigma = 0.04$. The other rate coefficients are chosen according to Table 10-1.

The variation of k_p^{app} with LPRR for BA polymerization at 20 °C has been evaluated from simulated MWDs. As long as it is detectable, the narrow peak in the first-derivative curve, which is associated with SPRs that escaped backbiting, was used to calculate k_p^{app} . The results presented in Figure 11-4 are calculated for primary radical concentrations of $c_R^0 = 1.0 \cdot 10^{-6}$ (squares) and $1.0 \cdot 10^{-5} \text{ mol}\cdot\text{L}^{-1}$ (circles), with the other rate coefficients as given in Table 10-1. The values of k_p^{app} vary between two limiting values that are relatively insensitive

to the input value of c_R^0 . At high repetition rates, k_p^{app} is close to the k_p^s value used within the model. This result is expected, as the peak is formed by the termination of SPRs that have not been subjected to backbiting. The slight offset between k_p^{app} and the input value of k_p^s for $c_R^0 = 1.0 \cdot 10^{-5} \text{ mol} \cdot \text{L}^{-1}$ is because the system is approaching the high termination limit, where the maximum of the MWD peak is a better measure of i_0 than the POI, as discussed elsewhere.^[280] At low LPRRs, k_p^{app} approaches a constant value which is close to k_p^{eff} , as calculated by Eq. (10-6) in combination with Eq. (10-10). Between these two plateau values, k_p^{app} decreases toward lower LPRR with a sigmoidal shape. The steepness of the decline is, however, affected by the concentration of radicals generated per pulse. The LPRR at which a sharp decrease in k_p^{app} is observed is denoted by f_0 . This repetition rate is also the lowest LPRR at which the sharp peak in the first-derivative curve associated with k_p^s is seen. The features of the curve in Figure 11-4 provide the basis for the procedures for evaluating individual rate coefficients.

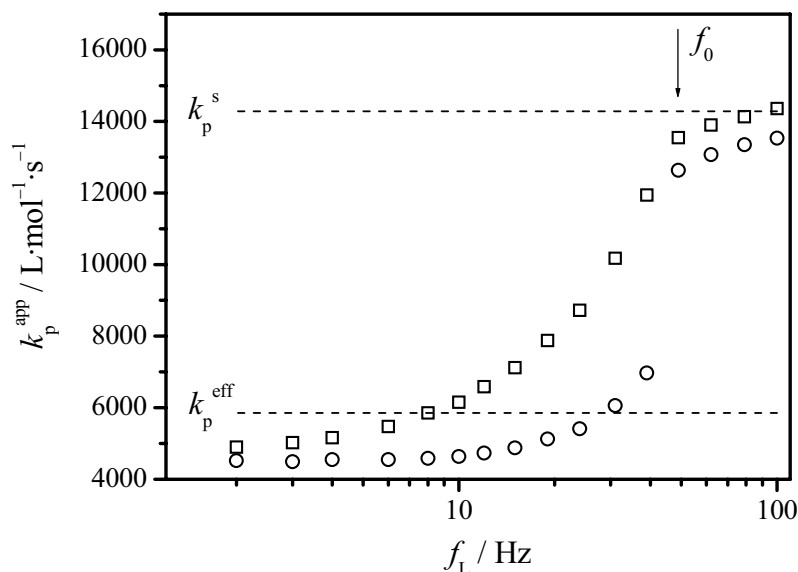


Figure 11-4: Variation of k_p^{app} with LPRR as obtained from simulated MWDs for PLP of BA at 20 °C. The modeling has been calculated for $c_M = 7.02 \text{ mol} \cdot \text{L}^{-1}$, $b\sigma = 0.04$, $c_R^0 = 1.0 \cdot 10^{-6}$ (□) and $1.0 \cdot 10^{-5}$ (○) $\text{mol} \cdot \text{L}^{-1}$, respectively. The other rate coefficients are chosen according to Table 10-1. Horizontal dashed lines indicate the input values of k_p^s (upper) and k_p^{eff} (lower) calculated by Eq. (10-6) in combination with Eq. (10-10).

11.2 Evaluation of k_{bb} , k_p^{eff} and k_p^t

The decrease of LPRR results in a broadening of the PLP-generated MWD as the fraction of chains that undergo intramolecular chain transfer increases, and a sharp decrease in k_p^{app} occurs at f_0 . The fraction of SPRs that survived one pulse separation time without undergoing backbiting to overall radical concentration at t_0 is given by Eq. (10-17). If this fraction is too low (LPRR less than f_0), an insufficient population of polymer molecules are formed to produce a sharp peak in MWD (and in the first-derivative plot). The lowest SPR fraction, x_{min} , that still allows for the observation of the sharp peak in the first-derivative curve associated with k_p^s can be assumed to be independent of the particular polymerization conditions:

$$x_{\text{min}} = \frac{c_{\text{SPR}}'(t = t_0)}{c_{\text{R}}^{\text{ov}}(t = t_0)} = \exp\left(-\frac{k_{bb}}{f_0}\right) = \text{const.} \quad (11-2)$$

The simulation results shown in Figure 11-4 indicate that f_0 is indeed not sensitive to c_{R}^0 , such that it is possible to conclude that k_{bb} is directly proportional to f_0 :

$$k_{bb} = a_p \cdot f_0 \quad (11-3)$$

This expression can be used to determine the absolute value of k_{bb} from the dependency of k_p^{app} on repetition rate, provided that the value of the proportionality constant a_p that relates k_{bb} to f_0 may be determined. In Figure 11-4, for example, the input value for k_{bb} is 109 s^{-1} and the critical repetition rate is 49 Hz; thus the value of a_p is evaluated to be 2.22.

To further confirm the validity of Eq. (11-3), values of f_0 have been evaluated by simulation of distributions calculated for different temperatures. The corresponding values of a_p determined according to Eq. (11-3) are shown in Figure 11-5, with the values of k_{bb} being calculated from the Arrhenius dependence in Table 10-1. The value of a_p is indeed seen to be constant, with a value of 2.16 ± 0.03 . Further simulations indicate that the value is dependent on the amount of SEC broadening that occurs. For the same input value of k_{bb} , f_0 shifts to a lower value as the broadening parameter $b\sigma$ is decreased (and the MWDs become sharper), such that the value of the proportionality constant a_p increases. Therefore the value of $b\sigma$ must be determined experimentally in order to relate f_0 to k_{bb} . Finally it is to be stressed that a_p may to some extent also depend on the rate coefficients used for modeling. For very

particular parameter combinations the outlined procedure for k_{bb} determination may even fail at all. However, this is only the case when rather unrealistic rate coefficients are chosen for modeling.^[281] Thus, the presented approach for measuring k_{bb} does not require knowledge of any other rate coefficient as long as the parameters for simulation are in reasonable ranges.

It is seen in Figure 11-4 that, although the values of k_p^{app} at low LPRRs approach a constant value close to the simulation input value for k_p^{eff} , there is an offset by as much as 30 %. At these low LPRRs, a larger fraction of the radicals terminate before the next pulse arrives, compared to a system at high LPRR. This increases the relative offset between k_p^{app} and k_p^{eff} compared to that between k_p^{app} and k_p^s . In addition, the peak formed from termination of radicals that are subjected to backbiting is broader compared to the peak formed as a result of termination of SPRs that have escaped intramolecular transfer-to-polymer. Thus, the associated POI in the MWD systematically underpredicts k_p^{eff} . The magnitude of the offset depends on c_R^0 and on the extent of broadening. An iterative approach has been developed to estimate k_p^{eff} (and thus k_p^t), as will be detailed with the experimental results in Chapter 11.4.

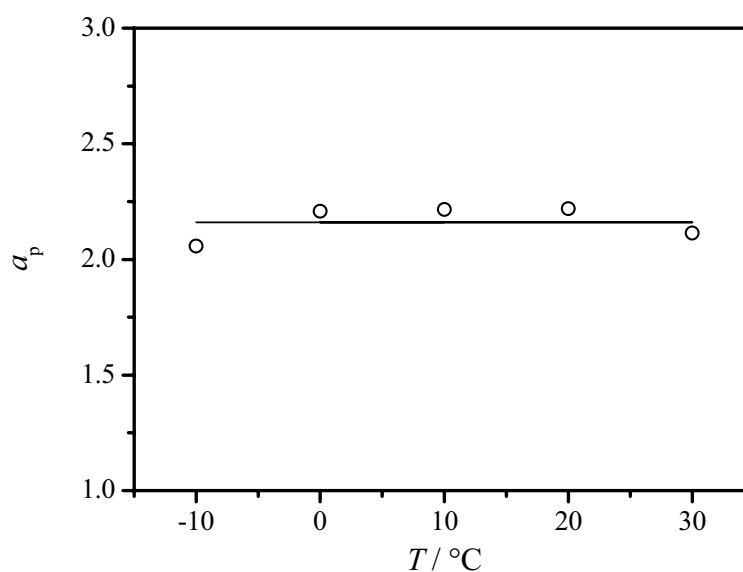


Figure 11-5: The proportionality constant a_p determined for different temperatures according to Eq. (11-3), with values of f_0 determined from simulated MWDs for BA polymerization at different LPRRs using the rate coefficients in Table 10-1, with $c_R^0 = 1.0 \cdot 10^{-5} \text{ mol} \cdot \text{L}^{-1}$ and $b\sigma = 0.04$.

11.3 Evaluation of c_R^0 and $b\sigma$

MWDs generated by PLP can exhibit broadening for numerous reasons. Many of them are related to experimental conditions during pulsing: radical concentrations may vary spatially or with the number of pulses because of initiator consumption, laser attenuation, non-uniform irradiation, and/or inhibition.^[283] As mentioned previously, every attempt was made to minimize these experimental broadening effects. In addition, natural broadening occurs due to the stochastic nature of FRP, and also results from dispersion effects during molecular weight separation in the SEC columns. As can be seen from experiments (Figure 11-1) and via simulation (Figure 11-2), the narrowest MWD peaks are obtained at higher LPRRs. Thus, it is these distributions that are selected for estimating the value of $b\sigma$. The width $\Delta_{\log M, h}$ of the peak at some height $h < h_{\max}$, where h_{\max} is the maximum height of the peak, is considered. This value of h should be selected large enough such that $\Delta_{\log M, h}$ is measured for the narrow peak associated with the termination of chain-end radicals controlled by the laser pulsing, as this width is mainly dependent on Poisson broadening, kinetic broadening (due to termination not occurring instantaneously at t_0), and instrumental broadening. The value of $b\sigma$ is then estimated by obtaining the best match between the experimental and simulated widths $\Delta_{\log M, h}$, as illustrated in Figure 11-6 for BA pulsed at 49 Hz and -10°C . The measured and simulated (with dispersion parameter $b\sigma = 0.049$) MWDs are normalized such that the ordinates of the peak maxima for both distributions are equal to unity. Within one series of experiments carried out at the same initiator concentration and pulse energy, the values of $b\sigma$ estimated for different distributions are close to each other. In addition, the value is not particularly sensitive to the choice of h ; the value of $b\sigma$ changes only from 0.048 to 0.050 as h is decreased from 0.95 to 0.55.

The sharp MWD peak results from termination of SPRs and thus is also influenced by the rate of termination, in particular by short-long termination. The termination rate coefficients k_t^{ss} , k_t^{st} and k_t^{tt} values are assumed to be known (see Table 10-1); only the value for c_R^0 must be estimated in order to characterize the termination event fully. In addition, the determination of c_R^0 is important for the procedure used to evaluate k_p^{eff} and k_p^t values. The fitting of experimental MWDs to estimate rate coefficients is well established. Moad et al.^[284] were the first to use the MWDs produced by PLP to estimate k_t with known values of c_R^0 . Here the opposite is done, the experimental MWDs are used to estimate c_R^0 assuming that the values of

k_t^{ss} , k_t^{st} and k_t^{tt} are known. The mode of termination is chosen to be predominantly by combination being in accordance with the recent observation that the distribution immediately before and after the termination-controlled peak have similar heights for PLP-generated MWDs obtained at conditions close to the high-termination-rate limit when termination occurs predominantly by combination.^[285] Figure 11-6 presents the result of fitting the measured MWD.

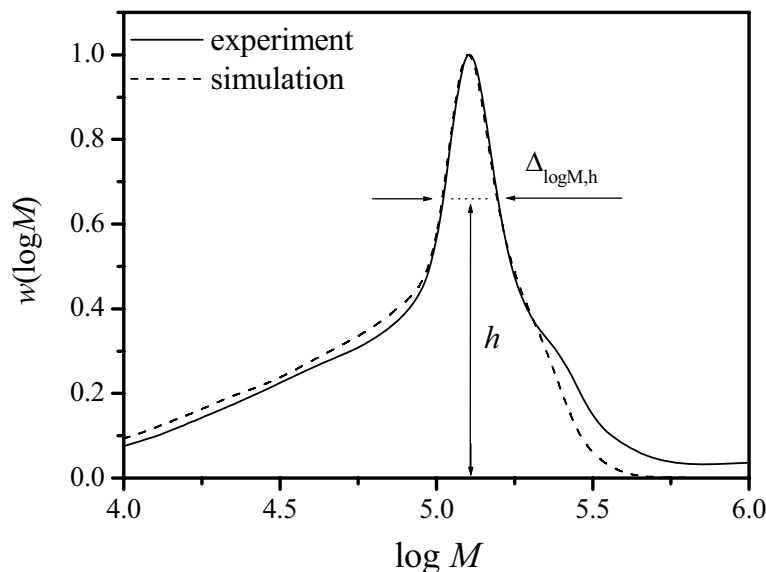


Figure 11-6: Experimental (solid line) and simulated (dashed line) MWDs for PLP of BA at $-10\text{ }^\circ\text{C}$ and an LPRR of 49 Hz. The simulated MWD has been calculated for $c_M = 7.26\text{ mol}\cdot\text{L}^{-1}$, $c_R^0 = 1.0\cdot 10^{-5}\text{ mol}\cdot\text{L}^{-1}$ and $b\sigma = 0.049$. Other rate coefficients are chosen according to Table 10-1.

According to this simulation, the best value of c_R^0 is found to be $1.0\cdot 10^{-5}\text{ mol}\cdot\text{L}^{-1}$. MWDs calculated for $c_R^0 = 8.0\cdot 10^{-6}$ and $1.25\cdot 10^{-5}\text{ mol}\cdot\text{L}^{-1}$ are compared to the same experimental MWD in Figure 11-7. Though the distribution of macromolecules before the peak is well fitted for the MWD calculated using $c_R^0 = 8.0\cdot 10^{-6}\text{ mol}\cdot\text{L}^{-1}$, the shoulder after the peak deviates clearly from the one in the experimental MWD. The distribution before the peak for MWD calculated with $c_R^0 = 1.25\cdot 10^{-5}\text{ mol}\cdot\text{L}^{-1}$ deviates considerably from the one in the experiment. Therefore the intermediate value $c_R^0 = 1.0\cdot 10^{-5}\text{ mol}\cdot\text{L}^{-1}$ (Figure 11-6) is chosen as the best value to reproduce the experimental MWD. Note that the estimate of the peak width ($\Delta_{\log M,h}$) and thus $b\sigma$ are relatively insensitive to c_R^0 , such that both parameters can be determined simultaneously from fitting.

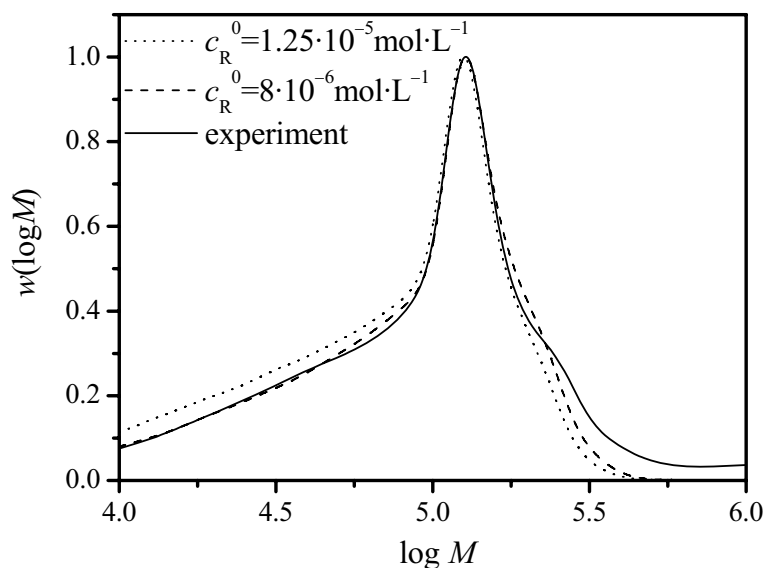


Figure 11-7: Experimental (solid line) and simulated (dashed and dotted lines) MWDs for PLP of BA at $-10\text{ }^{\circ}\text{C}$ and an LPRR of 49 Hz. The simulated MWD has been calculated for $c_M = 7.26\text{ mol}\cdot\text{L}^{-1}$, $b\sigma = 0.049$ and c_R^0 as indicated. The other rate coefficients are chosen according to Table 10-1.

11.4 Analysis of experimental MWDs

The measured dependencies of k_p^{app} on LPRR for BA at temperatures of -10 , 0 , 10 , 20 and $30\text{ }^{\circ}\text{C}$ are presented in Figure 11-8. The results of two series of PLP experiments are shown at temperatures of 10 and $30\text{ }^{\circ}\text{C}$. The horizontal dashed lines in each plot indicate the input values of k_p^s and k_p^{eff} , respectively. The k_p^{eff} value was calculated using Eqs. (10-6) and (10-10) with the Arrhenius parameters for k_{bb} and k_p^t estimated within this PLP-SEC study.

The k_p^{app} values obtained at high LPRRs are slightly lower than the IUPAC k_p^s values but in all cases within 20%. This difference is also seen in the simulation results shown as Figure 11-4 for $c_R^0 = 1.0\cdot 10^{-5}\text{ mol}\cdot\text{L}^{-1}$. Under these high termination rate limit conditions, it has been shown that the inflection point can underestimate the true experimental value.^[280] At $0\text{ }^{\circ}\text{C}$, a lower value of c_R^0 , $3.0\cdot 10^{-6}\text{ mol}\cdot\text{L}^{-1}$, is estimated, and the measured k_p^{app} value is in excellent agreement with the IUPAC k_p^s value.

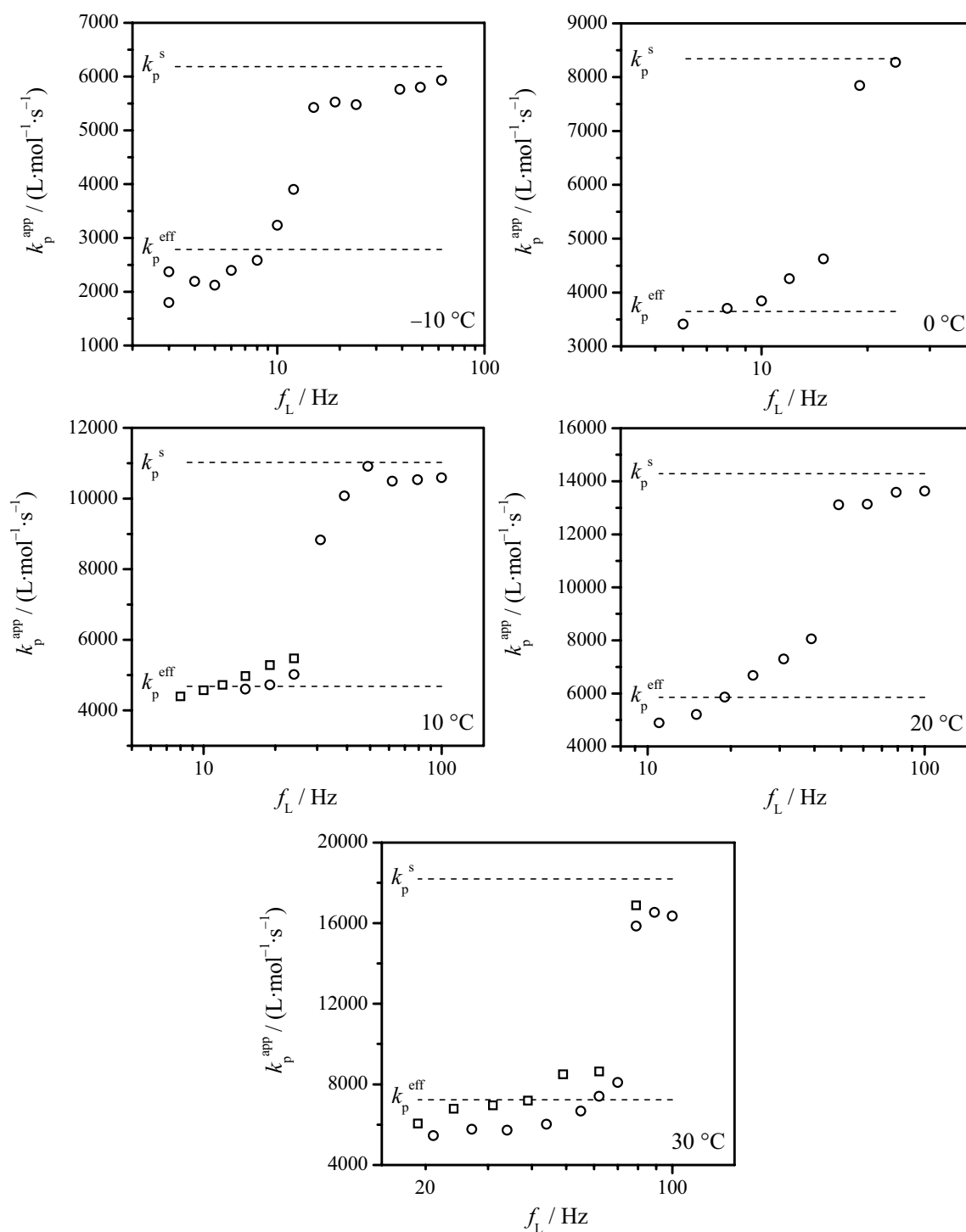


Figure 11-8: The dependency of k_p^{app} on LPRR obtained by PLP-SEC experiments for BA at -10 , 0 , 10 , 20 and 30 °C as indicated in the figure. At temperatures of 10 and 30 °C, the results of two series of experiments are shown (by circles and squares). The horizontal dashed lines indicate the IUPAC value of k_p^s and the estimated value of k_p^{eff} , respectively. k_p^{eff} was determined on basis of the Arrhenius parameters for k_{bb} and k_p^{t} which were finally obtained within this chapter (see Table 10-1).

The remaining task is to estimate k_{bb} and k_p^{eff} (and thus k_p^t) from the experimental MWDs and k_p^{app} values. This has been accomplished as follows:

- (i) MWDs for different LPRRs are calculated based on an initial guess of the rate coefficients as well as of c_R^0 and $b\sigma$ (assuming $b\sigma = 0.04$). a_p is determined via Eq. (11-3) by means of the f_0 values from the simulated distributions and the input value of k_{bb} , respectively.
- (ii) Using this preliminary a_p in combination with the experimental f_0 value, a first estimate for k_{bb} is obtained from Eq. (11-3).
- (iii) According to the simulation results of Figure 11-4, the values for k_p^{eff} are expected to be higher than k_p^{app} at low repetition rates. An initial guess for k_p^{eff} is made based upon the experimental results in Figure 11-8. The values 2600, 3700, 4700, 5600, 6850 $\text{L}\cdot\text{mol}^{-1}\cdot\text{s}^{-1}$ have been chosen at temperatures -10 , 0 , 10 , 20 and 30 $^{\circ}\text{C}$, respectively.
- (iv) Eq. (3-17) is then used to evaluate k_p^t values.
- (v) These first estimates for k_{bb} and k_p^t are applied to update the individual termination rate coefficients from ref.^[51] (see discussion to Table 10-1) and to simulate MWDs. Values of $b\sigma$ and c_R^0 are estimated for each series of experiments by fitting simulated distributions to the MWDs measured at high repetition rates, as described in Chapter 11.3.
- (vi) These values for $b\sigma$ and c_R^0 are used to update the k_{bb} estimates by passing through step (i) and (ii) again. The k_p^t data is re-evaluated using Eq. (3-17) and the refined k_{bb} values.
- (vii) The estimate for k_p^{eff} at each temperature is refined by simulating MWDs obtained at low LPRRs, using the predetermined values of $b\sigma$ and c_R^0 . The aim of these simulations is to determine the difference Δ_{eff} between the input value of k_p^{eff} and the value of k_p^{app} for the lowest LPRRs examined experimentally. This procedure is illustrated in Figure 11-9A for the set of experiments at -10 $^{\circ}\text{C}$. Within this figure, $k_p^{\text{th},0}$ represents the value of k_p^{app} determined from the simulated MWDs. The difference has been calculated for five LPRRs; at the lowest value (3 Hz) Δ_{eff} is estimated to be 655 $\text{L}\cdot\text{mol}^{-1}\cdot\text{s}^{-1}$. The variation in k_p^{app} with LPRR rate is well described by an exponential function in which a , b , and c are constants:

$$k_p^{\text{app}} = a + b \cdot \exp\left(\frac{c \cdot f_L}{\text{Hz}}\right) \quad (11-4)$$

(viii) Eq. (11-4) is suitable to describe the difference between k_p^{app} and k_p^{eff} for the experimental data. The non-linear least-squares fitting of the experimental points at $-10\text{ }^\circ\text{C}$ by Eq. (11-4) results in $k_p^{\text{app}}(\text{L}\cdot\text{mol}^{-1}\cdot\text{s}^{-1}) = 1802 + 152.3 \cdot \exp(0.206 \cdot f/\text{Hz})$. The fit to the data is also shown in Figure 11-9B. At the lowest LPRR of 3 Hz, the apparent propagation rate coefficient equals $2084\text{ L}\cdot\text{mol}^{-1}\cdot\text{s}^{-1}$. Therefore the corrected value for k_p^{eff} is calculated as $(k_p^{\text{exp},0} + \Delta_{\text{eff}}) = 2739\text{ L}\cdot\text{mol}^{-1}\cdot\text{s}^{-1}$.

(ix) With the so-obtained k_p^{eff} value, the final value k_p^{t} is determined from Eq. (3-17).

It should be stressed that the finally estimated k_p^{eff} values do not differ greatly from the corresponding initial guess and were within 5 % of the final converged values in all cases. Therefore, there was no need to re-estimate the values of $b\sigma$ and c_R^0 which to some extent depend on the choice of k_{bb} , k_p^{t} and the individual k_t values (see step (v)).

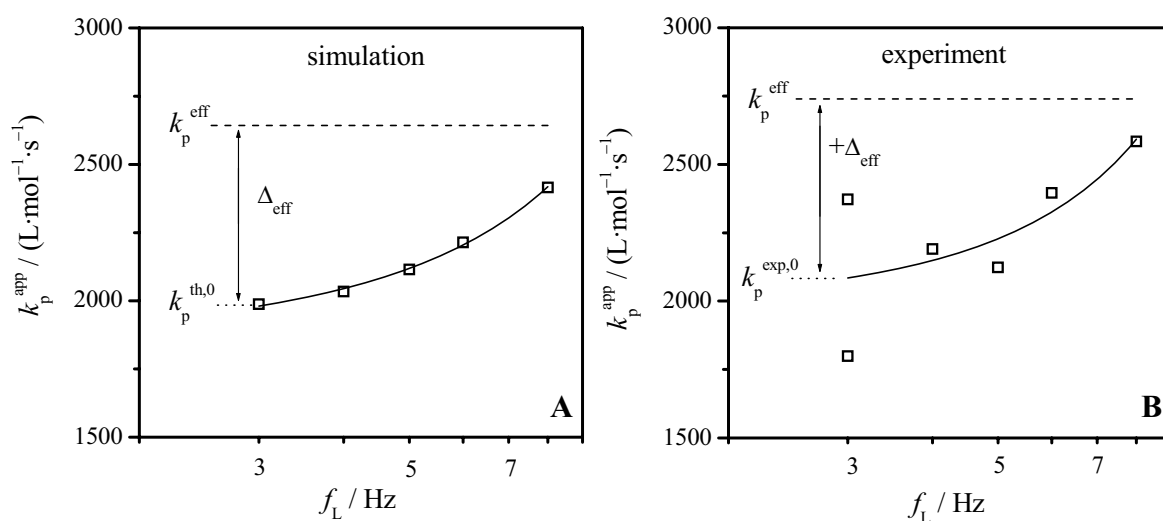


Figure 11-9: Methodology for evaluation of k_p^{eff} by considering the variation in k_p^{app} with LPRR for $f_L < 10\text{ Hz}$, illustrated for PLP-SEC experiments on BA at $-10\text{ }^\circ\text{C}$. The lines indicate the best fit of the simulated (A) and experimental (B) data using an exponential function, as described in the text.

Table 11-1: Values of parameters and rate coefficients estimated from the experimental dependency of k_p^{app} on LPRR measured by PLP-SEC for BA.

T °C	$b\sigma$	c_R^0 mol·L ⁻¹	f_0 Hz	a_p	k_{bb} s ⁻¹	k_p^{eff} L·mol ⁻¹ ·s ⁻¹	k_p^t L·mol ⁻¹ ·s ⁻¹
-10	0.051	$1.0 \cdot 10^{-5}$	15	1.67	25.1	2739	2.7
0	0.039	$3.0 \cdot 10^{-6}$	19	2.16	41.0	3727	4.7
10	0.040	$7.0 \cdot 10^{-6}$ a) $3.5 \cdot 10^{-6}$	31	2.16	67.0	4776	7.3
20	0.040	$6.5 \cdot 10^{-6}$	49	2.16	105.8	5802	10.6
30	0.040	$1.0 \cdot 10^{-5}$ a) $2.5 \cdot 10^{-5}$	79	2.16	170.6	7193	15.9

a) For data set shown by squares in Figure 11-8

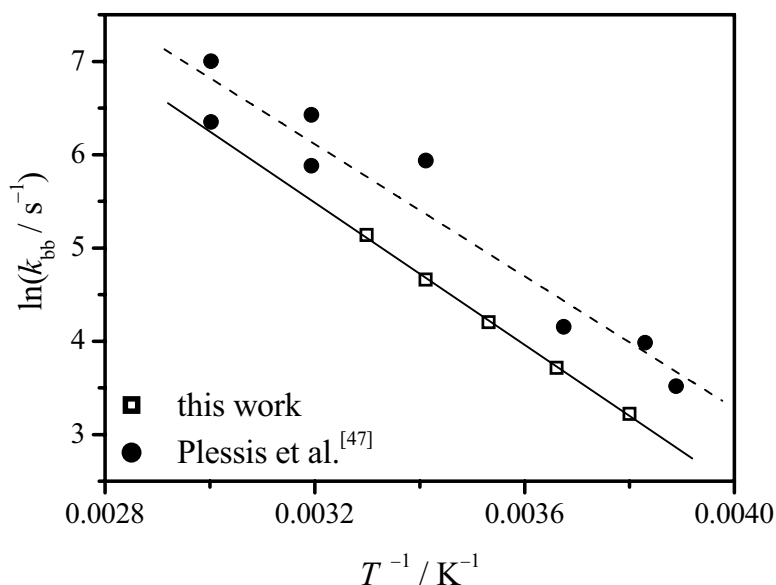
**Figure 11-10:** Arrhenius plot of k_{bb} for BA. The solid line represents the best fit of experimental data obtained in this work (\square). The dashed line represents the best fit of experimental data (\bullet) taken from ref.^[47]

Table 11-1 summarizes the final set of parameters and rate coefficients estimated from the experimental data. Recall that the reported values for f_0 are proportional to k_{bb} , with the proportionality constant being dependent on SEC broadening. For the distributions between 0

and 30 °C, $b\sigma$ is found to be close to the value of 0.04, resulting in an estimate for a_p of 2.16 according to simulation. At -10 °C, the distributions are well fit with $b\sigma = 0.051$, and an a_p value of 1.67 is estimated. Thus, k_{bb} values have been estimated at each temperature according to Eq. (11-3). The Arrhenius plot is shown in Figure 11-10. The associated values of pre-exponential factor and activation energy are $A(k_{bb}) = (4.84 \pm 0.29) \cdot 10^7 \text{ s}^{-1}$ and $E_a(k_{bb}) = (31.7 \pm 2.5) \text{ kJ} \cdot \text{mol}^{-1}$, respectively.

The Arrhenius plot of k_p^t is shown in Figure 11-11. The associated values of pre-exponential factor and activation energy are $A(k_p^t) = (1.52 \pm 0.14) \cdot 10^6 \text{ L} \cdot \text{mol}^{-1} \cdot \text{s}^{-1}$ and $E_a(k_p^t) = (28.9 \pm 3.2) \text{ kJ} \cdot \text{mol}^{-1}$, respectively.

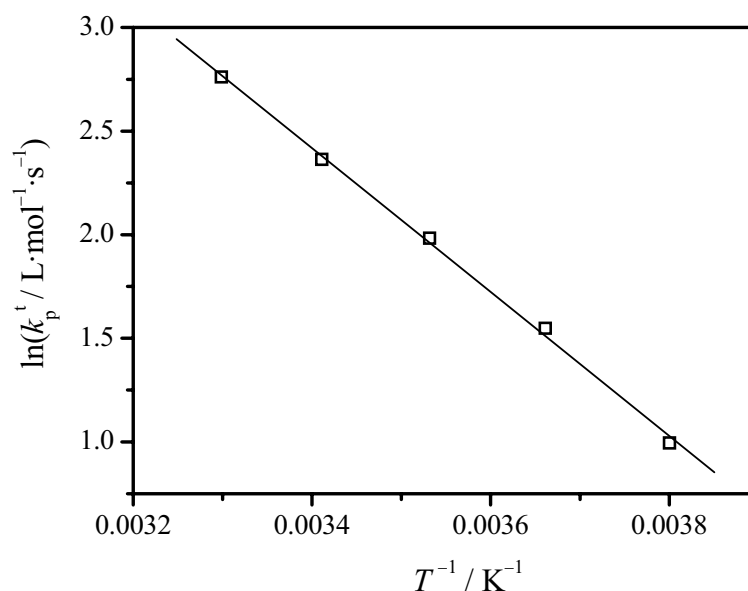


Figure 11-11: Arrhenius plot of k_p^t for BA. The line represents the best fit of experimental data.

11.5 Comparison of k_{bb} and k_p^t estimates with literature data

The Arrhenius parameters for k_{bb} obtained in this work ($E_a(k_{bb}) = 31.7 \text{ kJ} \cdot \text{mol}^{-1}$ and $A(k_{bb}) = 4.84 \cdot 10^7 \text{ s}^{-1}$) are not significantly different from the ones determined by Plessis et al.^[47] ($E_a(k_{bb}) = 29.8 \text{ kJ} \cdot \text{mol}^{-1}$ and $A(k_{bb}) = 4.31 \cdot 10^7 \text{ s}^{-1}$) via ^{13}C -NMR analysis of quaternary carbon atoms. The k_{bb} values of the present work are by about a factor of two below the ones

reported from Plessis et al. (see Figure 11-10). Although the experimental data in ref.^[47] provide a more direct measure of k_{bb} , the NMR signal-to-noise ratio may cause an appreciable scatter of the data, as can be seen from Figure 11-10. Interestingly, the k_{bb} data from the two independent experiments appears to be in closer agreement at the higher temperatures (see Figure 11-10), where the S/N ratio of the NMR measurements should be higher because of a larger content of quaternary carbon atoms. It should further be noted that the variation of k_p^{app} with LPRR, in particular the strong decrease at the repetition rate f_0 , as observed in our experiments, may not be simulated via the literature k_{bb} data. Furthermore, the Plessis et al. k_{bb} data cannot represent the sharp PLP peak found in BA polymerization experiments at 60 °C using an LPRR of 200 Hz.^[193] Simulation via the Arrhenius parameters obtained in this work, on the other hand, can predict this peak. Despite these differences, the agreement between the literature k_{bb} values and the ones from the present study must be considered as satisfactory.

The temperature dependence of the rate coefficient of monomer addition to an MCR (k_p^t) is best described by an activation energy of 28.9 kJ·mol⁻¹. This value differs substantially from the activation energy that can be inferred from the PLP-ESR results reported by Willemse et al.^[49] However, the origin of this apparent discrepancy will be discussed in Chapter 12.3. An upper bound of k_p^t may be estimated by examining BA addition to a BMA radical. While located on a tertiary carbon, this radical is not as hindered as the MCR that results from backbiting (compare Scheme 11-1a with Scheme 3-1). An approximate limiting value is estimated via the simplifying terminal model approach for copolymerization as follows:

$$k_{p,upper}^t / \text{L} \cdot \text{mol}^{-1} \cdot \text{s}^{-1} = \frac{k_{p,BMA}}{r_{BMA,BA}} \quad (11-5)$$

where $r_{BMA,BA}$ is the reactivity ratio for relative addition rate coefficients of BMA and BA to the BMA radical, and $k_{p,BMA}$ is the BMA homopropagation rate coefficient. As has been shown recently,^[267] the terminal model may be used for deducing approximate k_p values for acrylate-methacrylate copolymerizations with the two monomers having the same type of alkyl ester moiety. The IUPAC-recommended Arrhenius coefficients^[10] for the latter are $A(k_{p,BMA}) = 3.78 \cdot 10^6 \text{ L} \cdot \text{mol}^{-1} \cdot \text{s}^{-1}$ and $E_a(k_{p,BMA}) = 22.9 \text{ kJ} \cdot \text{mol}^{-1}$; and the reactivity ratio is taken from literature as:

$$r_{BMA,BA} = 0.827 \exp(282.1 \cdot T^{-1} / \text{K}^{-1}) \quad (11-6)$$

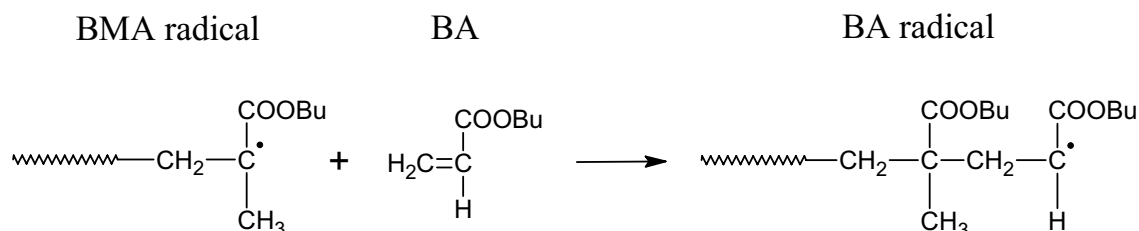
The latter expression actually is from a study of BA copolymerization with MMA,^[286] but was found to provide a good representation of the BMA-BA system.^[287] Thus:

$$k_{p,\text{upper}}^t / \text{L}\cdot\text{mol}^{-1}\cdot\text{s}^{-1} = 4.6\cdot 10^6 \exp(-3036\cdot T^{-1}/\text{K}^{-1}) \quad (11-7)$$

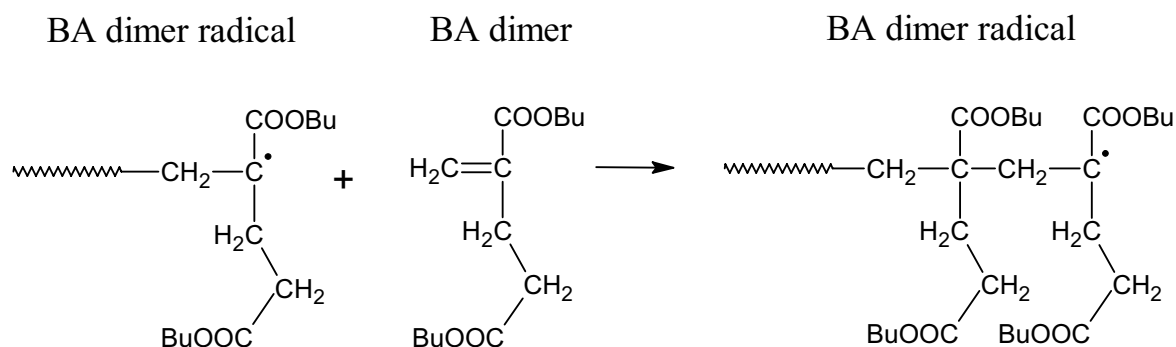
which corresponds to an activation energy of 25.2 kJ·mol⁻¹ and a value of 145 L·mol⁻¹·s⁻¹ for $k_{p,\text{upper}}^t$ at 20 °C.

Scheme 11-1: Reactions that provide upper and lower limiting estimates for BA addition to an acrylate MCR (shown as Scheme 3-1): a) BA addition to a BMA radical; b) BAD addition to the associated MCR. See text for further discussion.

(a)



(b)



The midchain radical structure of BA is similar to that formed by polymerization of BAD. Thus, the polymerization behavior of the dimer species of BA may provide a lower bound estimate for k_p^t ; although the radical structure is similar, the addition of bulky BAD to the radical may be hindered compared to addition of BA monomer (compare Scheme 11-1b to Scheme 3-1). Müller studied the propagation of BAD using the PLP-SEC technique and fit the following Arrhenius expression to the data:^[282]

$$k_{p,lower}^t / \text{L}\cdot\text{mol}^{-1}\cdot\text{s}^{-1} = k_{p,dimer} / \text{L}\cdot\text{mol}^{-1}\cdot\text{s}^{-1} = 9.31\cdot 10^6 \exp(-4065\cdot T^{-1}/\text{K}^{-1}) \quad (11-8)$$

which corresponds to an activation energy of 33.8 kJ·mol⁻¹ and a value of 8.8 L·mol⁻¹·s⁻¹ for $k_{p,lower}^t$ at 20 °C. k_p^t determined in this work has an activation energy (28.9 kJ·mol⁻¹) between these two limiting values, with the absolute rate coefficient ($k_p^t = 10.8 \text{ L}\cdot\text{mol}^{-1}\cdot\text{s}^{-1}$ at 20 °C) also intermediate, but much closer to the value for BAD polymerization.

12 Determination of Rate Coefficients for Acrylate Systems by SP-PLP-ESR

The impact of MCR build-up on the kinetics of acrylate polymerization was thoroughly discussed in Chapter 10. It was shown that individual k_t^{ss} , k_t^{st} and k_t^{tt} values may not be easily determined via SP-PLP-NIR as tracing of monomer conversion after single pulse initiation only provides indirect access to termination rate coefficients. Though the individual k_t values which were determined from analysis of R_p data for different c_M had proven to describe MWDs from PLP very well (see Chapter 11), the obtained k_t^{ss} , k_t^{st} and k_t^{tt} values are only chain-length-averaged quantities.^[51,53] It was outlined in Chapter 3.4.2 that k_t strongly depends on the degree of polymerization of the terminating radicals. Thus, a significant improvement of modeling capability may be obtained with chain-length dependent k_t values being available for simulation. Moreover, additional experimental evidence for k_{bb} and k_p^t would be valuable, as the PLP-SEC technique detailed in the previous chapter requires significant modeling support.

A particularly direct way of studying structurally different radicals is ESR spectroscopy. In fact, it was an ESR study by Gilbert et al.^[41] which first showed the simultaneous occurrence of SPRs and MCRs during acrylate polymerization. In ESR, the double integral of the dispersion spectra are proportional to the radical concentrations. However, determination of separate SPR and MCR concentrations for acrylate systems is not trivial as the associated individual spectra partially overlap. The experimental ESR spectra thus need to be deconvoluted as has been briefly outlined in Chapter 5.4.2. Spectra deconvolution yields x_{MCR} values for the particular reaction conditions containing kinetic information on the termination and transfer kinetics in the polymerizing system.

Particularly valuable information should be accessible from simultaneous time-resolved measurements of both, secondary and tertiary radical concentrations. Detailed insights into transfer kinetics and into individual $k_t(i,i)$ values for acrylate polymerizations may be assessed from c_{MCR} and c_{SPR} traces recorded after SP initiation. Such traces may be obtained by SP-PLP-ESR, a technique which was so far exclusively used for systems with one type of macroradical.^[32–34,97,149,208] However, via the calibration procedure detailed in Chapter 5.4.2,

this technique may also be applied to polymerization reactions where two structurally different macroradicals occur.

In the first sections of this chapter, ESR spectra measured for BA polymerization under stationary and pseudo-stationary conditions are discussed and evaluated. The major part is devoted to the analysis of SPR and MCR concentration traces detected via SP-PLP-ESR.

The investigations detailed in this chapter have been carried out in cooperation with Johannes Barth, Dr. Thomas Junkers, Dr. Tatiana Sergeeva, and Thomas Theis. Part of the work has already been published in refs.^[54,98,202]

12.1 The ESR spectrum of alkyl acrylates

The unpaired electrons of the SPR and MCR are located in different chemical environments. Thus the associated ESR spectra are dissimilar. The line splitting of the SPR may be explained by coupling of the unpaired electron with an α -hydrogen atom and a pair of equivalent β -hydrogen atoms with the corresponding hyperfine coupling constants for BA of $\alpha_{H\alpha} = 23.5$ G (1 H) and $\alpha_{H\beta} = 20.4$ G (2 H).^[49] For the MCR species coupling with two pairs of β -hydrogen atoms may be assumed with $\alpha_{H\beta 1} = 10.9$ G (2 H) and $\alpha_{H\beta 2} = 16.4$ G (2 H).^[49] The coupling constants were determined from low and high temperature ESR spectra which are dominated by the SPR and MCR species, respectively. The measured spectra and the assigned hyperfine coupling constants are in close agreement with the ones reported by Kajiwara for *tert*-BA.^[288] The simulated ESR spectra of the secondary and tertiary radicals are shown in Figure 12-1 with line widths of 4 G (black line) and 0.5 G (grey line). The line width of ESR spectra depends on the reaction conditions and spectroscopic parameters such as scanning rate. In the experimental studies of this work, rather broad lines were measured similar to the ones indicated in black. Due to the pronounced broadening, the SPR-6-line spectrum reduces to 4 lines and instead of a 9-line spectrum for the MCR only 7 lines are seen. Those broad simulated spectra may be used to deconvolute experimental spectra as outlined in Chapter 5.4.2. Sergeeva has recently shown that the agreement between simulated and experimental ESR spectra is significantly increased by introduction of small contributions of a 3-line spectrum ($\alpha_{H\beta} = 27$ G (2 H)) being indicated as MCR 2 in Figure 12-1.^[209] Such pattern implies that a radical species is present in which the electron spin couples with two

identical protons. This species is probably an MCR which has been formed via inter- or intramolecular transfer-to-polymer to random position along the polymer backbone (denoted as MCR 2 in previous studies^[97,98,208]). By such reactions, tertiary macroradicals are formed in which the electron spin is located between two long polymeric arms rather than one arm just being an SCB as for the MCR created via 1-5-hydrogen shift. Coupling occurs with only two out of four hydrogen atoms for MCR 2.^[41,289] Such situation may be met when rotations around the C-C bonds are strongly hindered by the long polymeric side chains. This may fix two of the protons in perpendicular position to the rotation axis of the p_z -orbital of the unpaired electron resulting in a coupling constant of zero.

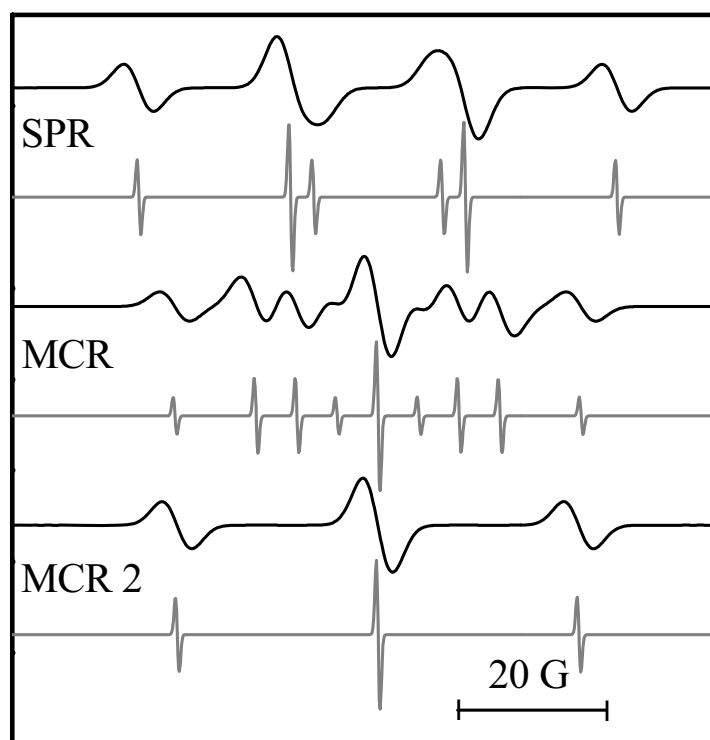


Figure 12-1: Simulated ESR spectra of the SPR, MCR and MCR 2 as indicated in the figure. The associated hyperfine coupling constants are given in the text. For simulation of the spectra line widths of 4 G (black) or 0.5 G (gray) were used.

A dominant 3-line spectrum was found within cross-linking polymerization^[41,289] under which conditions rotational restriction should become important. However, also Yamada and coworkers obtained 3-line spectra during conventional polymerization of acrylate-type monomers.^[43,44,48] Moreover, Yamada et al. reported a different coupling pattern for the SPR

as the one described above. They attributed different coupling constants to each of the β -hydrogen atoms.

Matsumoto and Giese^[290] obtained a 16-line spectrum for a monomeric MA radical which they attributed to identical $\alpha_{H\alpha}$ and $\alpha_{H\beta}$ values but with additional small line splitting due to the γ -hydrogen atoms of the ester group. Based on their assignment, it is possible to obtain a simulated SPR spectrum which is practically identical to the one shown in Figure 12-1 when pronounced line broadening is introduced (see Figure 12-2). In fact, coupling with γ -hydrogen atoms was also experimentally observed during polymerization of methacrylate monomers when slow scanning rates were used.^[202,291]

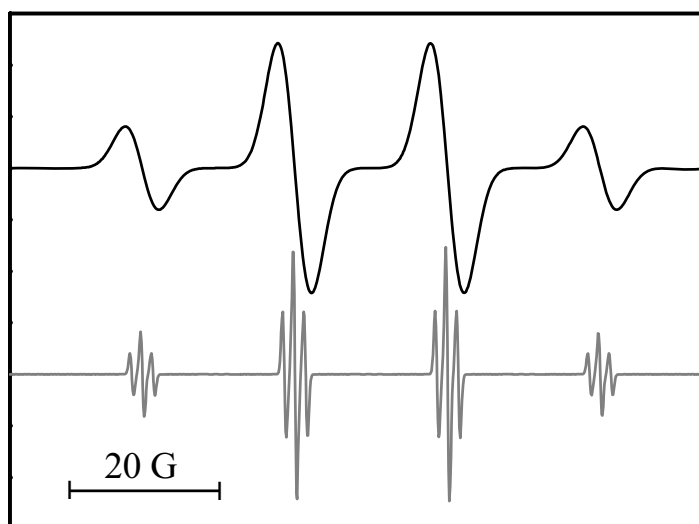


Figure 12-2: Simulated ESR spectra of the SPR. The hyperfine coupling constants are $\alpha_{H\alpha} = 20.77$ G (1 H), $\alpha_{H\beta} = 20.77$ G (2 H), and $\alpha_{H\gamma} = 1.45$ G (3 H) as reported in ref.^[290] For simulation of the spectra line widths of 4 G (black) or 0.5 G (gray) were used.

It was furthermore shown that hyperfine coupling constants may change with radical chain-length. This may cause broadened ESR spectra under conventional, i.e., not controlled polymerization conditions where macroradicals of different length occur.^[292]

The discussion above illustrates that the shape of the ESR spectra for SPR and MCR may strongly depend on experimental conditions such as temperature, radical chain length, solution viscosity, polymer content, and degree of cross-linking but spectroscopic parameters like scanning rate, microwave power and modulation amplitude seem equally important. Moreover, even for spectra of similar shape, different coupling mechanisms were proposed.

Though this situation is not very satisfactory, only the correct assignment of ESR bands to the SPR and MCR species is relevant for the kinetic investigations detailed in the thesis in hand. The SPR and MCR spectra shown in Figure 12-1 are unambiguously assigned by low and high temperature measurements and the MCR 2 spectrum is most likely due to tertiary macroradicals. A particularly simple method for identifying SPR and MCR lines in superimposed ESR spectra was recently introduced by Buback et al.^[54] and is detailed on example of BA polymerization in the next section.

12.2 PLP labeling of SPRs and MCRs in ESR analysis

ESR spectroscopy is well suited for analysis of different types of radicals. Contributions of SPRs and MCRs to the resulting ESR spectra may, however, not easily be separated because of (partial) band overlap. It was shown that the spectra measured at intermediate temperatures may be well expressed by a superposition of simulated SPR and MCR spectra with the coupling constants being determined from experimental spectra measured at low and high temperatures, respectively.^[49]

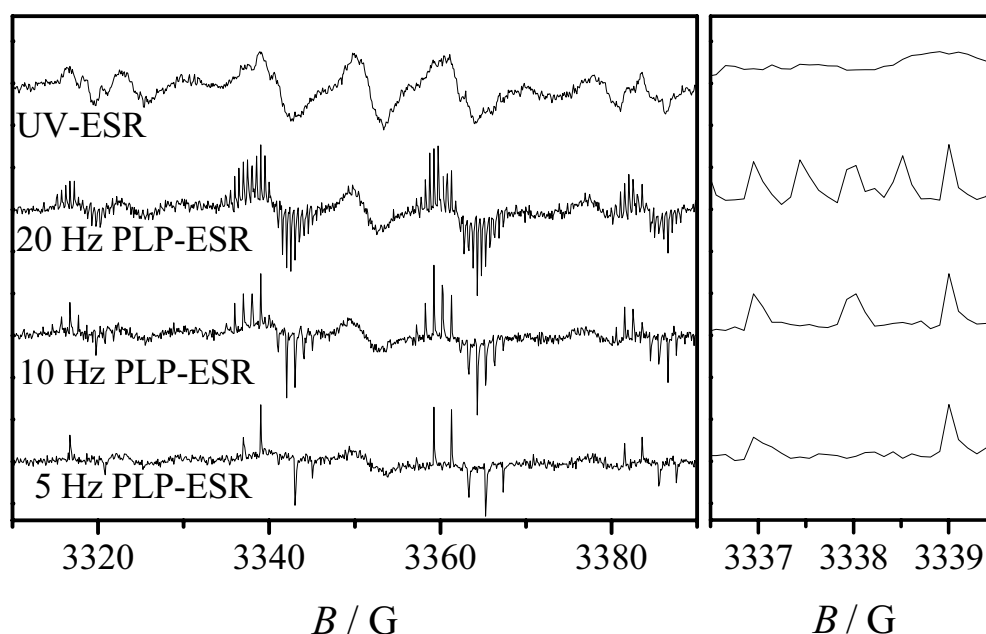


Figure 12-3: ESR spectra recorded during polymerization of $1.52 \text{ mol}\cdot\text{L}^{-1}$ BA in toluene. The spectra were recorded at 0°C under continuous illumination (UV) and under PLP conditions at different LPRRs (5, 10, and 20 Hz, as indicated in the figure).

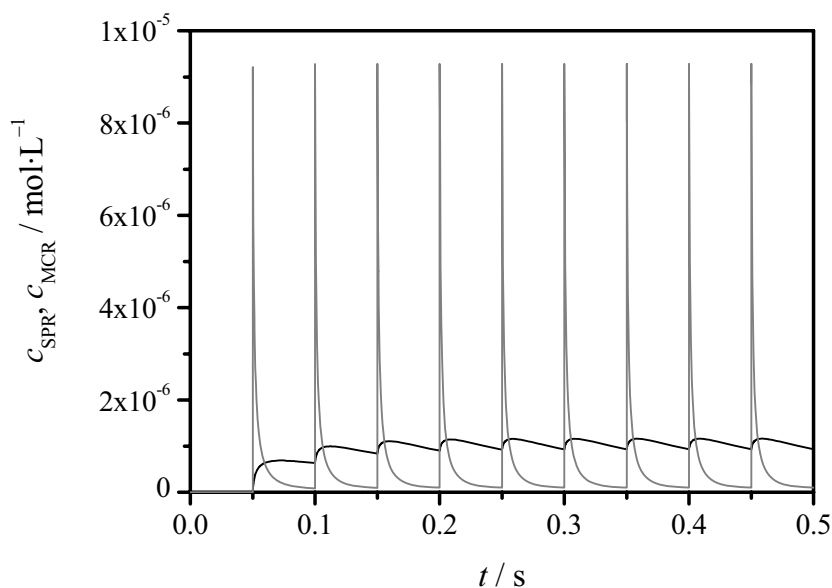


Figure 12-4: Simulated SPR (grey line) and MCR (black line) concentration traces for PLP-induced polymerization of $1.52 \text{ mol}\cdot\text{L}^{-1}$ BA in toluene at 0°C , an LPRR of 20 Hz, and primary radical concentrations of $c_{\text{R}}^0 = 10^{-5} \text{ mol}\cdot\text{L}^{-1}$. The rate coefficients collated in Table 10-1 were used for modeling.

A simple approach for labeling different types of structurally and kinetically different macroradicals has been presented for dodecyl acrylate (DA) solution polymerization^[54] and is shown in Figure 12-3 taking ESR spectra measured during a BA polymerization in toluene ($1.52 \text{ mol}\cdot\text{L}^{-1}$) at 0°C as an example. The scan rate was $10 \text{ G}\cdot\text{s}^{-1}$. For the upper spectrum (UV-ESR), polymerization was induced by continuous illumination with a UV lamp. The spectrum consists of several rather broad and smooth lines which cannot directly be assigned to particular radical species. The other ESR spectra in Figure 12-3 are scanned under pulsed laser initiation. They are composed of two types of ESR lines, with and without pronounced oscillation. There are four lines exhibiting oscillations whereas, e.g., the center line around 3350 G exhibits only minor intensity variations. The oscillating ESR lines are due to SPRs. Laser pulsing produces a burst of initiator-derived radicals which add to monomer and form SPRs. The SPRs may subsequently undergo termination or transformation to MCRs via backbiting. That the oscillations are due to laser pulsing is evident from the enlargement on the r.h.s. of Figure 12-3. The magnetic field domain can be transformed into a time domain based on the applied scanning rate. Thus, the peaks for 20, 10 and 5 Hz are spaced by 0.05, 0.1 and 0.2 s which exactly matches the associated pulse separation times. The fact that the

MCR lines (see, e.g., the central region) reflect laser pulsing to a much smaller extent directly shows that, under the above described reaction conditions, backbiting of SPRs, propagation from MCRs, and termination of MCRs are slow processes compared to termination of SPRs. To illustrate the above discussion, the SPR (grey line) and MCR (black line) concentration traces for polymerization of $1.52 \text{ mol}\cdot\text{L}^{-1}$ BA in toluene at 0°C under PLP-initiation of 20 Hz ($c_{\text{R}}^0 = 1\cdot 10^{-5} \text{ mol}\cdot\text{L}^{-1}$) were simulated via PREDICI and shown in Figure 12-4.

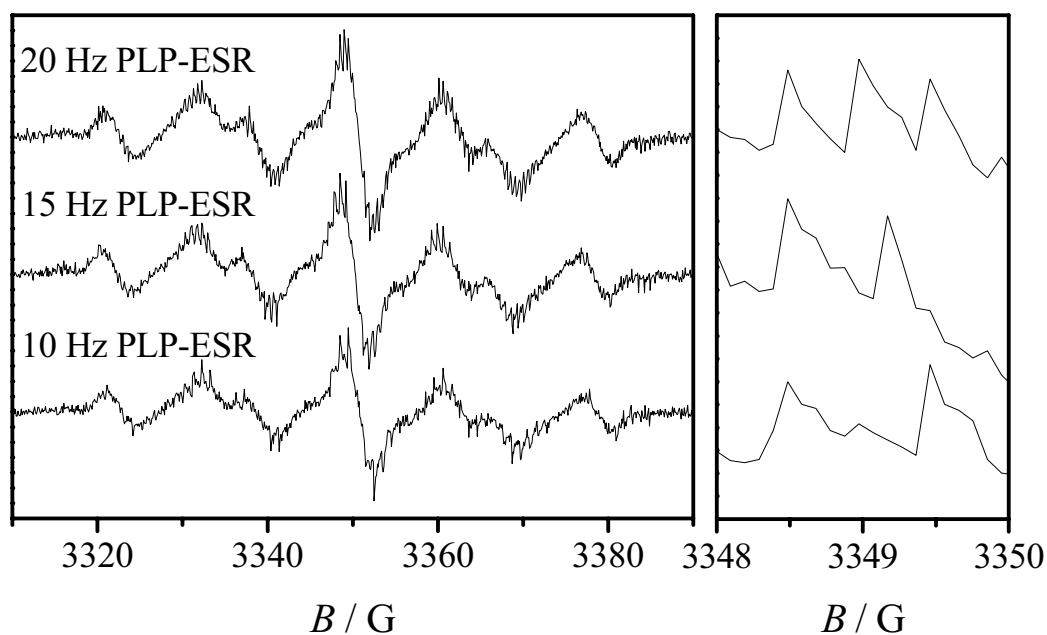


Figure 12-5: ESR spectra recorded during polymerization of $1.52 \text{ mol}\cdot\text{L}^{-1}$ BA in toluene at 72°C and under PLP conditions at different LPRRs (20, 15, and 10 Hz, as indicated).

Though MCR build up is relatively slow compared to formation of SPRs, pseudo-stationarity of MCR concentration is already reached after firing four to five laser pulses. However, after passing the initial transient period, only minor variations in MCR concentration are seen upon laser pulsing. c_{MCR} periodically changes between about $9\cdot 10^{-7}$ and $1.1\cdot 10^{-6} \text{ mol}\cdot\text{L}^{-1}$. However, c_{SPR} increases to almost $10^{-5} \text{ mol}\cdot\text{L}^{-1}$ directly after the laser pulse but decreases to less than $1\cdot 10^{-7} \text{ mol}\cdot\text{L}^{-1}$ during the pulse-separation time. Those strong variations in SPR concentration are also reflected in Figure 12-3 whereas no or only minor oscillations are seen for the MCR. Pronounced changes in MCR concentration may be observed when temperature is significantly increased. Under such conditions, the rates of MCR formation by backbiting and MCR loss by termination are strongly increased. This is illustrated in Figure 12-5 where ESR spectra recorded during PLP-induced polymerization of BA ($1.52 \text{ mol}\cdot\text{L}^{-1}$ in toluene) at 72°C

are shown. It can be seen that c_{MCR} oscillates with the applied LPRR within the spectra. SPR lines, however, cannot be clearly identified in Figure 12-5. This may be due to the extremely fast loss of the primary SPR concentrations by backbiting and termination which cannot be resolved with the applied scanning rate.

12.3 Evaluation of midchain radical fractions determined during stationary and pseudo-stationary polymerization

The temperature dependence of x_{MCR} under PLP-conditions was object of several studies by the Buback group.^[49,97,98,208] However, the results were in several perspectives curious as will be discussed for the BA system.

Figure 12-6 shows the experimentally obtained temperature dependence of x_{MCR} for PLP-induced polymerization of BA in toluene at an LPRR of 20 Hz and different monomer concentrations (data is taken from refs.^[49,97]). x_{MCR} is strongly increased toward higher temperature from a value close to zero at $-50\text{ }^{\circ}\text{C}$ to about 0.8 at $70\text{ }^{\circ}\text{C}$. Thus, for low temperatures almost no tertiary radicals are seen in the ESR spectrum whereas at high T less than 20 % of the radicals are SPRs. Such strong temperature dependence is at first glance surprising considering that, according to Table 10-1, $E_a(k_{\text{bb}})$ and $E_a(k_{\text{p}}^{\ddagger})$ differ by only about $3\text{ kJ}\cdot\text{mol}^{-1}$. This suggests a minor temperature dependence of x_{MCR} expressed by Eq. (10-10). Moreover, from Eq. (10-10) a pronounced monomer concentration dependence of x_{MCR} is expected as the re-initiation frequency scales with c_{M} . However, the data in Figure 12-6 closely overlap though wide ranges of monomer concentration are covered.

To overcome this dilemma, Willemsen et al.^[49] proposed a monomer-complexed transitional MCR species which adds to the monomer with the frequency $k_{\text{p}}^{\ddagger*}$. Definition of such unimolecular propagation step removes the monomer concentration dependence from Eq. (10-10):

$$x_{\text{MCR}} = \frac{k_{\text{bb}}}{k_{\text{bb}} + k_{\text{p}}^{\ddagger*}} \quad (12-1)$$

The pseudo-stationary SPR and MCR concentration profiles were simulated for identical reaction conditions as used within the experimental studies on BA. The primary radical

concentration was estimated to be $10^{-5} \text{ mol}\cdot\text{L}^{-1}$; a value which is typical for PLP-ESR (see Chapter 12.4). An example for simulated SPR and MCR traces under pseudo-stationary PLP conditions has already been shown in Figure 12-4. The c_{SPR} and c_{MCR} curves obtained for different monomer concentrations and temperatures were integrated over time to obtain a measure for the average radical concentration. From the associated integrals, x_{MCR} is calculated according to:

$$x_{\text{MCR}} = \frac{\int c_{\text{MCR}}(t)}{\int c_{\text{MCR}}(t) + \int c_{\text{SPR}}(t)} \quad (12-2)$$

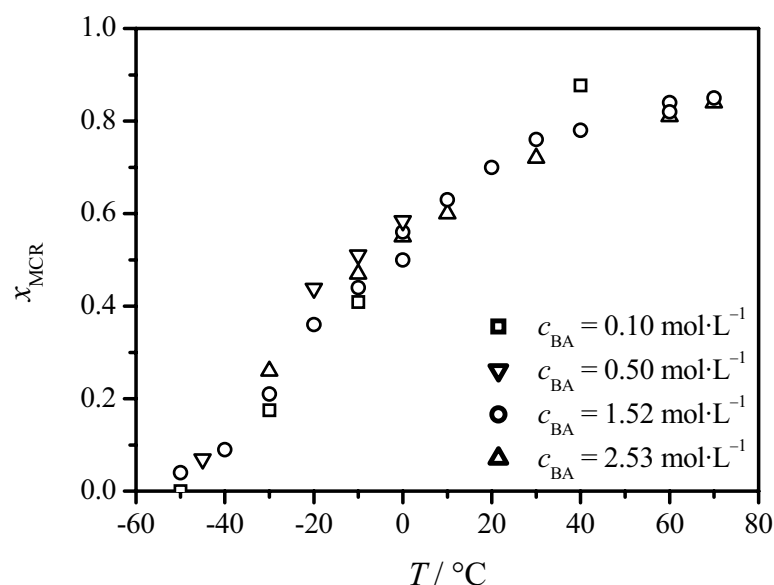


Figure 12-6: Temperature dependence of x_{MCR} during PLP-induced (20 Hz) polymerization of BA in toluene at different monomer concentrations as indicated in the figure. Data is taken from refs. ^[49,97]

The so-obtained simulated temperature dependencies of x_{MCR} for PLP-induced polymerization of BA at different monomer concentrations are depicted in Figure 12-7. It is clearly seen that x_{MCR} strongly depends on temperature and the curves simulated for different c_{BA} converge toward low T . Pronounced monomer concentration dependencies of x_{MCR} are only observed for high temperatures. Experimental high temperature x_{MCR} data for low c_{M} is limited to a single data point for $0.1 \text{ mol}\cdot\text{L}^{-1}$ of BA which is, however, indeed well above the values measured for monomer concentrations of 1.52 and $2.53 \text{ mol}\cdot\text{L}^{-1}$ (see Figure 12-6). The reason

behind those observations is that derivation of Eqs. (10-10) and (12-1) rests on two major assumptions which are the stationarity of c_{MCR} and, more importantly, the fulfillment of the long-chain hypothesis. Both restrictions are not met with the PLP-ESR measurements. c_{MCR} is not stationary but pseudo-stationary and at low temperatures the major loss reaction of MCRs is termination rather than monomer addition. At a temperature of $-50\text{ }^{\circ}\text{C}$ and a monomer concentration of $1.5\text{ mol}\cdot\text{L}^{-1}$, the average lifetime of an MCR before it adds to monomer is more than 2.5 s (according to Eq. (10-14)). However, termination of MCRs can still be assumed fast as the activation energies for k_t^{st} and k_t^{tt} are low and the radical concentrations are relatively high under PLP-conditions. Thus, even in case that the stationarity assumption was fulfilled, x_{MCR} at low T should be described by Eq. (10-8) and not by Eq. (10-10). Conclusively, at high temperatures x_{MCR} is controlled by monomer addition to the MCR and thus the MCR content depends on c_{M} . Toward lower T , a termination control of x_{MCR} sets in causing a pronounced decrease in MCR fraction and a monomer concentration independence of x_{MCR} at very low temperatures.

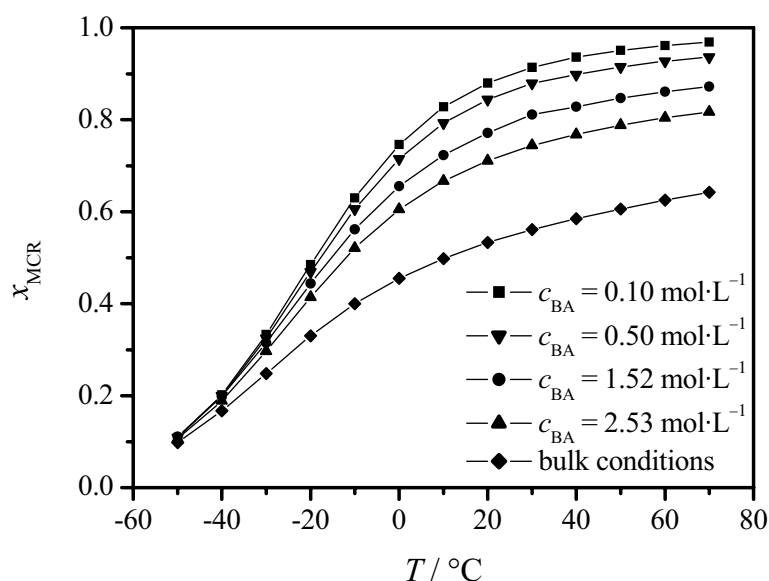


Figure 12-7: Simulated temperature dependence of x_{MCR} for PLP-induced polymerization of BA in toluene with an LPRR of 20 Hz, $c_{\text{R}}^0 = 10^{-5}\text{ mol}\cdot\text{L}^{-1}$, and different monomer concentrations as indicated in the figure. The rate coefficients for modeling were chosen according to Table 10-1.

A comparison of experimental (open symbols) and simulated (filled symbols) x_{MCR} data is shown in Figure 12-8 for BA concentrations of 2.53 (left) and $1.52\text{ mol}\cdot\text{L}^{-1}$ (right). This figure illustrates that not only qualitative but also close quantitative agreement between

experiment and simulation is obtained, especially for the higher BA concentration. Almost perfectly overlapping data may for example be achieved when the pre-exponential factor of k_t^{st} is increased by about 1.5 within the simulations. However, such minor discrepancies may also be explained by problems in experimental x_{MCR} determination. Strong oscillations of SPR lines as shown in Figure 12-3 may result in an underestimation of MCR fraction within the deconvolution procedure. The close agreement between experiment and simulation provides strong evidence for the accuracy of the rate coefficients collated in Table 10-1. x_{MCR} values estimated from Eq. (10-10) are included as full lines in Figure 12-8. Whereas those x_{MCR} values are close to the simulated and experimental data at high temperatures, they strongly diverge toward lower T . This again illustrates that x_{MCR} is controlled by termination at low temperatures and Eq. (10-10) is only valid at high temperatures and high c_{M} which, however, are the technically relevant conditions.

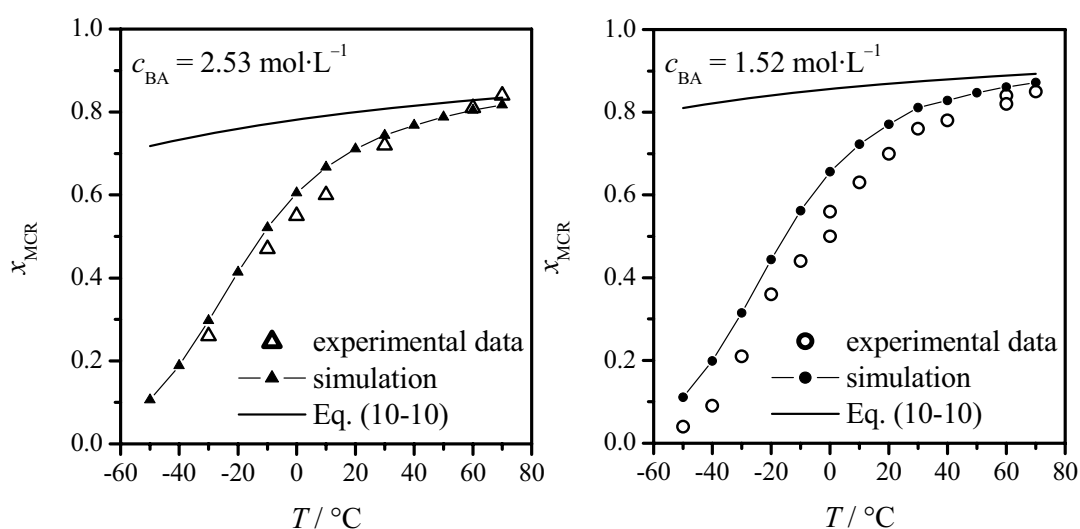


Figure 12-8: Comparison between experimental (open symbols) and simulated (full symbols) temperature dependencies of x_{MCR} for 2.53 (left) and 1.52 $\text{mol}\cdot\text{L}^{-1}$ (right) of BA in toluene (data is taken from Figure 12-6 and Figure 12-7). The full line was estimated using Eq. (10-10) with the k_{bb} and k_{p}^{t} values from Table 10-1.

In previous studies, the experimental x_{MCR} data was evaluated by Arrhenius plotting of $x_{\text{MCR}} \cdot (1 - x_{\text{MCR}})^{-1}$ to obtain the activation of $k_{\text{bb}}/k_{\text{p}}^{\text{t}*}$.^[49,97,98,208] The result from a corresponding plot to the entire BA data set shown in Figure 12-6 is $E_{\text{a}}(k_{\text{bb}}/k_{\text{p}}^{\text{t}*}) = 18.8 \text{ kJ}\cdot\text{mol}^{-1}$.^[49,97] This outcome is in conflict with the difference in the activation energies of k_{bb} and k_{p}^{t} according to Table 10-1 which is below $3 \text{ kJ}\cdot\text{mol}^{-1}$. Moreover, assuming that $E_{\text{a}}(k_{\text{bb}})$ is about $30 \text{ kJ}\cdot\text{mol}^{-1}$, as determined from the particularly direct method of branching level measurements,^[47] the

high $E_a(k_{bb}/k_p^{t*})$ value implies that $E_a(k_p^{t*}) \approx 12 \text{ kJ}\cdot\text{mol}^{-1}$. This value is well below all activation energies reported so far for monomer addition to tertiary macroradicals^[16] and may be obtained only for very special systems like secondary radical propagation of AA in dilute aqueous solution^[67,68]. However, the above described discrepancies only result from the invalidity of Eq. (12-1). Linear fitting of $\ln(x_{\text{MCR}}/(1-x_{\text{MCR}}))$ vs. T^{-1} should correctly yield $E_a(k_{bb}/(k_p^t \cdot c_M + 2 \cdot k_t^t \cdot c_{\text{MCR}} + 2 \cdot k_t^{\text{st}} \cdot c_{\text{SPR}} + k_{\text{tr},\text{M}}^t \cdot c_M))$. Figure 12-9 shows an Arrhenius plot of $x_{\text{MCR}} \cdot (1-x_{\text{MCR}})^{-1}$ of midchain radical fractions which were simulated for PLP-induced polymerization of $1.52 \text{ mol}\cdot\text{L}^{-1}$ BA. The full line represents a linear fit to the entire data set. The obtained activation energy of $21 \text{ kJ}\cdot\text{mol}^{-1}$ is in good agreement to the literature result of $18.8 \text{ kJ}\cdot\text{mol}^{-1}$. Exclusive regression of the two data points for the highest temperatures (dashed line) yields an activation energy of $9 \text{ kJ}\cdot\text{mol}^{-1}$ indicating propagation control of x_{MCR} with minor contribution of termination. From fitting of the two data points at the lowest temperatures (dotted line), an activation energy of $29 \text{ kJ}\cdot\text{mol}^{-1}$ is obtained which illustrates that termination controls x_{MCR} . It has to be noted that Junkers^[97] already pointed out that low $E_a(k_{bb}/k_p^{t*})$ values are obtained from exclusive regression of the high temperature data however without providing an explanation for this observation.

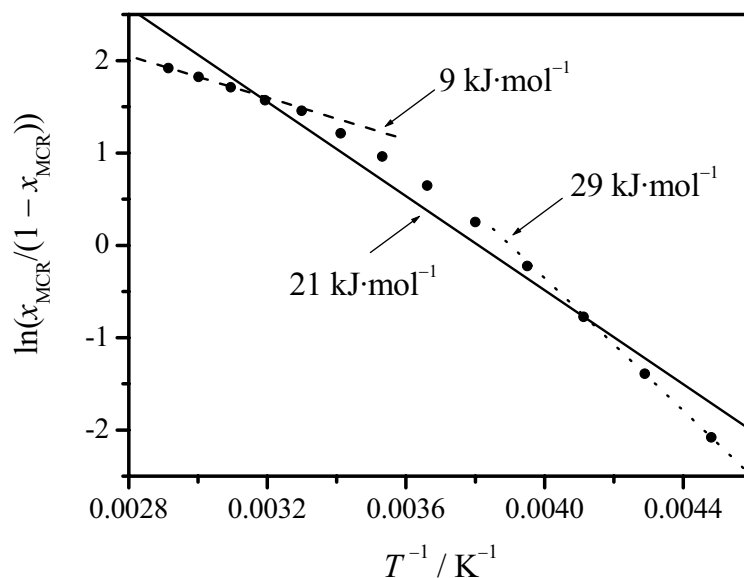


Figure 12-9: Arrhenius plot of $x_{\text{MCR}} \cdot (1-x_{\text{MCR}})^{-1}$ from simulated midchain radical fractions for PLP-induced polymerization of $1.52 \text{ mol}\cdot\text{L}^{-1}$ of BA in toluene ($f_L = 20 \text{ Hz}$ and $c_R^0 = 10^{-5} \text{ mol}\cdot\text{L}^{-1}$). The full line represents a linear fit to the entire data set whereas the dotted and dashed lines result from linear regression of the two data points at the lowest and highest temperatures, respectively.

Though PLP techniques usually afford for more detailed insights into kinetics than stationary methods, x_{MCR} values measured under stationary conditions are easier to evaluate. Under such conditions, $dc_{\text{MCR}}/dt = 0$ is fulfilled and thus Eq. (10-8) can directly be applied. Moreover, the ESR spectra are relatively smooth and no oscillations of SPR lines are seen (see Figure 12-3) allowing for precise determination of x_{MCR} via deconvolution.

Sergeeva determined MCR fractions for polymerizations of BA and DA in toluene induced by continuous illumination via a UV lamp.^[209] As an example, Figure 12-10 shows the experimentally obtained temperature dependence of x_{MCR} (open circles) for polymerization of $1.52 \text{ mol}\cdot\text{L}^{-1}$ of BA in toluene. As noted above, the $x_{\text{MCR}}(T)$ curve may be described by Eq. (10-8) but c_{MCR} and c_{SPR} are required for using this expression. However, these two quantities can be expressed by $c_{\text{MCR}} = c_{\text{R}} \cdot x_{\text{MCR}}$ and $c_{\text{SPR}} = c_{\text{R}} \cdot (1 - x_{\text{MCR}})$. The overall radical concentration may be determined from the experimental ESR spectra via calibration against TEMPO spectra (see Chapter 5.4.2). For c_{M} , the arithmetic mean monomer concentration before and after UV irradiation is used. This removes all unknown quantities from Eq. (10-8) and allows for solving this expression for x_{MCR} . The so-obtained predicted MCR fraction (using the rate coefficients from Table 10-1) is depicted in Figure 12-10 as filled circles. There is astonishingly good agreement between experimental and predicted data illustrating the validity of Eq. (10-8) and the predictive power of the set of rate coefficients collated in Table 10-1. The temperature dependence of x_{MCR} obtained from Eq. (10-10) is also included in Figure 12-10 to demonstrate again that this expression may only be used for high temperatures.

It has already been mentioned that x_{MCR} is controlled by termination at very low temperatures. Under such conditions transfer-to-monomer of the MCR can be neglected. MCR-MCR termination should also not significantly contribute to the loss of tertiary radicals as c_{MCR} is relatively low and k_{t}^{st} is well above k_{t}^{tt} . Based on those assumptions, Eq. (10-8) may be simplified and solved for k_{t}^{st} .

$$k_{\text{t}}^{\text{st}} = \frac{1}{2} \cdot \frac{k_{\text{bb}} - k_{\text{bb}} \cdot x_{\text{MCR}} - k_{\text{p}}^{\text{t}} \cdot c_{\text{M}} \cdot x_{\text{MCR}}}{c_{\text{R}} \cdot x_{\text{MCR}} \cdot (1 - x_{\text{MCR}})} \quad (12-3)$$

Via Eq. (12-3), k_{t}^{st} may be estimated from experimental x_{MCR} , c_{R} , and c_{M} values for low temperature polymerization conditions provided that k_{bb} and k_{p}^{t} are known; an approach which is currently explored.^[209]

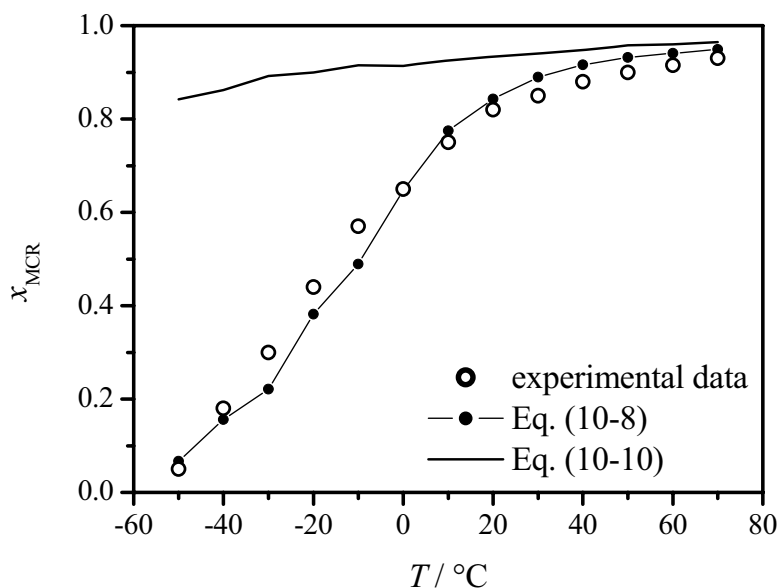


Figure 12-10: Experimental (open circles) temperature dependence of x_{MCR} for stationary UV-induced polymerization of $1.52 \text{ mol}\cdot\text{L}^{-1}$ of BA in toluene.^[209] The filled circles were estimated according to Eq. (10-8) and the full line was assessed from Eq. (10-10) both with the rate coefficients collated in Table 10-1.

12.4 SP-PLP-ESR of BA

SP-PLP-ESR is until now the most powerful experimental technique for kinetic investigations into acrylate systems, as it allows for obtaining k_{bb} and k_{p}^{\dagger} as well as chain-length dependent individual k_{t} values from a single experiment. However, application of SP-PLP-ESR is not trivial, as the calibration procedure is rather complex (see Chapter 5.4.2) and several experimental artefacts may occur which hamper tracing of c_{SPR} and c_{MCR} (see Chapter 5.4.3). The experimentally accessible range for time-resolved measurements of both, SPR and MCR concentration, is $0 \text{ }^\circ\text{C}$ to $60 \text{ }^\circ\text{C}$. At even lower temperatures, signal-to-noise quality of the MCR traces becomes too low whereas at temperatures above $60 \text{ }^\circ\text{C}$, the SPR lines in the full ESR spectra are no longer sufficiently resolved for accurate identification of the maximum position ($H_{\text{x,SPR}}$) used for tracing c_{SPR} . In the first part of this chapter, experimental SPR and MCR concentration curves for polymerization of BA are discussed. Subsequently, the general data evaluation procedure is outlined followed by the presentation of the results for the kinetic coefficients.

12.4.1 SPR and MCR concentration traces after single pulse initiation

The shape of $c_{\text{SPR}}(t)$ and $c_{\text{MCR}}(t)$ curves has already been briefly discussed for the simulations shown in Figure 10-10 and, indirectly, within Chapter 12.2 by means of the full ESR spectra measured under PLP conditions. The time evolution of SPR concentration after single pulse initiation at $t = 0$ for polymerization of BA in toluene ($1.52 \text{ mol}\cdot\text{L}^{-1}$) is shown in Figure 12-11 for different temperatures. SPRs are formed by monomer addition to initiator-derived radicals with the associated rate coefficient, k_i . As k_i is generally assumed to be even well above k_p and c_M is not close to zero, the maximum in c_{SPR} is reached shortly after the laser pulse. The steep increase in SPR concentration cannot be adequately resolved by SP-PLP-ESR, so far. Moreover, the laser signal (see Figure 5-13 and accompanying discussion) may strongly distort the SPR traces at short times after the laser pulse as can be seen from the of double maxima in the 273 and 333 K curves. Such $c_{\text{SPR}}(t)$ shape cannot be explained by a genuine kinetic effect. The maximum SPR concentration is almost independent of temperature as identical initiator concentrations and similar laser energies were used. The subsequent decrease in c_{SPR} is caused by termination and backbiting reactions, respectively. The dominant reaction at relatively short times after the pulse is SPR-SPR termination, as secondary radical concentration is very high and k_t^{ss} is well above k_t^{st} . SPR-MCR termination may only get significant at high temperatures and longer times after applying the pulse ($> 0.01 \text{ s}$) when a considerable MCR concentration has been formed. Due to the chain-length dependence of k_t^{ss} and the different reaction orders in SPR concentration of termination and backbiting, the influence of intramolecular transfer-to-polymer on $c_{\text{SPR}}(t)$ is negligible shortly after the laser pulse but becomes more and more important toward longer times. The impact of SPR loss via backbiting is more pronounced at high temperatures as $E_a(k_{\text{bb}})$ is well above $E_a(k_t^{\text{ss}})$ (see Table 10-1). Finally, it needs to be emphasized that the variation in signal-to-noise quality for the SPR traces in Figure 12-11 is due to the temperature dependence of spectrometer sensitivity (see Figure 5-8) as well as differences in the accumulations per data point and numbers of single trace co-additions (see Chapter 5.4.1).

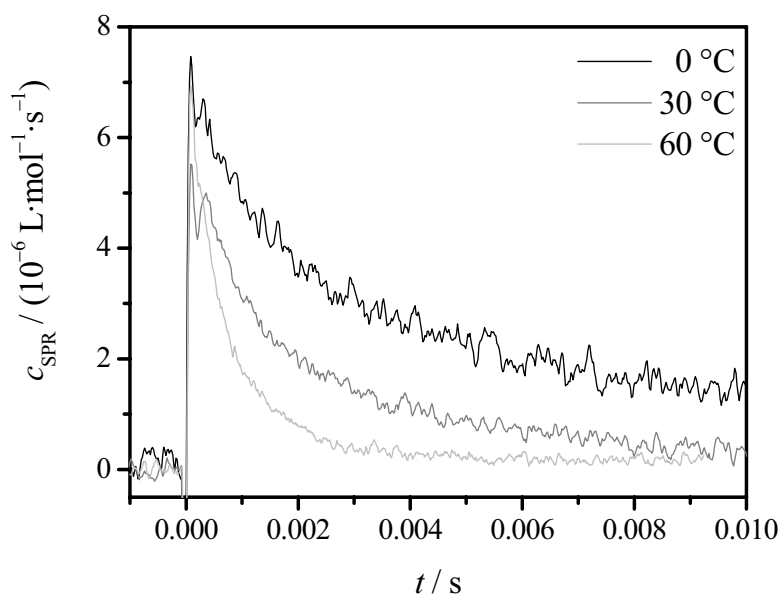


Figure 12-11: Variation of SPR concentration with time after SP initiation for polymerization of $1.52 \text{ mol}\cdot\text{L}^{-1}$ BA in toluene at 0, 30, and 60 °C (as indicated in the figure).

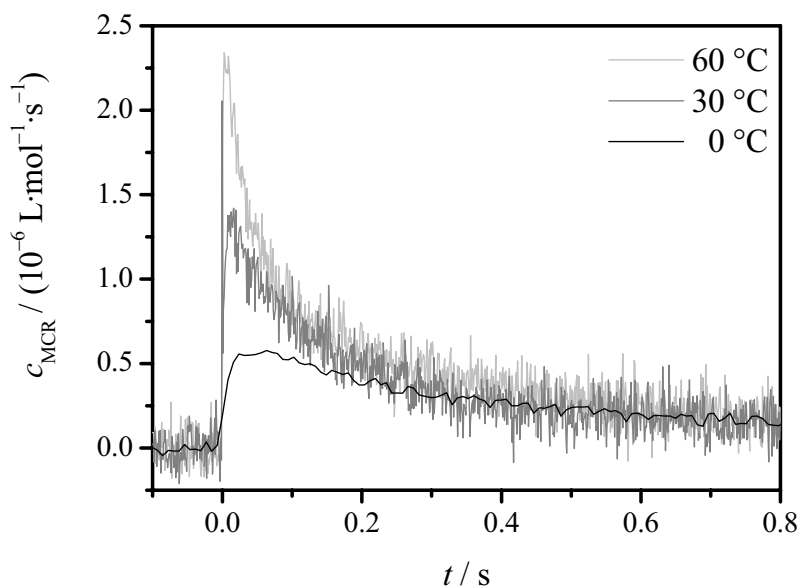


Figure 12-12: Variation of MCR concentration with time after SP-initiation for polymerization of $1.52 \text{ mol}\cdot\text{L}^{-1}$ of BA in toluene at 0, 30, and 60 °C (as indicated in the figure). The curve for 0 °C was measured at a lower time resolution compared to the traces at higher temperatures.

Figure 12-12 shows MCR traces measured during SP-PLP-induced polymerization of BA ($1.52 \text{ mol}\cdot\text{L}^{-1}$ in toluene) at 0, 30 and 60 °C. The slope of of the $c_{\text{MCR}}(t)$ curves during MCR build up increases toward higher temperature as k_{bb} grows. The maximum MCR concentration

strongly depends on temperature. Whereas only 5 % of the SPRs are transformed into MCRs at 0 °C, 25 % of the secondary radicals undergo intramolecular transfer-to-polymer rather than termination at 60 °C. This is, as mentioned above, due to the strong acceleration of k_{bb} toward higher T whereas k_t increases only to a minor extent. Comparison of Figure 12-12 with Figure 12-11 illustrates the enormous persistence of the MCR species compared to SPRs which is mainly caused by its low termination reactivity (see k_t^{ss} , k_t^{st} , and k_t^{tt} in Table 10-1). The maximum in $c_{MCR}(t)$ is reached when the rate of MCR formation by backbiting equals the sum of the rates of MCR loss by SPR-MCR termination, MCR-MCR termination and monomer addition to the tertiary radical. At relatively short times after the laser pulse SPR-MCR termination is dominant. However, as c_{SPR} rapidly decreases with time (see Figure 12-11) the impact of MCR-MCR termination and re-initiation reactions on the shape of $c_{MCR}(t)$ increases toward higher t . The more pronounced decrease in MCR concentration at higher temperatures illustrates the increase in k_t^{st} , k_t^{tt} and k_p^t toward higher T but is also partially due to the bimolecular nature of the termination step.

12.4.2 Strategy for kinetic analysis of $c_{SPR}(t)$ and $c_{MCR}(t)$ curves

The time evolution of SPR and MCR concentration after single pulse initiation was qualitatively discussed in the previous chapter. However, extraction of kinetic coefficients from these curves is not easily accomplished as already outlined in Chapter 10.4. The approach used in the thesis in hand was to separate termination and transfer kinetics. This was achieved by measuring $c_{SPR}(t)$ at low temperatures, i.e. at -40 °C. At this temperature backbiting is almost completely suppressed as is evident from x_{MCR} under PLP conditions being below 10 % (see Figure 12-6). In case of SP-PLP initiation, the influence of MCR formation should be even less pronounced, as there is no slow build-up of a pseudo-stationary tertiary radical concentration. The secondary radical concentration curves measured at -40 °C are evaluated by plotting $\log(c_R^0/c_{SPR}-1)$ vs. $\log(t)$. According to Eqs. (3-41) and (3-42), two linear regimes should be observed in such figure with the transition occurring at t_c (see Chapter 3.4.3). By linear fitting of the two ranges, α_s and $k_t^{ss}(1,1)$ as well as α_1 and k_t^0 are obtained. As discussed in Chapter 3.4.3, the chain-length dependence of k_t is not accurately assessed from the double-log plot but from non-linear curve fitting of the radical concentration traces to Eqs. (3-43) and (3-44). However, it turned out that regression of the

experimental data with Eq. (3-44) is rather insensitive and may result in even negative α_1 values.^[34] Thus, α_1 and t_c were determined from the double-log plot. The $c_{\text{SPR}}(t)$ data was subsequently cut at t_c and α_s as well as $k_t^{\text{ss}}(1,1)$ were evaluated by fitting the short-chain data to Eq. (3-43).

The so-obtained α_s , α_1 and i_c values were assumed to be independent of temperature. This hypothesis is reasonable because of the clear physical meaning behind these parameters (see Chapter 3.4.2). α_s describes the increase in hydrodynamic radius toward higher chain length. Chain stiffness is expected to decrease toward higher temperature which may facilitate coiling and thus results in a decrease of α_s . This effect is, however, assumed to be negligible. α_1 is governed by the shielding of the radical functionalities by polymeric chain segments within long-lived contact pairs. This parameter mainly depends on excluded volume effects which are governed by solvent quality.^[26] Also for α_1 no pronounced temperature dependence is thus anticipated. i_c is the chain length at which the transition between the short contact and long contact regime occurs. In other words, macroradicals start to entangle and form long-lived contact pairs from a chain length of i_c on. Thus, i_c is mainly governed by the dynamics of entanglement and disentanglement which should both be affected to similar extend by temperature resulting in an almost constant i_c .

The experimental $c_{\text{SPR}}(t)$ and $c_{\text{MCR}}(t)$ curves at temperatures between 0 and 60 °C were iteratively fitted by a comprehensive PREDICI model which explicitly accounts for the chain-length dependence of k_t^{ss} and k_t^{st} but is ostensibly identical to the one used within the previous chapters. The adjustable parameters within the model were $k_t^{\text{ss}}(1,1)$, $k_t^{\text{st}}(1,1)$, k_{bb} , k_p^t , and c_R^0 . The other rate coefficients were chosen according to Table 10-1 with the exception of k_i which was assumed to be $5 \cdot k_p^s$. The set of α_s , α_1 and i_c determined at low T was used to describe the chain-length dependence of k_t^{ss} with $k_t^{\text{ss}}(1,1)$ being the remaining fit-parameter. Within a previous data treatment, SPR-MCR termination was evaluated using $\alpha_s = 0.5$, $\alpha_1 = 0.27$ and $i_c = 20$ with $k_t^{\text{st}}(1,1)$ as adjustable parameter.^[202] However, it appears more reasonable to apply the same α_s and i_c values as were used for describing $k_t^{\text{ss}}(i,i)$ because both composite-model parameters are not expected to be significantly dependent on the position of the radical functionality within the chain. Moreover, α_1 is expected to decrease from 0.27 to 0.16 toward increasing degree of polymerization.^[26,128,129] Thus, an average value of 0.22 was implemented in the model rather than $\alpha_1 = 0.27$.

MCR-MCR termination does not significantly affect the SP-PLP-ESR traces for the reaction conditions examined within the thesis in hand. Thus, the chain-length-independent k_t^t contained in Table 10-1 was adopted for the model.

To finalize, the parameters which were adjusted by comparing experimental and simulated SPR and MCR traces are limited to c_R^0 , $k_t^{ss}(1,1)$, $k_t^{st}(1,1)$, k_{bb} , and k_p^t . This simplification allows for obtaining a one-to-one solution for the kinetic coefficients. $c_{SPR}(t)$ is particularly sensitive to the choice of c_R^0 and $k_t^{ss}(1,1)$. These two parameters were determined from the SPR trace using an estimate for $k_t^{st}(1,1)$, k_{bb} , and k_p^t . In the second step, the preliminary results for c_R^0 and $k_t^{ss}(1,1)$ were adopted in the model and $c_{MCR}(t)$ was simulated under refinement of $k_t^{st}(1,1)$, k_{bb} and k_p^t . These coefficients were subsequently used to re-evaluate the SPR trace for obtaining enhanced accuracy in $k_t^{ss}(1,1)$ and c_R^0 et cetera. Thus, final $k_t^{ss}(1,1)$ and c_R^0 as well as $k_t^{st}(1,1)$, k_{bb} and k_p^t values were obtained from cyclic refinement of the parameters on the basis of the experimental $c_{SPR}(t)$ and $c_{MCR}(t)$ curves.

12.4.3 Termination kinetics of BA at low temperatures

Figure 12-13 shows an ESR spectrum scanned during PLP-induced polymerization of BA in toluene at $-40\text{ }^\circ\text{C}$. The spectrum is mainly due to SPRs with the fraction of MCRs being below 10 %, as can be seen from the weak line around 3350 G. The SPR lines which strongly oscillate with the applied LPRR are in close agreement with the associated simulated spectra shown in Figure 12-1 and Figure 12-2, respectively.

The evaluation of an SPR trace via a $\log(c_R^0/c_{SPR}-1)$ vs. $\log(t)$ plot is exemplarily shown in Figure 12-14 for polymerization of $1.52\text{ mol}\cdot\text{L}^{-1}$ BA in toluene at $-40\text{ }^\circ\text{C}$. The data points at very short times (circles, segment I) were not used for regression as in this time region the approximation $i = k_p \cdot c_M \cdot t$ is not valid (see Chapter 3.4.3) and the data may additionally be affected by the influence of the laser pulse and initiator-derived radicals (see Chapter 5.4.3). Linear regression of the short-chain (crosses, segment II) and long-chain regime (crosses, segment IV) results in $\alpha_s \approx 0.56$ and $\alpha_l \approx 0.25$. From the crossing point of the two straight lines, $i_c = 30 \pm 8$ is obtained according to Eq. (3-8). The chain-length range of $25 < i < 50$ (circles, segment III) where the transition between the slopes $(1-\alpha_s)$ and $(1-\alpha_l)$ occurs was omitted from linear regression.

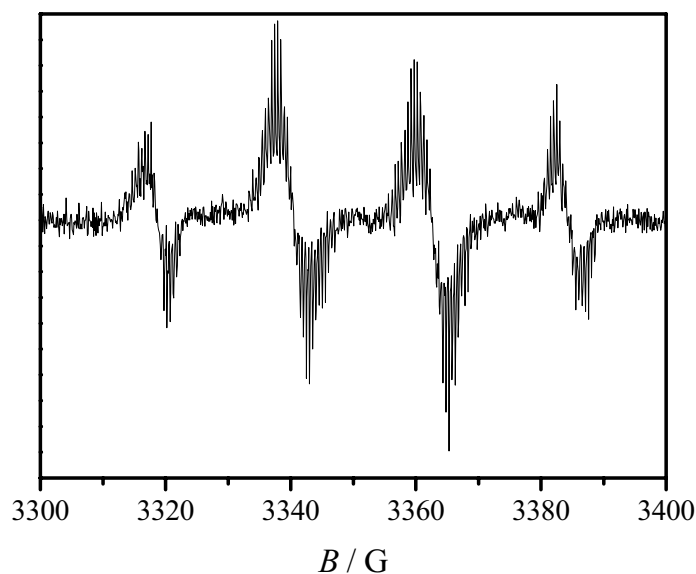


Figure 12-13: ESR spectrum recorded during PLP-induced polymerization of BA ($1.52 \text{ mol}\cdot\text{L}^{-1}$ in toluene) at -40°C and an LPRR of 20 Hz.

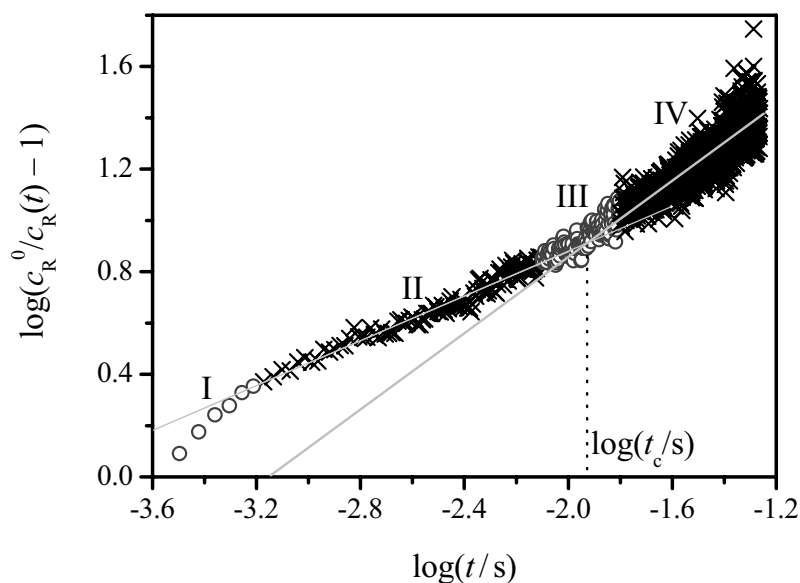


Figure 12-14: Analysis of BA-SPR traces according to Eqs. (3-41) and (3-42). SP-PLP-ESR was carried out for polymerization of $1.52 \text{ mol}\cdot\text{L}^{-1}$ of BA in toluene at -40°C . Data at very short times (corresponding to $i < 3$) indicated by the circles were not used for regression.

Figure 12-15 shows the refined analysis of the short-chain regime of the SPR trace from Figure 12-14. The regression according to Eq. (3-43) within the entire time interval of $0 < t < t_c$ yields $\alpha_s = 0.85$ and $k_t^{ss}(1,1) = 1.65 \cdot 10^8 \text{ L}\cdot\text{mol}^{-1}\cdot\text{s}^{-1}$. Only the very first one or two

data points were omitted, as they refer to the increase of the $c_{\text{SPR}}(t)$ curve which is not captured by Eq. (3-43). The higher power-law exponent compared to the evaluation by Eq. (3-41) results from the more accurate description of the chain length as detailed in Chapter 3.4.3. Regression of the long-chain regime by Eq. (3-44) did not result in reasonable values for α_1 .

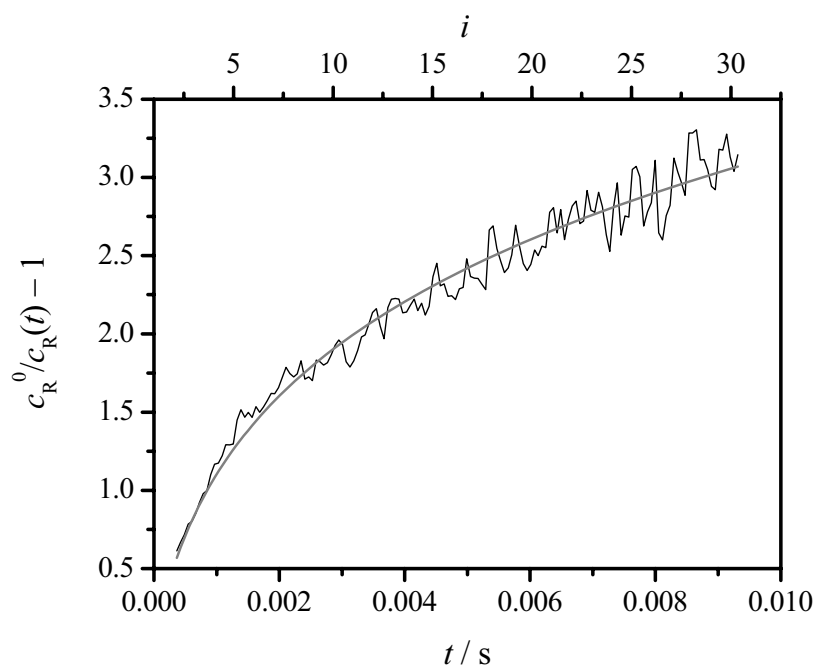


Figure 12-15: Analysis of the short-chain regime of the SPR trace from Figure 12-14 according to Eq. (3-43).

The SPR traces measured during SP-PLP experiments of BA ($1.52 \text{ mol}\cdot\text{L}^{-1}$ in toluene) at temperatures above $-40 \text{ }^\circ\text{C}$ were also analyzed by Eq. (3-43). The so-obtained temperature dependence of α_s is shown as squares in Figure 12-16. A pronounced decrease of α_s toward higher temperature is observed from $0 \text{ }^\circ\text{C}$ on. Also included in Figure 12-16 are the results from fitting simulated SPR traces to Eq. (3-43). The simulations were carried out using the final set of kinetic parameters collated in Table 12-1. Thus, a constant α_s of 0.85 was applied within all simulations. Nevertheless, a very similar decrease of the (apparent) power-law exponent toward higher T is obtained from the simulated data when evaluation according to Eq. (3-43) is processed. This indicates that the experimentally observed drop in α_s is mainly or even solely due to the influence of MCR build-up on the SPR traces. SPR loss by backbiting was not included in the derivation of Eq. (3-43). This process results in an

apparent increase of k_t^{ss} at longer times after the laser pulse thus reducing α_s . Moreover, the good overlap of experimental and simulated data in Figure 12-16 up to 40 °C illustrates the accuracy of the final converged rate coefficients. It is also demonstrated that the influence of backbiting on α_s determination at -40 °C is absolutely negligible.

It needs to be noted that the α_s from SP-PLP-ESR is well below $\alpha_s = 1.24$ obtained via SP-PLP-NIR-RAFT for BA.^[38] The potential origin of this difference will be discussed in Chapter 13.3.

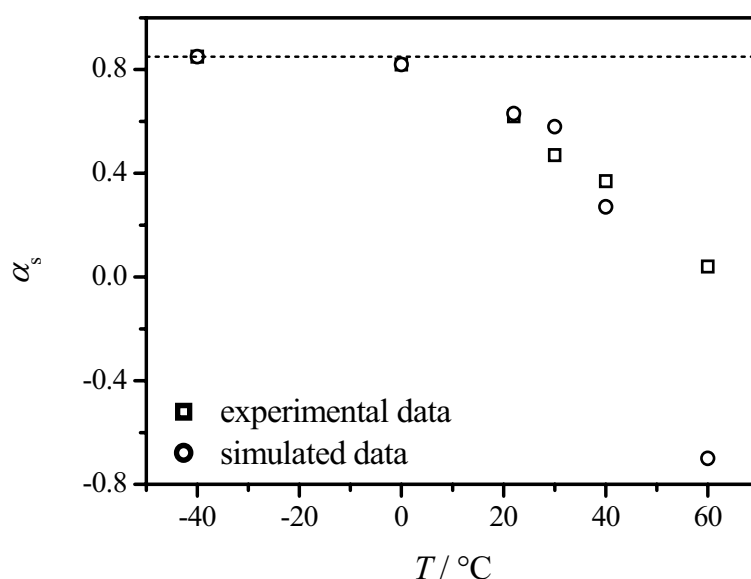


Figure 12-16: Temperature dependence of α_s obtained from analysis of the short-chain regime by Eq. (3-43). The circles indicate experimental α_s values for polymerization of 1.52 mol·L⁻¹ BA in toluene. The squares were obtained from fitting simulated SPR traces. The simulations were carried out using the kinetic coefficients collated in Table 12-1. A temperature independent α_s of 0.85 was thus applied (indicated by the dotted line).

It is not self-evident that also α_1 is obtained with high accuracy from fitting experimental SPR traces recorded at low T to Eq. (3-42). It was pointed out by Buback et al.^[34] that application of Eq. (3-42) leads to an overestimation of α_1 . Moreover, though the influence of backbiting is relatively small at short times after the pulse, it becomes increasingly important toward longer times due to its unimolecular nature. Figure 12-17 shows an experimental $c_{\text{SPR}}(t)$ curve recorded during polymerization of BA (1.52 mol·L⁻¹ in toluene). Also included are simulated SPR traces which were modeled by means of the final converged kinetic parameters collated in Table 12-1. The curve indicated by the thick full line was simulated with the full kinetic scheme whereas, for the dotted line, $k_{\text{bb}} = 0$ was used. It was assumed for the simulation that

α_1 was not 0.25 as determined experimentally but set to 0.16, as theoretically proposed. It is clearly seen that the simulation without MCR build up overestimates c_{SPR} at longer times after the laser pulse. However, perfect agreement between experiment and simulation is obtained when the full kinetic scheme is used. Accordingly, the simulation of $c_{\text{SPR}}(t)$ with $\alpha_1 = 0.25$ under consideration of MCR formation should yield an underestimation of SPR concentration in the long-chain regime. Thus, $\alpha_1 = 0.16$ was adopted for the simulations of the SPR and MCR traces at temperatures between 0 and 60 °C.

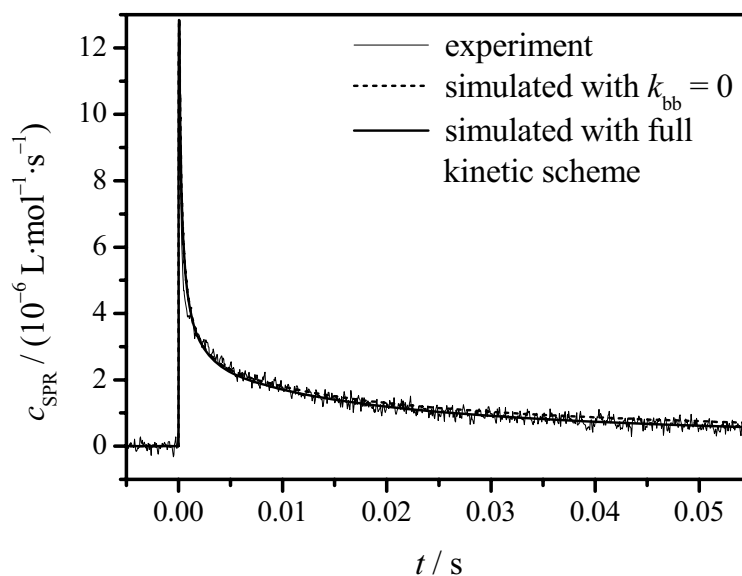


Figure 12-17: Comparison between simulated and experimental SPR (thin full line) traces for polymerization of BA at -40 °C. The rate coefficients collated in Table 12-1 were used for modeling. Simulations were carried out with the full kinetic scheme (thick full line) and for $k_{\text{bb}} = 0$ (dashed line).

12.4.4 Termination and transfer kinetics of BA between 0 and 60 °C

As outlined in Chapter 12.4.2, the termination and transfer kinetics of BA polymerization at 0 to 60 °C was analyzed via iterative parameter refinement within a comprehensive PREDICI model aimed at overlapping experimental and simulated SPR and MCR traces. The composite-model parameters for $k_t^{\text{ss}}(i,i)$ of $\alpha_s = 0.85$, $\alpha_1 = 0.16$, and $i_c = 30$ were assumed to be constant. It goes without saying that c_{R}^0 and $k_t^{\text{ss}}(1,1)$ can be determined with good accuracy from $c_{\text{SPR}}(t)$. c_{R}^0 is estimated from extrapolation of the decreasing part of the SPR trace to $t = 0$. $k_t^{\text{ss}}(1,1)$ is subsequently adjusted to fit the curvature of SPR concentration vs. time,

mainly at relatively short times after the pulse before backbiting becomes dominant. $k_t^{st}(1,1)$, k_{bb} and k_p^t are assessed from the MCR trace. The $c_{MCR}(t)$ curves are particularly sensitive toward k_{bb} and $k_t^{st}(1,1)$ at relatively short times after the laser pulse, that is up to about 0.2 s. The influence of k_p^t , or more precisely the ratio of k_{bb} to k_p^t , becomes more important toward longer times after SP initiation. An illustration of the sensitivity of parameter estimation from $c_{MCR}(t)$ curves is contained in the diploma thesis of Barth.^[202]

The change in SPR and MCR concentration after single pulse initiation for polymerization of $1.52 \text{ mol}\cdot\text{L}^{-1}$ of BA in toluene at $30 \text{ }^\circ\text{C}$ is shown in Figure 12-18. The grey lines are kinetic fits to the experimental data which were obtained as detailed above. The simulations afford for an excellent representation of both traces with a single set of kinetic parameters.

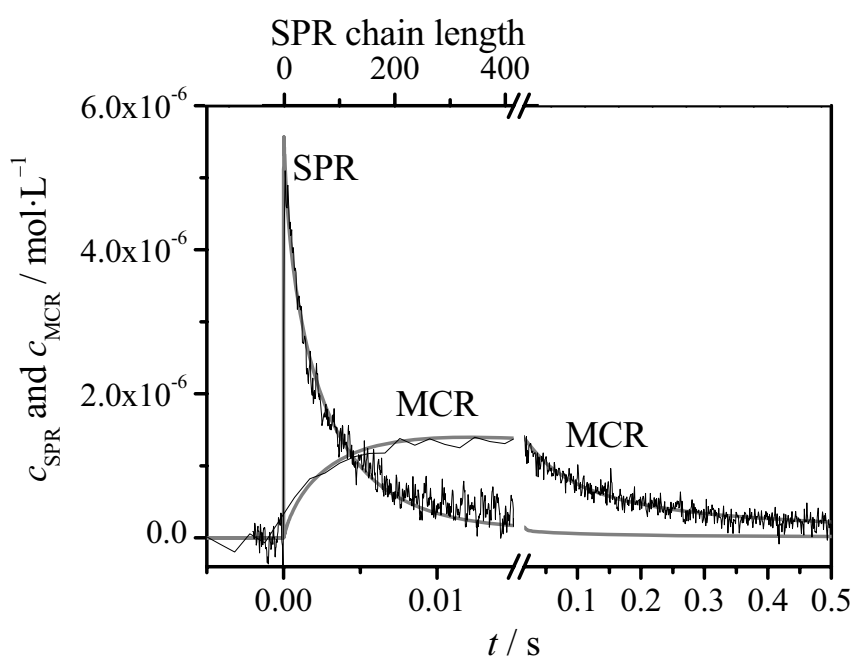


Figure 12-18: Change in secondary propagating radical (SPR) and midchain radical (MCR) concentration after single pulse initiation at time $t=0$ (black lines) monitored by time-resolved ESR spectroscopy during polymerization of $1.52 \text{ mol}\cdot\text{L}^{-1}$ BA in toluene at $30 \text{ }^\circ\text{C}$. The grey lines represent kinetic simulations of the data (see text).

The temperature dependence of $k_t^{ss}(1,1)$ for polymerization of $1.52 \text{ mol}\cdot\text{L}^{-1}$ of BA in toluene is shown in Figure 12-19. The corresponding Arrhenius parameters are $E_a(k_t^{ss}(1,1)) = (8.4 \pm 0.7) \text{ kJ}\cdot\text{mol}^{-1}$ and $A(k_t^{ss}(1,1)) = (1.3 \pm 0.4) \cdot 10^{10} \text{ L}\cdot\text{mol}^{-1}\cdot\text{s}^{-1}$. The temperature dependence of the termination rate of two monomeric radicals should be entirely governed by $\eta^{-1}(T)$ as R_c and $r_{s,i}$ can be assumed constant (see Eqs. (3-19) and (3-20)). In

fact, the temperature dependence of the fluidity of toluene, which is the main component of the reaction solution, may be expressed in terms of an activation energy of $8.9 \text{ kJ}\cdot\text{mol}^{-1}$.^[195,293] Thus, the result for $E_a(k_t^{ss}(1,1))$ is in excellent agreement with the theoretically expected value based on the center-of-mass diffusion controlled nature of primary radical termination. A thorough discussion of the termination rate kinetics of acrylate and methacrylate monomers is given in Chapter 14.

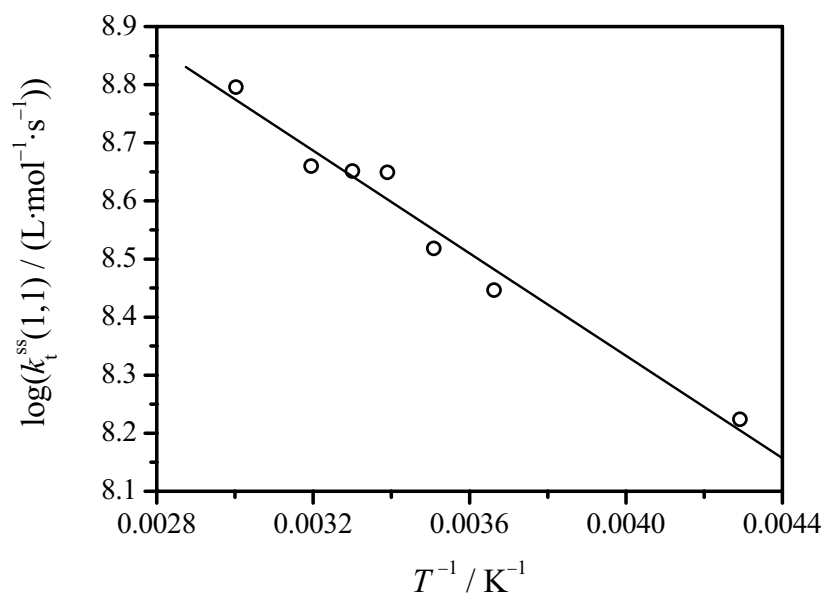


Figure 12-19: Temperature dependence of $k_t^{ss}(1,1)$ for polymerization of $1.52 \text{ mol}\cdot\text{L}^{-1}$ of BA in toluene.

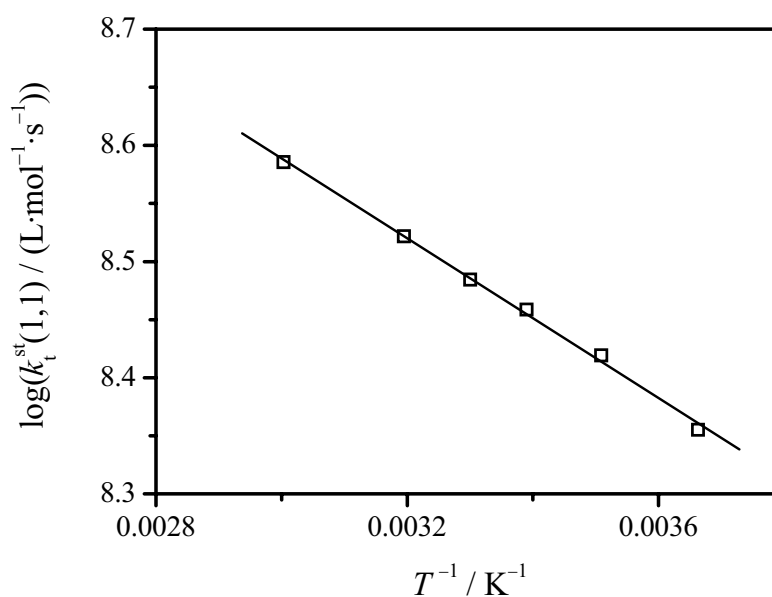
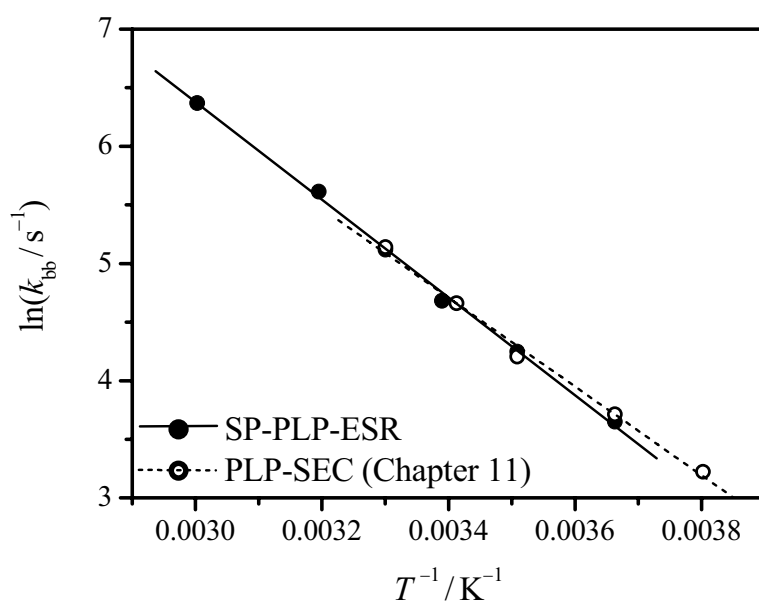


Figure 12-20: Temperature dependence of $k_t^{st}(1,1)$ for polymerization of $1.52 \text{ mol}\cdot\text{L}^{-1}$ of BA in toluene.

The variation of $k_t^{\text{st}}(1,1)$ with temperature for polymerization of $1.52 \text{ mol}\cdot\text{L}^{-1}$ of BA in toluene is depicted in Figure 12-20. The corresponding Arrhenius parameters are $E_a(k_t^{\text{st}}(1,1)) = (6.6 \pm 0.2) \text{ kJ}\cdot\text{mol}^{-1}$ and $A(k_t^{\text{st}}(1,1)) = (4.2 \pm 0.6) \cdot 10^9 \text{ L}\cdot\text{mol}^{-1}\cdot\text{s}^{-1}$. As expected for a center-of-mass diffusion controlled rate coefficient, $E_a(k_t^{\text{st}}(1,1))$ is again relatively close to $E_a(\eta^{-1})$. The $k_t^{\text{st}}(1,1)$ values are less than a factor of 2 below the $k_t^{\text{ss}}(1,1)$ data shown Figure 12-19. However, a more pronounced difference between $k_t^{\text{ss}}(i,i)$ and $k_t^{\text{st}}(i,i)$ is established for longer chain lengths due to the higher α_1 for SPR-MCR termination. Furthermore, it needs to be stressed that $k_t^{\text{st}}(1,1)$ is a hypothetical quantity as MCRs cannot be formed via backbiting, i.e. via 1,5-hydrogen shift, for chain lengths below 4.^[288]

Figure 12-21 shows the Arrhenius-type plots of k_{bb} for polymerization of BA determined via SP-PLP-ESR (filled circles, full line) and via PLP-SEC under wide variation of LPRRs (open circles, dashed line), respectively. Both data sets, obtained from different experimental approaches, closely overlap which provides strong evidence for the high accuracy of both techniques. Moreover, this at least partially imparts benchmark character to the k_{bb} data. The Arrhenius parameters from SP-PLP-ESR of $E_a(k_{\text{bb}}) = (34.7 \pm 0.8) \text{ kJ}\cdot\text{mol}^{-1}$ and $A(k_{\text{bb}}) = (1.6 \pm 0.7) \cdot 10^8 \text{ s}^{-1}$ are consequently close to the ones collated in Table 10-1. Linear fitting of the combined $\ln(k_{\text{bb}})$ vs. T^{-1} data results in $E_a(k_{\text{bb}}) = (33.3 \pm 0.7) \text{ kJ}\cdot\text{mol}^{-1}$ and $A(k_{\text{bb}}) = (9.3 \pm 2.9) \cdot 10^7 \text{ s}^{-1}$. The associated 95 % joint confidence ellipsoid is depicted in lower part of Figure 12-21.



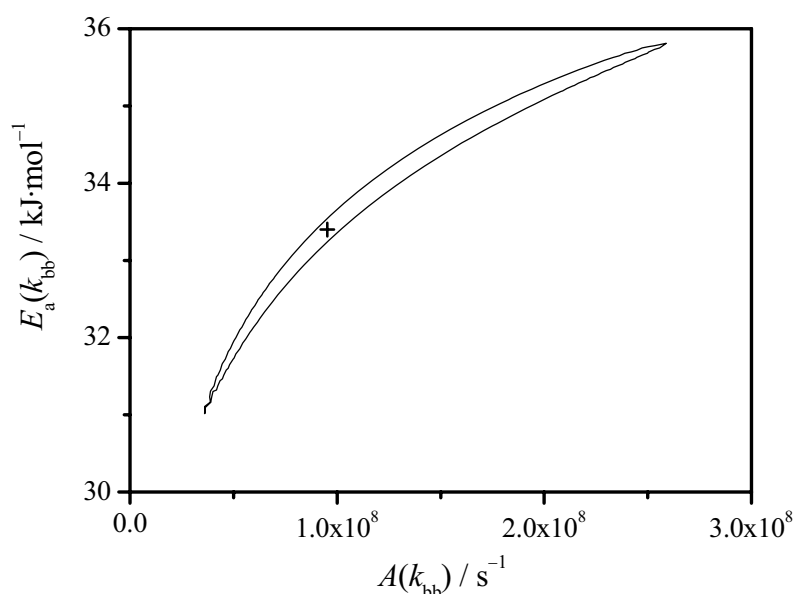


Figure 12-21: Arrhenius-type plot of k_{bb} for polymerization of BA determined via SP-PLP-ESR (filled circles, full line) as well as via PLP-SEC under wide variation of LPRRs (open circles, dashed line). The 95 % JCI associated with the combined k_{bb} data for polymerization BA at ambient pressure is depicted in the lower part.

The temperature dependencies of k_p^\ddagger for polymerization of BA determined via SP-PLP-ESR (filled triangles, full line) and via PLP-SEC (open triangles, dashed line) are shown in Figure 12-22. The activation energy assessed by SP-PLP-ESR ($E_a(k_p^\ddagger) = (28.3 \pm 1.7) \text{ kJ} \cdot \text{mol}^{-1}$) is, under consideration of experimental error, identical to the one from the PLP-SEC studies detailed in Chapter 11 (see Table 10-1). However, the pre-exponential factor of $A(k_p^\ddagger) = (9.2 \pm 6.3) \cdot 10^5 \text{ L} \cdot \text{mol}^{-1} \cdot \text{s}^{-1}$ is slightly lower though still within the margins of uncertainty. This results from an average difference between the experimental k_p^\ddagger from the two techniques of about 30 %. The reason for this discrepancy is not clear but may for example be related to SEC calibration or to uncertainties in conversion detection (and thus to c_M) within the SP-PLP-ESR studies. It is not possible to judge which experimental technique allows for better k_p^\ddagger evaluation, as both approaches have some shortcomings. Fitting the combined k_p^\ddagger data with a constant average activation energy of $E_a(k_p^\ddagger) = 28.6 \text{ kJ} \cdot \text{mol}^{-1}$ yields $A(k_p^\ddagger) = 1.17 \cdot 10^6 \text{ L} \cdot \text{mol}^{-1} \cdot \text{s}^{-1}$.

The final set of kinetic coefficients determined via SP-PLP-ESR on solutions of $1.52 \text{ mol} \cdot \text{L}^{-1}$ BA in toluene is collated in the upper part of Table 12-1. This data, together with the coefficients in the lower part of Table 12-1, allows for excellent representation of the

experimental $c_{\text{SPR}}(t)$ and $c_{\text{MCR}}(t)$ traces measured at temperatures of 0 to 60 °C. Moreover, k_{bb} and k_{p}^{t} were determined by two independent experimental approaches which, as mentioned above, imparts partial benchmark character to this data though the rate coefficients were collected within the same research group. The Arrhenius parameters from the combined sets of kinetic coefficients are contained in Table 12-2 and may nevertheless be considered highly reliable.

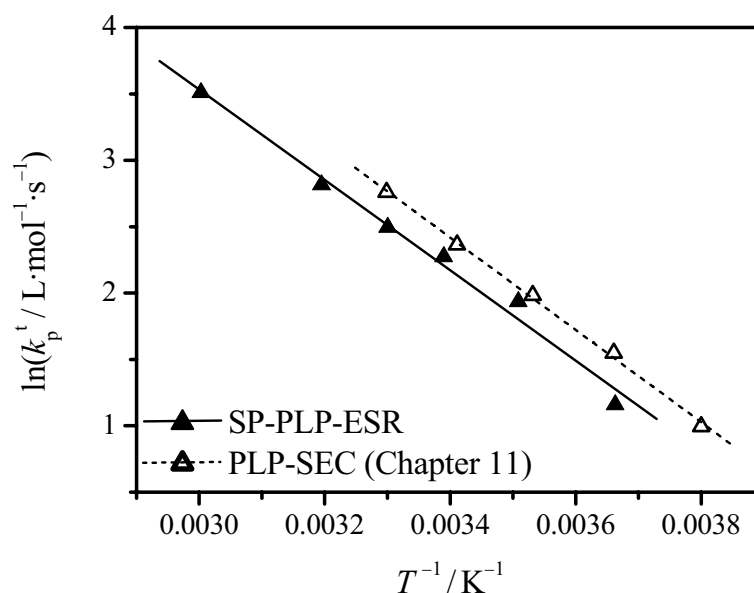


Figure 12-22: Arrhenius-type plot of k_{p}^{t} for polymerization of BA determined by SP-PLP-ESR (filled triangles, full line) as well as PLP-SEC under wide variation of LPRRs (open triangles, dashed line).

Table 12-1: Collection of kinetic parameters determined for polymerization of BA in toluene via SP-PLP-ESR. The lower part of the table collates further coefficients used for simulating the SPR and MCR traces (estimated or taken from Table 10-1).

	composite model parameter	pre-exponential factor $\text{L}\cdot\text{mol}^{-1}\cdot\text{s}^{-1}$ or s^{-1}	activation energy $\text{kJ}\cdot\text{mol}^{-1}$
$\alpha_{\text{s}}(k_{\text{t}}^{\text{ss}})$	0.85	—	—
$\alpha_{\text{i}}(k_{\text{t}}^{\text{ss}})$	0.16	—	—
$i_{\text{c}}(k_{\text{t}}^{\text{ss}})$	30	—	—
$k_{\text{t}}^{\text{ss}}(1,1)$	—	$1.3\cdot 10^{10}$	8.4

$k_t^{st}(1,1)$	–	$4.2 \cdot 10^9$	6.6
k_{bb}	–	$1.6 \cdot 10^8$	34.7
k_p^t	–	$9.2 \cdot 10^5$	28.3
$\alpha_s(k_t^{st})$	0.85	–	–
$\alpha_1(k_t^{st})$	0.22	–	–
$i_c(k_t^{st})$	30	–	–
$\langle k_t^{tt} \rangle$	–	$9.0 \cdot 10^6$	5.6
k_p^s	–	$2.21 \cdot 10^7$	17.9
k_i	–	$1.11 \cdot 10^8$	17.9
$k_{tr,M}^s$	–	$2.9 \cdot 10^5$	32.6
$k_{tr,M}^t$	–	$2.0 \cdot 10^5$	46.1

Table 12-2: Arrhenius parameters of k_{bb} and k_p^t for BA polymerization from combined data of independent experimental approaches.

	pre-exponential factor $L \cdot mol^{-1} \cdot s^{-1}$ or s^{-1}	activation energy $kJ \cdot mol^{-1}$	techniques
k_{bb}	$9.3 \cdot 10^7$	33.3	SP-PLP-ESR and PLP-SEC
k_p^t	$1.2 \cdot 10^6$	28.6	SP-PLP-ESR and PLP-SEC

13 Kinetics of Acrylic Acid Polymerization

Products from homo- and copolymerizations of AA in aqueous solution are of eminent technical importance. Thus, there is urgent need for establishing a comprehensive mechanistic description of AA polymerization based on kinetic rate laws with accurate coefficients. However, the kinetics of AA polymerization in aqueous solution is extremely complex as there is simultaneous occurrence of MCR formation via backbiting^[41,52] and strong solvent effects on the individual rate coefficients^[67–69,270]. Consequently, it is recommendable to separate influences from MCR build-up and solvent effects based on the knowledge obtained from studies into systems showing just one of the two features.

The influence of aqueous solvent composition on the propagation and termination kinetics of MAA and NVP (which are both not susceptible to backbiting reactions) was discussed in Chapters 6 to 9. It was shown that k_p for the non-ionized monomers strongly increases toward higher solvent content. This observation is in agreement with results from PLP-SEC on AA^[68] which were carried out at high LPRRs. The so-obtained k_p^{app} values should hence be close to k_p^s , as was shown by simulation of PLP for BA (see ref.^[13] and Chapter 10.3). Moreover, it has been found that k_p for both, aqueous MAA and NVP polymerization, increases toward higher degrees of monomer-to-polymer conversion due to changes in the solvent composition of the intra-coil environment for propagation. Recent investigations into the propagation kinetics of AA polymerization in aqueous solution with pre-mixed poly(AA) or propionic acid showed that also k_p^s of non-ionized AA increases toward higher X_{virtual} , provided that long-chain polymer is formed.^[271]

Not only the propagation, but also the termination kinetics of MAA and NVP is strongly dependent on monomer concentration in water. The solvent effects are very similar to the ones observed for non-aqueous solution polymerizations (see Chapters 8 and 9 as well as ref.^[96]), i.e. the solvent content strongly affects k_t in the TD-controlled regime whereas only a moderate acceleration of $\langle k_{\text{SD}} \rangle$ toward lower monomer concentration is seen. However, the chain-length-averaged low-conversion k_t values determined by Kukučkova showed a pronounced increase toward lower initial AA concentration in water.^[270]

The theoretical considerations in Chapters 10.3 and 10.4 illustrated that not only PLP-SEC is influenced by MCR formation but also SP-PLP-NIR which has been used for studying k_t of

AA. It was shown that k_t^{app} calculated by implementing k_p^s into k_t/k_p may strongly overestimate the actual k_t^{eff} and even k_t^{ss} . This effect is reduced when k_p^{eff} is used. k_p^{eff} may be deduced from k_p^s provided that x_{MCR} is known. The fraction of MCRs may be obtained from PLP-SEC experiments conducted under a wide variation of LPRRs (see Chapter 11). However, even with implementation of k_p^{eff} , the k_t^{app} values still exceed k_t^{eff} especially at low temperatures and low monomer concentrations.

In principle, SP-PLP-ESR should represent the perfect tool for studies into termination and transfer kinetics of AA. However, such experiments are strongly hampered by the high polymerization rate of AA in water and, more importantly, the strong solution polarity which significantly reduces ESR sensitivity.

Chain-length-dependent termination rate coefficients for AA polymerization may be determined by SP-PLP-NIR-RAFT, a technique which has previously been successfully applied for studying $k_t(i,i)$ of acrylic acid esters.^[37–39]

In the first sections of this chapter, PLP-SEC experiments on AA polymerization under variation of LPRR are outlined. The so-obtained x_{MCR} and k_{bb}/k_p^t data are subsequently used for re-evaluation of $\langle k_t^{\text{app}} \rangle$ for AA polymerization. In the last section, SP-PLP-NIR-RAFT data for polymerization of 40 wt.% AA in water at 40 °C and 2000 bar are presented and discussed.

The investigations detailed in this chapter have been partially carried out in cooperation with Dr. Igor Lacík and Dr. Silvia Kukučková. Aspects of the work have been published in refs.^[52,270]

13.1 Determination of x_{MCR} and k_{bb}/k_p^t by PLP-SEC experiments

The polymerization of $1.35 \text{ mol}\cdot\text{L}^{-1}$ AA in aqueous solution has been investigated at 6 °C via PLP-SEC using a wide range of LPRRs. The so-obtained dependence of k_p^{app} on LPRR is illustrated by the semi-log plot in Figure 13-1. In perfect agreement with the prediction by Nikitin et al.^[55] and the corresponding BA data presented in Chapter 11, a sigmoidal decrease of k_p^{app} toward lower LPRR is seen. In the range of LPRRs from 100 to 60 Hz, k_p^{app} is diminished by about 10 %. At LPRRs below 60 Hz, a more than twofold decrease of k_p^{app} is observed until, at approximately 30 Hz, k_p^{app} starts to level off again. The limiting values at high and low LPRRs are assigned to k_p^s and k_p^{eff} , respectively. The upper dashed line in

Figure 13-1 reflects the arithmetic mean of the two data points for 100 Hz and the lower dashed line is determined by the arithmetic mean of the data for 10 and 20 Hz. The k_p^s value resulting from the upper dashed line is $99\,750\text{ L}\cdot\text{mol}^{-1}\cdot\text{s}^{-1}$ which number is in close agreement with k_p values determined for similar AA concentrations in aqueous solution at $6\text{ }^\circ\text{C}$. The literature values are reported to be $91\,750\text{ L}\cdot\text{mol}^{-1}\cdot\text{s}^{-1}$ for an AA concentration of $1.54\text{ mol}\cdot\text{L}^{-1}$ and $110\,000\text{ L}\cdot\text{mol}^{-1}\cdot\text{s}^{-1}$ for an AA concentration of $0.7\text{ mol}\cdot\text{L}^{-1}$.^[68]

The effective propagation rate coefficient of $34\,490\text{ L}\cdot\text{mol}^{-1}\cdot\text{s}^{-1}$ is obtained from the 10 and 20 Hz data. Implementing the so-obtained k_p^s and k_p^{eff} values into Eq. (3-18) yields $x_{\text{MCR}} = 65 \pm 3\%$ as the fraction of MCRs under the selected polymerization conditions.

Upon neglecting the change in MCR concentration due to termination and chain transfer, x_{MCR} may be expressed by Eq. (10-10). As detailed in Chapter 10.3, ignoring termination during the dark-time period in between two laser pulses should not invalidate Eq. (10-10), as the termination product will show up as a low molecular weight shoulder of the PLP peak, whereas k_p^{eff} is obtained from the high molecular weight range of the SEC trace.

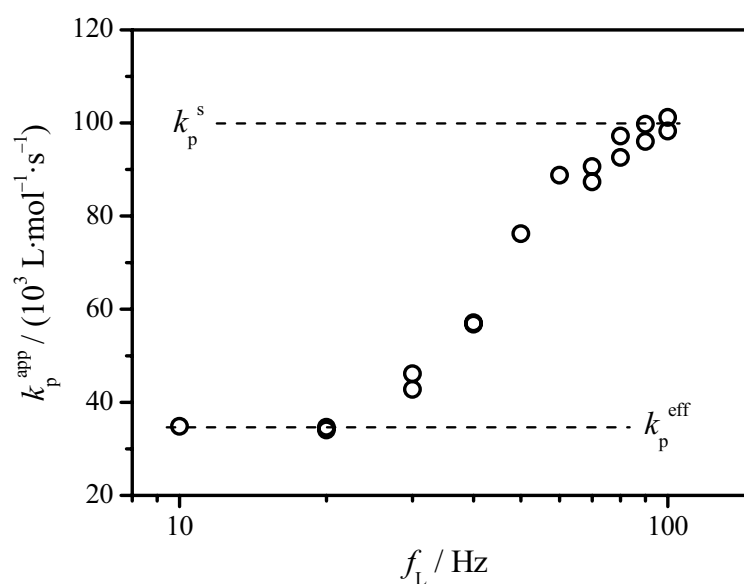


Figure 13-1: Dependence of k_p^{app} on LPRR for PLP-induced polymerizations of $1.35\text{ mol}\cdot\text{L}^{-1}$ AA in aqueous solution at $6\text{ }^\circ\text{C}$ and ambient pressure. The dashed lines indicate the limiting values of k_p^{eff} and k_p^{SPR} , respectively.

Rearrangement of Eq. (10-10) yields the simple expression given in Eq. (13-1), which allows for deducing the coupled parameter $k_{\text{bb}}/k_p^{\dagger}$:

$$\frac{k_{bb}}{k_p^t} = \left(\frac{x_{MCR}}{1 - x_{MCR}} \right) \cdot c_M \quad (13-1)$$

For an average concentration of $1.284 \text{ mol}\cdot\text{L}^{-1}$ acrylic acid (which takes AA conversion during PLP into account) in aqueous solution at 6°C and ambient pressure, the coupled parameter is $k_{bb}/k_p^t = 2.4 \pm 0.3 \text{ mol}\cdot\text{L}^{-1}$.

Knowledge of $b\sigma$ would be required for estimation of individual k_{bb} and k_p^t values according to the procedure detailed in Chapter 11. However, k_t^{ss} , k_t^{st} and k_t^{tt} need to be known for evaluation of $b\sigma$ via comparison of experimental and simulated MWDs. As these rate coefficients are so far not accessible for AA, no separate k_{bb} and k_p^t values were determined from the dependence of k_p^{app} on LPRR.

13.2 Re-consideration of $\langle k_t^{app} \rangle$ data for AA polymerization in water

Kukučkova studied the termination kinetics of AA polymerization in water within wide ranges of experimental conditions via SP-PLP-NIR.^[270] However, the obtained $\langle k_t^{app} \rangle$ data showed a strong acceleration of termination rate toward lower initial AA concentration. In fact, the $\langle k_t \rangle$ values for 5 wt.% of AA in D_2O at 25°C and 2000 bar are about $2 \cdot 10^9 \text{ L}\cdot\text{mol}^{-1}\cdot\text{s}^{-1}$ which is higher than typical values for $k_t(1,1)$ of alkyl acrylates under ostensibly the same conditions and may even be close to the diffusion limit.^[38,39]

A huge set of $\langle k_t^{app} \rangle$ data was collected for polymerizations of AA at 25°C , ambient pressure and initial AA concentrations of 10 to 60 wt.%.^[270] The dependence of $\langle k_t^{app} \rangle$ on fractional conversion for polymerization of AA in water at 25°C , 50 bar and different initial monomer concentrations is shown in Figure 13-2. The relatively low temperature of 25°C was selected as up to this temperature k_p data from PLP-SEC could be obtained. A pressure of 50 bar was used to fix the internal cell within the high pressure cell and to promote heat transfer. The differences in the kinetic coefficients for 50 bar and ambient pressure are assumed to be negligible.^[16] $\langle k_t^{app} \rangle$ in Figure 13-2A was calculated by decoupling k_t/k_p via a conversion independent k_p^s from PLP-SEC which, however, changes with initial monomer content in water. The so-obtained average $\langle k_t^{app} \rangle$ data increase by a factor of 36 between initial AA concentrations of 60 and 10 wt.% as well as by a factor of 13 between 60 and 20 wt.% of

monomer in water. This acceleration strongly exceeds the monomer-concentration induced changes in $\langle k_{SD} \rangle$ observed for MAA and NVP. In fact, an increase of $\langle k_{SD} \rangle$ by less than a factor of 2.5 between 60 and 20 wt.% of NVP in D₂O was found. The termination rate data was re-evaluated by implementing estimates of k_p^{eff} from Eq. (3-18) with the changes in k_p^s and x_{MCR} with initial monomer concentration and conversion being explicitly considered. The generalized k_p^s correlation was obtained in an analogous way as Eq. (8-5) for MAA and Eq. (9-2) for NVP, i.e. via fitting the k_p^s vs. w_{AA}^0 data from ref.^[68] with subsequent introduction of the relation $w_{\text{AA}} = w_{\text{AA}}^0 \cdot (1-X)/(1-w_{\text{AA}}^0 \cdot X)$. The dependence of x_{MCR} on initial AA concentration and conversion was estimated using the single k_{bb}/k_p^t value determined within Chapter 13.1. The coupled parameter was extrapolated to 25 °C using $E_a(k_{\text{bb}}/k_p^t) = E_a(k_{\text{bb}}) - E_a(k_p^t)$ with the associated activation energies for BA polymerization (see Table 12-2). x_{MCR} can finally be estimated from a transformed version of Eq. (10-10)

$$x_{\text{MCR}} = \left(1 + \frac{k_p^t}{k_{\text{bb}}} \cdot c_{\text{AA}} \right)^{-1} \quad (13-2)$$

with

$$c_{\text{AA}} = (1 - X) \cdot c_{\text{AA}}^0 \quad (13-3)$$

It needs to be emphasized that the calculation of k_p^{eff} from Eq. (3-18) in combination with Eqs. (13-2) and (13-3) is based on the rough assumption of a monomer concentration independence of k_{bb}/k_p^t . The re-evaluated $\langle k_t^{\text{app}} \rangle$ values are depicted in Figure 13-2B. The termination rate coefficients are strongly reduced compared to the ones in Figure 13-2A, especially for the low initial monomer concentrations where x_{MCR} is high. For example, the average $\langle k_t^{\text{app}} \rangle$ value for an initial AA content of 10 wt.% is diminished by about half an order of magnitude. The difference between $\langle k_t^{\text{app}} \rangle$ for 20 and 60 wt.% decreased to a factor of 9 which is, however, still much higher than observed for MAA and NVP. This effect may be caused by a slow equilibration velocity between the SPR and MCR species resulting in an artificial increase of $\langle k_t^{\text{app}} \rangle$ especially for systems with low monomer contents (see Chapter 10.4).

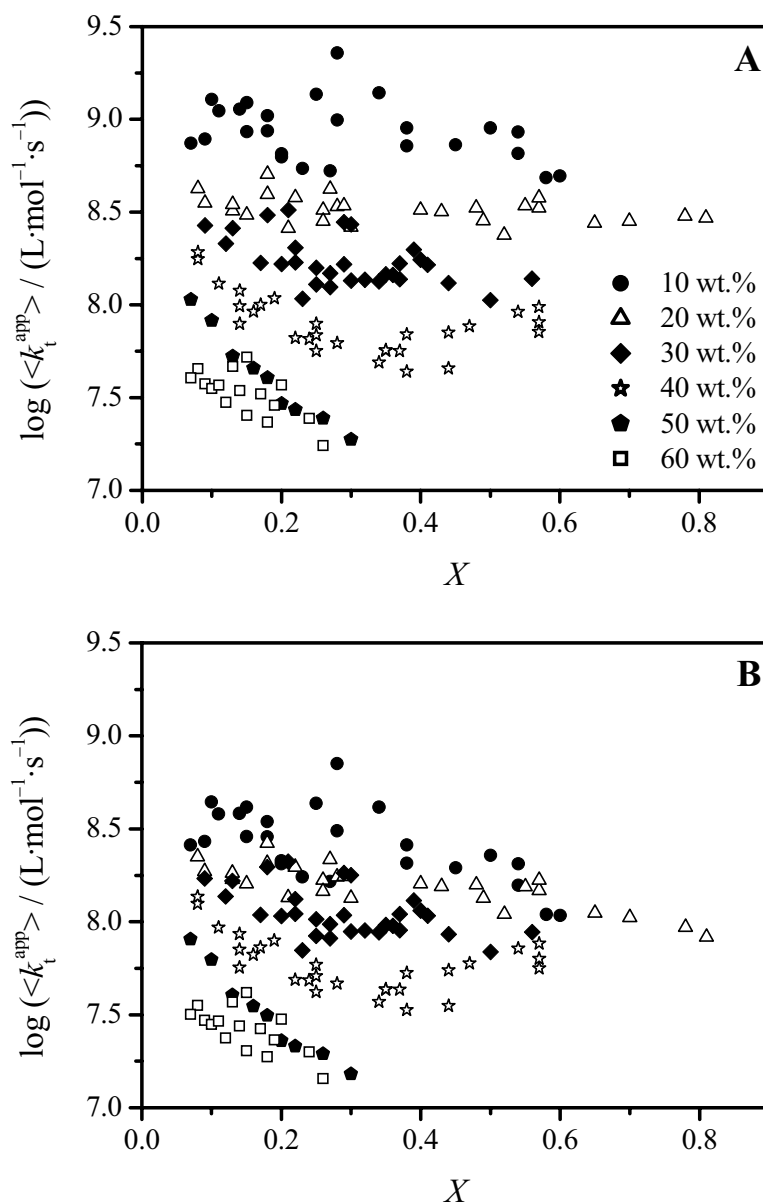


Figure 13-2: Dependence of $\langle k_t^{app} \rangle$ on fractional conversion for polymerization of AA in water at 25 °C, 50 bar and different initial monomer contents (as indicated in the figure). $\langle k_t^{app} \rangle$ was calculated from k_t/k_p by implementing a conversion independent k_p^s as within the thesis of Kukučková^[270] (A) or a conversion dependent k_p^{eff} (B) (for details see text).

The conversion dependencies of $\langle k_t^{app} \rangle$ for different initial AA concentrations are similar for the data in Figure 13-2A and Figure 13-2B which is due to the partial compensation of the increase in x_{MCR} toward higher conversions by the acceleration of k_p^s . The variation of $\langle k_t^{app} \rangle$ with X , especially at high initial monomer concentrations, is quite curious. There is, e.g., an increase of $\langle k_t^{app} \rangle$ between $X = 0.4$ and $X = 0.6$ within the 40 wt.% data. Such acceleration of k_t is unlikely to be a genuine kinetic effect considering the diffusion controlled nature of the

termination reaction and the continuous increase of solution viscosity toward higher degrees of monomer-to-polymer conversion. As an origin of this observation, not only slow MCR build up and its impact on SP-PLP-NIR traces has to be considered but also problems concerning the homogeneity of the reaction solution. However, the influence of both effects may be significantly reduced by using higher temperatures and high-pressure conditions (see Chapter 10.4).

The conversion dependence of $\langle k_t^{\text{app}} \rangle$ for polymerization of AA in water at 40 °C, 2000 bar and different initial monomer concentrations is depicted in Figure 13-3 (data taken from ref.^[270]). The termination rate coefficients were calculated using conversion-independent k_p^s values. The $\langle k_t^{\text{app}} \rangle$ data in Figure 13-3 shows considerably less scatter than the data in Figure 13-2. Moreover, $\langle k_t^{\text{app}} \rangle$ dependencies are much better behaved, i.e. $\langle k_t^{\text{app}} \rangle$ is almost constant for 20 wt.% of AA or slightly decreases toward increasing conversion for higher initial monomer contents. This observation may be explained by an RD control of k_t which, however, would result in unrealistically high C_{RD} values for low initial AA concentrations.

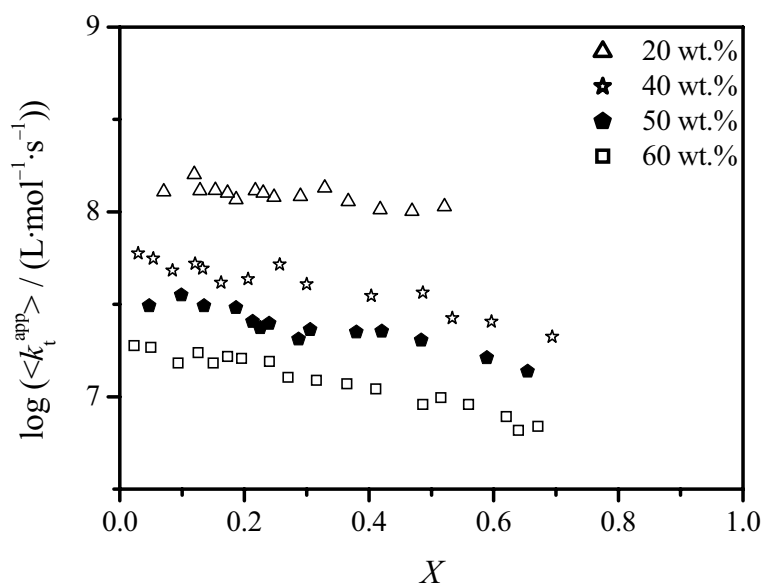


Figure 13-3: Dependence of $\langle k_t^{\text{app}} \rangle$ on fractional conversion for polymerization of AA in water at 40 °C, 2000 bar and different initial monomer contents (as indicated in the figure). $\langle k_t^{\text{app}} \rangle$ was calculated from k_t/k_p by implementing a conversion independent k_p^s .^[270]

It appears more reasonable to assume, in accordance to alkyl acrylate polymerization, an SD control followed by a weakly pronounced gel effect (see Chapter 3.3.3). Some additional evidence for the latter hypothesis is given in Chapter 13.3. In Figure 13-3, the difference in

the average low conversion $\langle k_t^{\text{app}} \rangle$ values for 20 and 60 wt.% of AA in water is only by a factor of 7.5 (compared to 13 in Figure 13-2A) which may even be further reduced by applying k_p^{eff} . However, k_p^{eff} data for AA polymerizations at 2000 bar are so far not accessible.

To finalize, the high-pressure k_t data for AA polymerization in water must be considered more accurate than the values obtained for ambient-pressure conditions and may provide more detailed insights into the termination kinetics. However, the knowledge of x_{MCR} under reaction conditions, i.e. temperature, pressure, initial monomer conversion, and monomer-to-polymer conversion, is urgently required for correct treatment of the primary k_t/k_p data.

13.3 Chain-length-dependent termination in AA polymerization

The RAFT process may be used for controlling the chain length of growing macroradicals, by which studies into chain-length-dependent termination become feasible even for short chain lengths.^[40] Through the addition of a RAFT agent to the polymerizing system, a correlation between X and molecular weight of the growing radicals may be established without affecting the propagating radical concentration. The SP-PLP-NIR-RAFT method takes advantage of the fact that, under RAFT control, the pulsed-laser induced chain growth of the macroradical ensemble is almost negligible during the time period of some hundred microseconds, which is typical for an SP experiment. Hence, chain-length independent kinetics may be applied for analysis of the monomer concentration vs. time traces. The experimental $c_M(t)/c_M(t=0)$ curves are fitted to Eq. (3-7), yielding the ratio k_t/k_p , from which k_t can be deduced by implementing k_p from independent PLP-SEC experiments. k_t as a function of monomer conversion can be transformed into chain-length dependent k_t values, due to the controlled characteristics of RAFT polymerization, which provides a correlation of fractional monomer conversion, X , and chain length, i , of the living polymer according to Eq. (13-4).^[38]

$$i = \frac{c_M^0}{\sigma \cdot c_{\text{RAFT}}^0} \cdot X + 1 \quad (13-4)$$

c_M^0 is the monomer concentration at $X = 0$, σ is the number of RAFT agent leaving groups (i.e. two in the case of trithiocarbonate-type RAFT agents) and c_{RAFT}^0 is the initial RAFT agent concentration.

The instationary SP-PLP-NIR-RAFT technique has several advantages in comparison to stationary methods.^[37,38] (i) The method is well suited for determining k_t in the short-chain length regime, because there is no requirement for stationary radical concentration, which needs to be reached in thermally initiated stationary polymerizations before fully reliable k_t data can be obtained. (ii) Neither the initiator decomposition rate coefficient, k_d , nor the initiator efficiency, f , are required to extract rate coefficients from the instationary polymerization experiments. (iii) Uncertainties introduced by k_p are affecting k_t data to a smaller extent, because k_t/k_p is determined in SP-PLP, whereas k_t/k_p^2 is the primary experimental result in stationary polymerization methods. (iv) The instationary SP-PLP-NIR-RAFT technique has proven to be a more robust method for $k_t(i,i)$ determination compared to the stationary RAFT-CLD-T^[40] approach, i.e. the resulting termination rate coefficients are less dependent on the magnitudes of k_{ad} and k_{frag} .^[97]

SP-PLP-NIR-RAFT has successfully been applied in MA, BA and DA bulk polymerizations,^[37-39] demonstrating the improved accuracy of the determined parameters compared to RAFT-CLD-T and providing evidence for a composite-model type behavior of $k_t(i,i)$. The objective of the study detailed in this chapter is to broaden the picture of termination during acrylate polymerization by measuring chain-length-dependent termination rate coefficients for polymerization of 40 wt.% AA in water at 40 °C and 2000 bar. The elevated pressure was used to improve system homogeneity, accelerate SPR-MCR equilibration and increase the ratio of propagation to termination rate which is beneficial for signal-to-noise quality in SP-PLP-NIR. Furthermore, elevated pressure applied to RAFT polymerization compensates for potential side reactions that may broaden the chain-length distribution.^[294] In previous SP-PLP-NIR-RAFT studies S-S'-bis(methyl-2-propionate)-trithiocarbonate (BMPT) has been used as mediating agent.^[37-39] However, due to insolubility of BMPT in aqueous solutions, the acidic RAFT agent S,S-bis(α,α' -dimethyl- α' -acetic acid)-trithiocarbonate (TRITT) was applied which also fulfills the requirements for SP-PLP-NIR-RAFT:^[37] (i) TRITT exhibits a low absorbance at the wavelength of the initiating XeF excimer laser and hence does not decompose upon irradiation. (ii) Trithiocarbonates have been reported to exhibit less pronounced rate retardation than dithiobenzoates and phenyl dithioacetates.^[295] (iii) AA polymerization proceeds under well controlled conditions, i.e. with

a direct proportionality between number average molecular weight and conversion (see further below).

In order to quantify the chain-length dependence of k_t , the primary experimental data, i.e. k_t/k_p vs. X , has to be transformed from the conversion into the chain-length domain via Eq. (13-4). To check for the applicability of Eq. (13-4), calibration samples of poly(AA) were produced by SP-PLP initiated RAFT polymerization at 40 °C and 2000 bar with reaction being stopped at different degrees of monomer-to-polymer conversion. The experimentally obtained number average molecular weights, M_n , were recalculated into macroradical chain lengths by:

$$i = \frac{M_n - M_{RG}}{\sigma \cdot M_M} \quad (13-5)$$

M_{RG} and M_M are the molecular weights of the RAFT group and one monomer unit within the living polymer, respectively. For the system under investigation, i.e. a TRITT-mediated AA polymerization, $M_{RG} = 108 \text{ g}\cdot\text{mol}^{-1}$, $M_M = 94 \text{ g}\cdot\text{mol}^{-1}$ (molecular weight of NaAA), and $\sigma = 2$. The experimentally obtained dependencies of i on X for the two different RAFT agent concentrations of this study are depicted in Figure 13-4 together with the associated polydispersity indices, PDI . The absence of a hybrid effect (see Chapter 3.5) allows for accessing even the short-chain regime by SP-PLP-NIR-RAFT. Additionally, there is good agreement between the measured data and the ones predicted by Eq. (13-4) which are indicated by the dashed lines. The overlap of the experimental data with Eq. (13-4) is excellent for the high RAFT agent concentration. At the low TRITT concentration, however, some discrepancies are seen which may be caused by higher amounts of dead polymeric material contributing to M_n ^[296] but may also result from inaccuracies in c_{RAFT}^0 determination. The empirical linear fits to the experimental data (full lines) were thus used for performing the transformation from monomer conversion to chain length. The low PDI values in the TRITT-mediated AA polymerizations provide additional evidence for a successful RAFT control. For $c_{TRITT} = 1.2 \cdot 10^{-2} \text{ mol}\cdot\text{L}^{-1}$ and high conversions, PDI s in the range of 1.2 are reached which is not possible in conventional FRP where $PDI = 1.5$ is the lower bound. Moreover the narrow MWDs obtained at high conversions indicate that there is no pronounced intermolecular transfer-to-polymer during AA polymerization at 40 °C and 2000 bar, as such reactions may give rise to multimodal MWDs and increased numbers of active RAFT-moieties per chain.^[76]

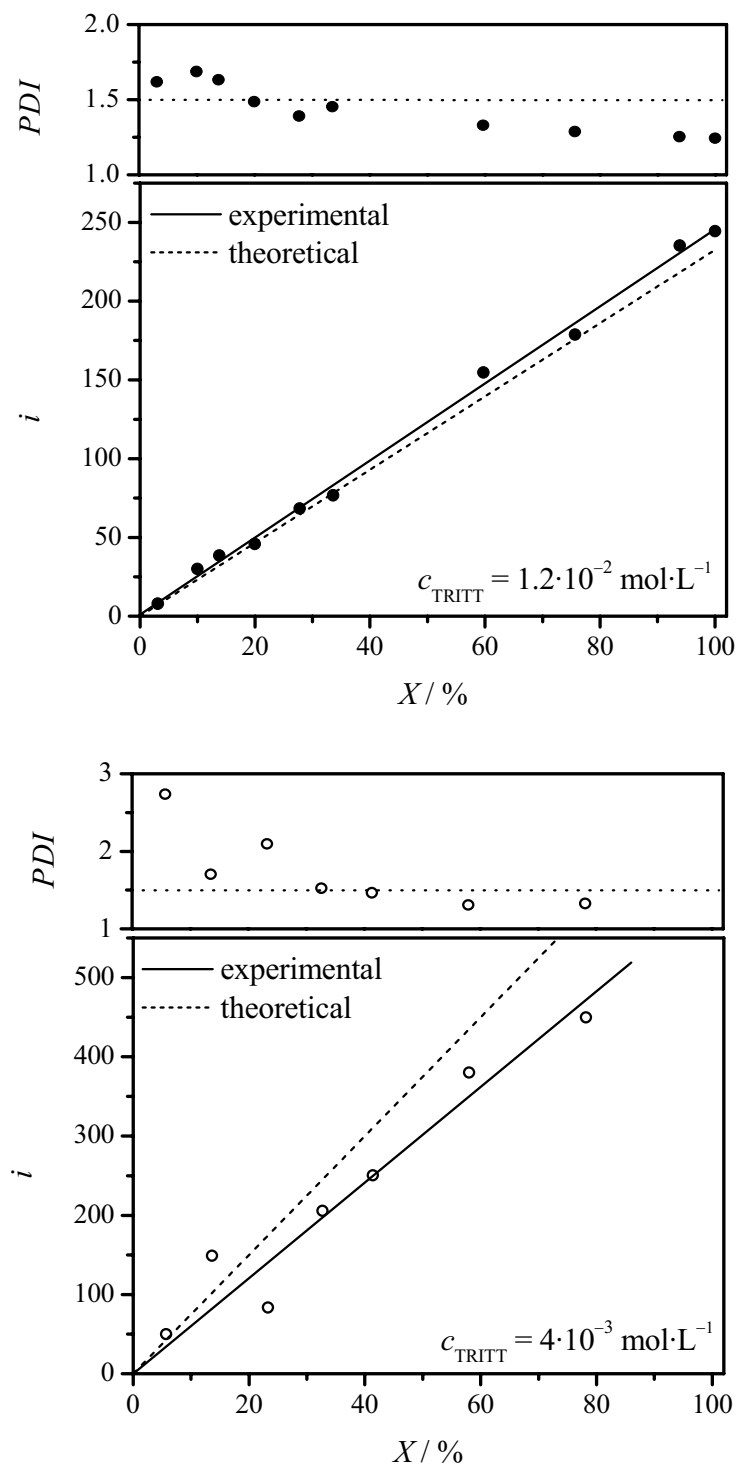


Figure 13-4: Dependence of chain length, i , of the macroradical which is expelled from the macroRAFT agent on monomer conversion, X , for SP-PLP induced RAFT polymerizations of 40 wt.% AA in water at 40 °C and 2000 bar using TRITT as the mediating agent. Also included are the polydispersities, PDI , of the poly(AA) MWDs. The full lines are linear fits to the i vs. X and the dashed lines are estimated according to Eq. (13-4).

The magnitude of this effect has recently been found to strongly decrease within the series $DA > BA > MA$.^[76] Consequently, AA seems to fit in this family-type behavior concerning intermolecular transfer-to-polymer.

The dependence of k_t/k_p on fractional conversion for RAFT mediated polymerization of 40 wt.% AA in water at 40 °C and 2000 bar is shown in Figure 13-5. The different TRITT concentrations, $1.2 \cdot 10^{-2} \text{ mol} \cdot \text{L}^{-1}$ and $4 \cdot 10^{-3} \text{ mol} \cdot \text{L}^{-1}$, are indicated by open and filled symbols. No individual k_t values were calculated due to the non-availability of accurate k_p^{eff} data. It has been found from SP-PLP-NIR investigations under ostensibly the same reaction conditions that the chain-length averaged k_t in conventional polymerization is almost constant up to monomer conversions of about 30 % followed by a marginal decrease (see stars in Figure 13-3). This data suggests that k_t values from RAFT polymerization obtained at monomer conversions below 30 % are not significantly affected by monomer-to-polymer conversion and that effects on k_t in this region may safely be attributed to the chain-length dependence of k_t . In fact, monomer conversion effects on the SP-PLP-NIR-RAFT data should even be negligible up to higher X as polymer of relatively low molecular weight is formed and thus higher polymer contents are required to provoke the onset of the gel effect.

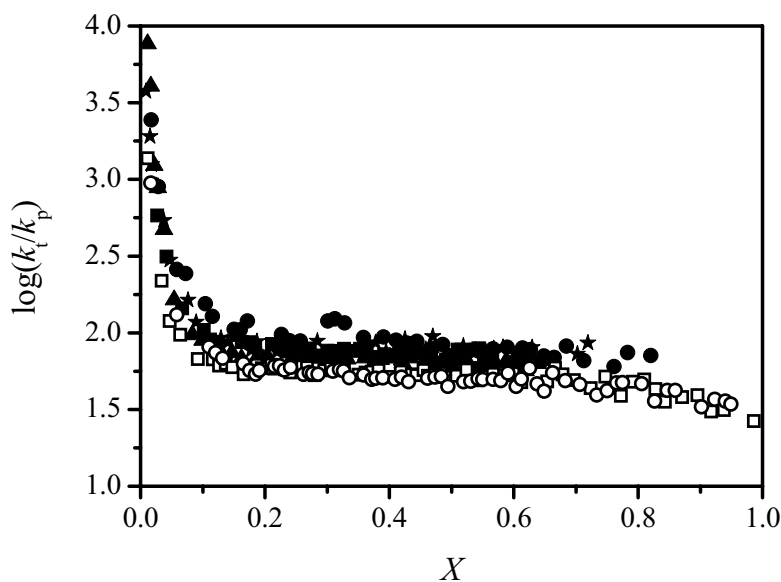


Figure 13-5: Dependence of k_t/k_p on fractional conversion determined via SP-PLP-NIR-RAFT for polymerization of 40 wt.% AA in water at 40 °C and 2000 bar. TRITT concentrations of $1.2 \cdot 10^{-2} \text{ mol} \cdot \text{L}^{-1}$ (filled symbols) and $4 \cdot 10^{-3} \text{ mol} \cdot \text{L}^{-1}$ (open symbols) were used. Individual experimental runs are marked by different symbol styles.

The k_t/k_p data for the higher RAFT agent concentration (filled symbols), and thus shorter chain lengths, is almost constant between 20 and 80 % conversion whereas some decrease of k_t/k_p for conversions above 70 % is seen within the data indicated by the open symbols.

Hence, for $c_{\text{TRITT}} = 4 \cdot 10^{-3} \text{ mol} \cdot \text{L}^{-1}$, only data up to 60 % monomer-to-polymer conversion were employed for deducing the chain-length dependence of k_t .

The k_t/k_p plot obtained by transforming the dependence on monomer conversion into a chain-length dependence is depicted in Figure 13-6. The overlap of the $\log(k_t/k_p)$ data from measurements at different TRITT concentrations is satisfactory (compare open and filled symbols). This figure provides the opportunity to extract quantitative information on the chain-length dependence of k_t/k_p , i.e. the slopes α_s and α_l for the respective chain-length regimes, the crossover chain length i_c as well as the ordinate intercept $k_t/k_p(1,1)$. As pointed out above, at elevated monomer conversions (corresponding to $\log(i) > 2.5$) the chain-length dependent k_t/k_p data is strongly decreasing, as k_t becomes affected by monomer conversion and runs into TD control. The k_t/k_p values for $\log(i) > 2.5$ are thus omitted from further evaluation. For $\log(i) < 2.5$, two distinct regimes can be observed, in which $\log(k_t/k_p)$ decreases linearly with different respective slopes. The observed slopes are the exponents $-\alpha_s$ for the short- chain-length regime, with $i < i_c$, in Eq. (13-6)

$$\frac{k_t}{k_p}(i,i) = \frac{k_t}{k_p}(1,1) \cdot i^{-\alpha_s} \quad (13-6)$$

and the exponent $-\alpha_l$ in Eq. (13-7) describing the long-chain-length regime, with $i > i_c$.

$$\frac{k_t}{k_p}(i,i) = \frac{k_t}{k_p}(1,1) \cdot i_c^{-\alpha_s + \alpha_l} \cdot i^{-\alpha_l} = \frac{k_t^0}{k_p} \cdot i^{-\alpha_l} \quad (13-7)$$

Note that Eqs. (13-6) and (13-7) are modified versions of Eqs. (3-33) and (3-34). In case k_p is independent of conversion and chain-length, the slopes α_s and α_l in Figure 13-6 are identical to the ones expressed by Eqs. (3-33) and (3-34) and $\log(k_t(1,1))$ is obtained by adding $\log(k_p)$ to the y-axis intercept of the linear fit to the short-chain regime. It has previously been shown that accounting for the conversion-induced change in k_p^{eff} , by implementing an apparent reaction order in monomer concentration (see Eq. (10-23)), does not significantly change the results for α_s and α_l .^[39] Moreover, the decrease in k_p^{eff} toward higher conversion, resulting from an increase in x_{MCR} , should at least partially be compensated by a growing $k_p^s(X)$ within

the AA system. Thus, the α_s and α_l values obtained from the linear fits to the $\log(k_t/k_p)$ vs. $\log(i)$ data should also well describe the change in $k_t(i,i)$ according to Eqs. (3-33) and (3-34).

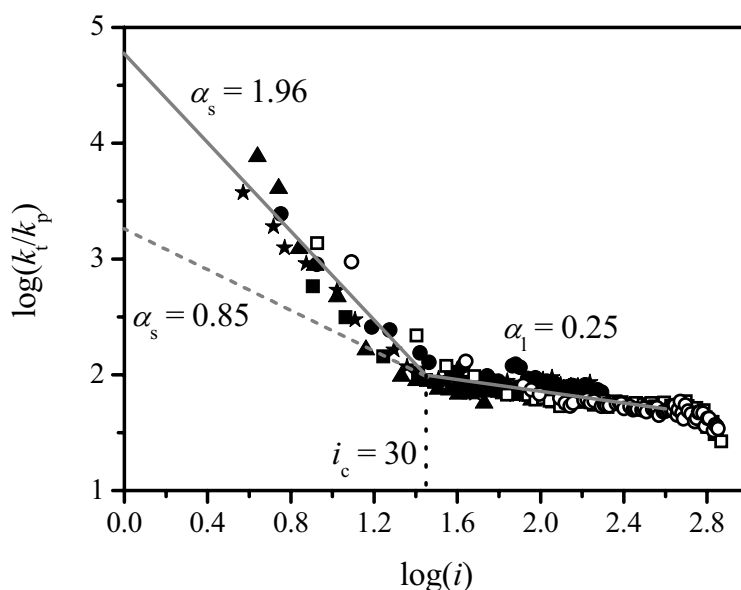


Figure 13-6: $\log(k_t/k_p)$ vs. $\log(i)$ for a polymerization of 40 wt.% AA in water at 40 °C and 2000 bar obtained from SP-PLP-NIR-RAFT measurements at TRITT concentrations of $1.2 \cdot 10^{-2} \text{ mol} \cdot \text{L}^{-1}$ (filled symbols) and $4 \cdot 10^{-3} \text{ mol} \cdot \text{L}^{-1}$ (open symbols). The full grey lines represent linear fits to the respective short- and long-chain regimes according to Eqs. (13-6) and (13-7). The grey dashed line was estimated for $i_c = 30$ and $\alpha_s = 0.85$.

The results from linear fitting to the short- and long chain regimes in Figure 13-6 are $\alpha_s = 1.96$, $\alpha_l = 0.25$, $i_c = 30$ and $\log(k_t/k_p(1,1)) = 4.8$. Consequently, $\log(k_t^{\text{app}}(1,1) / \text{L} \cdot \text{mol}^{-1} \cdot \text{s}^{-1}) = 10.0$ is obtained via $k_p^s = 165\,000 \text{ L} \cdot \text{mol}^{-1} \cdot \text{s}^{-1}$ which has been estimated for the corresponding reaction conditions.^[270] Whereas α_l and i_c are in the expected range, α_s and $k_t^{\text{app}}(1,1)$ are unusually high.

In order to provide a broader picture of the chain-length-dependent termination behavior of acrylate polymerization, the key parameters of this work are presented in Table 13-1 together with the data that have been obtained earlier for the MA, BA and DA systems via SP-PLP-NIR-RAFT. $k_t^{\text{app}}(1,1)$ for AA was extrapolated to the experimental conditions used for studies into the alkyl acrylates, i.e. to 60 °C and 1000 bar. The comparison tells that $k_t^{\text{app}}(1,1)$ of AA is indeed unrealistically high and appears to even exceed the diffusion limit. The viscosity of the aqueous AA mixture is expected to be higher than the one of BA in bulk. Thus, $k_t(1,1)$ for AA in water should even be lower than $k_t(1,1)$ for BA according to Eqs. (3-19) and (3-20). The reason for this discrepancy might be connected with an influence of MCR formation on

the magnitude $k_t^{\text{app}}(1,1)$ which, however, should not be very pronounced for short chain lengths. It appears more likely that strong RAFT specific effects affect $k_t(1,1)$. The correlated value α_s of 1.96 is very high, not only in comparison to MA, BA and DA, but also from a theoretical point of view. As outlined in Chapter 3.4.2, the hydrodynamic radius increases at most linearly toward higher chain lengths, i.e. $r_{s,i}$ is proportional to $i^{\leq 1}$. Thus, a strong reduction of the capture radius R_C toward increasing i would be required to explain α_s values which significantly exceed unity. However, independent experiments showed only minor changes of R_C with i .^[120] This discussion is further supported by the resulting value of $\alpha_s = 0.85$ for k_t^{ss} of BA determined via SP-PLP-ESR (see Chapter 12.4.4). This value is well below the associated α_s obtained by SP-PLP-NIR-RAFT. Thus, besides the influence of MCR formation, there may be some inhibition effect, introduced by the RAFT agent, which increases k_t for short chain-lengths. Moreover, the influence of monomer conversion on the center-of-mass diffusion controlled $k_t(i,i)$ values may affect the short-chain data. The huge difference between the experimental $k_t(i,i)$ data with $\alpha_s = 1.96$ and the more realistic value of 0.85 is illustrated by the full and dashed grey lines. For the latter case, a much more reasonable $k_t^{\text{app}}(1,1)$ value of $7.6 \cdot 10^8 \text{ L} \cdot \text{mol}^{-1} \cdot \text{s}^{-1}$ (for 60 °C and 1000 bar) is obtained.

In principle, further validation of the short-chain $k_t(i,i)$ data for AA is required. To improve the accuracy in this regime, higher RAFT agent concentrations need to be used which is, however, impeded by the weak solubility of TRITT in aqueous AA mixtures.

The values found for i_c decrease in the series of AA, MA, BA, and DA. According to the composite model, $k_t(i,i)$ for small chain lengths is assumed to be governed by center-of-mass diffusion, which may be described by the Smoluchowski equation predicting proportionality between the termination rate coefficient and the diffusion coefficient. At larger chain lengths when the macroradicals start to form long-lived contact pairs, $k_t(i,i)$ is determined by the intramolecular shielding of the radical center by surrounding polymer segments. The crossover between these two regimes occurs at i_c . Since DA is the largest monomer with the highest viscosity, the associated macroradicals diffuse rather slowly and may get entangled from relatively short chain lengths on. This is indeed indicated by the small i_c for DA in Table 13-1. It should be noted that in systems with polymer main chains of greater stiffness than with acrylates, the i_c values were found to be larger. E.g., for dodecyl methacrylate, i_c was found to be 50,^[34] which is significantly above the DA value of 20. This finding is in full agreement with the understanding that acrylates form more flexible coils than methacrylates.

The values found for α_1 (see Table 13-1) seem to slightly decrease toward longer ester chain. In this long-chain regime, k_t is governed by the radical encounter probability upon coil overlap. The associated exponent α_1 has been predicted to be close to 0.16^[26,125,126] for chain end-end reaction in a good solvent. For the encounter between a midchain and a chain-end radical an α_1 value of 0.27 is predicted. The observed exponents between 0.20 and 0.26 may hence be indicative of MCRs being involved in the termination with SPRs to some extent.

Table 13-1: Chain-length dependency parameters of the termination rate coefficient in AA, MA, BA and DA bulk polymerization determined via SP-PLP-NIR-RAFT.

	AA	MA ^[39]	BA ^[38]	DA ^[39]
$k_t^{\text{app}}(1,1) / \text{L}\cdot\text{mol}^{-1}\cdot\text{s}^{-1}$	$2.6\cdot 10^{10}$ ^(a)	$1.3\cdot 10^9$	$1.0\cdot 10^9$	$2.0\cdot 10^8$
α_s	1.96	0.78	1.24	1.12
α_1	0.25	0.26	0.22	0.20
i_c	30	30	27	20

^(a) extrapolated to 60 °C and 1000 bar

Comparing results from SP-PLP-NIR-RAFT for acrylate-type monomers is not without difficulties due to problems associated with MCR formation and possible influences of the RAFT agent on termination kinetics. Nevertheless, the data comparison indicates that the composite-model parameters of AA to some extent fit into the picture previously obtained for its alkyl esters. Thus, it is straightforward to assume that the same types of termination mechanisms are operative for AA, i.e. a center-of-mass diffusion control for short chains and an SD control for longer chain lengths.

14 General Aspects of Termination Kinetics in Free-Radical Polymerization

A huge amount of chain-length-dependent and chain-length-averaged termination rate data has been collected so far, primarily for acrylate- and methacrylate-type monomers. It is instructive to discuss the data based on the rate-controlling diffusion steps in order to test and broaden the mechanistic understanding. As detailed in Chapter 13, low conversion $k_t(i,i)$ values and the associated composite-model parameters obtained via SP-PLP-ESR may be considered more accurate than data from RAFT techniques, i.e. from SP-PLP-NIR-RAFT and RAFT-CLD-T, respectively. Thus, the discussion of the $k_t(1,1)$, α_s , α_l and i_c values primarily rests on SP-PLP-ESR data for methacrylic acid esters^[34,297] and BA (Chapter 12.4.4). For chain-length-averaged termination rate coefficients, $\langle k_t \rangle$ vs. X data from SP-PLP-NIR for acrylate- and methacrylate-type monomers will be considered.

Table 14-1 summarizes the composite-model parameters α_s , α_l , i_c and $k_t(1,1)$ for *n*-BMA,^[297] *t*-BMA,^[297] MMA,^[122] DMA,^[34] and BA (Chapter 12.4.4). The MMA data was obtained via RAFT-CLD-T whereas the other values are from SP-PLP-ESR. The composite-model parameters for BA refer to SPR-SPR termination, i.e. to $k_t^{ss}(i,i)$. The $k_t(1,1)$ values are given for a polymerization temperature of 0 °C.

The power-law exponent for the long-chain regime, α_l , is found to be almost the same for all monomers contained in Table 14-1. The parameter values are always sufficiently close to the theoretical prediction of 0.16 for SD controlled termination in good solvents.^[26,125,126] Olaj and Vana observed a drop of α_l from about 0.18 at 20 °C to ~ 0.10 at 70 °C for styrene polymerization, which they attributed to a decrease in solvent quality toward increasing temperature.^[135] However, constant α_l values were determined in a recent SP-PLP-ESR work on *n*- and *t*-BMA^[297] though a temperature interval of even 90 K was covered.

The crossover chain length i_c characterizes the radical size from which on two radicals may get entangled and thus experience a significantly enhanced contact time as compared to the short contact times with radicals of chain lengths $i < i_c$. As stiff macroradicals are less capable of forming entanglements, i_c should be mainly governed by chain flexibility. Moreover, flexible macroradicals screen their surrounding more efficiently and long-chain behavior should be reached from shorter chain lengths on. The major effect on chain flexibility results

from the type of chain segments. E.g., methacrylates are of significantly lower chain flexibility than acrylates, as is indicated by the higher glass transition temperatures of poly(methacrylates) as compared to associated poly(acrylates). Within the methacrylate family, a higher i_c is anticipated for monomers with bulky ester groups. According to this argument, the crossover chain length for *t*-BMA, $i_c = 70$, exceeds the one for *n*-BMA, $i_c = 50$, reflecting the higher steric demand of an *tert*-butyl group as compared to an *n*-butyl group. Higher chain flexibility is also indicated by the propagation rate coefficient under otherwise identical reaction conditions which is larger for *n*-BMA than for *tert*-BMA. The chain-flexibility argument with propagation rate comes into play via the hindrance of internal rotational motion of the transition structure for propagation, as is discussed elsewhere (see Chapter 6.1 and ref.^[138]). The crossover chain length of DMA, $i_c = 50$, is identical to the one measured for *n*-BMA which indicates that chain stiffness is essentially determined by the type of side-chain segments which sit next to the backbone. Alternatively, the similarity of i_c for DMA and *n*-BMA may be understood by assuming that the reduction in flexibility associated with the large dodecyl side chain is compensated by the fluidizing action of this longer alkyl moiety which serves as some kind of “internal” solvent. Relatively large crossover chain lengths, of about $i_c = 90$, have been found for two methacrylates with cyclic ester groups, CHMA and BzMA.^[34] The cyclic ester groups thus induce enhanced chain stiffness. That the i_c values for CHMA and BzMA even exceed the one for *t*-BMA may serve as an indication of significant mutual interactions of the cyclic moieties during segmental re-orientation of the associated polymeric chains. The crossover chain lengths of methacrylate monomers increase along the series: *n*-alkyl < *sec*-alkyl < *tert*-alkyl < cyclic. The i_c value of MMA is significantly above the other values in Table 14-1. It should be noted that the i_c data for MMA was obtained via RAFT-CLD-T and may thus be considered less accurate.

It needs to be tested whether the sequence above applies also to other families, e.g., to the acrylates. So far, three *n*-alkyl esters have been studied. As is to be expected from the chain-flexibility argument, the i_c values for MA,^[39] BA,^[38] and DA^[39] polymerization are significantly below the ones for alkyl methacrylates. They range from 20 to 30 with the lowest number ($i_c \sim 20$) being found for DA, the monomer with the largest alkyl ester side chain, and vice versa ($i_c \sim 30$ for MA). This finding supports the argument that a large alkyl ester group acts as an “internal” solvent and enhances the flexibility of the polymeric chain.

The magnitudes of $k_t(1,1)$ and α_s are governed by the velocity of center-of-mass diffusion of small radicals. A center-of-mass diffusion controlled rate coefficient, k_D , may be described by

the Smoluchowski equation (see Eq. (3-19)) in combination with diffusion coefficients from the Stokes-Einstein equation (see Eq. (3-20)). As discussed within the previous chapter, Eqs. (3-19) and (3-20) illustrate that no chain-length dependence of k_t is expected when R_C and $r_{s,i}$ grow to the same extent with chain length. Quenching experiments on polystyrene,^[120] however, revealed that R_C is almost independent of the degree of polymerization in the short-chain regime. Thus, the chain-length dependence of $k_t(i,i)$ is governed by $D_s(i)$. At infinite dilution the center-of-mass diffusion coefficient should progress according to $D_s(i) \propto i^{-0.5}$ for ideal random coils^[116-118] (which are formed in θ solvents) and according to $D_s(i) \propto i^{-0.6}$ when excluded volume effects are considered.^[119] The exponents determined for methacrylate-type monomers are in good agreement with the predicted value of 0.6. It should further be noted that the chain-length dependence of the diffusion coefficient has also been directly measured for n -BMA oligomers in solution of monomeric n -BMA resulting in the relation $D_s(i) \propto i^{-0.66}$ with the exponent almost exactly matching the α_s value in Table 14-1.^[298]

The maximum reaction rate is usually given by the so-called diffusion limit. From combination of Eqs. (3-19) and (3-20), $k_t^{\max}(1,1) = 4 \cdot R \cdot T / (3 \cdot \eta)$ is obtained under the assumption that $R_C = 2 \cdot r_{s,1}$. Implementation of monomer viscosities from ref.^[138] yields $k_t^{\max}(1,1) \approx 3 \cdot 10^9 \text{ L} \cdot \text{mol}^{-1} \cdot \text{s}^{-1}$ for termination in n -BMA and t -BMA at 0 °C. The diffusion limiting value exceeds $k_t(1,1)$ by more than one order of magnitude. This difference reflects that the capture radius for the termination reaction is governed by the dimension of the reactive center bearing the unpaired electron and not by the entire molecule, i.e. $r_{s1} \gg R_C$. To compare $k_t(1,1)$ values for polymerizations of different monomers, scaling with monomer (solution) viscosity and with hydrodynamic radius is instructive. Thus, relative monomer viscosities and hydrodynamic radii are also contained Table 14-1. The values were scaled with respect to n -BMA as this is the monomer with the most recent and probably also most accurate SP-PLP-ESR data. Viscosity data was sometimes not available for 0 °C. Thus, several viscosity ratios in Table 14-1 originate from higher temperatures. Moreover, the hydrodynamic radii of t -BMA and BA were estimated to be close to $r_{s,n\text{-BMA}}$. The thereby introduced errors are assumed to be negligible.

Table 14-1: Comparison of the $k_t(1,1)$ values obtained for bulk polymerizations of alkyl methacrylates and BA in toluene at 0 °C. Also contained are i_c , α_s , α_t , relative viscosities as well as relative hydrodynamic monomer radii (compared to *n*-BMA). The relative capture radii were calculated based on the $k_t(1,1)$, η and $r_{s,i}$ data (for details see text).

	<i>n</i> -BMA	<i>t</i> -BMA	MMA ^{a)}	DMA	BA ^{b)}
α_s	0.65	0.56	0.65	0.64	0.85
α_t	0.2	0.2	0.15	0.18	0.16
i_c	50	70	100	50	30
$k_t(1,1) / \text{L}\cdot\text{mol}^{-1}\cdot\text{s}^{-1}$	$1.3\cdot 10^8$	$9.1\cdot 10^7$	$4.7\cdot 10^8$ ^{c)}	$1.1\cdot 10^7$	$3.2\cdot 10^8$
$E_a(k_t(1,1)) / \text{kJ}\cdot\text{mol}^{-1}$	10.1	10.9	–	–	8.4
$\eta / \eta_{n\text{-BMA}}$	1	1	0.6	4.4	0.6
$r_s / r_{s,n\text{-BMA}}$	1	~ 1 ^{d)}	0.6	1.8	~ 1 ^{d)}
$R_C / R_{C,n\text{-BMA}}$	1	~ 0.7	~ 1.3	0.6	~ 1.5
ref.	[138], [297],[299]	[138], [297], [299]	[122], [299]	[34], [299]	this work

^{a)} $k_t(i,i)$ data from RAFT-CLD-T

^{b)} $k_t(i,i)$ data for SPR-SPR termination

^{c)} $k_t(1,1)$ was determined for 80 °C and extrapolated to 0 °C via $E_a(k_t(1,1)) = 10 \text{ kJ}\cdot\text{mol}^{-1}$

^{d)} hydrodynamic radii were interpolated according to the number of atoms in the monomer

Scaling of the $k_t(1,1)$ values with monomer viscosity and hydrodynamic radius according to Eqs. (3-19) and (3-20) yields the ratio of the capture radii shown in bold in Table 14-1. Whereas $k_t(1,1)$ differs by about one order of magnitude between DMA and the butyl methacrylates, it turns out that the capture radii are very similar, i.e. the differences in $k_t(1,1)$ are predominantly caused by dissimilar monomer viscosities and hydrodynamic radii. The similar $k_t(1,1)$ values of the isomers *n*-BMA and *t*-BMA illustrate that minor structural

differences do not significantly affect the center-of-mass diffusion controlled reaction between the monomeric radicals but may become important when longer chains are formed (see below). The slight increase of R_C in the series DMA < BMA < MMA may not be considered significant in view of the accuracy of $k_t(1,1)$ determination via SP-PLP-ESR and RAFT-CLD-T, respectively. Nevertheless, this result may reflect some increased shielding of the radical center by larger ester groups. Thus, strong family-type behavior for $k_t(1,1)$ of methacrylic acid esters is found when representing $k_t(1,1)$ as a function of monomer viscosity and size. The slightly higher R_C obtained for $k_t^{ss}(1,1)$ may be caused by the absence of an α -methyl group within the acrylate monomers which potentially results in a better availability of the radical site for termination.

Additional support for the simple description of $k_t(1,1)$ by Eqs. (3-19) and (3-20) is provided by the associated activation energies. The $E_a(k_t(1,1))$ values for polymerization of *n*- and *t*-BMA in bulk as well as of BA in solution of toluene (see Table 14-1) closely resemble the temperature dependence of solution fluidity, i.e. $E_a(\eta^{-1})$.^[138,195,293]

It is important to note that the discussion above is limited to low conversion data. Significantly higher α values (up to 2) may be obtained in the presence of high polymer concentrations where $\langle k_t \rangle$ is controlled by TD.^[122,123,137-141] Thus, it is a matter of priority to extend the SP-PLP-ESR studies into the chain-length dependence of termination to high polymer concentration conditions. These investigations may provide a deeper understanding of both, the chain-length and the conversion dependence of k_t .

A comparison of the low-conversion chain-length-averaged termination rate coefficients, $\langle k_{SD} \rangle$, for bulk polymerizations of different alkyl methacrylates obtained via SP-PLP-NIR is provided in Table 14-2. The data was extrapolated to 40 °C and 2000 bar using the activation volumes given in the respective references. When k_t is controlled by segmental diffusion, the magnitude of the termination rate coefficient is governed by the probability of two macroradicals forming a contact pair and the rate of segmental motion during contact (see e.g. ref.^[299]). The first effect, which may be interpreted by an equilibrium constant, is mainly dependent on the rates of entanglement and disentanglement as well as on the dimension of the entangled region. Thus, this parameter is primarily governed by excluded volume effects. The second term, i.e. the segmental mobility, depends on chain architecture, chain structure and interchain effects. Consequently, not only $k_t(1,1)$ but also $\langle k_{SD} \rangle$ should be scaled with bulk viscosity to obtain comparable results. In fact, the so-obtained $k_{SD} \cdot \eta(\eta_{MMA})^{-1}$ values are rather similar for the *n*-alkyl methacrylates collated in Table 14-2. However, the scaled

termination rate coefficient for *t*-BMA is significantly lower. This discrepancy is caused by the fact that bulk viscosity only accounts for the mobility of free monomer molecules but not for the ones which are fixed in a polymeric chain. Thus, chain stiffness induced by the bulky *t*-butyl group contributes to an additional reduction of the efficiency of termination via the SD mechanism. This is reflected by the higher i_c of *t*-BMA compared to *n*-BMA in Table 14-1 but equivalently results in a lower k_t^0 for *t*-BMA.

Table 14-2: Comparison of the low-conversion chain-length-averaged termination rate coefficients, $\langle k_{SD} \rangle$, for bulk polymerizations of different alkyl methacrylates obtained via SP-PLP-NIR. The data was extrapolated to reaction conditions of 40 °C and 2000 bar. Also contained are relative viscosities (compared to MMA) and scaled $\langle k_{SD} \rangle$ values (for details see text).

	MMA	<i>n</i> -BMA	<i>t</i> -BMA	DMA
$\langle k_{SD} \rangle / 10^6 \text{ L}\cdot\text{mol}^{-1}\cdot\text{s}^{-1}$	14	5.5	2.1	1.1
$\eta^* = \eta / \eta_{\text{MMA}}$	1	1.7	1.7	7.3
$\langle k_{SD} \rangle \cdot \eta^* / 10^6 \text{ L}\cdot\text{mol}^{-1}\cdot\text{s}^{-1}$	14	9.4	3.6	8.0
ref.	[16],[299]	[138]	[138]	[16],[299]

The remaining tasks are to incorporate the $\langle k_{SD} \rangle$ data from SP-PLP-NIR of alkyl acrylates as well as for polymerization of AA and MAA in water into this picture. A collection of k_p and $\langle k_{SD} \rangle$ values for bulk polymerization of several alkyl acrylates and alkyl methacrylates at 40 °C and 2000 bar is given in Figure 14-1.^[16,138] The k_p values for the acrylate type monomers refer to k_p^s . The apparent $\langle k_{SD} \rangle$ values for MA, BA and DA in Figure 14-1A were obtained from implementing k_p^s into k_t/k_p . Figure 14-1B also includes the individual k_t^{ss} , k_t^{st} and k_t^{tt} values for BA polymerization from Table 10-1 extrapolated to the above mentioned reaction conditions. Note that k_t^{ss} , k_t^{st} and k_t^{tt} are also chain-length-averaged quantities. The change in $\langle k_{SD} \rangle$ within the alkyl methacrylate family has already been discussed in connection with Table 14-2. A similar qualitative trend, i.e. an increase in $\langle k_{SD} \rangle$ toward shorter ester chain length, is observed for the alkyl acrylates in Figure 14-1A. Comparison

between alkyl acrylates and alkyl methacrylates reveals strong differences in $\langle k_{SD} \rangle$, especially between MA and MMA. However, as detailed in Chapter 10.4, the $\langle k_{SD} \rangle$ data for MA, BA and DA are highly fictitious in cases where they result from implementation of k_p^s into k_t/k_p .

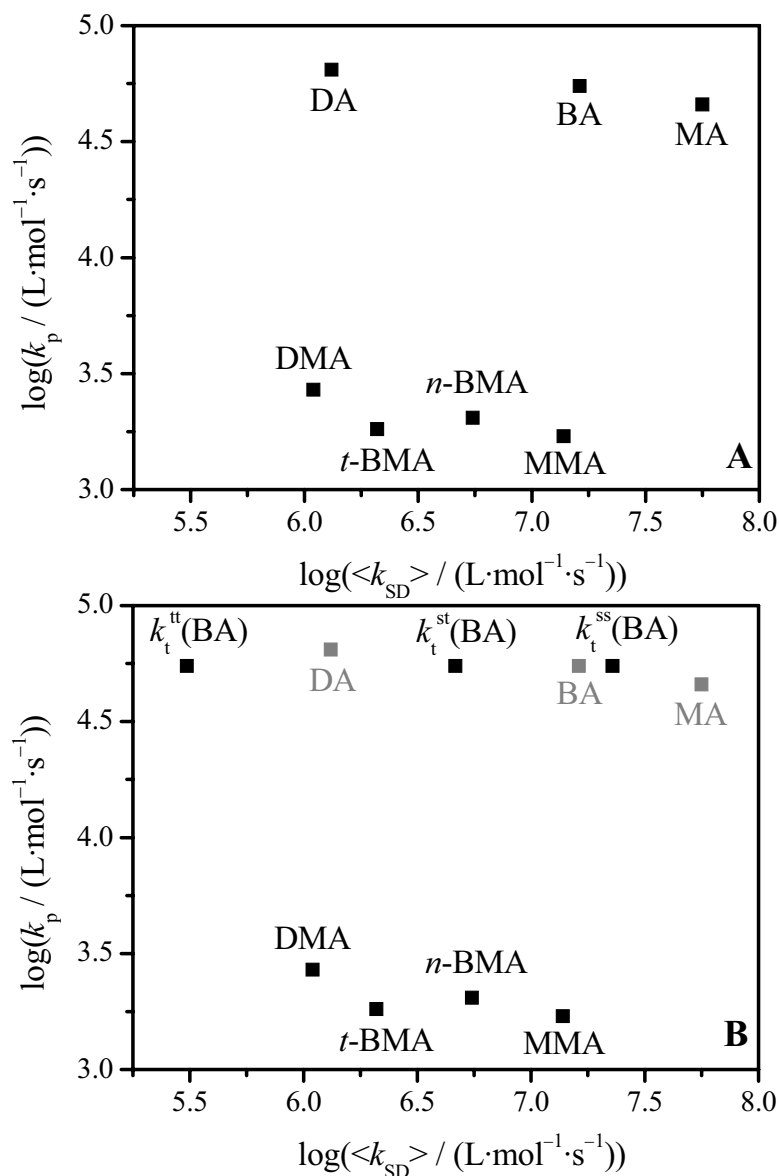


Figure 14-1: Collection of propagation rate coefficients, k_p , and (low conversion) chain length averaged termination rate coefficients, $\langle k_{SD} \rangle$, for bulk polymerization of several alkyl acrylates and alkyl methacrylates at 40 °C and 2000 bar.^[16,138] The k_p values for the acrylate type monomers refer to k_p^s . The apparent $\langle k_{SD} \rangle$ values for MA, BA and DA in Figure 14-1A were obtained from implementing k_p^s into k_t/k_p . Figure 14-1B includes the individual k_t^{ss} , k_t^{st} and k_t^{tt} values for BA from Table 10-1.

Thus, it is more conclusive to compare the individual k_t^{ss} , k_t^{st} and k_t^{tt} values for BA with the n -BMA data. k_t^{ss} of BA is well above $\langle k_{SD} \rangle$ for n -BMA reflecting the more efficient termination via the SD mechanism for acrylates due to the higher chain flexibility. This effect is also reflected in the considerably lower i_c for BA compared to n -BMA. However, k_t^{st} is close to $\langle k_{SD} \rangle$ of n -BMA though the BA chains should still show the same flexibility. However, the enhanced shielding of the radical site within the MCR hampers termination. This effect is even more pronounced for MCR-MCR termination for which a very low k_t is found. The influence of shielding induces a difference between k_t^{ss} and k_t^{tt} of a factor of 75 whereas $\langle k_{SD} \rangle$ for n -BMA and t -BMA differ by less than factor of 3. Thus, the shielding effect must be considered to be dominant when comparing different monomer families.

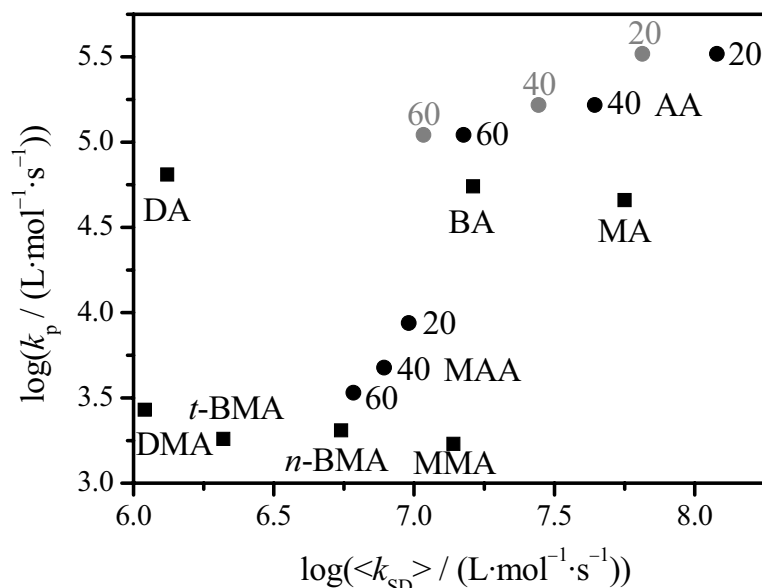


Figure 14-2: Collection of k_p and $\langle k_{SD} \rangle$ for bulk polymerization at 40 °C and 2000 bar of several alkyl acrylates and alkyl methacrylates including AA and MAA in water with the indicated monomer concentrations in wt.%.^[16,138] The AA data was obtained by extrapolation of the $\langle k_t^{app} \rangle$ values in Figure 13-2A (black points) and Figure 13-2B (grey points). The k_p values for the acrylate-type monomers refer to k_p^s . The apparent $\langle k_{SD} \rangle$ values for MA, BA and DA were obtained from implementing k_p^s into k_t/k_p .

In Figure 14-2, the k_p and $\langle k_{SD} \rangle$ values for polymerizations of AA and MAA in water are added to the data already presented in Figure 14-1A. The associated monomer concentrations in wt.% are indicated in the figure. The AA data was obtained by extrapolation of the $\langle k_t^{app} \rangle$ values in Figure 13-2A (black points) and Figure 13-2B (grey points), i.e. the values are based on polymerizations at 25 °C and 50 bar. The mechanistic origin of the increase of the

propagation rate coefficients toward lower AA and MAA concentrations has already been discussed in Chapter 6.1. The extrapolated $\langle k_{SD} \rangle$ for bulk polymerization of MAA is slightly below the associated value for *n*-BMA. Thus, the termination rate coefficient of pure MAA is quite low and not above $\langle k_{SD} \rangle$ of MMA as may be expected from the increase in termination rate within the series DMA < BMA < MMA. However, the viscosity of MAA is relatively high and exceeds the one of BMA by a factor of 1.5. Thus, the extrapolated $\langle k_{SD} \rangle \cdot \eta^*$ value for MAA bulk polymerization of about $11 \cdot 10^6 \text{ L} \cdot \text{mol}^{-1} \cdot \text{s}^{-1}$ would perfectly fit into the *n*-alkyl methacrylate data (see Table 14-2). The increase of $\langle k_{SD} \rangle$ toward lower monomer MAA concentration in water may reflect higher macroradical flexibility (see Chapter 8.2).

As mentioned previously, care must be taken when discussing the (apparent) $\langle k_{SD} \rangle$ data for the acrylate-type monomers. It is unreasonable to assign the strong acceleration of $\langle k_{SD} \rangle$ toward lower AA concentration in water to increased chain flexibility. As emphasized in the previous chapter, the AA termination rate data, especially at low monomer concentrations, must be considered highly fictitious. Improved evaluation procedures are urgently required for which, however, knowledge of individual k_{bb} and k_p^t values is obligatory.

15 Closing Remarks

In this work, the propagation and termination kinetics of MAA and NVP in aqueous solution were studied via PLP-SEC and SP-PLP-NIR, respectively. It is a matter of priority to use these rate coefficients for modeling rate of polymerization and MWD data from batch polymerizations of MAA^[277] and NVP in aqueous solution. Valuable information on the predictive power of the rate coefficients and on the reaction steps not considered so far, e.g. transfer-to-monomer, may be obtained from the comparison of simulated and experimental results. Furthermore, the SP-PLP-NIR and PLP-SEC studies may be extended to other technically relevant water-soluble monomers.^[200,265] The propagation kinetics for polymerization of water soluble monomers in non-aqueous solvents may be studied to broaden the current mechanistic picture. Moreover, the copolymerization kinetics in aqueous solution is of eminent scientific and industrial interest.

The polymerization kinetics of AA in aqueous solution is far from trivial due to the simultaneous occurrence of strong solvent effects on kinetic coefficients and MCR build-up by backbiting. As detailed in Chapter 13, k_{bb} and k_p^t values for the experimental conditions used for SP-PLP-NIR are urgently required for re-consideration of the experimental data. Thus, further PLP-SEC experiments under a wide variation of LPRRs (see Chapter 13.1) may be carried out, at least for estimating k_{bb}/k_p^t . Also individual k_{bb} and k_p^t values may be assessed from this technique for which, however, large simulation efforts are required (see Chapter 11). k_{bb} data for AA polymerization may alternatively be obtained by revisiting the determination of branching levels via ¹³C-NMR.^[47] The most appealing feature of this technique is the directness by which k_{bb} is determined (see Eq. (11-1)). However, long measurement times at NMR-spectrometers with high magnetic field strengths are required to obtain sufficient signal-to-noise quality of the spectra. Moreover, additional uncertainties are introduced by the Fourier transformation procedure, especially in terms of the phase correction. In case k_{bb} and k_p^t data for AA is available, the SP-PLP-NIR traces may be re-evaluated based on an improved kinetic model from which at least separate $\langle k_t^{ss} \rangle$ and $\langle k_t^{st} \rangle$ values should be accessible.

In principle, the perfect method for studies into the termination and transfer kinetics of acrylate-type monomers is tracing of $c_{SPR}(t)$ and $c_{MCR}(t)$ via SP-PLP-ESR as introduced for BA polymerization (see Chapter 12). However, this technique is not easily applied to aqueous

solution polymerizations of AA primarily due to the high polarity of the reacting system. Further studies should be devoted to additional acrylic acid esters, especially to MA and DA in order to reveal the effect of ester chain length on k_{bb} , k_p^t and the individual termination rate coefficients.

A considerable increase in time resolution of SP-PLP-ESR has recently been achieved^[149] which allows for studying fast terminating species. Thus, the SP-PLP-ESR investigations may be extended to monomers like styrene, MMA and vinyl acetate. However, full ESR spectra, required for the purpose of calibration and identification of H_x , are not easily measured with high scanning rates due to the low pseudo-stationary radical concentration under PLP-conditions. This limitation may be overcome by initiating polymerization via a continuous UV-lamp.

It was shown in Figure 5-16 and Figure 5-17 that two MMMP fragments with distinctly different termination rates are formed upon laser irradiation. The structure of those fragments may be determined via ESI-MS. Moreover, the associated rate coefficients of primary radical termination may be obtained from SP-PLP-ESR measurements on monomer-free solutions.

So far, the SP-PLP-ESR technique is so far limited to studies at low monomer-to-polymer conversions. However, it is of eminent scientific interest to study the chain-length dependence of termination at conversions where $\langle k_t \rangle$ is controlled by TD. This may be achieved by pre-mixing of polymer or via thermally induced pre-polymerization followed by the actual SP-PLP experiment.^[201]

SP-PLP-ESR studies may also be used for copolymerization systems (consisting of monomer A and B). The full ESR spectrum measured under copolymerization conditions is supposed to result from an overlap of two individual ESR spectra of macroradical chain ends of A- and B-type, respectively, as long range hyperfine coupling should be negligible. Due to the fast exchange of the terminal units via cross-propagation, identical $c_R(t)$ traces may be obtained from each line in the ESR spectrum providing access to an effective termination rate coefficient, k_t^{copo} .

Although SP-PLP-ESR is an extremely versatile experimental technique, only overall termination rate coefficients (i.e. the sum of the rate coefficient for disproportionation, $k_{t,d}$, and the rate coefficient for combination, $k_{t,c}$) can be obtained. However, the mode of termination may be determined from PLP-SEC experiments conducted under high termination rate limit conditions.^[285] Investigations into the temperature and pressure dependence the mode of termination during MMA and BMA polymerization are currently underway.^[300]

Moreover, the approach of applying PLP-SEC experiments to the determination of backbiting rate coefficients (see Chapter 11) may be generalized and used for measuring any kind of transfer coefficient, e.g. the one of transfer to a chain-transfer agent.^[300]

16 Glossary of Abbreviations

A	absorbance
a	Mark-Houwink parameter
α	power-law coefficient describing the chain-length dependence of k_t
AA	acrylic acid
α_D	degree of monomer ionization
α_H	coupling constant (with a hydrogen atom)
$A(k_x)$	(Arrhenius) pre-exponential factor of coefficient k_x
α_l	α in the long chain-length regime
AMPS	2-acrylamido-2-methylpropane sulfonic acid
a_p	proportionality constant that relates k_{bb} to f_0
α_s	α in the short chain-length regime
ATRP	atom transfer radical polymerization
B	integrated molar absorbtivity
BA	butyl acrylate
BAD	butyl acrylate dimer
BL	branching level
BMA	butyl methacrylate
$b\sigma$	dispersion parameter used to represent SEC broadening
C_η	viscosity parameter according to Eq. (8-7)
CI	chemically initiated
CLD-T	chain length dependent termination
CR	chemical reaction
C_{RD}	reaction diffusion constant
$c_{SPR}^?$	residual concentration of growing macroradicals at time t after the initiating laser pulse which escaped backbiting reactions
CTA	chain-transfer agent
$C_{tr,x}$	transfer constant
c_x	concentration of substance x
c_x^0	initial concentration of substance x

DA	dodecyl acrylate
Darocur	2-hydroxy-2-methylpropiophenone
Δ_{eff}	difference between the input value of k_p^{eff} and the value of k_p^{app} for the lowest LPRRs examined experimentally
$\Delta_{\log M, h}$	width of a peak in the molecular weight distribution at height $h < h_{\text{max}}$, where h_{max} is the maximum height of the peak
DMA	dodecyl methacrylate
DMPA	2,2-dimethoxy-2-phenyl acetophenone
D_s	diffusion coefficient
ε	molar absorption coefficient
$E_a(k_x)$	activation energy of coefficient k_x
E_λ	energy of one mole of photons at wavelength λ
E_P	energy of one laser pulse
ESI-MS	electrospray ionization – mass spectrometry
ESR	electron spin resonance
Eq.	equation
Φ	primary quantum yield
f	initiator efficiency
f_0	laser pulse repetition rate at which the sharp decrease in the apparent propagation rate coefficient occurs
FD	fast digitizer
f_L	laser pulse repetition rate (coefficient)
FRP	free-radical polymerization
FT	Fourier transformation
η	viscosity
$[\eta]$	intrinsic viscosity
η_0	viscosity at zero conversion
h_1, h_2, h_3, h_4	calibration constants in SP-PLP-ESR
η_r	relative viscosity
HQ	hydroquinone
HV	hydrodynamic volume
H_x	fixed magnetic field position used for time-resolved ESR experiments

I	intensity
i, j	radical chain length
I_0	starting intensity
IBA	<i>iso</i> -butyric acid
i_c	cross-over chain length according to the composite model
JCI	joint confidence interval
K	Mark-Houwink parameter
k_{ad}	addition rate coefficient of propagating radicals to RAFT agents
k_B	Boltzmann constant
k_{bb}	backbiting rate coefficient
k_{CR}	rate coefficient of a chemical reaction
k_d	initiator decomposition rate coefficient
K_{eq}	RAFT equilibrium constant
k_{frag}	fragmentation rate coefficient of RAFT intermediates
k_i	rate coefficient of monomer addition to initiator derived radicals
k_p	propagation rate coefficient
$k_{p,0}$	propagation rate coefficient without the contribution of diffusion
$k_{p,D}$	rate coefficient of the diffusive stage of propagation
$k_{p,D}^0$	diffusion controlled part of the propagation rate coefficient zero conversion
k_p^s	propagation rate coefficient of secondary propagating radicals
k_p^t	propagation rate of midchain radicals
k_p^{t*}	unimolecular propagation rate coefficient for monomer-complexed midchain radicals
$k_p^{th,0}$	apparent propagation rate coefficient determined from simulated molecular weight distributions
k_p^{eff}	effective propagation rate coefficient
$k_{p,max}$	propagation rate coefficient extrapolated to a monomer concentration of zero
$k_{p,X}$	rate coefficient of monomer addition to species X
k_{SD}	rate coefficient of segmental diffusion
$\langle k_{SD} \rangle$	arithmetic mean chain-length averaged termination rate coefficient in the low conversion plateau range

k_t	termination rate coefficient
$\langle k_t \rangle$	chain-length averaged termination rate coefficient
k_t^0	termination rate coefficient of (hypothetical) coiled monomeric radicals
$k_t(1,1)$	termination rate coefficient of radicals of chain length unity
k_t^{app}	apparent termination rate coefficient
$k_{t,c}$	rate coefficient for termination by combination
k_t^{copo}	effective termination rate coefficient in a copolymerization
k_{TD}	rate coefficient of translational diffusion
$k_{t,D}$	diffusion controlled termination rate coefficient
$k_{t,d}$	rate coefficient for termination by disproportionation
k_{TD}^0	translational diffusion rate coefficient at zero conversion
k_t^{eff}	effective termination rate coefficient
$k_t(i,i)$	termination rate coefficient of radicals of identical chain length i
$k_t(i,j)$	termination rate coefficient of radicals of size i and j
$k_{t,\text{RD}}$	reaction diffusion controlled termination rate coefficient
$k_{\text{tr},X}$	rate coefficient of chain transfer to a species X
k_t^{ss}	termination rate coefficient of two secondary propagating radicals
k_t^{st}	termination rate coefficient of a secondary propagating radical and a midchain radical
k_t^{tt}	termination rate coefficient of a two midchain radicals
l	optical path length
LC regime	long contact regime
M	molecular weight
LPRR	laser pulse repetition rate
M_1, M_2	molecular weight at the first / second point of inflection of the molecular weight distribution
MA	methyl acrylate
MAA	methacrylic acid
MEHQ	hydroquinone monomethyl ether
MH	Mark-Houwink
MMA	methyl methacrylate
MMMP	2-methyl-4-(methylthio)-2-morpholino-propiophenone
M_n	number average molecular weight

MWD	molecular weight distribution
$\tilde{\nu}$	wave number
N_A	Avogadro's number
n_c	number of backbiting and re-initiation cycles during one dark-time period
NEP	<i>N</i> -ethyl pyrrolidone
NIR	near infrared
NMP	<i>N</i> -methyl pyrrolidone
NMR	nuclear magnetic resonance
NVP	<i>N</i> -vinyl pyrrolidone
p	pressure
PA	propionic acid
<i>PDI</i>	polydispersity index
PLP	pulsed laser polymerization
POI	point of inflection
poly(X)	polymer of monomer X
R	leaving group of the RAFT agent
RAFT	reversible addition fragmentation transfer (polymerization)
R_C	capture radius
RD	reaction diffusion
<i>res</i>	residual
RI	refractive index
R_p	rate of polymerization
$r_{X,Y}$	reactivity ratio
σ	number of RAFT agent leaving groups
SC	signal channel
SC regime	short contact regime
SD	segmental diffusion
SEC	size exclusion chromatography
SP	single pulse
T	temperature
t	time
t_0	pulse separation time

t_p	propagation time
TD	translational diffusion
TEMPO	2,2,6,6-tertramethyl-1-piperidinyloxy
THF	tetrahydrofuran
τ_{MCR}	lifetime of a midchain radical until it undergoes monomer addition
TRITT	<i>S,S</i> -bis(α,α' -dimethyl- α' -acetic acid)-trithiocarbonate
TS	transition state
τ_{SPR}	lifetime of a secondary propagating radical until it undergoes backbiting
UV	ultra violet
V50	2,2'-azobis (2-methylpropionamidine) dihydrochloride
$\Delta V^\ddagger(k_x)$	activation volume of coefficient k_x
ν_i	rate of initiation
ω	reaction order in monomer concentration determined from stationary polymerization methods
w_X	weight fraction of substance X
w_X^0	initial weight fraction of substance X
X	monomer-to-polymer conversion
x_i	molar fraction of species i
x_{min}	lowest secondary propagating radical fraction that allows for observation of the sharp peak in the first-derivative curve of the molecular weight distribution
$X_{virtual}$	virtual monomer-to-polymer conversion
Z	stabilizing group of the RAFT agent

17 References

- [1] Baekeland, L. H. *US Patent 942,699*, **1907**.
- [2] Staudinger, H. *Berichte der Deutschen Chemischen Gesellschaft* **1920**, *53*, 1073–1085.
- [3] Staudinger, H. *Helv. Chim. Acta* **1922**, *4*, 785–806.
- [4] “*Chemie in Zahlen*”, VCI Broschüre, 2007.
- [5] “*Macromolecular Engineering. Precise Synthesis, Materials, Properties, Applications*”, Matyjaszewski, K.; Gnanou, Y.; Leibler, L. (Eds.), Wiley-VCH, Weinheim, 2007.
- [6] Buback, M.; Garcia-Rubio, L.-H.; Gilbert, R. G.; Napper, D. H.; Guillot, J.; Hamielec, A.; Hill, D.; O’Driscoll, K. F.; Olaj, O. F.; Shen, J.; Solomon, D.; Moad, G.; Sickler, M.; Tirrell, M.; Winnik, M. A. *J. Polym. Sci., Polym. Lett. Ed.* **1988**, *26*, 293–297.
- [7] Buback, M.; Gilbert, R. G.; Russell, G. T.; Hill, D. J. T.; Moad, G.; O’Driscoll, K. F.; Shen, J.; Winnik, M. A. *J. Polym. Sci., Polym. Chem. Ed.* **1992**, *30*, 851–863.
- [8] Buback, M.; Gilbert, R. G.; Hutchinson, R. A.; Klumperman, B.; Kuchta, F.-D.; Manders, B. G.; O’Driscoll, K. F.; Russell, G. T.; Schweer J. *Macromol. Chem. Phys.* **1995**, *196*, 3267–3280.
- [9] Beuermann, S.; Buback, M.; Davis, T. P.; Gilbert, R. G.; Hutchinson, R. A.; Olaj, O. F.; Russell, G. T.; Schweer, J.; van Herk A. M. *Macromol. Chem. Phys.* **1997**, *198*, 1545–1560.
- [10] Beuermann, S.; Buback, M.; Davis, T. P.; Gilbert, R. G.; Hutchinson, R. A.; Kajiwarra, A.; Klumperman, B.; Russell G. T. *Macromol. Chem. Phys.* **2000**, *201*, 1355–1364.
- [11] Buback, M.; Egorov, M.; Gilbert, R. G.; Kaminsky, V.; Olaj, O. F.; Russell, G. T.; Vana, P.; Zifferer, G. *Macromol. Chem. Phys.* **2002**, *203*, 2570–2582.
- [12] Beuermann, S.; Buback, M.; Davis, T. P.; Gilbert, R. G.; Hutchinson, R. A.; Kajiwarra, A.; Kamachi, M.; Lacík, I.; Russell G. T. *Macromol. Chem. Phys.* **2003**, *204*, 1338–1350.

- [13] Asua, J. M.; Beuermann, S.; Buback, M.; Castignolles, P.; Charleux, B.; Gilbert, R. G.; Hutchinson, R. A.; Leiza, J. R.; Nikitin, A. N.; Vairon, J.-P.; van Herk, A. M. *Macromol. Chem. Phys.* **2004**, *205*, 2151–2160.
- [14] Barner-Kowollik, C.; Buback, M.; Egorov, M.; Fukuda, T.; Goto, A.; Olaj, O. F.; Russell, G. T.; Vana, P.; Yamada, B.; Zetterlund, P. *Prog. Polym. Sci.* **2005**, *30*, 605–643.
- [15] Beuermann, S.; Buback, M.; Hesse, P.; Kuchta, F.-D.; Lacík, I.; van Herk, A. M. *Pure Appl. Chem.* **2007**, *79*, 1463–1469.
- [16] Beuermann, S.; Buback, M. *Prog. Polym. Sci.* **2002**, *27*, 191–254.
- [17] Heuts, J. P. A.; Gilbert, R. G.; Radom, L. *Macromolecules* **1995**, *28*, 8771–8781.
- [18] Heuts, J. P. A.; Gilbert, R. G.; Maxwell, I. A. *Macromolecules* **1997**, *30*, 726–736.
- [19] Thickett, S. C.; Gilbert, R. G. *Polymer* **2004**, *45*, 6993–6999.
- [20] Izgorodina, E. I.; Coote, M. L. *Chemical Physics* **2006**, *324*, 96–110.
- [21] Değirmenci, I.; Avcı, D.; Aviyente, V.; van Caeter, K.; van Speybroeck, V.; Waroquier, M. *Macromolecules* **2007**, *40*, 9590–9602.
- [22] Buback, M. *Makromol. Chem.* **1990**, *191*, 1575–1587.
- [23] Buback, M.; Huckestein, B.; Russell, G. T. *Macromol. Chem. Phys.* **1994**, *195*, 539–554.
- [24] de Gennes, P. G. *J. Chem. Phys.* **1982**, *76*, 3322–3326.
- [25] Mahabadi, H. K. *Macromolecules* **1985**, *18*, 1319–1324.
- [26] Friedman, B.; O’Shaughnessy, B. *Macromolecules* **1993**, *26*, 5726–5739.
- [27] Smith, G. B.; Russell, G. T.; Heuts, J. P. A. *Macromol. Theory Simul.* **2003**, *12*, 299–314.
- [28] Nikitin, A. N.; Hutchinson, R. A. *Macromolecules*, **2005**, *38*, 1581–1590.
- [29] Olaj, O. F.; Bitai, I.; Hinkelmann, F. *Macromol. Chem.* **1987**, *188*, 1689–1702.

- [30] Olaj, O. F.; Schnöll-Bitai, I. *Eur. Polym. J.* **1989**, *25*, 635–641.
- [31] Buback, M.; Hippler, H.; Schweer, J.; Vögele, H.-P. *Makromol. Chem., Rapid Commun.* **1986**, *7*, 261–265.
- [32] Buback, M.; Egorov, M.; Junkers, T.; Panchenko, E. *Macromol. Rapid Commun.* **2004**, *25*, 1004–1009.
- [33] Buback, M.; Egorov, M.; Junkers, T.; Panchenko, E. *Macromol. Chem. Phys.* **2005**, *206*, 333–341.
- [34] Buback, M.; Müller, E.; Russell, G. T. *J. Phys. Chem. A* **2006**, *110*, 3222–3230.
- [35] Chiefari, J.; Chong, Y. K.; Ercole, F.; Krstina, J.; Jeffery, J.; Le, T. P. T.; Mayadunne, R. T. A.; Meijs, G. F.; Moad, C. L.; Moad, G.; Rizzardo, E.; Thang, S. H. *Macromolecules* **1998**, *31*, 5559–5562.
- [36] Mayadunne, R. T. A.; Rizzardo, E.; Chiefari, J.; Chong, Y. K.; Moad, G.; Thang, S. H. *Macromolecules* **1999**, *32*, 6977–6980.
- [37] Buback, M.; Junkers, T.; Vana, P. *Macromol. Rapid Commun* **2005**, *26*, 796–802.
- [38] Junkers, T.; Theis, A.; Buback, M.; Stenzel, M. H.; Davis, T. P.; Vana, P.; Barner-Kowollik, C. *Macromolecules* **2005**, *38*, 9497–9508.
- [39] Buback, M.; Hesse, P.; Junkers, T.; Theis, T.; Vana, P. *Aust. J. Chem.* **2007**, *60*, 779–787.
- [40] Vana, P.; Davis, T. P.; Barner-Kowollik, C. *Macromol. Rapid. Commun.* **2002**, *23*, 952–956.
- [41] Gilbert, B. C.; Lindsay Smith, J. R.; Milne, E. C.; Whitwood, A. C.; Taylor, P. *J. Chem. Soc. Perkin Trans.* **1994**, *2*, 1759–1769.
- [42] Ahmad, N. M.; Heatley, F.; Lovell, P. A. *Macromolecules* **1998**, *31*, 2822–2827.
- [43] Yamada, B.; Azukizawa, M.; Yamazoe, H.; Hill, D. J. T.; Pomery, P. J. *Polymer* **2000**, *41*, 5611–5618.

- [44] Azukizawa, M.; Yamada, B.; Hill, D. J. T.; Pomery, P. J. *Macromol. Chem. Phys.* **2000**, *201*, 774–781.
- [45] Plessis, C.; Arzamendi, G.; Leiza, J. R.; Schoonbrood, H. A. S.; Charmot, D.; Asua, J. M. *Macromolecules* **2000**, *33*, 4–7.
- [46] Farcet, C.; Bellenev, J.; Charleux, B.; Pirri, R. *Macromolecules* **2002**, *35*, 4912–4918.
- [47] Plessis, C.; Arzamendi, G.; Alberdi, J. M.; van Herk, A. M.; Leiza, J. R.; Asua, J. M. *Macromol. Rapid Commun.* **2003**, *24*, 173–177.
- [48] Sato, E.; Emoto, T.; Zetterlund, P. B.; Yamada, B. *Macromol. Chem. Phys.* **2004**, *205*, 1829–1839.
- [49] Willemse, R. X. E.; van Herk, A. M.; Panchenko, E.; Junkers, T.; Buback, M. *Macromolecules* **2005**, *38*, 5098–5103.
- [50] Quan, C.; Soroush, M.; Grady, M. C.; Hansen, J. E.; Simonsick Jr., W. J. *Macromolecules* **2005**, *38*, 7619–7628.
- [51] Nikitin, A. N.; Hutchinson, R. A. *Macromol. Theory Simul.* **2006**, *15*, 128–136.
- [52] Buback, M.; Hesse, P.; Lacík, I. *Macromol. Rapid Commun.* **2007**, *28*, 2049–2054.
- [53] Nikitin, A. N.; Hutchinson, R. A.; Buback, M.; Hesse, P. *Macromolecules* **2007**, *40*, 8631–8641.
- [54] Buback, M.; Hesse, P.; Junkers, T.; Sergeeva, T.; Theis, T. *Macromolecules* **2008**, *41*, 288–291.
- [55] Nikitin, A. N.; Castignolles, P.; Charleux, B.; Vairon, J.-P. *Macromol. Rapid Commun.* **2003**, *24*, 778–782.
- [56] Arzamendi, G.; Plessis, C.; Leiza, J. R.; Asua, J. M. *Macromol. Theory Simul.* **2003**, *12*, 315–324.
- [57] Nikitin, A. N.; Castignolles, P.; Charleux, B.; Vairon, J.-P. *Macromol. Theory Simul.* **2003**, *12*, 440–448.
- [58] Peck, A. N. F.; Hutchinson, R. A. *Macromolecules* **2004**, *37*, 5944–5951.

- [59] “*Handbook of polyelectrolytes and their applications*”, Tripathy, S. K.; Kumar, J.; Nalva, H. S. (Eds.), American Scientific Publishers, Stevenson Ranch, California, 2002.
- [60] Katchalsky, A.; Blauer, G. *Faraday Soc. Trans.* **1951**, *47*, 1360–1370.
- [61] Gromov, V. F.; Galperina, N. I.; Osmanov, T. O.; Khomikovskij, P. M.; Abkin, A. D. *Eur. Polym. J.* **1980**, *16*, 529–535.
- [62] Gromov, V. F.; Bune, E. V.; Teleshov, E. N. *Russ. Chem. Rev.* **1994**, *63*, 530–542.
- [63] Anseth, K. S.; Scott, R. A.; Peppas, N. A. *Macromolecules* **1996**, *29*, 8308–8312.
- [64] Galperina, N. I.; Gugunava, T. A.; Gromov, V. F.; Khomikovskij, P. M.; Abkin, A. D. *Vysokomol. Soed.* **1975**, *A17*, 1455–1460.
- [65] “*Polymer Handbook*”, Brandrup, J.; Immergut, E. H.; Grulke, E. A. (Eds.), 4th edition, John Wiley & Sons, Inc. New York, 1999.
- [66] Kuchta, F.-D.; van Herk, A. M.; German, A. L. *Macromolecules* **2000**, *33*, 3641–3649.
- [67] Lacík, I.; Beuermann, S.; Buback, M. *Macromolecules* **2001**, *34*, 6224–6228.
- [68] Lacík, I.; Beuermann, S.; Buback, M. *Macromolecules* **2003**, *36*, 9355–9363.
- [69] Lacík, I.; Beuermann, S.; Buback, M. *Macromol. Chem. Phys.* **2004**, *205*, 1080–1087.
- [70] Ganachaud, F.; Balic, R.; Monteiro, M. J.; Gilbert, R. G. *Macromolecules* **2000**, *33*, 8589–8596.
- [71] Seabrook, S. A.; Tonge, M. P.; Gilbert, R. G. *J. Polym. Sci. Part A: Polym. Chem.* **2005**, *43*, 1357–1368.
- [72] Beuermann, S.; Buback, M.; Hesse, P.; Lacík, I. *Macromolecules* **2006**, *39*, 184–193.
- [73] Beuermann, S.; Buback, M.; Hesse, P.; Kukučková, S.; Lacík, I. *Macromol. Symp.* **2007**, *248*, 23–32.
- [74] Beuermann, S.; Buback, M.; Hesse, P.; Kukučková, S.; Lacík, I. *Macromol. Symp.* **2007**, *248*, 41–49.

- [75] Beuermann, S.; Buback, M.; Hesse, P.; Hutchinson, R. A.; Kukučková, S.; Lacík, I. *Macromolecules* **2008**, *41*, 3513–3520.
- [76] Boschmann, D.; Vana, P. *Macromolecules* **2007**, *40*, 2683–2693.
- [77] Chiefari, J.; Jeffery, J.; Mayadunne, T. A.; Moad, G.; Rizzardo, E.; Thang, S. H. *Macromolecules* **1999**, *32*, 7700–7702.
- [78] Achilias, D. S. *Macromol. Theory Simul.* **2007**, *16*, 319–347.
- [79] von Smoluchowski, M. *Z. phys. Chem.* **1917**, *92*, 129–168.
- [80] Hutchinson, R. A. *Polym. React. Eng.* **1992-3**, *1*, 521–577.
- [81] Yamazoe, H.; Zetterlund, P. B.; Yamada, B.; Hill, D. J. T.; Pomery, P. J. *Macromol. Chem. Phys.* **2001**, *202*, 824–829.
- [82] Ballard, M. J.; Gilbert, R. G.; Napper, D. H.; Pomery, P. J.; O’Sullivan, P. W.; O’Donnell, J. H. *Macromolecules* **1986**, *19*, 1303–1308.
- [83] Zhu, S.; Tian, Y.; Hamielec, A. E.; Eaton, D. R. *Polymer* **1990**, *31*, 154–159.
- [84] Carswell, T. G.; Hill, D. J. T.; Londero, D. I.; O’Donnell, J. H.; Pomery, P. J.; Winzor, C. L. *Polymer* **1992**, *33*, 137–140.
- [85] Ballard, M. J.; Napper, D. H.; Gilbert, R. G. *J. Polym. Sci., Polym. Chem. Ed.* **1984**, *22*, 3225–3253.
- [86] Zetterlund, P. B.; Yamazoe, H.; Yamada, B.; Hill, D. J. T.; Pomery, P. J. *Macromolecules* **2001**, *34*, 7686–7691.
- [87] Zetterlund, P. B.; Yamazoe, H.; Yamada, B. *Macromol. Theory Simul.* **2003**, *12*, 379–385.
- [88] Zetterlund, P. B.; Yamauchi, S.; Yamada, B. *Macromol. Chem. Phys.* **2004**, *205*, 778–785.
- [89] Benson, S. W.; North, A. M. *J. Am. Chem. Soc.* **1959**, *81*, 1339–1345.
- [90] Benson, S. W.; North, A. M. *J. Am. Chem. Soc.* **1962**, *84*, 935–940.

- [91] Schulz, G. V. *Z. Phys. Chem. (Munich)* **1956**, *8*, 290–317.
- [92] Andrzejewska, E. *Prog. Polym. Sci.* **2001**, *26*, 605–665.
- [93] Buback, M.; Schweer, J. *Z. Phys. Chem. (Munich)* **1989**, *161*, 153–165.
- [94] Norrish, R. G. W.; Smith, R. R. *Nature* **1942**, *150*, 336–3367.
- [95] Trommsdorff, E.; Köhle, H.; Lagally, P. *Makromol. Chem.* **1948**, *1*, 169–198.
- [96] Beuermann, S.; Buback, M.; Russell, G. T. *Macromol. Chem. Phys.* **1995**, *196*, 2493–2516.
- [97] Junkers, T. *PhD thesis*, Göttingen, 2006.
- [98] Theis, T. *diploma thesis*, Göttingen, 2006.
- [99] Moad, G.; Rizzardo, E.; Solomon, D. H.; Beckwith, A. L. J. *Polym. Bull.* **1992**, *29*, 647–652.
- [100] Zetterlund, P. B.; Busfield, W. K.; Jenkins, I. D. *Macromolecules* **2002**, *35*, 7232–7237.
- [101] Gridnev, A. A.; Ittel, S. D. *Macromolecules* **1996**, *29*, 5864–5874.
- [102] Olaj, O. F.; Vana, P.; Zoder, M. *Macromolecules* **2002**, *35*, 1208–1214.
- [103] Olaj, O. F.; Vana, P.; Zoder, M.; Kornherr, A.; Zifferer, G. *Macromol. Rapid Commun.* **2000**, *21*, 913–920.
- [104] Willemsse, R. X. E.; Staal, B. B. P.; van Herk, A. M.; Pierik, S. C. J.; Klumperman, B. *Macromolecules* **2003**, *36*, 9797–9803.
- [105] Olaj, O. F.; Zoder, M.; Vana, P.; Kornherr, A.; Schnöll-Bitai, I.; Zifferer, G. *Macromolecules* **2005**, *38*, 1944–1948.
- [106] Smith, G. B.; Russell, G. T.; Yin, M.; Heuts, J. P. A. *Eur. Polym. J.* **2005**, *41*, 225–230.
- [107] Heuts, J. P. A.; Russell, G. T. *Eur. Polym. J.* **2006**, *42*, 3–X.
- [108] Smith, G. B.; Heuts, J. P. A.; Russell, G. T. *Macromol. Symp.* **2005**, *226*, 133–146.
- [109] Heuts, J. P. A.; Russell, G. T.; Smith, G. B.; van Herk, A. M. *Macromol. Symp.* **2007**, *248*, 12–22.

- [110] Heuts, J. P. A.; Russell, G. T.; Smith, G. B. *Aust. J. Chem.* **2007**, *60*, 754–764.
- [111] Olaj, O. F.; Zifferer, G. *Macromolecules* **1987**, *20*, 850–861.
- [112] Olaj, O. F.; Kornherr, A.; Zifferer, G. *Macromol. Theory Simul.* **1998**, *7*, 501–508.
- [113] Russell, G. T. *Aust. J. Chem.* **2002**, *55*, 399–414.
- [114] de Kock, J. B. L., van Herk, A. M.; German, A. L. *J. Polym. Sci., Polym. Rev.* **2001**, *41*, 199–256.
- [115] Piton, M. C.; Gilbert, R. G.; Chapman, B. E.; Kuchel, P. W. *Macromolecules* **1993**, *26*, 4472–4477.
- [116] Kirkwood, J. G.; Riseman, J. *J. Phys. Chem.* **1948**, *16*, 565–573.
- [117] Mahabadi, H. K.; O’Driscoll, K. F. *Macromolecules* **1977**, *10*, 55–58.
- [118] Mahabadi, H. K.; O’Driscoll, K. F. *J. Polym. Sci., Polym. Chem. Ed.* **1977**, *15*, 283–300.
- [119] “*Principles of Polymer Chemistry*”, Flory, P. J., Cornell University Press, Ithaca, New York, 1953.
- [120] Strukelj, M.; Martinho, J. M. G.; Winnik, M. A. *Macromolecules* **1991**, *24*, 2488–2492.
- [121] Johnston-Hall, G.; Theis, A.; Monteiro, M. J.; Davis, T. P.; Stenzel, M. H.; Barner-Kowollik, C. *Macromol. Chem. Phys.* **2005**, *206*, 2047–2053.
- [122] Johnston-Hall, G.; Stenzel, M. H.; Davis, T. P.; Barner-Kowollik, C.; Monteiro, M. J. *Macromolecules* **2007**, *40*, 2730–2736.
- [123] Johnston-Hall, G.; Monteiro, M. J. *Macromolecules* **2008**, *41*, 727–736.
- [124] Theis, A.; Feldermann, A.; Charton, N.; Davis, T. P.; Stenzel, M. H.; Barner-Kowollik, C. *Polymer* **2005**, *46*, 6797–6809.
- [125] Khokhlov, A. R. *Makromol. Chem., Rapid Commun.* **1981**, *2*, 633–636.
- [126] Olaj, O. F.; Zifferer, G. *Macromolecules* **1987**, *20*, 850–861.
- [127] Karatekin, E.; O’Shaughnessy, B.; Turro, N. J. *Macromol. Symp.* **2002**, *182*, 81–101.

- [128] Fröhlich, M. G.; Vana, P.; Zifferer, G. *Macromol. Theory Simul.* **2007**, *16*, 610–618.
- [129] Fröhlich, M. G.; Vana, P.; Zifferer, G. *J. Chem. Phys.* **2007**, *127*, 164906/1–164906/7.
- [130] Mahabadi, H. K. *Macromolecules* **1991**, *24*, 606–609.
- [131] Olaj, O. F.; Vana, P. *Macromol. Rapid Commun.* **1998**, *19*, 433–439.
- [132] Olaj, O. F.; Vana, P. *Macromol. Rapid Commun.* **1998**, *19*, 533–538.
- [133] Olaj, O. F.; Vana, P.; Kornherr, A.; Zifferer, G. *Macromol. Chem. Phys.* **1999**, *200*, 2031–2039.
- [134] Buback, M.; Busch, M.; Kowollik, C. *Macromol. Theory Simul.* **2000**, *9*, 442–452.
- [135] Olaj, O. F.; Vana, P. *J. Polym. Sci., Polym. Chem. Ed.* **2000**, *38*, 697–705.
- [136] Buback, M.; Egorov, M.; Feldermann, A. *Macromolecules* **2004**, *37*, 1768–1776.
- [137] Theis, A. Davis, T. P.; Stenzel, M. H.; Barner-Kowollik, C. *Polymer* **2006**, *47*, 999–1010.
- [138] Buback, M.; Junkers, T. *Macromol. Chem. Phys.* **2006**, *207*, 1640–1650.
- [139] de Gennes, P. G. *J. Chem. Phys.* **1971**, *55*, 572–579.
- [140] de Gennes, P. G. *J. Chem. Phys.* **1982**, *76*, 3322–3326.
- [141] Johnston-Hall, G.; Monteiro, M. J. *Macromolecules* **2008**, *41*, 727–736.
- [142] de Kock, J. B. L. *PhD thesis*, Eindhoven, 1999.
- [143] Smith, G. B.; Russell, G. T. *Z. Phys. Chem. (Munich)* **2005**, *219*, 295–323.
- [144] Feldermann, A. *PhD thesis*, Göttingen, 2003.
- [145] Matyjaszewski, K.; Patten, T. E.; Xia, J. H. *J. Am. Chem. Soc.* **1997**, *119*, 674–680.
- [146] Matyjaszewski, K.; Xia, J. H. *Chem. Rev.* **2001**, *101*, 2921–2990.
- [147] Hawker, C. J.; Bosman, A. W.; Harth, E. *Chem. Rev.* **2001**, *301*, 3661–3688.
- [148] Fischer, H. *J. Polym. Sci., Part A: Polym. Chem.* **1999**, *37*, 1885–1901.

- [149] Buback, M.; Hesse, P.; Junkers, T.; Vana, P. *Macromol. Rapid Commun.* **2006**, *27*, 182–187.
- [150] Barner-Kowollik, C.; Quinn, J. F.; Morsley, D. R.; Davis, T. P. *J. Polym. Sci., Part A: Polym. Chem.* **2001**, *39*, 1353–1365.
- [151] Davis, T. P.; Barner-Kowollik, C.; Nguyen, T. L. U.; Stenzel, M. H.; Quinn, J. F.; Vana, P. *ACS Symp. Ser.* **2003**, *854*, 551–569.
- [152] Feldermann, A.; Coote, M. L.; Stenzel, M. H.; Davis, T. P.; Barner-Kowollik, C. *J. Am. Chem. Soc.* **2004**, *126*, 15915–15923.
- [153] Monteiro, M. J.; de Brouwer, H. *Macromolecules* **2001**, *34*, 349–352.
- [154] Kwak, Y.; Goto, A.; Tsujii, Y.; Murata, Y.; Komatsu, K.; Fukuda, T. *Macromolecules* **2002**, *35*, 3026–3029.
- [155] Wang, A. R.; Zhu, S.; Kwak, Y.; Goto, A.; Fukuda, T.; Monteiro, M. S.; *J. Polym. Sci., Part A: Polym. Chem.* **2003**, *41*, 2833–2839.
- [156] Monteiro, M.; Bussels, R.; Beuermann, S.; Buback, M. *Aust. J. Chem.* **2002**, *55*, 433–437.
- [157] Chernikova, E.; Morozov, A.; Leonova, E.; Garina, E.; Golubev, V.; Bui, C.; Charleux, B. *Macromolecules* **2004**, *37*, 6329–6339.
- [158] Drache, M.; Schmidt-Naake, G.; Buback, M.; Vana, P. *Polymer* **2005**, *46*, 8483–8493.
- [159] Kwak, Y.; Goto, A.; Komatsu, K.; Sugiura, Y.; Fukuda, T. *Macromolecules* **2004**, *37*, 4434–4440.
- [160] Buback, M.; Vana, P. *Macromol. Rapid Commun.* **2006**, *27*, 1299–1305.
- [161] Buback, M.; Janssen, O.; Oswald, R.; Schmatz, S.; Vana, P. *Macromol. Symp.* **2007**, *248*, 158–167.
- [162] Barner-Kowollik, C.; Quinn, J. F.; Nguyen, T. L. U.; Heuts, J. P. A.; Davis, T. P. *Macromolecules* **2001**, *34*, 7849–7857.
- [163] Gallot-Grubisic, Z.; Rempp, P.; Benoit, J. *J. Polym. Sci., Polym. Lett.* **1967**, *5*, 753–759.

- [164] Flory, P. J. *J. Chem. Phys.* **1945**, *13*, 453–465.
- [165] Mark, H. *Der feste Körper*, Hirzel, Leipzig 1938.
- [166] Houwink, R. *J. Prakt. Chem.* **1940**, *157*, 15–18.
- [167] Reed, W. F. *Macromol. Chem. Phys.* **1995**, *196*, 1539–1575.
- [168] Wyatt, P. J. *Anal. Chim. Acta* **1993**, *272*, 1–40.
- [169] Lai, J. T.; Filla, D.; Shea, R. *Macromolecules* **2002**, *35*, 6754–6756.
- [170] Poulter, T. C. *Phys. Rev.* **1932**, *40*, 860–869.
- [171] Buback, M.; Hinton, C. “*High-pressure Techniques in Chemistry and Physics: A Practical Approach*”, Isaacs, N. S.; Holzapfel, W. B. (Eds.), Oxford Univ. Press., 1997, 151–186.
- [172] Kuchta, F.-D. *PhD thesis*, Göttingen, 1995.
- [173] Beuermann, S.; Paquet Jr, D. A.; McMinn, J. H.; Hutchinson, R. A. *Macromolecules* **1996**, *29*, 4206–4215.
- [174] Hutchinson, R. A.; Beuermann, S.; Paquet Jr., D. A.; McMinn, J. H. *Macromolecules* **1997**, *30*, 3490–3493.
- [175] Tackx P., Bosscher F. *Anal. Commun.* **1997**, *34*, 295–297.
- [176] Huglin, M. B. *J. Appl. Polym. Sci.* **1965**, *9*, 4003–4024.
- [177] Schweer, J. *PhD thesis*, Göttingen, 1988.
- [178] Kowollik, C. *PhD thesis*, Göttingen, 1999.
- [179] Deufelhard, P.; Wulkow, M. *Preprint SC94-22* **1994**.
- [180] Wulkow, M. *Macromol. Theory Simul.* **1996**, *2*, 393–416.
- [181] Buback, M.; Busch, M.; Lämmel, R. A. *Macromol. Theory Simul.* **1996**, *5*, 845–861.
- [182] Schulz, G. V.; Romatowski, J. *Makromol. Chem.* **1965**, *85*, 195–226.

- [183] (a) Aleksandrov, A. P.; Genkin, V. N.; Kitai, M. S.; Smirnova, I. M.; Sokolov, V. V. *J. Quantum Electron.* **1977**, *4*, 976–981.; (b) Genkin, V. N.; Sokolov, V. V. *Dokl. Akad. Nauk SSSR* **1977**, *234*, 94–96.
- [184] Davis, T. P.; O’Driscoll, K. F.; Piton, M. C.; Winnik, M. A. *Polym. Int.* **1991**, *24*, 65–70.
- [185] Buback, M.; Degener, B. *Makromol. Chem.* **1993**, *194*, 2875–2883.
- [186] Lyons, R. A.; Hutovic, J.; Piton, M. C.; Christie, D. J.; Clay, P. L.; Manders, B. G.; Kable, S. H.; Gilbert, R. G. *Macromolecules* **1996**, *29*, 1918–1927.
- [187] Hutchinson, R. A.; Paquet Jr, D. A.; McMinn, J. H.; Beuermann, S.; Fuller, R. E.; Jackson, C. *DECHEMA Monographs* **1995**, *131*, 467–492.
- [188] Manders, B. *Ph.D. Thesis*, Eindhoven, 1997.
- [189] Beuermann, S.; Buback, M.; Schmaltz, C. *Macromolecules* **1998**, *31*, 8069–8074.
- [190] Beuermann, S.; Buback, M.; Schmaltz, C.; Kuchta, F.-D. *Macromol. Chem. Phys.* **1998**, *199*, 1209–1216.
- [191] Buback, M.; Kurz, C. H.; Schmaltz, C. *Macromol. Chem. Phys.* **1998**, *199*, 1721–1727.
- [192] Couvreur, L.; Piteau, G.; Castignolles, P.; Tonge, M.; Coutin, B.; Charleux, B.; Vairon, J. P. *Macromol. Symp.* **2001**, *174*, 197–207.
- [193] Pierik, S. C. J.; van Herk, A. M.; Plessis, C.; van Steenis, J. H.; Loonen, T.; Bombeeck, A. *Eur. Polym. J.* **2005**, *41*, 1212–1218.
- [194] data provided by BASF AG
- [195] “*Handbook of Chemistry and Physics*”, 76th ed.; Lide, D. R., Ed., CRC Press, Boca Raton, 1995–96.
- [196] Buback, M. *Angew. Chem.* **1991**, *103*, 658–670.
- [197] Buback, M.; Kuchta, F.-D. *Macromol. Chem. Phys.* **1995**, *196*, 1887–1898.
- [198] Beuermann, S.; Buback, M.; Hesse, P.; Junkers, T.; Lacík, I. *Macromolecules* **2006**, *39*, 509–516.

- [199] Hesse, P. *diploma thesis*, Göttingen, 2004.
- [200] Schrooten, J. *diploma thesis*, Göttingen, 2007.
- [201] Junkers, T. *diploma thesis*, Göttingen, 2002.
- [202] Barth, J. *diploma thesis*, Göttingen, 2008.
- [203] Kamachi, M. *J. Polym. Sci. Part A: Polym. Chem.* **2002**, *40*, 269–285.
- [204] Yamada, B.; Westmoreland, D. G.; Kobatake, S.; Konosu, O. *Prog. Polym. Sci.* **1999**, *24*, 565–630.
- [205] Ranby, B.; Rabek, J. F. “*ESR Spectroscopy in Polymer Research*“, Springer Verlag, Berlin-Heidelberg-New York, 1977.
- [206] Tonge, M. P.; Kajiwara, A.; Kamachi, M.; Gilbert, R. G. *Polymer* **1998**, *39*, 2305–2313.
- [207] Kubota, N.; Kajiwara, A.; Zetterlund, P. B.; Kamachi, M.; Treurnicht, J.; Tonge, M. P.; Gilbert, R. G.; Yamada, B. *Macromol. Chem. Phys.* **2007**, *208*, 2403–2411.
- [208] Müller, E. *PhD thesis*, Göttingen, 2005.
- [209] Sergeeva, T. *unpublished results*
- [210] Gruber, H. F. *Prog. Polym. Sci.* **1992**, *17*, 953–1044.
- [211] Külpmann, A. *diploma thesis*, Göttingen, 2000.
- [212] Buback, M.; Külpmann, A. *Macromol. Chem. Phys.* **2003**, *204*, 632–637.
- [213] Vana, P.; Davis, T. P.; Barner-Kowollik, C. *Aust. J. Chem.* **2002**, *55*, 315–318.
- [214] Leopold, D.; Fischer, H. *J. Chem. Soc. Perkin Trans. 2* **1992**, *4*, 513–517.
- [215] Fischer, H.; Baer, R.; Hany, R.; Verhoolen, I.; Walbiner, M. *J. Chem. Soc. Perkin Trans.* **1990**, *2*, 787–798.
- [216] Vana, P.; Davis, T. P.; Barner-Kowollik, C. *J. Polym. Sci., Part A: Polym. Chem.* **2002**, *40*, 674–681.
- [217] Szablan, Z.; Junkers, T.; Koo, S. P. S.; Lovestead, T. M.; Davis, T. P.; Stenzel, M. H.; Barner-Kowollik, C. *Macromolecules* **2007**, *40*, 6820–6833.

- [218] Buback, M.; Kowollik, C.; Kurz, C.; Wahl, A. *Macromol. Chem. Phys.* **2000**, *201*, 464–469.
- [219] “*Data Reduction and Error Analysis for Physical Science*” Bevington, P., McGraw Hill, New York, 1969.
- [220] “*Numerical Recipes*” Press, W. H.; Flannery, B. P.; Teukolsky, S. A.; Vetterling, W. T., Cambridge University Press, Cambridge, 1989.
- [221] Kurz, C. *PhD thesis*, Göttingen, 1995.
- [222] Kratochvil, P.; Straková, D.; Stejskal, J.; Tuzar, Z. *Macromolecules* **1983**, *16*, 1136–1143.
- [223] Katchalsky, A. *J. Polym. Sci.* **1951**, *7*, 393–412.
- [224] Silberberg, A.; Eliassaf, J.; Katchalsky, A. *J. Polym. Sci.* **1957**, *23*, 259–284.
- [225] Sakurai, M.; Imai, T.; Yamashita, F.; Nakamura, K.; Komatsu, T.; Nakagawa, T. *Polymer J.* **1993**, *25*, 1247–1255.
- [226] Chapiro, A. *Eur. Polym. J.* **1973**, *9*, 417–427.
- [227] van Herk, A. M. *J. Chem. Educ.* **1995**, *72*, 138–140.
- [228] Buback, M.; Mähling, F.-O. *J. Supercrit. Fluids* **1995**, *8*, 119–126.
- [229] Kabanov, V. A.; Topchiev, D. A.; Karaputadze, T. M. *J. Polym. Sci. Symp.* **1973**, *42*, 173–183.
- [230] Kabanov, V. A.; Topchiev, D. A. *Vysokomol. Soed.* **1971**, *A13*, 1324–1347.
- [231] Popov, V. G.; Topchiev, D. A.; Kabanov, V. A.; Kargin, V. A. *Vysokomol. Soed.* **1972**, *A14*, 117–130.
- [232] Topchiev, D. A.; Shakirov, V. Z.; Kalinina, L. P.; Karaputadze, T. M.; Kabanov, V. A. *Vysokomol. Soed.* **1972**, *A14*, 581–586.
- [233] Kabanov, V. A.; Topchiev, D. A.; Karaputadze, T. M.; Mkrtchian, L. A. *Eur. Polym. J.* **1975**, *11*, 153–159.

- [234] Cutié, S. S.; Smith, P. B.; Henton, D. E.; Staples, T. L.; Powell, C. J. *Polym. Sci. B Polym. Phys.* **1997**, *35*, 2029–2047.
- [235] “*Characterization of Macromolecular Parameters in Polyelectrolyte Solutions.*” In: Dautzenberg, H.; Jaeger, W.; Kötz, J.; Philipp, B.; Seidel, C.; Stscherbina, D. “*Polyelectrolytes: Formation, Characterization and Application*”, Hauser Publishers, Munich, Vienna, New York, 1994, Chapter 5, 166–247.
- [236] Dobrynin, A.V.; Rubinstein, M. *Prog. Polym. Sci.* 2005, *30*, 1049–1118.
- [237] Sedláč, M. “*Polyelectrolytes in solution.*” In: “*Light scattering: Principles and development*”, Brown, W. Ed. Clarendon Press, Oxford, 1996, Chapter 4, 120–163.
- [238] “*Applications of Polyelectrolytes.*” In: Dautzenberg, H.; Jaeger, W.; Kötz, J.; Philipp, B.; Seidel, C.; Stscherbina, D. “*Polyelectrolytes: Formation, Characterization and Application.*” Hauser Publishers, Munich, Vienna, New York, 1994, Chapter 7, 272–327
- [239] de Stefano, C.; Gianguzza, A.; Piazzese, D.; Sammartano, S. *React. Funct. Polym.* **2003**, *55*, 9–20.
- [240] Sedláč, M. *Polymer* **1990**, *31*, 253–257.
- [241] Horský, J.; Morawetz, H. *Makromol. Chem.* **1988**, *189*, 2475–2483.
- [242] Morawetz, H.; Wang, Y. *Macromolecules* **1987**, *20*, 194–195.
- [243] Morawetz, H. *Macromolecules* **1996**, *29*, 2689–2690.
- [244] Nakashima, K.; Fujimoto, Y.; Anzai, T.; Dong, J.; Sato, H.; Ozaki, Y. *Bull. Chem. Soc. Jpn.* **1999**, *72*, 1233–1238.
- [245] Eliassaf, J.; Silberberg, A. *Polymer* **1962**, *3*, 555–564.
- [246] “*Polyelectrolyte Models and Theoretical Predictions.*” In: Dautzenberg, H.; Jaeger, W.; Kötz, J.; Philipp, B.; Seidel, C.; Stscherbina, D. “*Polyelectrolytes: Formation, Characterization and Application*”, Hauser Publishers, Munich, Vienna, New York, 1994, Chapter 3, 87–129.

- [247] Wandrey, C.; Hunkeler, D. "Study of Polyion Counterion Interactions by Electrochemical Methods." In: "Handbook of Polyelectrolytes and Their Applications." Tripathy, S.K.; Kumar, J.; Nalwa, H. S. American Science Publishers, 2002, Volume 2, Chapter 5, 147–172.
- [248] Wandrey, C.; Hunkeler, D.; Wendler, U.; Jaeger, W. *Macromolecules* **2000**, *33*, 7136–7147.
- [249] Sedlák, M.; Koňák, Č.; Štěpánek, P.; Jakeš, J. *Polymer* **1987**, *28*, 873–880
- [250] Nishida, K.; Kaji, K. Kanaya, T. *J. Chem. Phys.* **2001**, *115*, 8217–8220.
- [251] "Influence of Monomer Concentration and Temperature on the Free-Radical Propagation Rate Coefficients of Partially and Fully Ionized Methacrylic Acid in Aqueous Solution Studied by PLP-SEC" Beuermann, S.; Buback, M.; Hesse, P.; Kukučková, S.; Lacík, I.; Učňová, L. *in preparation*
- [252] Mukherjee, A. K.; Schmitz, K. S.; Bhuiyan, L. B. *Langmuir* **2004**, *20*, 11802–11810.
- [253] Tanaka, M.; Grosberg, A.Yu. *Phys. Rev. Lett.* **2000**, *85*, 1568–1577.
- [254] Harrison, S.; Mackenzie, S. R.; Haddleton, D. M. *Macromolecules* **2003**, *36*, 5072–5075.
- [255] Woecht, I.; Schmidt-Naake, G.; Beuermann, S.; Buback, M.; Garcia, N. *J. Polym. Sci. Part A: Polym. Chem.* **2008**, *46*, 1460–1469.
- [256] Yee, L. H.; Coote, M. L.; Chaplin, R. P., Davis, T. P. *J. Polym. Sci. Part A: Polym. Chem.* **2000**, *38*, 2192–2200.
- [257] Lee, C. M.; Kumler, W. D. *J. Am. Chem. Soc.* **1961**, *83*, 4593–4596.
- [258] Rothschild, W. G. *J. Am. Chem. Soc.* **1972**, *94*, 8676–8683.
- [259] Sengwa, R. J.; Abhilasha; Moore, N. M.; Mehrotra, S. C. *J. Polym. Sci., Part B: Polym. Phys.* **2005**, *43*, 1134–1143.
- [260] Kirsh, Y. E. *Water soluble poly-N-vinylamides: synthesis and physicochemical properties*, John Wiley & Sons, Chichester, 1998

- [261] Agasandyan, V. A.; Trosman, E. A.; Bagdasaryan, K. S.; Litmanovich, A. D.; Shtern, V. Y. *Vysokomol. Soedin.* **1966**, *8*, 1580–1585.
- [262] Stamm, E. V.; Skurlatov, J. I.; Karaputadze, T. M.; Kirsh, Y. E.; Purmal, A. P. *Vysokomol Soedin B* **1980**, *22*, 420–424
- [263] “*Propagation rate coefficient for radical polymerization of N-vinyl pyrrolidone in aqueous solution obtained by PLP–SEC*” Stach, M.; Lacík, I.; Chorvát Jr, D.; Buback, M.; Hesse, P.; Hutchinson, R. A.; Tang, L. *Macromolecules* **2008**, accepted.
- [264] Yin, M.; Barner-Kowollik, C.; Heuts, J. P. A.; Davis, T. P. *Macromol. Rapid Commun.* **2001**, *22*, 1035–1040.
- [265] Lacík, I.; Stach, M. *unpublished results*
- [266] Hu, Y.; Motzer, H. R.; Etxeberria, A. M.; Fernandez-Berridi, M. J.; Iruin, J. J.; Painter, P. C.; Coleman, M. M. *Macromol. Chem. Phys.* **2000**, *201*, 705–714.
- [267] Buback, M.; Müller, E. *Macromol. Chem. Phys.* **2007**, *208*, 581–593.
- [268] Breitenbach, J. W. *J. Polym. Sci.* **1957**, *23*, 949–953.
- [269] Olaj, O. F.; Kornherr, A.; Zifferer, G. *Macromol. Theory Simul.* **2000**, *9*, 131–140.
- [270] Kukučkova, S. *PhD thesis*, Bratislava, Slovak Republic, 2006.
- [271] Hesse, P. *unpublished results*
- [272] Beuermann, S.; Buback, M.; Russell, G. T. *Macromol. Rapid Commun.* **1994**, *15*, 351–355.
- [273] Sack-Kouloumbri, R.; Meyerhoff, G. *Makromol. Chem.* **1989**, *190*, 1133–1152.
- [274] Beuermann, S. *PhD thesis*, Göttingen, 1993.
- [275] Wako chemicals information brochure
- [276] Buback, M.; Kowollik, C. *Macromolecules* **1999**, *32*, 1445–1452.
- [277] “*Kinetics and modeling of free-radical polymerization of non-ionized methacrylic acid in aqueous solution*” Buback, M.; Hesse, P.; Hutchinson, R. A.; Lacík, I.; Utz, I. *in preparation*

- [278] Maeder, S.; Gilbert, R. G. *Macromolecules* **1998**, *31*, 4410–4418.
- [279] Castignolles, P. *PhD Thesis*, University Pierre et Marie Curie, Paris, France, 2003.
- [280] Sarnecki, J.; Schweer, J. *Macromolecules* **1995**, *28*, 4080–4088.
- [281] Nikitin, A. N. *private communication*, 2007.
- [282] Müller, M. *PhD Thesis*, Göttingen, 2005.
- [283] Castignolles, P.; Nikitin, A. N.; Couvreur, L.; Mouraret, G.; Charleux, B.; Vairon, J-P. *Macromol. Chem. Phys.* **2006**, *207*, 81–89.
- [284] Moad, G.; Shipp, D. A.; Smith, T. A.; Solomon, D. H. *Macromolecules* **1997**, *30*, 7627–7630.
- [285] Nikitin, A. N.; Hutchinson, R. A. *Macromol. Theory Simul.* **2007**, *16*, 29–42.
- [286] Hakim, M.; Verhoeven, V.; McManus, N. T.; Dubé, M. A.; Penlidis, A. *J. Appl. Polym. Sci.* **2000**, *77*, 602–609.
- [287] Li, D.; Grady, M. C.; Hutchinson, R. A. *Ind. Eng. Chem. Res.* **2005**, *44*, 2506–2517.
- [288] Kajiwara, A. *Macromol. Symp.* **2007**, *248*, 50–59.
- [289] Best, M. E.; Kasai, P. H. *Macromolecules* **1989**, *22*, 2622–2627.
- [290] Matsumoto, A.; Giese, B. *Macromolecules* **1996**, *29*, 3758–3772.
- [291] Kamachi, M.; Kajiwara, A. *Macromol. Symp.* **2002**, *179*, 53–74
- [292] Kajiwara, A.; Kamachi, M. “*Advances in Controlled/Living Radical Polymerization*” ACS Symposium series 854, Matyjaszewski, K. (Ed.), American Chemical Society: Washington, DC, 2003.
- [293] Harris, K. R. *J. Chem. Eng. Data* **2000**, *45*, 893–897.
- [294] Arita, T.; Buback, M.; Janssen, O.; Vana, P. *Macromol. Rapid Commun.* **2004**, *25*, 1376–1381.
- [295] Szablan, Z.; Toy, A. A.; Davis, T. P.; Hao, X. J.; Stenzel, M. H.; Barner-Kowollik, C. J. *Polym. Sci., Part A: Polym. Chem.* **2004**, *42*, 2432–2443.

- [296] Arita, T.; Buback, M.; Vana, P. *Macromolecules* **2005**, *38*, 7935–7943.
- [297] “Chain length dependent termination in *n*- and *tert*-butyl methacrylate polymerization studied via SP-PLP-ESR” Barth, J.; Buback, M.; Hesse, P.; Sergeeva, T. *in preparation*
- [298] Griffiths, M. C.; Strauch, J.; Monteiro, M. J.; Gilbert, R. G. *Macromolecules* **1998**, *31*, 7835–7844.
- [299] Mahabadi, H. K. *Makromol. Chem.; Macromol. Symp.* **1987**, *10-11*, 127–150.
- [300] Nikitin, A. N.; Buback, M.; Hesse, P. *unpublished results*

Danksagung / Acknowledgements

Herrn Prof. Dr. Michael Buback danke ich für die interessante Themenstellung, die wertvollen Diskussionen und die stete Förderung dieser Arbeit.

I wish to thank Dr. Igor Lacík for fruitful cooperation, many valuable discussions and for taking the crucial part of PLP-SEC, i.e. for measuring and evaluating a multitude of SEC traces. Contributions of Dr. Marek Stach and other coworkers at the *Polymer Institute of the Slovak Academy of Sciences* are also gratefully acknowledged.

Dr. Anatoly N. Nikitin is acknowledged for giving me the opportunity to participate in his work and for numerous discussions. I certainly learned a lot.

I wish to thank Prof. Dr. Robin A. Hutchinson for steady and effective cooperation on both, the water soluble and the acrylate-type monomers.

Prof. Dr. Sabine Beuermann danke ich für die gute Betreuung während meiner Diplomarbeit und am Anfang der Doktorarbeit.

Ebenso möchte ich mich bei PD Dr. Philipp Vana, MBA für wertvolle Diskussionen und Anmerkungen bedanken.

Dr. Thomas Junkers danke ich für die Einarbeitung in die SP-PLP-Techniken und für seine stete Diskussionsbereitschaft.

Weiterhin danke ich Johannes Barth, Dr. Silvia Kukučková, Jens Schrooten, Dr. Tatiana Sergeeva und Thomas Theis für die angenehme und zumeist auch erfolgreiche Zusammenarbeit innerhalb der Arbeitsgruppe. Vielen Dank an dieser Stelle auch an Dr. Hans-Peter Vögele, Sandra Lotze und Heike Rohmann.

Ebenfalls bedanken möchte ich mich für finanzielle Unterstützung durch den Fonds der Chemischen Industrie, die Deutsche Forschungsgemeinschaft (im Rahmen des Graduiertenkollegs "Microstructural Control in Free-Radical Polymerization") und die BASF SE.

Volker Meyer, Andreas Knorr und allen weiteren Mitarbeitern der Werkstätten gilt mein Dank für die stets schnelle und gewissenhafte Bearbeitung von Fertigungs- und Reparaturaufträgen. Besondere Erwähnung gebührt in dem Zusammenhang auch Herrn Reinhard Bürsing für die zahlreichen Reparaturen der Laser.

Prof. Dr. Franc Meyer danke ich für die Bereitstellung des ESR-Spektrometers. Für ihre Hilfestellung bei ESR-Problemen und die unkomplizierte Zusammenarbeit möchte ich mich bei Frau Dr. Claudia Stückl bedanken.

Besonderer Dank gilt Björn, Daniel, Fabian, Florian, Henning, Johannes, Olaf, Silvia und Thomas für Auflockerung des Arbeitsalltages (und zum Teil auch danach). Auch allen anderen ehemaligen und derzeitigen Mitgliedern der Arbeitsgruppe Buback sei gedankt für die insgesamt gute Atmosphäre.

Zu meinem geistigen Wohlbefinden trug maßgeblich das tägliche Mittagessen mit Caro, Corte, Daniel und Sabine bei.

Meinen Eltern gebührt mein Dank für ihre moralische und materielle Unterstützung während des gesamten Studiums und der Doktorarbeit.

Abschließend möchte ich meiner Freundin Sabine für ihre große Geduld und fortwährende Unterstützung danken. Ohne sie wären die letzten Monate und Jahre nicht so schön gewesen.

Lebenslauf

07.07.1980 geboren in Nordhausen

Schulbildung

1987 – 1991 Grundschule: POS „Geschwister Scholl“, Heringen

1991 – 1999 Johann Gottfried Herder Gymnasium, Nordhausen

Juni 1999 Abitur

Wehrersatzdienst

Juli 1999 – Juni 2000 Johanniter-Unfallhilfe e.V. Kreisverband Nordhausen;
Abteilung Rettungsdienst

Hochschulausbildung

Okt. 2000 – Jan. 2005 Studium der Chemie an der Georg-August-Universität
Göttingen

Okt. 2000 – Sept. 2002 Stipendiat des Fonds der Chemischen Industrie

Jan. 2002 – Jan. 2005 Mitglied der Studienstiftung des Deutschen Volkes

Okt. 2002 Diplomvorprüfung im Fach Chemie

seit April 2004 Kollegiat im DFG-geförderten Graduiertenkolleg 585
„Microstructural Control in Free-Radical Polymerization“

April 2004 – Jan. 2005 studentische / wissenschaftliche Hilfskraft am Institut für
Physikalische Chemie der Universität Göttingen

Mai 2004 – Jan. 2005 Anfertigung einer Diplomarbeit am Institut für Physikalische
Chemie der Universität Göttingen unter Anleitung von Herrn
Prof. Dr. M. Buback „Kinetik radikalischer Polymerisationen in
wässriger Phase“

Jan. 2005 Diplomprüfung im Fach Chemie

seit Jan. 2005 wissenschaftlicher Mitarbeiter am Institut für Physikalische
Chemie der Universität Göttingen

seit Jan. 2005 Anfertigung einer Dissertation am Institut für Physikalische
Chemie der Universität Göttingen unter Anleitung von Herrn
Prof. Dr. M. Buback

Juli 2005 – Juni 2007 Stipendiat des Fonds der Chemischen Industrie

seit Juli 2007 Stipendiat des DFG-geförderten Graduiertenkollegs 585

